Functional screening for gene trap mutants involved in perineuronal net formation.

A thesis presented by
Adil Abbasi

In fulfilment for the degree of Doctor of Philosophy

2023

Strathclyde institute of Pharmacy and Biomedical Sciences
University of Strathclyde

Declaration

This thesis is the result of the author's original research. It has been composed by the author and has not been previously submitted for examination which has led to the award of a degree. The copyright of this thesis belongs to the author under the terms of the United Kingdom Copyright Act as qualified by the University of Strathclyde Regulation 3.49

Due acknowledgment must always be made of the use of any material contained in or derived from this thesis.

Signed: **Adil Abbasi**

Date 31/05/2023

Acknowledgments

First of all, I would like to thank Allah SWT, the most merciful and the most gracious for giving me the opportunity to get to this part of my studies. I would also like to thank my supervisor Dr Benjamin Pickard for his mentorship, guidance, and support throughout the course of my studies. Due to his patience, discussions, criticisms and questions, Ben has brought out the best in me and he made my research and studies at Strathclyde a very enjoyable time despite me being a very challenging individual to deal with. I would also like to give a special thanks to Dr Christine Dufes the head of the graduate school for doing an outstanding job and providing me with the necessary support and guidance when my mental health issues were spiralling out of control.

I would like to give special thanks for my beautiful wife, Arooj Tariq for her immense support, patience and encouragement throughout all of this. Special thanks also go to my mum and dad and my brothers Aali Abbasi, Saoud Tariq Abbasi and Zeeshan Abbasi for their continued support and my father-in-law Tariq Mustafa Abbasi and my mother-in-law Naheed Tariq Abbasi for their continued support and encouragement. Further thanks are also extended to my sister Anab Tariq Abbasi who is my partner in crime. I would like to also thank my aunty and uncle (Sadaf Mustafa Abbasi) and (Zahid Imtiaz) for always guiding me and providing me with excellent guidance and life skills even when I was considerably testing their patience levels. Without all these people helping me and guiding me today, I do not think I would be in the place I am today. I owe a lot to these individuals for helping me become the person I am today. I would also like to give special acknowledgment and thanks to Naweed Safdar for his continued guidance and knowledge which has helped change my attitude to life immensely. However, nothing happens without the permission of Allah the most merciful and I am truly grateful for everything I have been given in my life and the opportunity to complete this PhD. Despite all the numerous challenges and hardships, I have faced recently, I would like to say Al-ḥamdullilah. I would also like to pay a final tribute to Haji Ghulam Mustafa Abbasi who is one of the greatest Islamic characters of the 21st century. His honesty and directness showed me the way to be happy in life. Though he is no longer with me, I owe a lot to him for seeing the best in me when others were putting me down.

This PhD has taught me one thing. Money and status aren't important. Good character and behaviour are. Don't look down on anyone and don't think you are better than anyone. Be humble and simple.

Contents

List of Figures and Tables

List of figures

List of tables

Table 7.1 Top ten proteins identified that were not annotated as 'contaminants' by the FingerPrints Laboratory.

List of Abbreviations

ACAN-Aggrecan

ADAMST- disintegrin and metalloproteinase with a thrombospondin type 1 motif, member 13

AMPA- α -amino-3-hydroxyl-5-methyl-4-isoxazole-propionate

BBB-blood-brain barrier

BCAN-*Brevican*

ChABC- Chondroitinase ABC

CLD- C-terminal lectin-like domain

CNS- Central nervous system

CRISPR- Clustered regularly interspaced short palindromic repeats

CSPGs-chondroitin sulphate proteoglycan

C6STs -chondroitin-6-sulphate sulphotransferases

C4STs)-4-O sulphotransferases

CSK-cytoskeleton buffer

DAPI- 4'6'-diamino-2-phenylindole

DCC-deleted in colorectal cancer

DMSO- dimethyl sulfoxide

DNA- Deoxyribonucleic acid

DMEM-Dulbecco's Modified Eagle Medium

ECACC-European Collection of Authenticated Cell Cultures

ECL- Enhanced chemiluminescence

ECM- Extracellular matrix

ER-endoplasmic reticulum

FAF1-Fas-associated factor 1

FCS- Foetal Calf serum

GAG-glycosaminoglycan

GAG-glycosaminoglycan

Glc-Glucuronic acid-Glc

GlcNAc -Glc-NAc-N-acetylglucosamine

GSK-3Glycogen Synthase Kinase-3

HA-Hyaluronan- HA

HAS-hyaluronan synthases

HAPLN- Hyaluronan and proteoglycan binding link protein

HEK293- human embryonic kidney 293

LTP-hippocampal long-term potentiation

MMP- Matrix metalloproteinase

MS- Multiple sclerosis

NES-nestin

NCAN- *Neurocan*

NMDA- n-methyl-D-aspartate

NPY-Neuropeptide Y

PAM- Protospacer adjacent motif

PBS-T PBS + 0.1% TIen20

PCR- polymerase chain reaction

PFA- paraformaldehyde

PGs-proteoglycans

PNS- Peripheral nervous system

PNN- perineuronal net

PCR- polymerase chain reaction

PTPσ -receptor-type tyrosine-protein phosphatase S

RACE-rapid amplification of cDNA ends'

TN-c-Tenascin C

TN-R Tenascin R

TBE-Tris/Borate/EDTA

TH-tyrosine hydroxylase

VCAN- *Versican*

WFA- Wisteria floribunda agglutinin

Abstract

A tissue's cells function within the context of an extracellular matrix (ECM) of glycosylated and cross-linked proteins that provide structural support and adhesion, while also modulating intercellular communication. In the central nervous system (CNS), the ECM is vital for the complex neuronal migration and neurite projection stages during embryonic development that create the precise anatomies and morphologies of functioning brain circuitry.

The historical discovery of a plant-derived molecule, *Wisteria floribunda* agglutinin (WFA), revolutionised the study of brain ECM because it binds to (and, therefore, is used to stain) one specific form of ECM called the perineuronal net (PNN). As its name suggests, this creates a 'cage' specifically around the soma of parvalbumin-containing interneurons. The critical role of this class of neurons in brain activity regulation, and known involvement in specific neuropsychiatric pathologies, ignited much investigation of the PNN. It is now known that its dysfunction is associated with multiple conditions. In our laboratory, a previous cellular 'gene trap' genetic screen identified that the mutation of protein components of the PNN contributed to the response to lithium, a mood stabiliser treatment for the psychiatric disorder bipolar disorder.

In this thesis, the further application of gene trap screening to search for genes encoding proteins that contribute directly to, or regulate, the formation of the perineuronal net on *SH-SY5Y* neuroblastoma cells, a commonly used model of neurons is described. The hypothesis was that identified genes would not only provide greater insight into the PNN structure but might offer new targets for the treatment of CNS disorders. A 'library' of randomly mutated cells was created, and WFA was used to identify mutant colonies with reduced staining, indicative of PNN dysfunction.

Several PNN-defective cell colonies were isolated, and their mutated genes identified using a modified polymerase chain reaction (PCR) protocol. Three genes, *DCC*, *FAF1*, and *GALNTL6* were among those that were identified and considered the best candidates to take forward for further analysis. *DCC* protein is the netrin-1 receptor, which has important roles in CNS development. *FAF1*, the FAS associated factor 1 protein, which participates in apoptosis and autophagy processes. *GALNTL6* is a glycosyl transferase enzyme that modifies proteins through O-linked glycosylation – a very strong candidate in light of the substantial glycosylation that occurs to PNN proteins, and which is thought to be the target of WFA staining.

These three proteins required validation through the generation of independent mutations/inhibition in cells. CRISPR, siRNA and pharmacological means was used to attempt this. Multiple genetic ablations failed to produce successful defective gene alleles meaning that full validation of these three candidate genes was not possible, and their role in PNN function remains unclarified.

However, the still-unknown targets of WFA in a 'pull-down' assay of proteins lysed from *SH-SY5Y* cells was pursued-associated protein material was assessed by mass spectrometry. Among the top hits was the protein vimentin which is known to exist within the cytoplasm of the cells but also to be secreted into the ECM, where it reportedly shows post-translational modification by O-linked glycosylation.

In summary, despite failure to fully validate screen findings, these studies identified a number of candidates for further investigation in the context of PNN function and role in associated disease. The protein vimentin should also be pursued in terms of its potential contribution to PNN function and as the target of the WFA stain.

Chapter 1

Introduction

1. The Perineuronal Net (PNN)

The central nervous system (CNS) is composed of the brain and spinal cord and is key for the integration of information sent by physiological and sensory systems, and subsequent processing and control of responses to promote survival and reproduction (Bonneh-Barkay & Wiley, 2009). The central nervous system integrates and adapts to this information through learning and memory through its ability to establish, withdraw and modify synaptic connections between neurons. Modulation of the synaptic connections between neurons in response to environmental stimuli is referred to as neuronal or synaptic plasticity and is thought to be the basis of learning and memory.

Neuronal plasticity is achieved, in part, by changes in the extracellular matrix (ECM) as well as the increased number and sensitivity of neurotransmitter receptors and synapses. The ECM can be classified into regionally specialised forms such as the perineuronal net (PNN) – the focus of the work described in this thesis. The PNN plays a key role in the regulation of neuronal plasticity (Sood *et al.*, 2015) but that is just one functional aspect of an extracellular structure that is hugely complex in its molecular composition, highly limited in its distribution, and consistently linked to neuropsychiatric and neurodegenerative disease states. PNNs are typified by their enrichment in a specific type of glycosaminoglycan (GAG), chondroitin sulphate. The following sections will explore the extracellular matrix and specifically, PNNs, thus providing the rationale for the experimental investigations described in this thesis.

1.1 Extracellular matrix in the central nervous system

The extracellular matrix (ECM) helps connect cells, resulting in formation of tissues (Warren *et al.*, 2018). The composition of the ECM varies according to the cell type of the tissue thus permitting it to undergo many specific functions. The neuronal ECM is considered unique within the human body with regards to its composition and diversity. It represents approximately 20% of the total volume of the adult brain and has key roles in early development as well as in adult neuronal function. Within the adult CNS, functions include proliferation, differentiation, migration, plasticity, and regeneration of neural cells.

Secretion of the neural ECM occurs from both neurons and glia. In contrast to other tissues, the neural ECM possesses limited numbers of structural (load-bearing) fibrous proteins such as collagen, laminin and elastin, but enhanced levels of proteoglycans (PGs). Major components of the neural ECM include hyaluronic acid, proteoglycans, link proteins and tenascins (Reichardt & Prokop,

2011) while associated proteins such as reelin, ECM receptors and integrins also play a considerable role in development processes.

The extracellular matrix typically provides a structural support for the cells and maintains tissue integrity (Warren *et al.*, 2018). In the brain, the ECM also permits communication between adjacent and distant cells by stimulating the transport and availability of various molecules (Warren *et al.*, 2018). The ECM offers a pertinent environment for enzymes involved in post-synthesis modifications and for signalling molecular cleavage of myelin around axons. Production of myelin occurs via oligodendrocytes in the CNS and promotes efficient propagation of the action potential. Within the peripheral nervous system (PNS), ECM components such as laminin and collagen stimulate myelination of peripheral nerves via regulation of Schwann cell proliferation, adhesion and spreading.

1.1.1 ECM types in the central nervous system

The ECM within the central nervous system is organised within various compartments with differing composition and function (See Figure 1.1) (Lau *et al.*, 2013).The basement membrane (basal lamina) is a specialized extracellular matrix surrounding the blood vessels and surface of the CNS and is essential for the development of epithelial tissues and organs. The basement membrane is involved in neurogenesis, CNS injury repair and nerve regeneration and is a significant component of the blood-brain barrier (BBB). Another compartment within the CNS is the interstitial matrix which corresponds to molecules which fill the space between the CNS cells in the parenchyma, which is the functional part of the brain. This can be divided into both the loose matrix as well as the membrane-associated matrix. Within some regions of the CNS, the interstitial matrix can become more complex, resulting in the production of a condensed matrix structure termed the perineuronal net. Historically, perineuronal nets were reported by Camello Golgi in the 19th Century. However, over the last few decades, the molecular composition and anatomy of the PNN has been substantially documented (Soleman *et al.*, 2013).
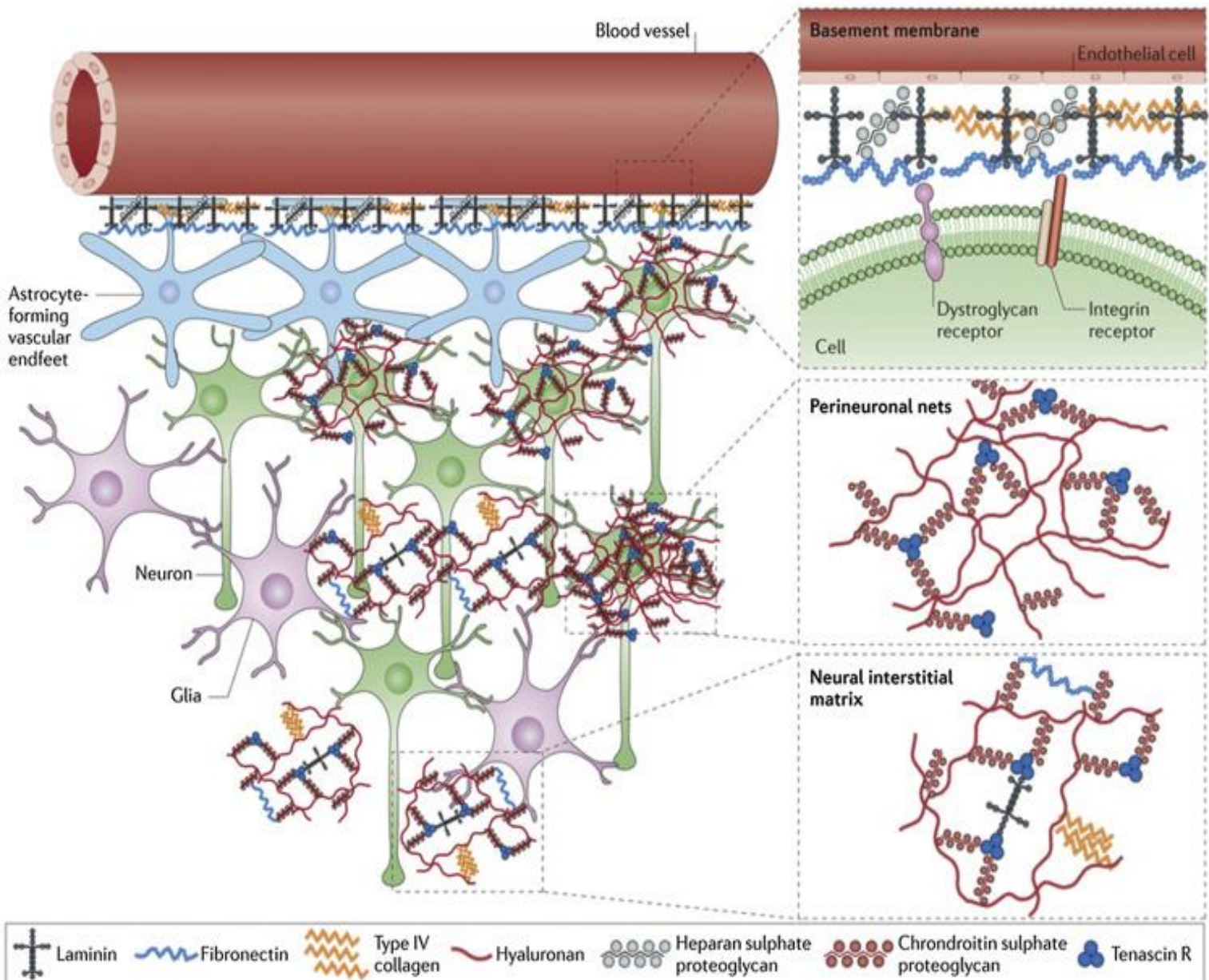
Figure 1.1 The central nervous system extracellular matrix is a complex and diverse molecular structure. *The ECM of the CNS has three major components: the basement membrane, perineuronal net and the neuronal interstitial matrix. The basement membrane is located around surrounding cerebral blood vessels, whereas the perineuronal net is a dense matrix which surrounds neuronal cell bodies and dendrites. The neuronal interstitial matrix occupies the space between the neurons and glial cells. Taken from (Lau et al.,2013).*

1.2 Components of the perineuronal net

Perineuronal nets produce large and stable aggregates via specific interactions on the surface of the soma and proximal dendrites in sub-populations of neurons described in more detail in section 1.3 (Kwok *et al.*, 2011). At the cellular level, the PNN appears as a meshed coat on the neuronal soma resulting in the compartmentalisation and regulation of synaptic formation and connection (Kwok *et al.*,2011).

The perineuronal net is a specialized complex of cross-linked, glycosylated proteins and oligosaccharides and is described as having a typical honeycomb-like structure within the literature (John *et al.,2022).* With regards to protein glycosylation, there are two types which are defined as N-linked and O-linked glycosylation both which require the import of the target polypeptide into the endoplasmic reticulum (ER). N-linked glycosylation begins in the endoplasmic reticulum, but O-linked glycosylation does not occur until the polypeptide has been transported into the Golgi apparatus. N-linked glycosylation is the attachment of an oligosaccharide to a nitrogen atom of an asparagine residue of a protein. Glycosylation is an important modification of eukaryotic proteins because the added sugar residues are often used as molecular flags or recognition signals to other cells which can interact with them or as a means to modify protein-protein interactions. N-linked glycosylation is a co-translational mechanism, whereas O-linked glycosylation must be occurring post-translationally. Other major differences in the two types of glycosylation are (1) N-linked glycosylation occurs on asparagine (N) residues within an N-X-S or N-X-T consensus sequence (X is any amino acid other than P or D) while O-linked glycosylation occurs on the side chain hydroxyl oxygen of either serine or threonine residues determined not by surrounding sequence, but by secondary and tertiary structure; (2) N-linked glycosylation begins with 14 specific sugar residues that are then pruned and remodelled, while O-linked glycosylation is based on sequential addition of individual sugars, and does not usually extend beyond a few residues. Though the perineuronal net component chondroitin sulphate proteoglycans undergo N-linked glycosylation, it is known that due to the sequential addition of individual sugars, O-linked glycosylation is also occurring during perineuronal net development. For example, protein cores are post translationally modified by O-linked glycosylation via glycosyltransferases producing proteoglycans. In the figure below (Fig. 1.2), the main components of the PNN are indicated and subsequently described in the text.
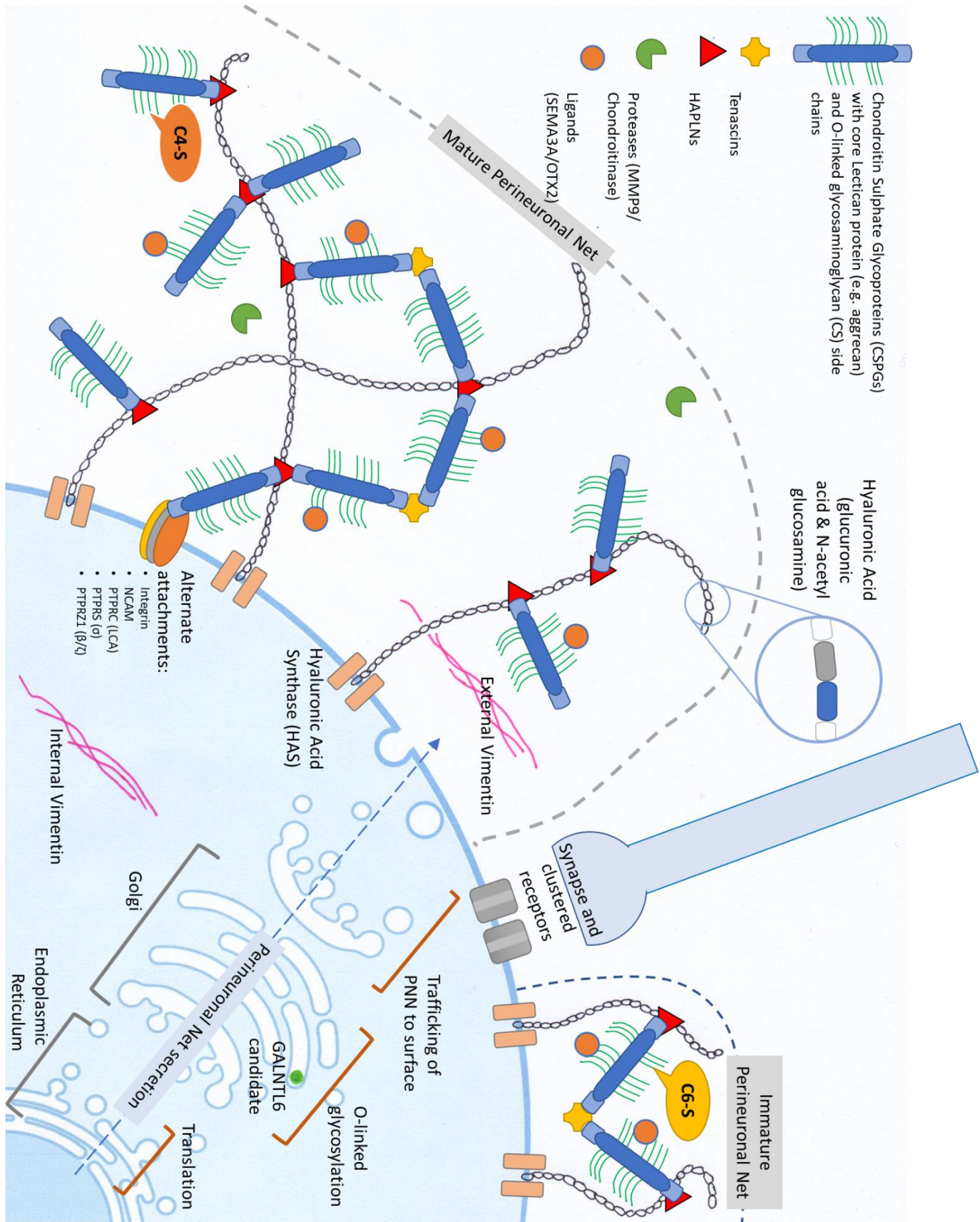
Figure 1.2 The composition and function of the perineuronal net (PNN) and its relation to the work described in this thesis. *The PNN is a complex form of extracellular matrix that is primarily*

based on secreted and anchored hyaluronic acid chains that are cross-linked by chondroitin sulphate proteoglycans (CSPGs). At the core of the CSPG is a protein member of the lectican family with Aggrecan, Neurocan, Versican, Brevican, and phosphacan being the principal members. These proteins are substantially modified by the addition of chondroitin sulphate side-chains through the process of O-linked glycosylation. CSPGs bind to each through tenascin-mediated interactions, and to the hyaluronic acid chains through HAPLN-mediated interactions. CSPGs are known to interact with other cell surface proteins such as integrins, NCAM, and several receptor-type protein tyrosine phosphatases. The thickness of the PNN around a neuron increases as a function of maturity - matched by a shift in chondroitin sulphation pattern from C6-S to C4-S. This thickness can be reduced by the action of proteases such as MMP9 and Chondroitinase. The journey of the PNN component proteins begins with transcription in the nucleus, translation and translocation into the luminal space of the endoplasmic reticulum, and trafficking through the Golgi body (where O-linked modification occurs), and eventual secretion. One the candidate proteins identified in the screen described in Chapter 6 is GALNTL6, an enzyme contributing to O-linked glycosylation. Also shown, both internally and in an extracellular form (with potential O-linked glycosylation), is the intermediate filament, vimentin. This protein is identified from an experimental pull-down of proteins that interact with the Wisteria floribunda agglutinin molecule (Chapter 7) that is a commonly used stain for the presence of the PNN. The actions of the PNN in neurotransmitter receptor clustering, restriction of synaptic connections, and the binding of specific signalling molecules (e.g., SEMA3A and OTX2) are also illustrate*d in the figure. Figure created using BioRender, Powerpoint, and by hand.*

1.2.1 PNN component- Glycosaminoglycans

Glycosaminoglycans (GAGs) are divided into four groups which are based on their core disaccharide structures. These include heparin sulphate and chondroitin sulphate which are produced in the Golgi apparatus whilst their lectican protein cores are produced in the rough endoplasmic reticulum (Bonneh-Barkay & Wiley, 2009). These are post translationally modified via O-linked glycosylation via glycosyl transferases producing proteoglycans. On the other hand, keratan sulphate can modify proteins via N-linked glycosylation or O-linked glycosylation of the proteoglycan. Furthermore, the fourth class of GAG is hyaluronic acid (HA) is a large linear polysaccharide composed of repeating disaccharide units of glucuronic acid (Glc) and N-acetylglucosamine (GlcNAc) in the sequence [-β(1,4)-GlcA-β(1,3)-GlcNAc-] (see Fig.1.2 and Fig.1.3). HA represents the backbone of the ECM upon

which other ECM molecules aggregate and assemble, and is the only component entirely based on disaccharides. During physiological conditions, HA is composed of 2,000-20,000 disaccharide units, corresponding to 1,000-10,000 kDa and 2-25 μm in length. Synthesis of HA occurs via the hyaluronan synthases (HAS1-3), and degradation occurs via hyaluronidases. Use of *in situ* hybridisation indicates that PNN neurons within the cerebellum possess HAS-2 and HAS-3 activity, while spinal cord neurons express the isoforms HAS-1 and HAS-3. These neural HAS enzymes are transmembrane and synthesise HA chains of various lengths and at various speeds. Chain length differences arising from differential HAS expression have an effect on PNN structure and mechanical strength. In agreement with this, studies reported pig heart valves with high regions of tensile strength are associated with decreased levels of GAG chain length and content (Stephens *et al.*,2008). The HA chain is extruded via the plasma membrane into the ECM as synthesis occurs. Results from studies conducted with *in vitro* models provide a strong basis that neuronal surface associated HAS can anchor hyaluronan chains to the neuronal surface. Due to its large size, negative charge, random coil structure, and hydrophobic faces (resulting from its 16 carboxyl groups and hydrogen clusters), HA has the ability to influence physicochemical and hydrodynamic properties of the surrounding tissue (Bonneh-Barkay & Wiley, 2009). The most abundant GAG within the foetal rat brain is HA (25%) but its level decreases significantly (to 10%) after birth (Warren *et al.*, 2018). During development, HA is concentrated within the intermediate zone – helping give rise to white matter (Warren *et al.*, 2018). With regards to adult animals, HA localizes around myelinated fibres in white matter, but it is also located within grey matter in PNNs (Warren *et al.*, 2018).
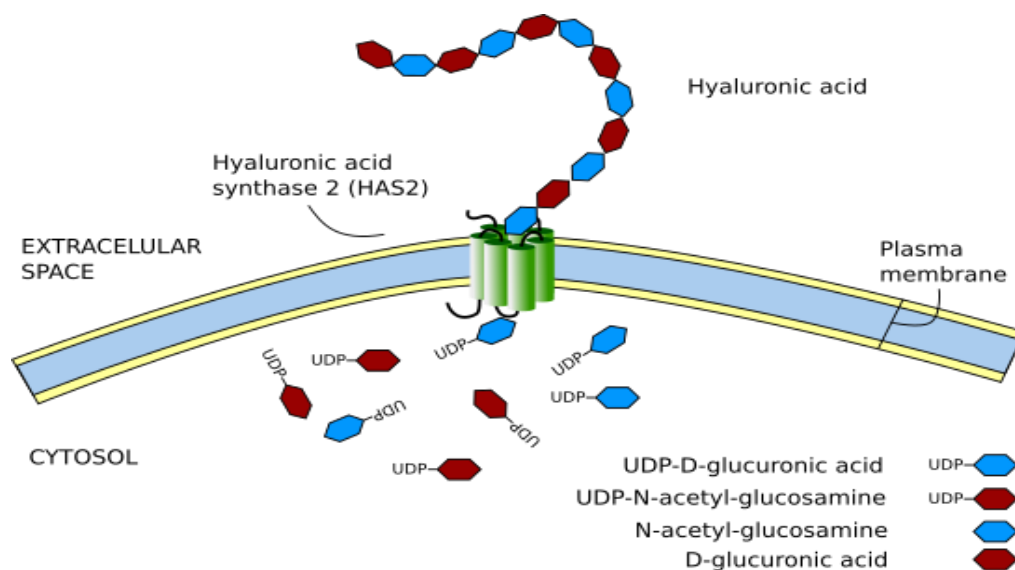
Figure 1.3. Synthesis of Hyaluronic acid is necessary for PNN assembly. *The process of hyaluronic acid synthesis occurs via hyaluronic acid synthase. Occurring in the cytosol and*

extracellular space, production of hyaluronic acid is undertaken where the building blocks such as UDP and its other similar family members are bound to the sugar precursors are then utilised by hyaluronic synthase 2 resulting in formation of hyaluronic acid. Taken from (Escudero; 2011)

1.2.2 PNN component- Hyaluronan and proteoglycan binding link protein (HAPLN)

Hyaluronan and proteoglycan binding link protein (HAPLN) is a family of proteins with four members (HAPLN 1-4) (Dityatev *et al.*, 2010). These are involved in stabilising interactions between HA and CSPGs (Dityatev *et al.*, 2010). HAPLNs are composed of Ig-like V-type, link 1 domain and link 2 domain and are 38-43 kDa (Dityatev *et al.*, 2010). Their structures are homologous to G1 lectican domains (described below) which also bind to HA (Dityatev *et al.*, 2010). HAPLN1 interacts with both HA and lecticans (such as *Aggrecan*) and is thus vital for cross-linking the components of the specialised PNN matrix (Dityatev *et al.*, 2010). Studies have shown that animals lacking HAPLN1 or HAPLN4 in the CNS have abnormal PNNs (Dityatev *et al.*, 2010). The absence of HAPLN1 in PNN-bearing cells hinders production of a compact pericellular matrix (Kwok *et al.*,2010).

1.2.3 Perineuronal net component - Lecticans

Another key component of the PNN is the lectican family. Lecticans are classified as members of the chondroitin sulphate proteoglycan (CSPG) family - the proteoglycan status indicates that they are 'more glycan than protein' (compared to glycoproteins). These possess the ability to bind to both hyaluronan and lectins such as WFA - a plant molecule that will figure heavily in this thesis as a PNN detection tool (Kwok *et al.*,2010). The structure of these lecticans involve a protein core onto which is covalently attached linear and unbranched chondroitin sulphate GAG chains (Fig. 1.2). This covalent attachment occurs via serine residues on the core protein through the process of O-linked glycosylation producing the complete CSPG.

There are five lectican members: *Aggrecan*, *Neurocan*, *Phosphacan*, *Versican* and *Brevican*. Of the five, *Brevican* (BCAN) resides in both the ECM and is also linked to the cell membrane exterior. This linkage occurs via a glycosylphosphatidylinositol anchor. It is important to note that while the presence of *Aggrecan* (*ACAN*) is detected on all PNN-positive neurons, the other lecticans reside in

sub-populations of PNNs. PNNs have been shown to have reduced *Brevican* levels but no alterations in *Aggrecan* expression in the absence of HAPLN4 (bral2) (Carulli & Verhaagen, 2021).

The importance of *Aggrecan* is further confirmed in *in vitro* HEK293 cell mutant models and also organotypic cultures derived from *Aggrecan* knockout animals. These models result in failed production of normal PNNs (Giamanco *et al.*,2010).

The size of the lectican molecule and the extent of glycosylation in the middle GAG attachment regions can alter levels of crosslinking in perineuronal nets and thus alter compactness (Table 1). Lectican-CSPGs can also interact with receptor-type tyrosine-protein phosphatase S (PTPRS; also known as PTPσ) and PTPRC (also known as LCA/LAR) receptors, among other molecules (Fig. 1.2) which are expressed widely by CNS neurons and on PNN-bearing cells. Despite no established role for these receptors in PNN function, the consequences for axon regeneration are well documented (Yamaguchi, 2000). Another proposed PNN signalling route is via reticulon 4 receptor (the Nogo receptor) whose function can also be modulated by Lectican-CSPG.

Proteoglycan	Name	Core protein size (kDa)	Number of GAG chains	Type
CSPG	*Aggrecan*	224	100	Secretory
	Versican V0	370	17-23	Secretory
	Versican V1	262	12-15	Secretory
	Versican V2	180	5-8	Secretory
	Brevican	97	0-5	Secretory
	Neurocan	133	3	Secretory
	Phosphacan	173	3-4	Secretory

Table 1. Proteoglycans expressed within the central nervous system. *Table 1 shows the proteoglycans expressed within the central nervous system. As can be seen above, most chondroitin sulphate proteoglycans are secretory and Versican also has 3 isoforms differing in sizes of 262, 180 and 370 kDa respectively.*
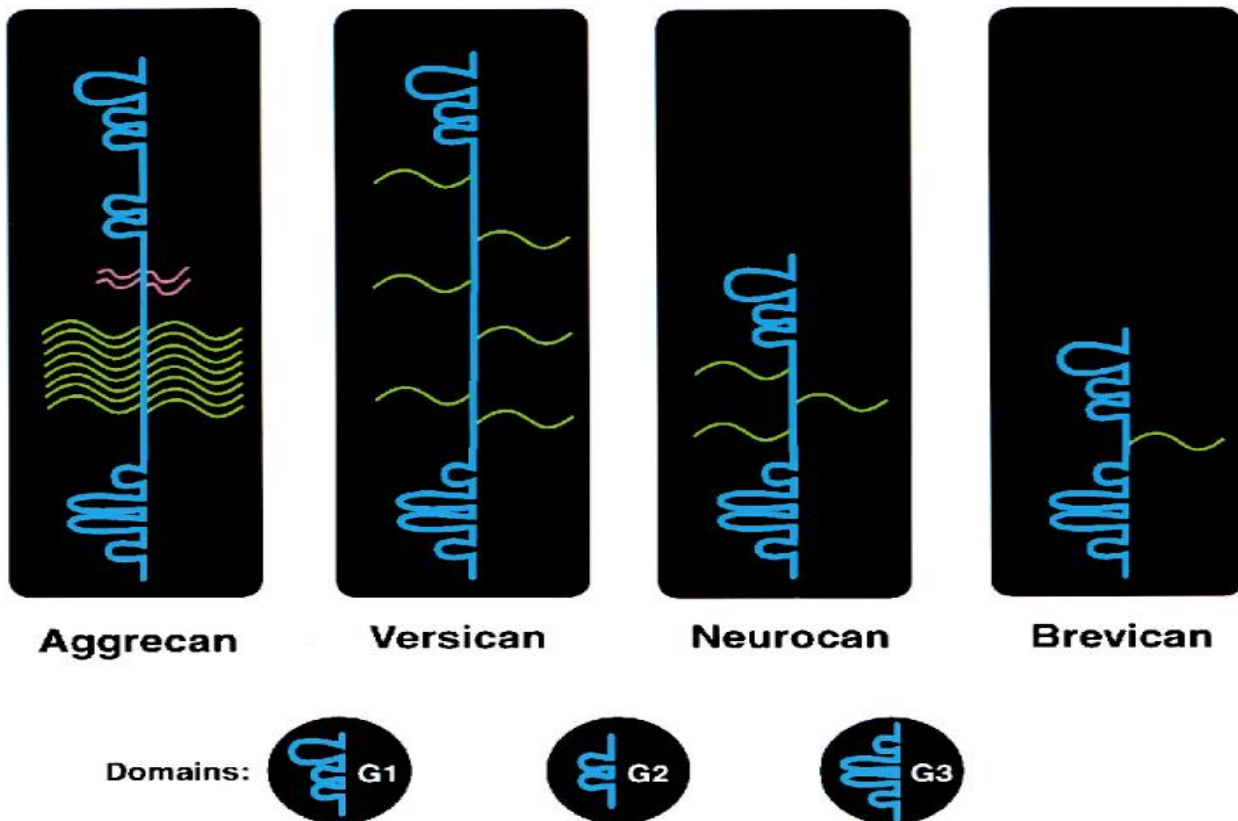
Figure 1.4 Lectican Domain Structure. *Figure 1.4 above adapted from (Yamaguchi, 2000). Lecticans possess N-term G1 domains as well as C-ter G3 domains. The G1 domain is composed of Ig-like loops and two link modules. On the other hand, the G2 domain consists of only two link modules. The G3 domain is composed of one or two EGF repeats, a C-type lectin domain as well as a CRP-like domain. Lecticans possess chondroitin sulphate chains (yellow) within the central domain. Keratan sulphate chains (pink) are also present within the N terminal part of the central domain of Aggrecan only.*

Aggrecan is distributed through the entire body with the majority in the cartilage and brain *ACAN*'s structure involves a N-terminal domain (G1) which is separated from a second globular domain (G2) via a short interglobular domain (See Figure 1.4). Other regions include an elongated domain carrying keratan sulphate and chondroitin sulphate chains as well as a C-terminal globular G3 domain. Proteoglycan tandem repeats located in the G1 domain are responsible for *ACAN*'s interaction with hyaluronan. *Aggrecan* possesses a significant role in production and formation of complex PNN structure with *ACAN* knockout animals displaying abnormal PNN formation.

NCAN is also classified as a major component of the extracellular matrix and has a full-length protein composed of 1,321 amino acids with a molecular weight of 220 kDa (Siebert, Conta Steencken and Osterhout, 2014). It possesses 5/6 N-linked and 40 O-linked potential glycosylation sites as Well as three active domains (Siebert, Conta Steencken and Osterhout, 2014). These domains include an N-terminal hyaluronan-binding domain, a C-terminal lectin-like domain (CLD), and a central GAG attachment region (See Figure 1.4) which possesses no homology with other family members (Siebert, Conta Steencken and Osterhout, 2014). Importantly, lectican family members have similar characterization with regards to CLDs and N-terminal globular hyaluronan binding domains but differ in central regions (Siebert, Conta Steencken and Osterhout, 2014). Functional studies on *NCAN* indicates it contributes to the mesh-like structure of the PNN by binding multiple ECM components (hyaluronan, heparin, Neural cell adhesion molecule (NCAM) *Tenascin C* (TN-c) and *Tenascin R* (Siebert, Conta Steencken and Osterhout, 2014). Brain expression of *NCAN* occurs during embryonic and post-natal brain development. Embryonic studies show that *NCAN* is first detected at the tenth embryonic day and maximum expression occurs at birth with reduced levels in mature mouse brains (Kwok *et al.*, 2011). Importantly, after birth, CS chains on *Neurocan* have altered sulphation patterns (Warren *et al.*, 2018). *NCAN* expression occurs in various areas including the thalamus, spinal cord, hypothalamus and the cerebellum (Kwok *et al.*, 2011). A lack of *Neurocan* decreases late phase hippocampal long-term potentiation (LTP) (Warren *et al.*, 2018).

Like the other lecticans, *Versican* (1,000 kDa) has a globular domain involving an N-terminal, C-terminal and a GAG side chain (Kwok *et al.*, 2011). *Versican* possesses four isoforms, V0, V1, V2, and V3 expressed in various tissues including the brain. The structure of *Versican* isoforms include N-terminal domains (G1), GAG attachment region and a C-terminal domain (G3) (Kwok *et al.*, 2011). However, the V3 isoform possess no GAG attachment region but still crucially possesses the ability to bind to hyaluronan via the G1 domain and to EGF receptors (Kwok *et al.*, 2011). In some studies, it has been demonstrated that *Versican* impacts immunity and inflammation via regulation of cell trafficking and activation (Wight *et al.*, 2020). Consequently, *Versican* is emerging as a potential target within the control of inflammation within various diseases (Wight *et al.*, 2020)

Brevican has a molecular mass of 140 kDa and has been shown to interact with *Tenascin R* (Kwok *et al.*, 2011). Other studies have demonstrated upregulated *Brevican* expression with glial cell proliferation during early nervous system development and it also plays a role in cell adhesion, neurite outgrowth as well as synaptic plasticity (Kwok *et al.*, 2011).

Versican, *Neurocan* and *Aggrecan* have all been shown to inhibit axonal regeneration and neurogenesis after central nervous system injury. *Neurocan* polymorphisms have been associated with risk of bipolar disorder and schizophrenia (Siebert, Conta Steencken and Osterhout, 2014) and one study indicated decreased levels of CSPG labelled perineuronal nets in PM brain tissue from patients diagnosed with schizophrenia (Siebert, Conta Steencken and Osterhout, 2014).

1.2.4 PNN component- Chondroitin sulphate proteoglycans and their synthesis, sulphation, and epimerisation

I have already discussed the Hyaluronan and Lectican-associated glycosaminoglycans (GAGs). These are members of a wider family of Chondroitin sulphate proteoglycans. This family of linear polysaccharides are located in the 'glycocalyx' (meaning the shell of heavy glycosylation around a cell) and the ECM of most animal tissues. Composed of repeating disaccharide units such as hexosamine and uronic acid (apart from keratan sulphate) and sulphated at various positions, this gives rise to two subfamilies, glucosaminoglycans and galactosaminoglycans. Members of the glucosaminoglycan family include heparin/heparin sulphate, keratan sulphate and HA (non-sulphated). Chondroitin sulphate and dermatan sulphate make up the other subfamily. With the exception of HA, other GAGs are produced as part of a proteoglycan molecule which is formed of a core protein and at least one GAG. Heparin/Heparin sulphate and CS/DS are linked covalently to protein serine residues via a O-glycosylation post translational modification. This occurs at a specific amino acid sequence Gly-Ser-Gly and starts with the addition of a specific linker tetra saccharide. The sequence of this tetra saccharide linker is Ser-Xyl- Gal- Gal- GlcA.

Subsequent additions to the tetra saccharide linker indicate whether the proteoglycan will result in a chondroitin sulphate proteoglycan or dermatan sulphate proteoglycan (Pomin and Mulloy, 2018). GalNAc residue addition to the tetra saccharide linker in chondroitin occurs via an enzyme, GalNAcT-I. This is encoded by the *CSGALNACT1* gene. Subsequently, multiple additions of GlcA of UDP-GlcA and GalNAc of UDP-GalNaC occur to produce the GAG polymer attached to the proteoglycan.

Further modification of the GAG backbone may occur via epimerisation. This occurs during GAG synthesis in the Golgi apparatus to produce stereoisomers. Epimerisation involves inverting the configuration of the asymmetric centre at C5 position of the glucuronic acid resulting in production

of an epimer iduronic acid (IdoA). Catalysis of this reaction occurs via glucuronyl C5-epimerase. GAG backbones have a relatively simple structure. However, due to the epimerisation of the glucoronic acid, the position and number of sulphate on one monosaccharide, and the size variety between molecules leads to plethora of isoforms within subfamilies and huge variation of potential glycosylation structures. The structure of each GAG molecule could be unique because there is no underlying blueprint as there is for mRNA to peptide sequence.

Subsequently, polymerization then occurs in various highly organized processes regulated by two types of polymerases such as GlcAT-II and GalNAc-TII to result in production of the repeating disaccharide motif GlcA-GalNac. Both these enzymes then add an individual sugar to the non-reducing end of the growing nascent chain. GalNAcT1 is not able to polymerize the CS chain whereas GalNACT-II is not able to identify the tetra saccharide of the linkage region. This is also true of both GlcAT-I and GlcAT-II.

Glycosaminoglycans may also be modified via a process called sulphation: the transfer of a sulphate group (SO_4^{2-}) to various positions on the disaccharide units - within the Golgi apparatus. Required for this process are specific sulfotransferases (STs), enzymes that transfer the sulpho- group from the universal sulphate donor 3' phosphoadenosine 5'-phosphosulpate (PAPS) to the GAG backbone. Synthesis of PAPS occurs in the cytosol and then it is translocated to the Golgi apparatus via PAPS translocase. GalNAc and GlcA are sulphated at various positions involves various CS sulfotransferase. Within the same chain, all sulphation patters can be located. Sulphation of C6 is catalysed via chondroitin-6-sulphate sulphotransferases (C6STs) of which C6ST1 was the first characterized. With regards to 4-O sulphation, this is catalysed by 4-O sulphotransferases (C4STs), and this is most common within sulphation processes in CS and DS chains. Various isoforms of C4ST occurs and can sulphate different regions. During PNN formation, 6-O-sulphation pattern is dominant in the juvenile brain this producing C6-S which is more permissive (Siebert, Conta Steencken and Osterhout, 2014). In contrast, 4-O-sulphation is more dominant within the adult brain to result in production of C4-S which is an inhibitory form of chondroitin sulphates (see Fig. 1.2). Changes in sulphation pattern are crucial for PNN formation (Siebert, Conta Steencken and Osterhout, 2014). This is demonstrated in studies where transgenic mice overexpress C6ST-1 displaying juvenile state sulphation patterns. Also, overexpressing C6ST-1 prevents the maturation of electrophysiological properties of PV-expressing interneurons (Siebert, Conta Steencken and Osterhout, 2014). This also decreases the inhibitory effects of PV cells due to improper PNN formation. Therefore, these transgenic mice display juvenile levels of ocular dominance plasticity

even in adulthood (Siebert, Conta Steencken and Osterhout, 2014). By overexpressing C6ST-1, this reduces *Aggrecan* levels in the aged brain without altering other PNN components (Siebert, Conta Steencken and Osterhout, 2014). This suggests that CS sulphation patterns of *Aggrecan* chains affect CSPG stability therefore maintaining PNN formation. With regards to neuropsychiatric disorders, altered C6ST-1 expression and CS sulphation patterns are present in brains of bipolar patients. Similar results are also obtained in schizophrenia and in mice with cortical brain injury (Siebert, Conta Steencken and Osterhout, 2014).

GAG	Localization	Comments
Hyaluronate	synovial fluid, articular cartilage, skin, ECM of loose connective tissue	large polymers: molecular weight can reach 1 million Daltons
Chondroitin sulphate	cartilage, bone, heart valves	most abundant GAG: principally associated with protein to form proteoglycans. Sulphation of chondroitin sulphates occurs on the C-2 position of the uronic acid residues and the C-4 and/or C-6 positions of GalNAc residues. the chondroitin sulphate proteoglycans form a family of molecules called lecticans and includes *Aggrecan*, *Versican*, *Brevican*, and *Neurocan*; major component of the ECM
Heparan sulphate	basement membranes, components of cell surfaces	contains higher acetylated glucosamine than heparin and is associated with protein forming heparin sulphate proteoglycans (HSPG); major HSPG forms are the syndecans and GPI-linked glypicans; HSPG binds numerous ligands such as fibroblast growth factors (FGFs), vascular endothelial growth factor (VEGF), and hepatocyte growth factor (HGF); HSPG also binds chylomicron remnants at the surface of hepatocytes; HSPG derived from endothelial cells act as anti-coagulant molecules
Heparin	component of intracellular granules of mast cells, lining the arteries of the lungs, liver and skin	more sulphated than heparin sulphates; clinically useful as an injectable anticoagulant although the precise role *in vivo* is likely defence against invading bacteria and foreign substances
Dermatan sulphate	skin, blood vessels, heart valves, tendons, lung	was originally referred to as chondroitin sulphate B. The sulphation of dermatan sulphates occurs on the C-2 position of the uronic acid residues and the C-4 and/or C-6 positions of GalNAc residues; may

		function in coagulation, wound repair, fibrosis, and infection; excess accumulation in the mitral valve can result in mitral valve prolapse
Keratan sulphate	cornea, bone, cartilage aggregated with chondroitin sulphates	usually associated with protein forming proteoglycans; keratan sulphate proteoglycans including keratin, fibromodulin, *Aggrecan*,

Table 1.2 GAGs characteristics. *Table 1.2 adapted from (Themedicalbiochemistrypage.org, 2018) above represents the various characteristics of GAGs. As detailed above, the most abundant GAGs are chondroitin sulphate proteoglycans, and they form the family of lecticans.*

1.2.5 PNN components- Tenascins

Tenascins are classified as multimeric ECM molecules falling into several categories: -C, R, W, X and Y. Expression of *Tenascin C* and *X* occurs outside the nervous system in many areas such as dense connective tissue and smooth muscle. Contrastingly, *Tenascins R, C* and *W* possess restricted expression with W occurring in bone and *R* and *C* within the nervous system (Kimura *et al.*, 2007).

Tenascins C and *R* have been reported to play significant roles in cell proliferation, migration, differentiation, synaptic plasticity, axonal guidance and myelination (Warren *et al.*, 2018). Tenascin C is an 1,800 kDa protein which is produced from six monomers which are linked covalently with disulphide bonds. The monomers are formed of a tenascin assembly domain, a cysteine rich domain, 14.5 EGF like domains, 8 fibronectin-type III homologous domains and a fibrinogen like domain (Warren *et al.*, 2018). *Tenascin C* expression has been reported to be enhanced during development and within the adult brain (Warren *et al.*, 2018). Within early development of the CNS, it is highly expressed by various types of cells including immature astrocytes and a restricted population of immature neurons (Warren *et al.*, 2018). Tenascin C has also been linked to proliferation of progenitor cells, migration and neurite outgrowth as Well as having a role in learning/neuronal plasticity (Warren *et al.*, 2018). *Tenascin R* (TN-R) is expressed solely within the CNS (Reichardt & Prokop, 2011). This is a 180 kDa protein from which production of a 160 kDa form occurs via proteolytic cleavage (Reichardt & Prokop, 2011). Both isoforms can be expressed during CNS development (Reichardt & Prokop, 2011). The fully active form of *Tenascin R* is produced from two-three monomers which are linked via disulphide bonds (Reichardt & Prokop, 2011). Similar to *Tenascin C*, the monomer is also formed of a tenascin assembly domain, cysteine-rich N terminal

region, 4.5 EGF like domains, 8 fibronectin type III repeats, a carboxyl terminal region and a fibrinogen like domain (Reichardt & Prokop, 2011). *Tenascin R* undergoes post-translation modifications which results in addition of three sulphated oligosaccharides (Reichardt & Prokop, 2011). One of these is a CS oligosaccharide which can mediate Tn-R interaction with Tenascin C and fibronectin to inhibit neurite outgrowth (Reichardt & Prokop, 2011). *Tenascin R* is expressed in a certain subpopulation of neurons and oligodendrocytes specifically the cortical region and laminae (Reichardt & Prokop, 2011). *Tenascin R* possesses dual roles where it plays a significant role in oligodendrocytes differentiation (Reichardt & Prokop, 2011). With regards to PNNs, Tenascin- R immunostaining displayed co localisation with WFA staining in PNNs (Carruli *et al*., 2006). In association with the G3 domain of lecticans, fibronectin III repeats bind in *Tenascin R* trimers (Zimmerman and Dours Zimmerman, 2008). This occurs in a calcium dependent manner. One *Tenascin R* trimer bonds up to 3 lectican molecules. As well as structural differences, tenascins can also vary in the expression patterns where *Tenascin C* can be detected within the developing mouse brain at week 10 whilst *Tenascin R* expression is more predominant in adults (Jakovljevic *et al*., 2021). Within the first few weeks of life, the brain extracellular matrix is composed of *Tenascin C*, as well as *Neurocan* and *Versican*, and this structural composition indicates a more diffuse extracellular matrix organisation which permits the modulation of connectivity within the developing brains (Jakovljevic *et al*.,2021). As time goes on, proteoglycan expressions move towards smaller molecules such as *Aggrecan Brevican* and *Tenascin R* with downregulation of *Tenascin C* which is able to ensure a more condensed extracellular matrix and perineuronal net therefore restricting and stabilizing established synaptic connections (Jakovljevic *et al*., 2021). Importantly, this *Tenascin R*-lectican interaction aids in strengthening PNNs.

Furthermore, it has been shown that *Tenascin R* and phosph*acan* (RPTPζ) cooperate to promote building of PNNs. *Tenascin R* associates with the (RPTPζ) ectodomain and provides a structural basis for these interactions (Sinha *et al*., 2023). Phosph*acan* has also been shown to produce a similar complex with *Tenascin C* promoting neural plasticity. Further studies have indicated that mutating residues at the RPTPζ- *Tenascin R* interface hinders the formation of PNNs in dissociated neuronal cultures (Sinha *et al*., 2023). Of utmost importance, studies utilising Tn-R knockout mice displayed abnormal PNN staining. Irregular WFA staining distribution occurred around the perikarya. Finally, decreased levels of punctuate staining occurred in dendritic shafts (Iber *et al*.,1999)

1.3 The development and functions of the PNN

PNNs have numerous physical and functional roles. By wrapping the whole cell body of the neuron, PNNs hinder the formation of new neuronal contacts and synapses thus restricting plasticity. Production of PNNs occur on various types of neurons including excitatory principal neurons and inhibitory GABAergic neurons (Lee *et al.*, 2017). PNNs play a role in several cellular functions such ionic buffering, restriction of AMPA receptor motility and clustering, neuroprotection, synaptogenesis, and regulation of neural plasticity (Lee *et al.*, 2017). Within certain brain regions, PNN production is only associated with a single class of inhibitory interneurons which express parvalbumin (Miyata and Kitagawa, 2017). Interestingly, PNNs may regulate parvalbumin cell function through capture of secreted proteins at the cell surface (Lee *et al.*, 2017). One example is Otx2, a transcription factor which is produced in the retina and choroid plexus, and its association with the PNN initiates maturation of the underlying parvalbumin cells (Lee *et al.*, 2017). Otx 2 also known as orthodenticle homeobox 2 is required to be captured by PNNs to be internalized by the neurons. Importantly, this is required for Parvalbumin positive neuron maturation within the cortex to regulate plasticity (Beurdeley *et al.*, 2012). Use of Chondroitinase ABC (ChABC) degrades PNNS and decreases Otx2 levels within the neuron (Beurdeley *et al.*, 2012). Another study indicates that PNNs alter PV expression levels and therefore plasticity capacity of the neuron. Animal models with Otx2 gene point mutation leads to delayed maturation of parvalbumin interneurons (Beurdeley *et al.*, 2012).

Various components of PNNs possess specific binding capacities for proteins. Growth factors such as midline and fibroblast growth factor 2 have been shown to bind to CS-E which is enriched within PNNs. Also, Semaphorin 3A, a chemo repulsive molecule binds to PNNs via CS-E. Degradation of PNNs using ChABC results in removal of Sema3a from the neuronal surface (Berretta *et al.*, 2015). This indicates that Sema3a is presented to approaching axons from other neurons by PNNs (Berretta *et al.*, 2015). Essentially, this permits Sema3a to function as a repulsive signalling molecule. In the brain, Neuropeptide Y(NPY) interacts with a family of G protein–coupled receptors that includes the Y1 (Y1R), Y5 (Y5R), and Y2 receptors, the last one considered to function mainly as a presynaptic receptor (Eva *et al.*, 2006). NPY plays both inhibitory and stimulatory effects in learning and memory, depending on the type of memory, brain region and receptor subtype. There is compelling evidence that the NPY-Y1R signal differently modulates learning and memory processes and synaptic transmission (Gøtzsche and Woldbye, 2016). Some studies have shown that activation of TrkB in parvalbumin interneurons is essential for the stimulation of reversal learning in spatial and fear

memory by anti-depressants such as fluoxetine which is known to decrease WFA staining in *post mortem* brains of patients diagnosed with bipolar disorder (Jetsonen *et al.*,2023). It has also been shown that hippocampal parvalbumin interneurons play a significant role in memory development (Miranda *et al.*,2022).

Studies have shown that cavities located within PNNs have synapses which act as memory stores and that they remain stable after events leading to synaptic withdrawal symptoms such as hibernation or anoxia (Ruzicka *et al.*,2022). Recent studies further monitored place memory before and after synaptic withdrawal occurring as a result of acute hibernation-like state (HLS) (Ruzicka *et al.*,2022). Animals with no perineuronal nets due to enzymatic digestion occurring via ChABc or *Aggrecan* knockout were compared with wild type controls (Ruzicka *et al.*, 2022). This showed that HLS induced synapse withdrawal resulted in memory deficit but not to the levels of untreated animals which was not worsened by PNN attenuation (Ruzicka *et al.*, 2022). After HLS, only animals deficient of PNNs displayed memory restoration or relearning (Ruzicka *et al.*,2022). Lack of PNNs altered the restoration of excitatory synapses on PNN-bearing neurons (Ruzicka *et al.*, 2022). Taking into consideration all of the above, there appears to be a role for hippocampal PNNs within learning but not long-term memory storage.

PNNs, by virtue of the negatively charged GAGs, provide an ion buffering capacity around various subpopulations of neurons - mostly for the cations linked to fast spiking interneurons. This buffering capacity also prevents oxidative stress by the retention of Fe^{3+} ions. PNNs have, therefore, been shown to play a role in oxidative stress, particularly that generated by the fast-spiking interneurons. One study involving a triple knockout in mice of the main constituent of PNNs: *Aggrecan*, *Tenascin R* and *Hapln1*. resulted in protection against oxidative stress stimulated by FeCL3 (van 't Spijker and Kwok, 2017). In a similar manner, degradation of PNNs using ChABC results in parvalbumin neurons becoming vulnerable to oxidative stress (van't Spijker and Kwok, 2017). With regards to neurodegenerative disorders, PNNs have been shown to protect neurons from amyloid beta toxicity in comparison with those neurons with no PNNs (Miyata *et al.*, 2007). This demonstrates that importance of PNNs acting as a physical barrier against neurotoxic molecules.

PNNs also act as a barrier for the lateral diffusion of AMPA receptors. AMPA receptors are glutamate-gated ion channels and required for fast excitatory neurotransmission (Pantazopoulos and Berretta, 2016). AMPA receptor mobility on the plasma membrane is essential for regulation of

receptor numbers at the synapse and their availability is decreased via the compartmentalisation of synapses of the synaptic membrane through the action of PNNs (Frischknecht et al., 2009).PNNs decrease the mobility of membrane-bound proteins on the neuronal surface. Use of hyaluronidase to remove PNNs in neuronal cultures leads to increased lateral diffusion of AMPA receptor subunits (Pantazopoulos and Berretta, 2016). Studies involving whole-cell patch clamp recordings indicated that induced diffusion increase permits fast exchange of desensitized receptors under high stimulation (Pantazopoulos and Berretta, 2016). Consequently, this leads to increases in paired-pulse ratio which is classified as short-term synaptic plasticity. The PNNs ability to inhibit synaptic plasticity arises from the limitation to the lateral mobility of membrane bound proteins (Pantazopoulos and Berretta, 2016).

For animals to establish normal anatomical and physiological properties of neurons, patterned neuronal activity within the early postnatal period is significant. Studies involving rodents enriched in total darkness from birth reduced PNN formation as well as Tn-R and *Aggrecan* within the visual cortex (Wang and Fawcett, 2012). This also extended to PNN formation within deep cerebellar nuclei (Wang and Fawcett, 2012). These results indicate association between external stimuli as well and synthesis and PNN maintenance (Wang and Fawcett, 2012). Dark rearing decreases Crtl1, HA synthase 2/3 though Crtl1 expression levels can be restored within days of light exposure (Wang and Fawcett, 2012).

Other studies have shown that PNNs are produced within the neocortical layers 2-6 neurons during postnatal days and stabilize around PD42 within the mouse primary visual cortex. This suggests full production of PNNs occurs by the end of the critical period (Wang and Fawcett, 2012). One key point to note is various key PNN components are upregulated during the developmental period. However, during adulthood, these are downregulated as displayed in rats indicating that increased protein levels are required for PNN formations (Wang and Fawcett, 2012). This is in contrast to the level of proteins required for stabilized PNNs. *Aggrecan* and link protein mRNA are demonstrated in studies to be up-regulated during PNN formation occurring in postnatal development. This once against demonstrates the importance of these components in initiating PNN formation (Wang and Fawcett, 2012).

PNNs also regulate the synapse through parvalbumin. Various neurons surrounded by PNNs are parvalbumin expressing interneurons (Härtig *et al*., 1995; Baig *et al*., 2005; Yamada *et al*.,

2015). Parvalbumin is classified as a calcium binding protein which maintains short term synaptic plasticity. This was confirmed via electrophysiology experiments on a parvalbumin knockout mouse model (Cawellard *et al.*, 2000). Possibly, parvalbumin regulates the short-term plasticity via binding of calcium ions. In the mouse hippocampus, PNN digestion leads to decreased parvalbumin levels inside neurons (Yamada *et al.*,2015). Both parvalbumin mRNA as well as the amount of the protein itself are decreased by ChABC injection into the brain. These results conclude that PNNs assist in regulating the parvalbumin levels in the neuron thus permitting them to regulate plasticity. The PNN can limit neuronal plasticity in adulthood (See figure 1.5). PNNs become stabilised during adulthood (Slaker, Blacktop and Sorg, 2016) and experimental degradation of PNNs using the bacterial enzyme Chondroitinase ABC can result in a return to juvenile states of plasticity (Slaker, Blacktop and Sorg, 2016).
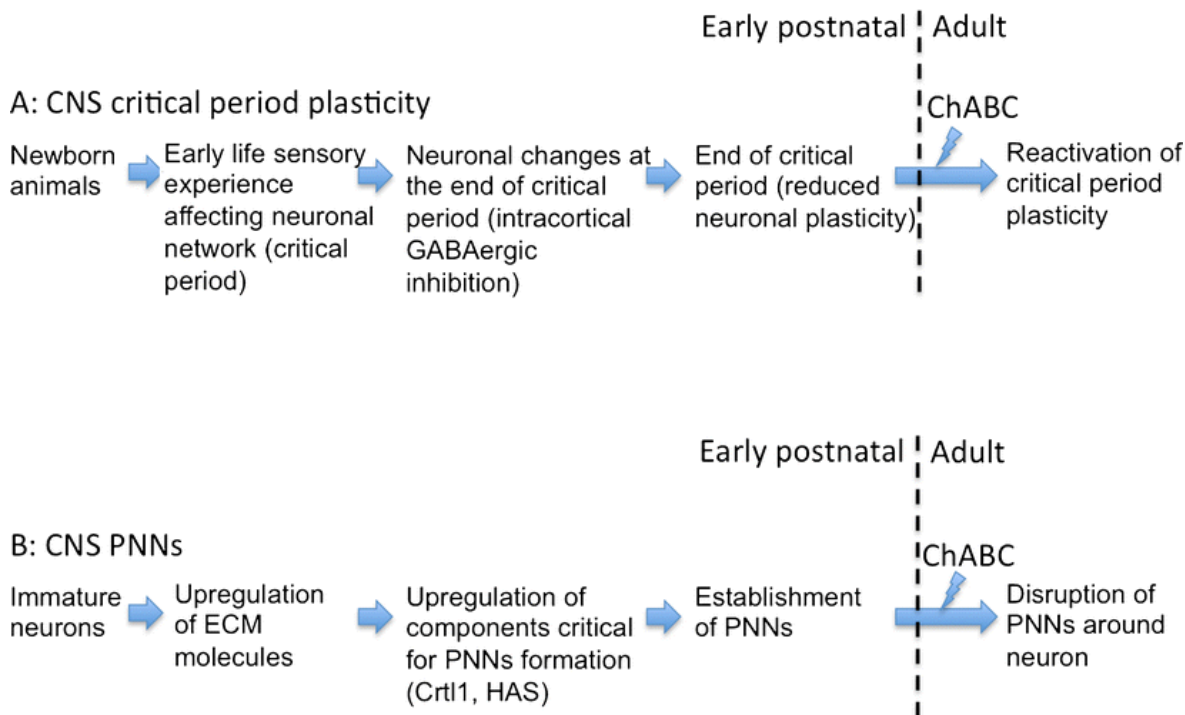
Figure 1.5 Critical period of plasticity. *Figure 1.5 above adapted from (Wang and Fawcett, 2012) shows the mechanisms involved in critical period plasticity. A: This shows the progression from new-born animals all the way through to the early post-natal period. By use of ChABC, a bacterial enzyme involved in degrading PNNs, this reactivates the critical period of plasticity, B: This shows the immature neurons within central nervous system PNNs develop and upregulation of various*

extracellular matrix components. Through use of ChABC, this disrupts PNNs wrapped around neurons (Wang and Fawcett, 2012).

1.3.1 PNN detection by a plant molecule, wisteria floribunda agglutinin, and association of this staining with a specific neuronal cell type

The analysis of PNNs has been substantially assisted by the availability and use of WFA (Wisteria floribunda agglutinin), a plant lectin that specifically binds to PNNs (Slaker, Harkness and Sorg, 2016). WFA staining is accepted as an indirect measure of PNN maturity: brighter WFA staining represents a more mature PNN, whereas dimmer staining indicates an immature PNN (Slaker, Harkness and Sorg, 2016). WFA staining has identified that PNN formation often occurs around parvalbumin-containing (PV) inhibitory interneurons (Pantazopoulos and Berretta, 2016). At the molecular level, WFA lectin is thought to bind to an unidentified sulphation motif present in the CS-GAG chains of most PNNs. Transgenic mice overexpressing juvenile type CS sulphation pattern had reduced levels of Otx2 in PV interneurons (Sorg *et al.*, 2016). Though WFA is a broad marker of PNNs, other markers also exist. 3B3 is an antibody raised against native chondroitin sulphate motifs involvingchondroitin-6-sulphate. 3B3 immunolabelled PNNs are more numerous and display broader distribution within the human amygdala (Slaker, Blacktop and Sorg, 2016).

Importantly, CS chains and sulphation patterns alter function and interaction with growth factors and cytokines (Eskici *et al.*, 2018). CS 4 and CS6 are common sulphation patterns within the brain (Sorg *et al.*, 2016). In essence, CS 6 in conjunction with *Aggrecan* plays a significant role in regulation of astrocyte maturation (Sorg *et al.*, 2016). As well as the others mentioned above, 3B3 labels a broad distribution of PNNs. 3B3 (antibody raised against *Aggrecan*) functions by detecting a non-reducing terminal end saturated disaccharide consisting of glucuronic N acetyl galactosamine 6 sulphate (Sorg *et al.*, 2016). Other antibodies involved in labelling PNNs include CS56 which recognises CS-C and CS-D chains. CS-C is classified as the major form during early development and decreased with the closure of critical periods. Decreased levels of CS56 labelled and 3B3 PNNs have also been reported in bipolar disorder and schizophrenia (Sorg *et al.*, 2016). Other studies have depicted that WFA may not detect CS 6 sulphation patterns which are recognised by 3B3 and CS56. Similarly, 3B3 and CS56 do not express CSPGs labelled by WFA (Sorg *et al.*, 2016). CSPGs receptors have been demonstrated to be crucial to pyramidal neurons and GABAergic interneurons. Through

interactions, PNNs may alter the functions of these (Siebert *et al.*, 2014). It has been proposed that CSPG receptors function as part of multicomponent molecular systems as a signalling platform various intracellular pathways. These pathways are key in gating neuronal maturation and structural stability this altering brain function and plasticity (Siebert *et al.*, 2014),

PNN formation results in upregulation of various CSPG core proteins and changes in the GAG sulphation patterns including removal of CS-6 and increased levels of CS-4 Cartilage link proteins has also been shown to trigger PNN formation (Siebert *et al.*, 2014). Interestingly, studies using mice with Crtl1 deletion indicate that lack of this protein leads to aberrant PNN formation (Siebert *et al.*, 2014),

1.4 Defects in the PNN are associated with disease.

ECM abnormalities are associated with the pathophysiology of psychiatric disorders such as schizophrenia, bipolar disorder, autism among others. PNN disruption has been reported in schizophrenia, with reduced levels of CSPG labelled PNNs within the amygdala, entorhinal cortex and prefrontal cortex (Pantazopoulos and Berretta, 2016). Decreased levels of PNNs also occur associated with abnormal CSPG expression within glial cells. In addition, evidence from human genetic and *post mortem* studies indicates that CSPGs, reelin, *SEMA3A*, and integrins are involved in PNN interactions. Others such as matrix metalloproteinases have also been implicated (Pantazopoulos and Berretta, 2016). MMPs are released by neurons in response to activity. These have been shown to be involved in plasticity and memory. Some studies have shown that induction of ocular dominance plasticity in mice via monocular deprivation both during and after the critical period results in PNN degradation via release of MMP-9 (Murase *et al.*, 2022). Further studies have indicated that *Brevican* is degrade by two other metalloproteinases such as ADAMST1 and ADAMST4 during excitotoxicity (Nakamura *et al.*, 2000). Parvalbumin positive interneurons also express metalloproteinase mRNAs and it has been shown that MMP3 and MMP13 are upregulated after seizures in these types of neurons (Beroun *et al.*, 2019).

With regards to bipolar disorder, reduced *reelin* expression has been noted within the prefrontal cortex, hippocampus, and cerebellum as well as within bipolar patients' blood samples. *Post mortem* studies of bipolar patients indicate reduced PNN levels across various nuclei within the amygdala

(Carulli *et al.*, 2016). Other neuropsychiatric disorders such as autism display ECM abnormalities. Where genome wide association studies have occurred, this indicate ECM molecules mentioned above as well as hyaluronan surface receptor, *CD44* and *Otx-2* are key regulators. However, most evidence focuses on Reelin. Altered reelin expression has been demonstrated in patients with autism (Carulli *et al.*,2016).

With regards to schizophrenia, disruption of glutamatergic/GABAergic function suggests that PNNs are involved heavily in the excitatory/inhibitory balance because they surround PV-containing fast spiking GABAergic interneurons within the pre-frontal cortex (Sorg *et al.*, 2016). These interneurons play a major role in production of gamma oscillations (30–120 Hz). Removal of these results in alterations of these oscillations. Gamma oscillations are instrumental in their synchronous network activity, which monitors information processing and cognitive flexibility (Sorg *et al.*, 2016). This is in agreement with other studies that indicate that PV neurons have abnormal production within schizophrenia and autism (Wohr *et al.*, 2015). In some psychiatric conditions such as schizophrenia, autism and bipolar disorder have been associated with abnormalities in inhibitory interneurons. Decreases in the number and staining intensity of pnns in the amygdala, thalamic reticular nucleus, entorhinal cortex and prefrontal cortex has been noted within post-mortem brain tissue from patients with schizophrenia (Bitanihirwe *et al.*, 2014). A further study which examined thalamic reticular nucleus of post-mortem schizophrenia patients reported a loss of PV+ interneurons and PNNs (Steullet *et al.*, 2017). Similarly, in another study of amygdala and entorhinal cortex of patients with schizophrenia, the number of parvalbumin neurons was normal but the levels of PNN decreased (Enwright *et al.*, 2016).

PNNs have been implicated in animal models of a number of other neurological disorders. Epilepsy results in long term increases in the excitability of various affected brain regions leading to an upregulation of 6-sulphated chondroitin glycan's within perineuronal nets (Chaunsali *et al.*, 2021). Biochemical and immunohistochemical studies of both animal models and human temporal lobe epilepsy tissue samples reveal abnormal expression of individual extracellular matrix molecules such as chondroitin sulphate proteoglycans, heparin sulphate proteoglycans, hyaluronan, *Aggrecan* and *Brevican* (Chaunsali *et al.*, 2021). There is also shown to be disruption of perineuronal net integrity and often decreased perineuronal net density and decreased parvalbumin neurons (Chaunsali *et al.*,2021). In a recent study involving a mouse model of human glioma-associated epilepsy, cortical PNNs were altered by glioma-released MMPs which enhanced the membrane capacitance of the PV neurons resulting in decreased spike firing activity leading to decreased overall inhibitory drive

(Tewari *et al.*, 2022). This suggests a key role of PNNs in initiating the fast-spiking properties of PV neurons.

Furthermore, digestion of PNNs via MMPs render the brain regions more susceptible for further seizures. In the cases of amyotrophic lateral sclerosis, perineuronal nets display damage around affected motor neurons but can be preserved via protected stem cell therapy (Sorg *et al.*,2016). Degradation of perineuronal nets by MMPs within disease results in PV interneuron dysfunction which can alter the balance of excitation and inhibition within affected brain regions (Soles *et al.*, 2023) Decreased PNNs lead to reduced growth factor levels, loss of neuroprotection against oxidative stress, modified ion concentrations within neuronal microenvironment and altered expression of neurotransmitter receptors and ion channels resulting in altered neuroplasticity (Soles *et al.*,2023). MMP-9 has also been implicated in perineuronal net maintenance and it has been shown that increased MMP-9 levels could contribute to perineuronal net degradation as well as altered levels of β- amyloid within Alzheimer's disease (Pinter & Alpar, 2022)

PNN reduction can also occur via microglia involved in phagocytosis. This is mediated by microglia phagocytosis which is involved in spinal cord injury promoting a pain phenotype (Tansley *et al.*, 2022). PNNs within the spinal cord are located around the large somas of spinoparabrachial projecting neurons within Lamina 1 of the dorsal horn (Tansley *et al.*, 2022). Reduced WFA staining was identified after three days of spinal nerve injury around these neurons. The WFA signal was located within microglial lysosomes suggesting that microglia were phagocytosing PNNs (Tansley *et al.*, 2022). Interestingly, removal of microglia hindered PNN degradation and pain phenotypes demonstrating that microglia-mediated degradations of PNNs on spinoparabrachial projection neurons stimulates pain behaviour (Tansley *et al.*, 2022)

Neurodegenerative diseases are classified as a group of chronic, progressive disorders characterized by gradual loss of neurons. Alzheimer's disease is the most common type affecting millions worldwide and is a chronic degenerative disorder that destroys memory and other important functions. Alzheimer's is characterized by beta aggregated fibrils of neurotoxic elements such as amyloid beta and Tau-protein. PNNs are known to have a neuroprotective role and thus they have the ability to restrict the processes of distribution and internalization of Tau protein thus protecting the neuron that they surround (Sorg *et al.*, 2016). Neurons that are enwrapped by PNNs are not affected by increased levels of neurofibrillary tangles despite the severity of the damaged region.

CSPGs usually provide the neuroprotective effect in Alzheimer's disease. Various studies have shown that in Alzheimer's diseased brains, there is an alteration in glycan sulphation patterns (Logsdon *et al*., 2021). Sulphation has been shown to key factor in developing a stable perineuronal net. Also, there is the presence of CS-E chains in perineuronal nets. However, recent studies have shown that neurons in culture which express CSPG rich PNNs withstand amyloid beta treatment whilst neurons without PNNs succumb to the treatment (Sierbert *et al*., 2014). Also, CSPGs protect neurons in culture from delayed cell death via glutamate stimulation of AMPA-R and NMDA-R (Sierbert *et al*., 2014). In addition, *Brevican* levels are upregulated in PNNs of Alzheimer's patients as well as HAPLN1 (Thon *et al*., 2000). Moreover, PNNs protect the neurons from oxidative stress in both normal aged brains and Alzheimer's disease. Ions produced from oxidative stress are repelled by negative charges of HA and CS (Sorg *et al*., 2016). PNNs protect from oxidative stress and amyloid beta accumulation but also removal of PNNS by ChABC stimulates plasticity to compensate for functional loss of neurons thus increasing memory as demonstrated in previous studies (Fawcett *et al*., 2022). PNNs have also been implicated in other neurodegenerative diseases such as multiple sclerosis and Parkinson's disease (Sorg *et al*., 2016).

1.5 The aims of this screen and the technologies to be used (Gene traps and CRISPR)

Taking into consideration all of the above, it is clear that the PNN is a highly specialised structure with roles in the healthy and diseased brain. Its coordinated composition, profile of developmental change, and restriction to certain neurons, suggests a tightly controlled regulation that is poorly understood. Therefore, it is important to investigate this regulation and what therapeutic insights or potential it might offer. This thesis describes the use of a technique previously applied in the laboratory in which laboratory cells are randomly mutated to form a 'gene trap' library which can be functionally screened for mutants with particular phenotypes of interest. As I have a molecular tool, WFA, for assessing PNN expression I chose to interrogate a gene trap library for PNN regulation mutants. By initiating a live screen, plating out the gene trap library and searching for instances of reduced WFA staining, it was reasoned that it would help us identify regulator genes. Furthermore, a gene trap only results in a heterozygous gene knockout meaning only 50 percent of the gene is lacking. The benefits and disadvantages of this feature will be discussed later, but I planned to

validate candidate genes with CRISPR-mediated homozygous knockout analysis. Below, both gene trapping and CRISPR are explained in more detail.

1.5.1   Gene trapping

Gene trapping is used for cellular mutagenesis and after transfection or electroporation of the gene trap vector into a cell, it stably integrates within nuclear genomic DNA (Gow *et al.*, 2013). Crucially, if this integration occurs within gene introns, then the splice acceptor/donor sequences divert and hinder the normal exon-exon splicing (Gow *et al.*, 2013). This results in three outcomes (Figure 1.6). Firstly, mRNA from the trapped allele of the endogenous gene is truncated or becomes unstable thus leading to a loss-of-function mutation. Secondly, the endogenous gene and gene trap sequence splicing events result in the production of translated fusion mRNAs producing neomycin/G418 resistance in productively mutated cells. Finally, the fusion mRNAs can be processed in a 'rapid amplification of cDNA ends' (RACE) PCR protocol to permit identification of the trapped gene (Gow *et al.*, 2013). By using this process to induce mutations within a cell line, functional screening can then identify genes of interest. It is important to note that the gene trap screen results in only a heterozygous knockout and some genes that have no introns or very small introns will be unable to be targeted. Previous studies using gene trap mutants derived from the *SH-SY5Y* neuroblastoma cell line identified various genes linked to functional cellular response to the mood stabiliser, lithium (Gow *et al.*,2013) (Table 1.3).These studies linked lithium response to genes associated directly or indirectly with the construction or function of perineuronal nets such as *Versican*, Tenascin C, *Sema3a* and CCL2. Interestingly, *Versican* is closely related to *Neurocan*, one of the higher genetic risk factors for bipolar disorder, the psychiatric disorder for which lithium is prescribed. The importance of the genes identified in the lithium gene trap screen has been highlighted in many other studies. *Versican*, for example, has been shown to be an extracellular matrix regulator of inflammation within the brain whereas *Neurocan* has been shown to be a risk factor for bipolar disorder and is required for early development of the brain (Wight *et al.*, 2020, Zhou *et al.*, 2001) With regards to *Tenascin C* and *Tenascin R*, these has been respectively shown as risk factors for depression, schizophrenia whilst also playing a key role in tissue injury and repair as well as neurogenesis and neuronal plasticity (Xu *et al.*, 2013). *CCL2* has been shown to play a role in depression and is released as an inflammatory marker in response to neurodegenerative diseases (Leighton *et al.*, 2017). Finally, SEMA3A which forms neuronal contacts with the surface of the

perineuronal net has been shown as a risk factor for various psychiatric diseases and is also involved in axonal guidance and neuronal plasticity (Carulli *et al.*, 2021). These circumstantial, but compelling, results paint a picture whereby lithium may reverse disease-associated abnormalities in PNN function – and further support the rationale for a direct genetic investigation of PNN regulation.

PNN component identified in lithium screen	Links with neuropsychiatric diseases
Versican	Extracellular matrix regulator of inflammation in brain
Neurocan	GWAS risk factor for bipolar disorder and required for early development in the brain
Tenascin C	Risk factor for unipolar depression as detailed in GWAS catalogue, key role in tissue injury and repair
Tenascin R	GWAS catalogue shows ADHD and schizophrenia risk factor and depression, regulates neurogenesis and plays role in plasticity
CCL2	Plays role in depression and released in response to neurodegenerative diseases
Sema3a	GWAS shows risk factor for ADHD, unipolar depression, bipolar disorder, autism spectrum disorder, schizophrenia, involved in axonal guidance and neuronal plasticity

Table 1.3 *Role of perineuronal net components identified in initial lithium gene trap screen and association with psychiatric* well*ness. Table 1.3 shows the genes that were identified in the initial lithium gene trap screen which identified various perineuronal components as failing to respond to lithium treatment. Information regarding the various components mentioned above was collated from GWAS catalogue (https://www.ebi.ac.uk/gwas/). Further information presented in the table is also referenced in text above detailing the roles of these perineuronal net components in psychiatric disease.*

(0) **AgeI**

Ad SA

BspDI - ClaI (134)

NsiI (485)

pUC replication origin

pIRES-Neo3 synthetic IVS

eukaryotic IRES

Venus

(4865) **AhdI**

5000

Amp

(4496) **PvuI**

bgh poly a

pGTIV3 gene trap plasmid
5743 bp

BsrGI (1392)
Eco53kI (1432)
SacI (1434)
BclI * (1438)

BbsI (1640)
AscI (1717)
BstAPI (1742)
EcoNI (1768)
AvrII (1858)
StuI * (1913)

ARE

b-globin SD

b-act pro

4000

(3946) **AatII**
(3944) **ZraI**

2000

Neo

(3483) **KflI**
(3454) **BamHI**

PaeR7I - PspXI - XhoI (2180)

(3320) **Bsu36I**
(3299) **NruI**

3000

(3140 .. 3167)   3'RACE 1 (RACE2)

(3126) **BstBI**

BsaAI (2742)

(3072 .. 3099)   SD5-P3 (RACE)

Figure 1.6 *The gene trap construct used in the original lithium gene trap screen known as PGTIV3. This gene trap vector was initially created and utilised with studies involved embryonic stem cells. As mentioned above, gene trapping involves the insertion of a gene trap vector into an intron of a gene resulting in three outcomes which are normal splice acceptor/splice donor sequences divert the normal exon to exon splicing and this results in formation of a truncated protein. Secondly, this results in production of fusion mRNAs between the neomycin resistance gene and trapped exon and finally these can be rapidly amplified via cDNA ends. However, it is important to note that this gene trap vector has several properties which results in heterozygous knockouts. Firstly, there is synthetic intron present which contains a cis-acting ARE element full of adenine and uridine residues resulting in mRNA degradation. If the intron integrates itself outside the genome, neomycin will not be expressed meaning the cells will die. There is an adenovirus splice acceptor site present which is commonly used in molecular studies and is known to be a good splice acceptor site. There is also the presence of an internal ribosomal entry site which drives the production of yellow venus protein and rather than having a 1 in 3 chance of matching reading frame and being expressed, this*

increases the likelihood of the venus yellow fluorescent protein being expressed. A poly A site is also present to stop production and a beta actin promoter is also present to drive the expression of the neomycin resistance gene. Cells which have the presence of the neomycin resistance gene means that the gene trap has integrated itself into the genome.

1.5.2   CRISPR

Clustered regularly interspaced repeats are classified as a modified form of bacterial immune system (Guell, Yang and Church, 2014). In recent times, this system has been adapted and utilised to target specific regions of DNA and manipulate the DNA (Guell, Yang and Church, 2014). CRISPR provides the ability to knock down genes which have been identified using gene trapping (Guell, Yang and Church, 2014). CRISPR arrays contain a DNA sequence classified as the PAM region which shares sequence homology with invading DNA. This provides a genetic memory of past invasions, and it utilised on secondary infections to target Cas nucleases to the invading pathogen genomes resulting in DNA degradation (Hsu *et al.,* 2014). CRISPR involves various components such as an endonuclease, guide RNA and a PAM motif. The guide RNA permits Cas9 endonuclease to cut a precis genomic locus of many possible loci. However, without binding to the guide RNA, Cas9 cannot cut. This Cas9 endonuclease binding to the target genome locus occurs via the target sequence within the guide RNA and the PAM (3bp). For the double stranded DNA to be cut via Cas9, the PAM sequence must be present immediately downstream (3') of the site targeted by the guide RNA. The guide RNA binds to the target sequence, cas9 binds to the guide RNA and cuts both DNA strands and the cut is repaired inducing a mutation which shuts off the targeted gene.

1.5 Hypothesis/Aims

<u>Aim of project</u>

- To identify *SH-SY5Y* mutant genes via gene trapping that result in reduced PNN staining
- To produce CRISPR KO cell lines to validate candidate genes identified.
- To confirm reduced expression of CRISPR-mutated candidate genes
- To analyse the effect of CRISPR mutated candidate genes on WFA staining as well as other key PNN components

<u>Hypothesis</u>

Gene trap mutants producing reduced PNN staining will be key regulators in the function and maturation of the perineuronal net and are potentially important targets in neuropsychiatric disease therapy.

Chapter 2

Materials and Methods

2. Materials

Equipment	Supplier	Catalogue/Model Number
Nikon TMS Inverted Phase Contrast Microscope	Marshal Scientific	NI-TMS
MSC-Advantage™ Class II Biological Safety Cabinet	Thermo Fisher Scientific	51025411
Galaxy S CO_2 Incubator	Samson Scientific	Model 170-200
PipetBoy	Thermo Fisher Scientific	-
Starstedt Serological Pipette	Starstedt	86.1254.001
Corning cell culture flasks	Sigma Aldrich, Dorset UK	CLS430639-200EA
Corning 50mL Centrifuge tubes	Sigma Aldrich, Dorset UK	CLS4558
Nalgene™ General Long-Term Storage Cryogenic Tubes	Thermo Scientific™	5005-0015
MSE Micro Centaur	DJB Labcare	-
Heraeus™ Labofuge™ 400 Centrifuge	Thermo Fisher Scientific	75008164
Sigma® cell culture plate	Sigma Aldrich	SIAL0516
Secuflow Fume Cupboard	Waldner, Oxford UK	-
Microscopic Slides	Sailing Boat, China	7101
Stuart™ Scientific Roller Mixer	Sigma Aldrich, Dorset UK	Z316474
Nikon Eclipse e600 Microscope	SpachOptics	-
Nunc™ Cell Scrapers	Thermo Scientific™	179693
4-20% gradient Mini-PROTEAN TGX Precast Gels	Bio-Rad Laboratories	456-1093
Nitrocellulose/Filter Paper Sandwiches 0.45µm	Bio-Rad Laboratories	1620214
Mini-PROTEAN Tetra Cell	Bio-Rad Laboratories	-

Mini Trans-Blot Electrophoretic Transfer Cell	Bio-Rad Laboratories	-
CL-XPosure™ Film	Thermo Scientific™	34090
Hypercassette, neutral (standard), 18 × 24 cm	GE Life Sciences	RPN11642
Automatic X-Ray Film Processor	-	-

Cells & Solutions	Supplier	Catalogue/Model Number
SH-SY5Y (ATCC® CRL-2266™)	ATCC	-
pSpCas9(BB)-2A-Puro (PX459) V2.0 CRISPR Plasmid	Addgene	62988
Bpil (BbsI) restriction enzyme	Thermo Fisher Scientific	ER1011
T4 DNA Ligase	Thermo Fisher Scientific	EL0011
Isolate Plasmid II Minikit	Bio-Rad Laboratories, Perth Scotland	-
Anza™ 27 PvuI restriction enzyme	Invitrogen™	IVGN0274
UltraPure™ Agarose	Invitrogen™	16500500
Pierce™ 10X TBE Buffer	Thermo Fisher Scientific	28355
SYBR Safe DNA Gel Stain	Invitrogen™	S33102
HyperLadder™ 1Kb	Bioline, London UK	BIO-33053
DMEM/F-12, GlutaMAX™ supplement	Gibco™	10565018
Fetal Bovine Serum	Biosera	FB-1090/500
Penicillin Streptomycin	Sigma Aldrich, Dorset UK	P4458-100ML
TrypLE Express 1x	Gibco™	12604-013
Dimethyl Sulfoxide	Sigma Aldrich, Dorset UK	D4540

Lipofectamine 2000 Reagent	Invitrogen™	11668019
Opti-MEM 1X reduced serum media	Gibco™	31985070
Puromycin (10mg/mL)	Sigma Aldrich, Dorset UK	P9620
Paraformaldehyde, 97%	Alfa Aesar	A11313
Methanol	Fisher Scientific	-
Phosphate Buffered Saline (Dulbecco A)	Oxoid, Basingstoke UK	BR0014G
Tlen® 20	Sigma Aldrich, Dorset UK	93773
HI Horse-Serum	Gibco™	26050-088
Sample Buffer, Laemmli 2X Concentrate	Sigma Aldrich, Dorset UK	S3401-1VL
2-Mercaptoethanol	Sigma Aldrich, Dorset UK	M6250
Prestained Molecular light Marker (26,600-180,000 Da)	Sigma Aldrich, Dorset UK	SDS7B2
Cell lytic solution	Sigma Aldrich, Dorset UK	C2978
Protease Inhibitor cocktails	Sigma Aldrich, Dorset UK	P8340-205

Table 2.1 List of materials used.

Name of solution	Constituent parts
Freezing medium	90% FBS 10% Dimethyl sulfoxide (DMSO)
Transfer buffer	78.6% ddH$_2$O 19.7% methanol 1.4% glycine 0.3% TRIS base
1% agarose gel	99% Tris-borate-EDTA 0.99% agarose 0.01% Cybrsafe
Laemelli lysis buffer	20% glycerol 4% SDS

	0.004% bromophenol blue 0.125M TRIS 400mM DTT
Phosphate-buffered saline (PBS)	PBS tablets (OXOID cat. BR0014G). One tablet dissolved in 100mLs H_2O.
5 x CSK buffer	95% CSK buffer (PIPES/KOH (1 M, pH 6.8), NaCl (5 M), Sucrose, EGTA (250 mM) MgCl$_2$ (1 M), DTT (1 M) Protease inhibitor cocktail (e.g., Roche 05056489001) 5% complete mini cocktail tablets (Roche, cat. 11836153001)

Paraformaldehyde in CSK buffer	80% CSK buffer
	
	    (663% ddH$_2$O
	
	    30% 1M sucrose
	
	    2% 5M NaCl
	
	    2% 0.5M PIPES)
	
	25% paraformaldehyde (1.8g (3.6%) paraformaldehyde dissolved in 35 mL water (made alkaline with NaOH) at 65°CMade neutral, made up to 40 mL with water then 10 mLs of 5xCSK buffer added. (CSK recipe). Cooled on ice or frozen and used within 3 days.

PBS/ TIEN	99.9% PBS 0.1% TIen® 20 Detergent

Table 2.2 List of solutions used.

Antibody/stain	Dilution for IF	Dilution for WB	Supplier	Catalogue number	Supplier headquarters
Anti-α-Tubulin monoclonal mouse IgG	1:1000	n/a	Oncogene Research Produce	CP06-100UG	La Jolla, United States
Rabbit Anti-*DCC* primary antibody	1:500	1:1333	Abcam	ab118918	Cambridge, United Kingdom
Rabbit polyclonal anti-*GALNTL6* antibody	1:2000	1:500	Abcam	Ab122149	Cambridge, United Kingdom
Recombinant Monoclonal anti-*FAF1* antibody (Rabbit)	1:500	1:2000	Abcam	Ab183045	Cambridge, United Kingdom
Biotinylated Wisteria Floribunda Lectin (WFA, WFL)	1:2000	1:3333	Vector Laboratories Inc.	B-1355	Burlingame, United States
Fluorescein labelled Wisteria Floribunda Lectin (WFA, WFL)	1:1000	n/a	Vector Laboratories Inc.	FL-1351	Burlingame, United States
Goat anti-Mouse IgG (H+L) Cross-Adsorbed Secondary Antibody, Alexa Fluor 594	1:2000	n/a	Invitrogen by ThermoFisher Scientific	A-11005	Waltham, United States
Donkey anti-Rabbit IgG (H+L) Highly Cross-Adsorbed Secondary Antibody, Alexa Fluor 488	1:2000	n/a	Invitrogen by ThermoFisher Scientific	A-21206	Waltham, United States
Streptavidin, Alexa Fluor™ 594 Conjugate	1:2000	n/a	Invitrogen by ThermoFisher Scientific	S32356	Waltham, United States

Goat anti-Mouse IgG (H+L) Cross-Adsorbed Secondary Antibody, Alexa Fluor 488	1:2000	n/a	Invitrogen by ThermoFisher Scientific	A-11001	Waltham, United States
β-Actin Loading Control Monoclonal Antibody	n/a	1:2000	Invitrogen by ThermoFisher Scientific	MA5-15739	Waltham, United States
Streptavidin HRPO conjugate	n/a	1:3333	Invitrogen by ThermoFisher Scientific	SA1007	Waltham, United States

Table 2.3 List of antibodies used.

2.1 Gene Trap Screen to identify WFA expression mutants.

2.1 Cell culture

SH-SY5Y is a human-derived cell line sub-cloned from an original cell line (SK-N-SH) that was isolated from a bone marrow biopsy taken from a four-year-old female neuroblastoma patient (Kovalevich and Langford, 2016).

Cell culture conditions

SH-SY5Y neuroblastoma cells (passage 21) were obtained originally from European Collection of Authenticated Cell Cultures (ECACC) and subsequently propagated and archived in the Pickard lab. Lines HEK293T, Lan 5 and A549were also Pickard lab stocks. Cells were grown in 1:1 of DMEM and Ham's F12 medium supplemented with 10 % foetal bovine serum (Kovalevich and Langford, 2016) and 1% penicillin/streptomycin. Cells were cultured at 37 *℃* with 95 % air and 5 % carbon dioxide (Kovalevich and Langford, 2016) in a humidified incubator. Once confluent, cells were trypsinised (TrypLExpress), centrifuged at 12,000 rpm for 5 minutes, resuspended in 8.5 ml fresh media and plated at various densities to allow mutant colonies to grow sparsely.

Recovery of frozen cells

Frozen cell lines at -80 *°C* were thawed by the pipetting of warm Dulbecco's Modified Eagle Medium (DMEM)/F-12, glutamax (Thermo-Fisher Scientific, UK) supplemented with 10 % FBS and 1 % Penicillin/Streptomycin over the frozen cells. Cells were then centrifuged at 12,000 rpm for 5 minutes. Cell pellets were resuspended in 10 ml fresh media, pipetted into culture vessel (flask/plate) and allowed to grow for a period until 70% confluent growth (2-5 days).

Freezing down cells

Once relevant colonies had reached confluence, cells were frozen down as a backup and stored for molecular analysis. For freezing down, cells were trypsinised, centrifuged at 1,200 g for 5 minutes. Subsequently, media was removed, and 1 mL freezing mix (stock composed of 90 % FCS and 10 % DMSO) was added and pipetted up and down to resuspend the cells. These cells were stored in 2 mL Cryotubes at -80 *°C* for future use.

Gene trap library creation

A pre-existing gene trap mutant library in SH-SY-5Y cells was available in the Pickard lab. This library had been generated through electroporation of cells with a linearised pGTIV3 gene trap plasmid (fig. 2.1 and (Tsakiridis *et al*., 2009) and subsequent selection for cells ls with productive mutational events using G418/Neomycin.
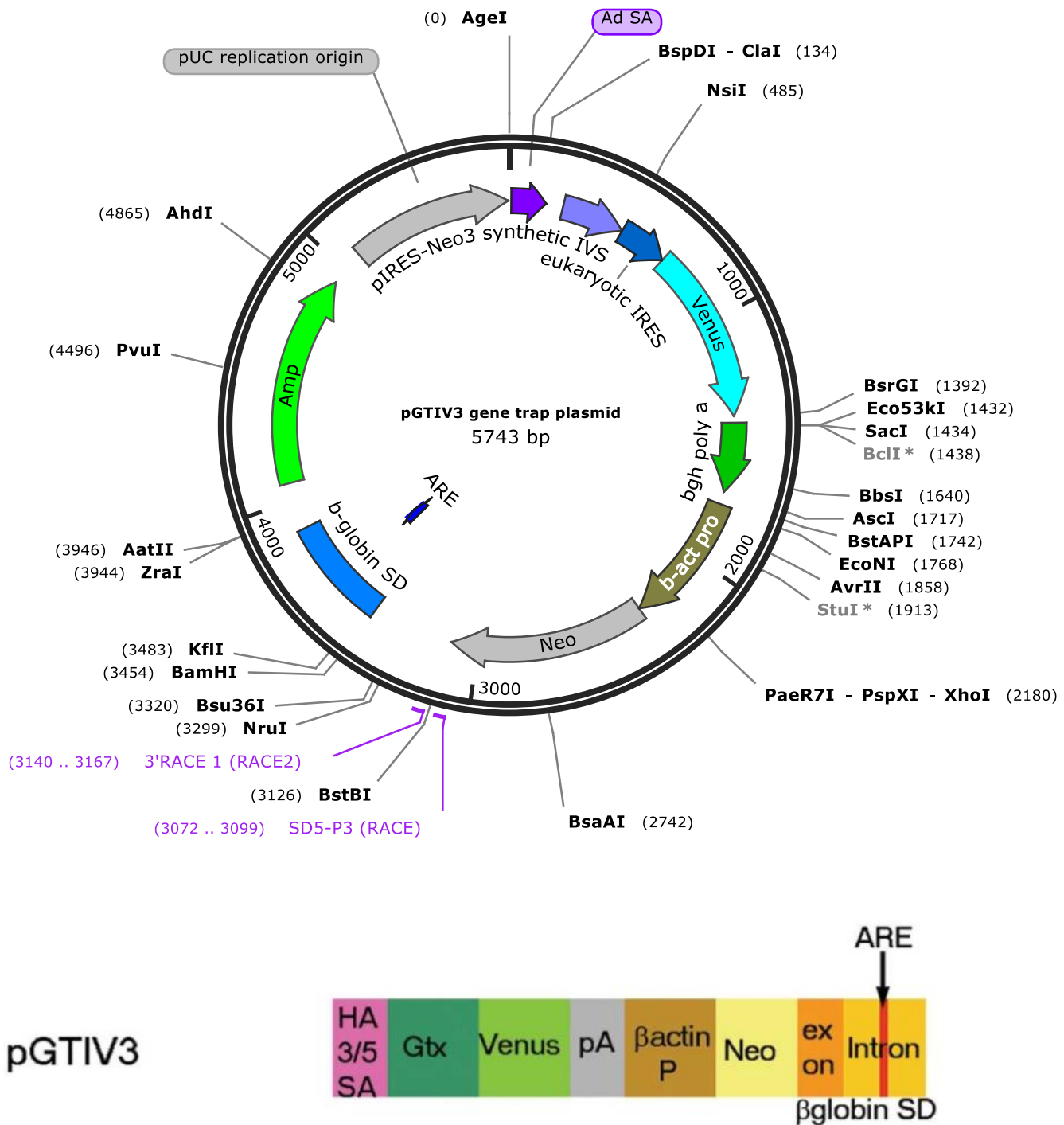
Figure 2.1. The pGTIV3 gene trap plasmid used in the creation of the mutant SH-SY5Y gene trap library (map created in SnapGene). *Schematic representation of the Poly A trap constructs employed. SA, splice acceptor; pA, polyadenylation signal; P, promoter; neo, neomycin phosohotransferase gene; SD, splice donor; ARE, AU-rich element; Gtx, synthetic sequencing*

containing Gtx motifs; HA 3/5. Human adenovirus type 3/5; βhygro, fusion between β-galactosidase and hygromycin resistance genes.

2.1.2 Live cell staining for PNN expression with WFA

The purpose of live cell staining was to determine which mutant colonies were failing to produce a PNN or displaying reduced staining levels. SH-SY5Y mutant cells were grown to confluence and plated out in 6 well plates and these were then allowed to grow to approximately 80 % confluence. The purpose was to ensure that cells were able to be stained with WFA and identification could occur. Once confluent, cells were treated with 2 µl WFA/Biotin and 2 µl Streptavidin conjugated to fluorophore Alexa594 complex in the dark. Cells were then incubated at 37 *°C* for approximately 1 hour in the dark. Following incubation, cells were washed twice with fresh media and immediately analysed under an epifluorescent Inverted Microscope (Nikon Eclipse TE300). Colonies failing to produce any signal or a dim signal with WFA staining were marked on the plate lid with a pen and were then subjected to isolation.

Isolation of mutant colonies

Cells under the pen marks were plucked and isolated to grow in firstly 24 well plates followed by further WFA staining. Once cells had been screened again with WFA/Biotin Streptavidin complex, these were then plucked using sterile tweezers and isolated into 6 well plates and allowed to grow until confluent. 6 well plates were then further analysed for WFA staining and relevant mutant colonies were grown in T75 flasks until fully confluent. Once fully confluent, cells were frozen down in freezing medium as archived stocks, frozen at -80 *°C* as pellets for future molecular analysis and plated on coverslips for immunofluorescence microscopy.

2.1.3 Immunofluorescence Microscopy

Fixation of cells for immunofluorescence

Cells grown on coverslips were fixed using 3.6% w/v paraformaldehyde (PFA) fix (Table 2.2) within a fume hood. 1.8g of powdered PFA (Alfa Aesar, Lancashire, UK) was added to 35ml of distilled water. 1M sodium hydroxide was then added in a dropwise manner until pH 10 was obtained. This solution was warmed to approximately 65°C. Subsequent to PFA dissolving, 1M hydrochloric acid

was added in a dropwise fashion until a neutral pH was obtained. Water was added to take the volume to 40 mL and then 10 mLs of 5x CSK buffer was added to create the final fix.

Living cells on coverslips were washed once with ice-cold PBS and then fixed in PFA on ice for 10 minutes. Three PBS washes were undertaken followed by fixation at -20°C in methanol for 20 minutes followed by another three PBS washes. Following fixation, cells were either subjected to further staining or stored for a maximum of one week submerged in PBS in the cold room (4°C).

Cells were then subjected to PBS + 0.1% Tween20 (PBS-T) (Alfa Aesar, UK) and incubated on ice for 10 minutes to permit cell permeabilization. Cells were blocked for 1 hour at room temperature 1ml PBS-T + 1% donkey serum (DS). Subsequently, primary antibodies (Table 2.3) (1:1000 diluted in PBS-T/1% DS) were added to the cells and left overnight at 4°C. Three x 5-minute washes were carried out using PBS-T. Addition of secondary antibodies in PBS-T then occurred with incubation for 1 hour with plates wrapped in foil to prevent light-induced degradation of the fluorophore. Three x PBS-T washes were then undertaken before mounting. Coverslips, cell side down, were directly mounted onto microscope slides on which 15 µL antifade mountant containing DAPI (Invitrogen, UK) had been spotted. Coverslips were then lightly blotted dry with cartridge paper and sealed with superglue. Once prepared, slides were stored in the refrigerator prior to imaging. All slides were examined under an epifluorescent upright microscope (Nikon Eclipse 600), and relevant images were obtained. Analysis of raw immunofluorescence data was undertaken using the Image J processing and analysis software. Cellular area, mean grey value, and integrated density was measured on Image TM (Schneider *et al*., 2012). An average was taken of background readings and WFA intensity. Immunofluorescence data was expressed as mean ± SEM. Two-tailed student's t-test was used for determining statistical significance and data was then analysed using Microsoft Excel. A p-value of less than 0.05 was considered to be statistically significant.

Mouse Brain staining with WFA

Once mounted on 3-amino-propyl-tri-ethoxy-silane (APES)-coated slides, sections were immediately frozen and stored at -80 °C. Sections when required were left to warm at room temperature for 5 minutes. Acetone fixative was added to a glass tank in an ice bucket and sections in a rack lowered in with fixation time of 15 minutes. Sections were then rinsed 3-4 times in PBS and air dried completely for 30 minutes under airflow. Sections were blocked with donkey serum as previously

described and stained overnight (4 °C) with biotinylated WFA and, subsequently, with streptavidin conjugated to a red fluorophore, and then mounted/sealed under a coverslip with DAPI counterstain and antifade solution. Images were taken with an epifluorescence microscope (as above) and were processed, and colour composites created using ImageJ.

2.1.4 Mutant gene identification

SH-SY5Y cells had been previously inserted with a gene trap vector (pGTIV3) during the gene trap process to induce mutations within the cell line. Those colonies which failed to produce a mature PNN – as described above -were then subjected to RNA isolation to allow the identification of the mutated gene. Total RNA from each mutant colony was purified using the BIOLINE ISOLATE II RNA mini kit (Bioline, London, UK). This kit purifies RNA from various sample types via a simple, column-based method. Steps were undertaken as stated in the manual (https://www.bioline.com/isolate-ii-rna-mini-kit.html). Gel electrophoresis was then undertaken to determine whether successful, high quality RNA Isolation had occurred.

Reverse transcription to produce cDNA

To create cDNA from the RNA, 5μl of RNA was mixed with 1μl of dNTPs, 1 μl of RACE oligo dT and 5.5μl dH2O and incubated at 65°C for 5 minutes. Subsequently this was placed on ice to prevent reformation of the secondary structure. 4 μl of FS Buffer, 2μl of DTT, 0.5μl of RNase inhibitor and 1μl of Superscript RTII (Life Technologies) was added to the linearized RNA solution. This was then placed in the thermocycler and held at 42°C for 50 minutes to create cDNA and then at 70°C for 15 minutes to inactivate the enzyme.

RACE PCR

Following cDNA synthesis, the resulting cDNA was amplified using a Rapid Amplification of cDNA Ends (RACE) protocol in order to amplify fusion transcripts between neomycin resistance and the trapped/mutated gene. In the RACE 1 protocol, 3μl of the cDNA was combined with 0.5 μl of RACE1 Primers, 18.8μl of dH2O, 0.4μl of MyTaq DNA Polymerase and 5μl of 5 x MyTaq PCR Buffer (Bioline). The parameters for the PCR machine were: 94 °C 2 min, 5 cycles of (94 °C 30 sec, 70 °C 30 sec, 72 °C 3 min) followed by 30 cycles of (94 °C 30 sec, 68 °C 30 sec, 72 °C 3 min) followed by the final extension which was 72 °C for 5 minutes.

For the second, nested PCR step (RACE2), 2.5µl of the RACE1 products were added to 122.5µl of dH2O and mixed thoroughly to dilute the RACE1 DNA and primers. To specifically amplify the products of interest, RACE 2 PCR was then undertaken on these diluted products from RACE1. 0.3µl of the diluted RACE1 products were combined with 0.5 µl of RACE2 Primers (18.8µl of dH2O, 0.4µl of MyTaq DNA Polymerase and 5µl of 5 x MyTaq PCR Buffer. RACE 2 conditions were as follows: 94 ºC 2 min, 5 cycles of (94 ºC 30 sec, 70 ºC 30 sec, 72 ºC 3 min) followed by 25 cycles of (94 ºC 30 sec, 68 ºC 30 sec, 72 ºC 3 min) followed by the final extension which was 72 ºC for 5 minutes. To confirm presence of PCR products, 5µl of the RACE2 products were run on a 1% agarose gel at 60 volts for 45 minutes.

Gel Electrophoresis

PCR products sizes were quantified using gel electrophoresis. Samples were prepared using PCR products, 5x blue loading dye (Bioline, London, UK) and ethidium bromide (5µl/50ml) (Sigma-Aldrich, Dorset, UK). Samples were then run on a 1 % agarose gel with Tris/Borate/EDTA (TBE) running buffer. 1 kb ladder (Bioline, London, UK) was used to estimate product size after images were captured on a UV transluminator using Genesnap software (Syngene, UK). Successfully amplified PCR products were subjected to the PCR product purification process using Thermo Scientific GeneJET PCR purification kit (Thermoscientific K0701) prior to cloning and sequencing.

Cloning and Sequencing of RACE PCR products

PCR products were purified and then ligated into the pGEM-T Vector (Promega) (See figure 2.2) using Quick Stick Ligase (Promega). A forward primer (5') and a reverse (5′) primer was used for the amplification of the PCR product. Both primers were dissolved in ultrapure water at a stock concentration of 20 pmol/µl. The template plasmid was diluted in ultrapure water at a stock concentration of 50 ng/µl and made up with water to a total volume of 50 µl: 1 µl plasmid DNA (1 ng/µl final concentration), 1.25 µl of each primer (0.5 pmol/µl final concentration for each primer), 1 µL dNTP (10 mM each). 1 µl of vector (50 ng/µl), 50 ng/µl of the PCR product, and 10 µl of 2X reaction buffer were mixed and filled with water to a total volume of 20 µl. 1 µl of T4 DNA ligase (5 U/µl) was added to the mixture, mixed, and incubated at room temperature for 30 minutes. For bacterial transfection, 10 µl of the mixture was mixed with 100 µl of DH5 alpha *E. coli* competent cells and incubated on ice for 45 minutes. The mixture was then heat-shocked at 42°C for 2 minutes

placed on ice again for 5 minutes and mixed with 1 ml LB medium and incubated in a thermomixer (Eppendorf) for 45 minutes at 37°C at 450G. The bacteria were then spun down for 4 minutes and the pellet was cultured overnight at 37°C on an agarose Petri dish containing 100 µg/mL of Ampicillin. Colonies were selected and cultured overnight in 3 ml LB containing 100 µg/mL of ampicillin. Following overnight incubation, the plasmid was isolated from the cultured bacteria using the Isolate Plasmid II minikit (Bioline) according to the manufacturer's instructions. Following this, restriction digest of the plasmid colonies occurred with the EcoRI to determine which plasmid colonies contained both the vector and insert. 800 ng of plasmid DNA in a total of 10 µl water were sent for sequencing (Source Bioscience) in Eppendorf tubes. The sequencing primers forward and reverse were generated by the company. Sequence results were analysed using NCBI Blast.
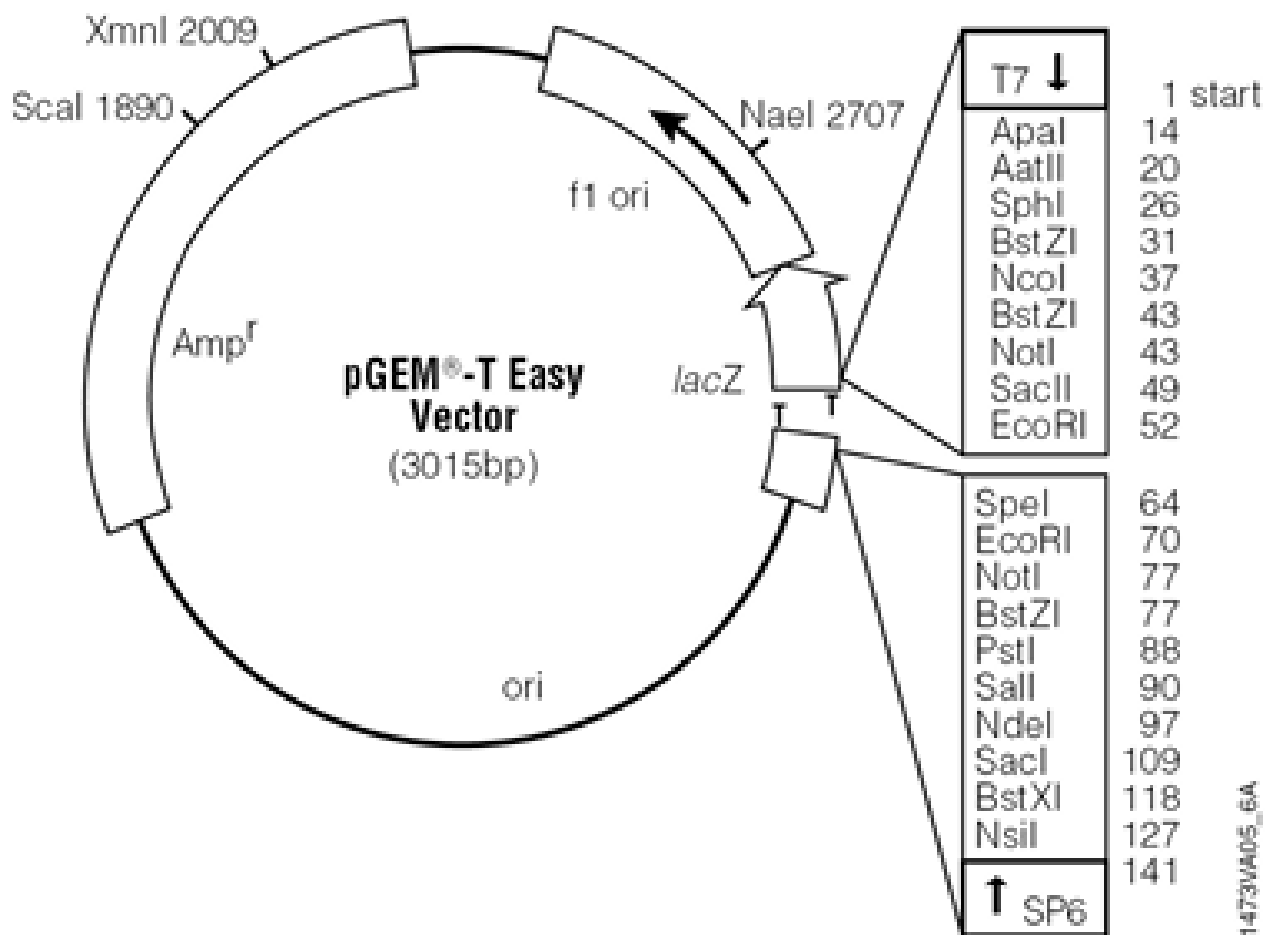
Figure 2.2 pGEM T Easy Vector. *pGEM T Easy Vector above represents the restriction map of the vector used in the PCR cloning process to determine the identification of the mutated gene in colonies with reduced WFA staining.*

2.2 Creation of CRISPR constructs

sgRNA oligonucleotide preparation

10 µL of each complementary pair of oligonucleotides (e.g., *top1/*bot1) were mixed with 5 µL of 5x annealing buffer (50 mM Tris-HCL, pH 8.0, 100 mM NaCl, 5 mM EDTA. Oligonucleotide solutions were then placed in a water bath at 100 °C and allowed to cool down slowly for 2 hours.

Primer sequences

*DCC*_sgrna_top1	[Phos]CACCTTGAAGATGCGCGCTGAACA
*DCC*_sgrna_bot1	[Phos]AAACTGTTCAGCGCGCATCTTCAA
*DCC*_sgrna_top2	[Phos]CACCGATGCCGTCACAATGCGGGG
*DCC*_sgrna_bot2	[Phos]AAACCCCCGCATTGTGACGGCATC
*galntl6*_sgrna_top1	[Phos]CACCTGTTACCATTTGCAATGAAG
*galntl6*_sgrna_bot1	[Phos]AAACCTTCATTGCAAATGGTAACA
*galntl6*_sgrna_top2	[Phos]CACCCTATGAAAGCATTCAGAAAG
*galntl6*_sgrna_bot2	[Phos]AAACCTTTCTGAATGCTTTCATAG
*Faf1*_sgrna_top1	[Phos]CACCGGACCGGGAGATGATCCTGG
*Faf1*_sgrna_bot1	[Phos]AAACCCAGGATCATCTCCCGGTCC
*Faf1*_sgrna_top2	[Phos]CACCCTGCAAACAAGAAACAGAGA
*Faf1*_sgrna_bot2	[Phos]AAACTCTCTGTTTCTTGTTTGCAG

Cloning of the annealed sgRNA sequences into the CRISPR plasmid

Plasmid pU6-(BbsI)_CBh-Cas9-T2A-mCherry (Addgene) was provided as an agar stab. Bacteria were streaked onto agar plates, and colonies picked and incubated in liquid LB media overnight. The following day plasmid DNA was isolated using Isolate Plasmid II minikit (Bioline). Following this, plasmid DNA was digested with BbSI, purified using Thermo Scientific GeneJET PCR purification kit (Thermoscientific K0701), and then the ligation reaction was set up using 1 µL quick stick DNA ligase, 5 µL DNA ligase buffer, 2 µL long oligonucleotide, 2 µL short guide oligonucleotide and 1 µL digested plasmid gRNA and incubated at room temperature for 5 minutes. Digested plasmid was ligated with the annealed oligonucleotides. The annealed oligonucleotides had overhangs which were complementary to BbsI. Three µL of the ligation products were added to 100 µL of chemically competent *E. coli* cells and incubated on ice for 30 minutes and then subsequently heat shocked for 45 seconds at 42 °C. 300 µL of LB broth was then added and the mixed solution was then incubated at 37 °C on a rotating incubator for one hour. The mixture was then spread on agar plates containing

µg/µL Ampicillin. Plasmid colonies were, grown overnight in liquid culture, as before, to generate purified plasmids.

<u>Gel electrophoresis of uncut plasmid and sequencing to confirm successful ligation</u>

Agarose gel electrophoresis was employed to confirm the presence of plentiful plasmid DNA before it was sent for sequencing (Source Bioscience, Nottingham, UK). The plasmid was also run on a 1% agarose gel at 70mV for 40 minutes. Returned sequences (Figure 2.3,2.4,2.7) were then analysed using FinchTV™ software (Geospiza, Inc.) to determine if successful ligation of gRNAs into the plasmid vector had taken place.

2.3 Production of stable cell line mutant KOs

<u>Cell Transfection with CRISPR Plasmids</u>

<u>*FAF1*</u>

For cellular transfection, two cell transfections were undertaken. One transfection utilised an uncut form of the mixed CRISPR plasmids whereas the other utilised a linearized form. Cells were grown until 90 % confluence, washed, and incubated in Opti-MEM™ media. Lipofectamine 2000® DNA Transfection reagent was diluted in Opti-MEM™ media to a dilution ratio of 1:15, producing a mixture of Lipofectamine 2000® (6.25%)/Opti-MEM™ media. Mixed CRISPR plasmid constructs were both added to Opti-MEM™ media to produce a F1A (1.3%)/F2A (1.3%)/Opti-MEM™ media mixture. Both mixtures were incubated at RT for 5 minutes, then combined and incubated for 20 minutes at RT. Following this, Lipofectamine 2000®/F1A/F2A/Opti-MEM™ media solution was then added to SH-SY5Y cells and incubated at 37C for a few hours. Media was then replaced with DMEM/F-12 GlutaMAX™ media (10%) per well.
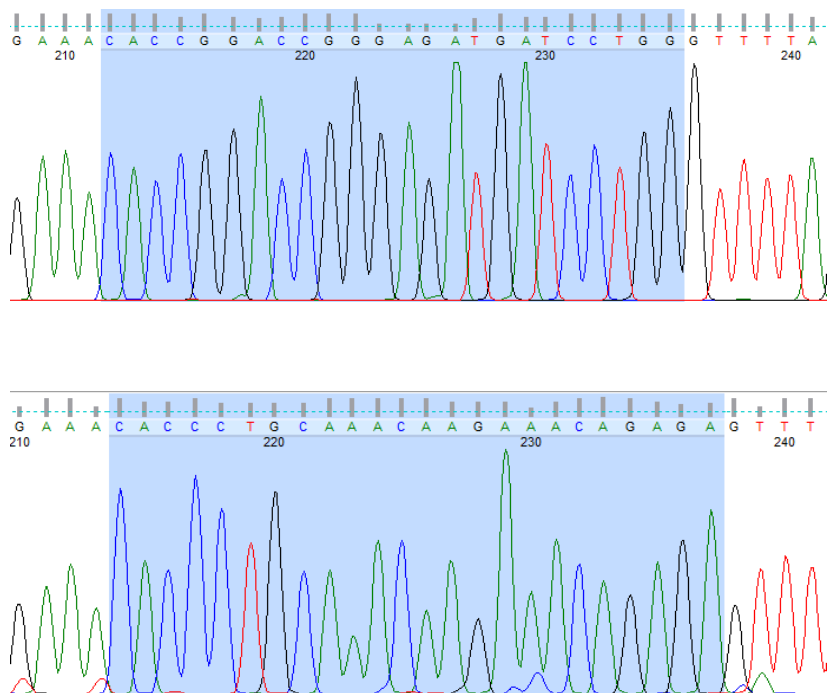
Figure 2.3 *Sequencing results to confirm successful cloning of FAF1 targeting gRNAs into CRISPR plasmids.*

GALNTL6

pSpCas9 (BB)-2A-Puro (PX459) V2.0 CRISPR plasmid with guide RNA (gRNA) was designed. Grna's were annealed and ligated into separate sets of CRISPR plasmids at the BbsI restriction site using BbsI restriction enzyme and ligase to produce two sets of *GALNTL6*-targeting CRISPR-gRNA plasmids. Heat shock transformation was undertaken for CRISPR-gRNA plasmid into competent *Escherichia coli* cells at 42°C for 45 secs, stored on ice for 2 min and broth media added for 1 hr at 37°C. Subsequently this was plated onto ampicillin-treated agar for selective amplification overnight. Isolation of CRISPR-gRNA plasmid was undertaken using Isolate Plasmid II minikit according to manufacturer's protocol with centrifugation (6'700 G). To linearise the CRISPR-gRNA plasmid they were treated with Pvu1 restriction enzymes and incubated at 37°C overnight.
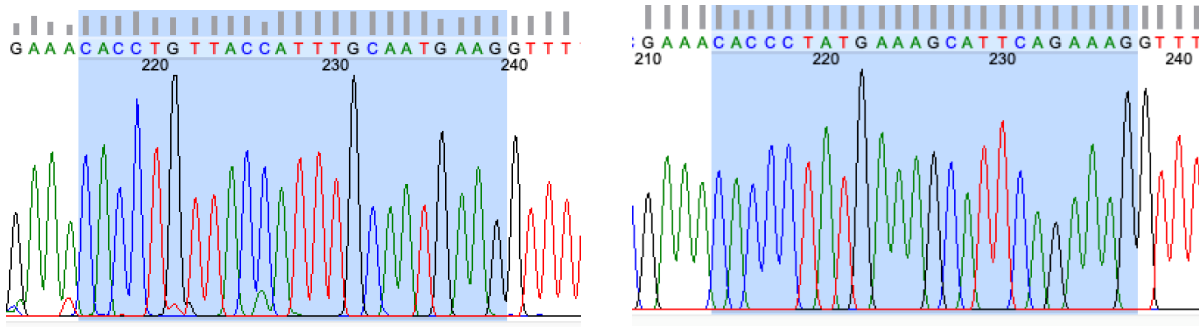
Figure 2.4- *Sequencing results to confirm successful cloning of Galntl6 targeting gRNAs into CRISPR plasmids.*

SH-SY5Y cells were grown to 80% confluence and Lipofectamine 2000 Reagent was utilised according to manufacturer's protocol, for transfection of CRISPR-gRNA plasmid or the original CRISPR plasmid as an empty vector control, in Opti-MEM 1X reduced serum media. Only one cloned non-linear CRISPR-gRNA plasmid was ready for use for the first sample of cell transfection and two cloned linear CRISPR-gRNA plasmids were co-transfected for the second sample of cells. Transfected cells were then incubated for 5 hr at 37°C. Selection of stable transfects of sham (empty vector control) and CRISPR-gRNA plasmid-treated SH-SY5Y cells were carried out using puromycin (1.5-3.5 µg/mL) for a maximum of 12 days. Non-linear or linear CRISPR-gRNA plasmid transfected SH-SY5Y cells were cultured for colony growth. Sham or pooled mutant *GALNTL6* cell colonies were grown after subculture by trypsinisation when individual colonies were observed, incubated for 5 min at 37°C and 5% CO2.Cells were centrifuged at 1200 g for 5 minutes. Cells were resuspended in DMEM/20% FBS/1% p/s and cultured as NP/LP-sham or CRISPR-treated-NP/LP cells in T25 flasks. Single mutant *GALNTL6* cell colonies were isolated by scraping and slowly pipetting up cell colony solution, or trypsinised if only one colony presents on the plate, then transferred for growth in DMEM/20% FBS/1% p/s as CRISPR-treated-N1 or L1 and L2 cells.

DCC

The CRISPR/Cas9 system was utilised to disrupt the expression of the _DCC_ gene, with p5pCas9 (BB)-2A-Puro (Addgene) (PX459) (Figure 2.6). Two pairs of oligonucleotide sequences were designed (D1A and D2A) to target _DCC_ were ordered and annealed. The gRNAs were designed to target _DCC_ at an early exon in the upstream promoter region to resulting in _DCC_ knockout. Two pairs of optimised gRNAs rather than one were utilised to essentially create a double knockout effect. PX459 was digested with _Bbs1_ enzyme, and the gRNA oligonucleotide pairs were ligated into the _Bbs1_ sites to create a plasmid expressing Cas9 and _DCC_ gRNA (_DCC_/PX459). SH-SY5Y cells were 80% confluent at time of transfection. For each transfection, media was removed from each well of the 6-ell plates in which SH-SY5Y cells were growing. Cells were gently washed in media in preparation for the addition of DNA-lipid complexes. DNA-lipid complexes were prepared using both CRISPR constructs and Lipofectamine® 2000 DNA Transfection Reagent and were diluted separately with Opti-MEM® Medium and incubated for 5 minutes at room temperature (RT). Both solutions were then mixed in a 1:1 ratio and incubated for a further 20 minutes at room temperature to permit formation of complexes. Subsequently, DNA-lipid complexes were added to cells and incubated for a few hours at 37ºC, 5% CO_2. Opti-MEM® / Lipofectamine® medium was then removed and replaced with DMEM/F-12/Glutamax growth medium supplemented with 10% FBS and 1% penicillin/streptomycin and left for overnight incubation. Transfected cells were visualised immunofluorescence microscopy and identified via western blotting. PX459 void of _DCC_ gRNA was also transfected into SH-SY5Y cells in order to produce empty vector control cells, hereafter "sham" or "sham control" cells.

Puromycin Selection of Transfected Cells

Puromycin selections of each transfection was then undertaken in parallel. A "sham" control was utilised composed of SH-SY5Y cells treated with the original CRISPR plasmid (Figure 2.5). This was to generate a 'control CRISPR cell line' that had undergone the transfection process but did not have a sgRNA. Therefore, I was controlling for the effects of expressing CAS9.Through use of puromycin, identification of mutant SH-SY5Y cells successfully transfected with each relevant CRISPR plasmid constructs occurred. Wild type SH-SY5Y cells were also treated with puromycin. Both transfections were treated initially with media containing 1.5µg/ml puromycin, which was increased to 3.5µg/ml puromycin upon observation of insufficient selection until all wild type cells had been killed off

indicating that any surviving cells in the transfection groups were puromycin resistance and therefore possessed the CRISPR construct. Through use of puromycin, identification of mutant SH-SY5Y cells successfully transfected with each relevant CRISPR plasmid constructs occurred.

Figure 2.5 pU6-(BbsI) _CBh-Cas9-T2A-mCherry CRISPR construct plasmid. *Figure 2.5 above represents the CRISPR construct plasmid used to create CRISPR KOs of each of the identified mutant colonies via sequencing such as FAF1, DCC and GALNTL6. This plasmid contains an expression vector for sgRNAs cloned into the BbsI sites and for expression of Cas9 linked to mCherry via a T2A peptide.*

Figure 2.6 p5pCas9(BB)-2A-Puro (PX459) CRISPR construct plasmid. *Figure 2.6 above represents the CRISPR construct plasmid used to create CRISPR KOs of each of the identified mutant colonies via sequencing such as FAF1, DCC and GALNTL6.*
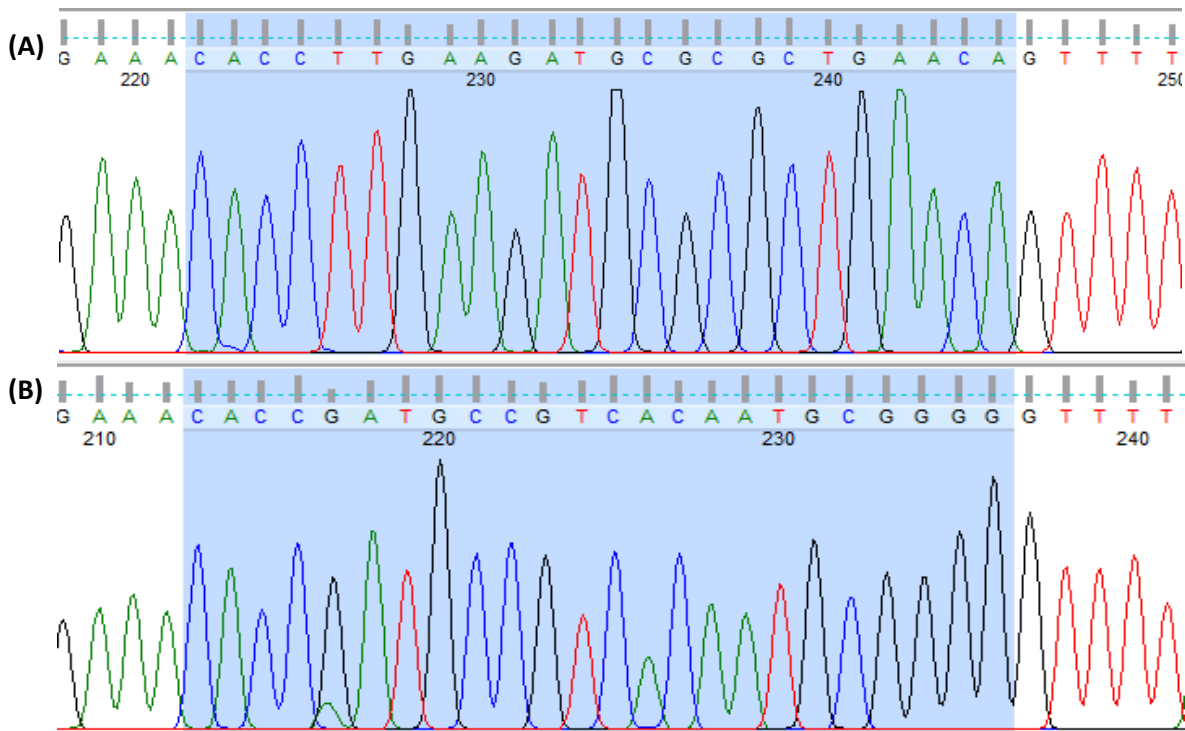
Figure 2.7. *Sequencing results to confirm successful cloning of DCC targeting gRNAs into CRISPR plasmids.*

2.4 CRISPR Validation

Western blotting

Cells were grown to confluence in 6-well plates and were treated as required. Following incubation at 37℃, media was removed via an aspirator, cells were scraped using cell lysis/scraping method and an equal volume of 2 x Laemmli sample buffer was added into the cells immediately. Cells were then harvested, and the mixture transferred to labelled micro centrifuge tubes and samples stored at -20 ℃ for Western blotting.

Cell lysates were thawed on ice and prepared for Western blotting. Equivalent loadings (determined by Bradford Assay) of each protein sample were loaded onto 10 % polyacrylamide gels and were electrophoresed at 120 V for 90 minutes. Proteins were transferred to the nitrocellulose membrane at 100 V for 60 minutes at 4°C. Pierce ™ Fast Western blot kit, ECL substrate (Catalog number: 35055) was then utilised and the blot was removed from the transfer apparatus and placed in a clean incubation tray. Blots were stained with respective primary antibodies such as anti-*DCC* (1:500) anti-

FAF1 (1:1,000) anti-*Galntl6* (1: 1,000). With regards to blots examining WFA staining, primary was biotinylated WFA (1: 1,000) and secondary instead of using generic secondary present in fast western blot kit, streptavidin conjugated horse radish peroxidase (following manufacturer's protocol) was utilised. Steps were undertaken as detailed in the kit manual and blots were subsequently developed on X-OMAT operating system. Bands were photographed, membrane was stripped and re stained with beta actin loading control and entire lanes were analysed and quantified using Image J TM software and Microsoft excel. The relative densities of protein of interest divided by beta actin loading control normalised the data and produced relative protein levels. Band sizes were calculated from their migration distance using a standard curve of migration ratio (distance over full length) versus known molecular size of a ladder.

2.5 Drug inhibitor effect on WFA staining

Wild type cells and *FAF1* pool cells were grown to confluence in two T25 flasks each respectively. One of each flask was extracted using cell scraping and lysis. The other flasks were digested for 15 minutes at 37 degrees Celsius with trypsin to remove the perineuronal net. Flasks were then washed with PBS and cell lysis was undertaken. For the second experiment, a 1000-x stock of the KR-33493 *FAF1* inhibitor was produced in DMSO. Two plates labelled A and B were used seeded with SH-SY5Y cells followed immediately by the drug dilution at 10 micro molar concentrations. This was to ensure that the cells were not allowed to attach overnight to hinder the production of the perineuronal net. Plates were then incubated for 72 hours at 37 degrees Celsius.

2.6 siRNA knockdown of *GALNTL6*

25% confluent cells were plated in 6 well plates with or without coverslips and then left overnight. Following overnight growth, each Well was treated respectively with either 0 μL, 100 μL or 300 μL of *GALNTL6* in 1 ml of serum-free media for 6 hours and then 2 ml full media was added. Cells were then left for 48 hours. Cells were seeded to 60-80 % confluence ready for transfection. Transfection was undertaken using Lipofectamine® RNAiMAX Reagent. Firstly, Lipofectamine® RNAiMAX Reagent was diluted in Opti-MEM® Medium. The siRNA was then diluted in Opti-MEM® Medium the diluted siRNA was added to the diluted Lipofectamine® RNAiMAX Reagent (1:1 ratio) Cells were then incubated at 37°C and siRNA-lipid complex was added to the cells. The cells were then

incubated for 3 days at 37°C and analysis of the transfected cells was then undertaken. Cells were subsequently lysed for either protein analysis or placed on coverslips fixed in paraformaldehyde /methanol. Adherent cell layers were fixed to cover slips using 3.6% w/v paraformaldehyde (PFA) fix within a fume hood. Where cells were cultured, they were fixed in the wells of plates. 3x PBS washes occurred and then fixed in PFA on ice for 30 minutes. Further PBS washes were undertaken followed by fixation at -18°C in methanol for 20 minutes. Following fixation, cells were either subjected to further staining or stored overnight submerged in PBS. Cells were then further subjected to PBS + 0.1% TIen20 (PBS-T) (Alfa Aesar, UK) and incubated on ice for 10 minutes to permit cell permeabilization. Cells were blocked for 1 hour at room temperature 1ml PBS-T + 1% donkey serum (DS). Subsequently, primary antibodies (1:1000 diluted in PBS-T/1% DS). 3 x 5 minutes' washes then occurring PBS-T. Secondary antibodies were also diluted in a mixture of PBS/0.1% TIEN-20 to a dilution ratio of 1:2000. Biotinylated WFA was paired with a Streptavidin, Alexa Fluor® 594 conjugate and fluorescent red. Plates were then wrapped in foil in dark conditions to prevent light induced degradation.3 x PBS-T washes were then undertaken before the mounting process. Cover slips were directly mounted onto microscope slides which were compared with antifade mountant containing DAPI (Invitrogen, UK). Coverslips were prepared so that for each round of microscopy there was (i) cytoskeletal & WFA-stained cells and (ii) cytoskeletal and *FAF1* stained cells. Coverslips were then mounted on glass slides with SlowFade™ Diamond Antifade Mountant with DAPI. Once prepared, slides were stored in the refrigerator prior to imaging. All slides were examined under an epifluorescent upright microscope (Nikon Eclipse 600), and relevant images were obtained. Analysis of raw immunofluorescence data was undertaken using the Image J processing and analysis software at 100 x magnification of 400 x magnification.

2.7 Pull-down Assay.

Two T75 flasks of SH-SY5Y cells were grown to confluence and then lysed for protein extraction in exactly the same way as for the preparation of protein for SDS-polyacrylamide gel electrophoresis/Western analysis (CelLytic/protease inhibitor cocktail to a total volume of 700 µL per flask). The combined extract was added to 49 mL PBS and 50 µL Biotinylated WFA (B-1355 Vector Laboratories, CA, USA) in a 50 mL Corning tube and incubated overnight at 4°C on a roller (Fisher Scientific, Model 11676251). The following morning, 100 µL Pierce Streptavidin Ultra Link Resin was added and the suspension left rolling at 4°C for an additional 2 hours.

Meanwhile a column was prepared using a 10 mL syringe cylinder with plunger removed. This was clamped vertically in a retort stand in the cold room (4°C). Deactivated glass wool (Restek US/EN) was packed into the bottom of the syringe using forceps. The column was washed with 2 x 10 mL PBS. The PNN protein-WFA-biotin-streptavidin-resin suspension was loaded onto the column in 10 mL batches, ensuring that no cloudiness was seen in the flow through (the glass wool plug was working to retain/trap the resin). The plunger was used if flow rates decreased. After the column had been completely loaded, it was washed by 3 x 10 mL PBS which was fully removed after the last wash by applying plunger pressure. 500 µL of CelLytic extraction buffer was heated to 80°C and pipetted directly onto the column. After 1 minute this was eluted using the plunger into microfuge tube. This was mixed with an equal volume of 2 x Laemmli buffer and loaded into several wells of a pre-cast SDS-polyacrylamide gel. After 3 minutes' electrophoresis another loading was carried out and the procedure repeated until all protein had been loaded into the top portion of the gel. This process was carried out to maximise the concentration of the eluted PNN component in the gel prior to slice excision and downstream mass spectrometry analysis.

The top ~0.5 cM of the gel under each well used was removed using a scalpel and then fixed for one hour in 45% methanol:45% H_2O:10% acetic acid at room temperature. The gel pieces were extensively air dried to remove traces of fix and then sent to The University of Dundee 'FingerPrints' Proteomics Facility for their in-house protein fragment identification pipeline:

1. In-gel processing
2. In-gel reduction/alkylation
3. In-gel trypsin digestion
4. Peptide extraction and dry down
5. MS Analysis (Thermo Fisher Scientific Q Exactive Plus)
6. Database searching for protein ID (Human)

CHAPTER 3

Characterisation of the Perineuronal Net (PNN) in human *SH-SY5Y* neuroblastoma cells

3.1 SH-SY5Y cells express PNNs

I chose *SH-SY5Y* cells to identify genes which, when mutated, fail to produce a perineuronal net. A neuroblastoma cell line *SK-N-SH* cell line was produced in 1960 from metastatic cells located in the bone marrow aspirate of a four-year-old female (Kovalevich & Langford, 2013). *SK-N-SH* was then sub cloned three times; first to *SH-SY*, then to *SH-SY5*, and finally to *SH-SY5Y* (Kovalevich & Langford, 2013). This cell line has served as a model for neurodegenerative disorders as well as neuropsychiatric disorders because it can be differentiated to different types of functional neurons via the addition of specific compounds (Lopes *et al.*, 2010). In addition, the *SH-SY5Y* cell line has been used in experimental neurological studies for analysis of neuronal metabolism and neurodegenerative processes including neurotoxicity and neuroprotection (Lopes *et al.*, 2010). The *SH-SY5Y* neuroblastoma cell line is the most cited *in vitro* model in neuropsychiatric research, and has various benefits including low cost, ease of culture, reproducibility, and available literature (Kovalevich & Langford, 2013). This cell line has been shown to display neuronal properties such as neurite outgrowth, neuro-transmitter synthesis, and receptor expression (Kovalevich & Langford, 2013). Previous studies using these cells have demonstrated that the first DNA variant displaying genome wide significant association with psychosis modifies the binding of a transcription factor, which controls expression of the ZNF04A gene – emphasising their use as a functional model of CNS disease (Lopes *et al.*, 2010).

SH-SY5Y cells have similarities to immature neurons and the cell lineage has been shown to possess dopaminergic and adrenergic properties as well as proliferative markers such as proliferating cell nuclear antigen (PCNA) and immature neuronal markers such as nestin (NES) (Kovalevich & Langford, 2013).Differentiation of *SH-SY5Y* can be promoted using retinoic acid and neurobasal medium supplemented with B-27 and BDNF (Kovalevich & Langford, 2013).This differentiation also results in upregulation of the axonal guidance signalling pathway, growth of neurites and conversion into a neuron-like phenotype. Both undifferentiated and differentiated *SH-SY5Y* express dopamine biosynthesis pathway enzymes and secrete dopamine and the surface of *SH-SY5Y* cells possess dopamine, GABA, acetylcholine, and glutamate receptors (Kovalevich & Langford, 2013). Dopaminergic markers expressed by *SH-SY5Y* also include tyrosine hydroxylase (TH) which is an enzyme required for catalysis of dopamine as well as noradrenaline and adrenaline (Encinas *et al.*, 2002) Furthermore, muscarinic, and nicotinic acetylcholine receptors have also been reported in *SH-SY5Y* cells (Encinas *et al.*, 2002).

SH-SY5Y cells have been previously shown to express perineuronal nets using the widely recognised marker Wisteria floribunda agglutinin (WFA) which binds to either an unidentified sulphation motif of chondroitin sulphate proteoglycans or the N-acetyl galactosamine residues of chondroitin sulphate proteoglycans (Kovalevich & Langford, 2013). Importantly, in brain tissue sections, WFA has been shown to recognise a specific type of perineuronal net which resides on parvalbumin-positive GABAergic interneurons, suggesting that SH-SY5Y cells may also have an overlapping phenotype with these neurons.

To confirm our protocol for staining the PNN with WFA, I carried out staining on mouse brain sections. Frozen 12-micron mouse brain sections were sourced from previously prepared laboratory stocks (B. Pickard). After acetone fixation, sections were stained overnight (4°C) with biotinylated WFA and, subsequently, with streptavidin conjugated to a red fluorophore, and then mounted under a coverslip with DAPI counterstain and antifade solution. Images taken with an epifluorescence microscope were processed and colour composites created using ImageJ (Fig.3.1).
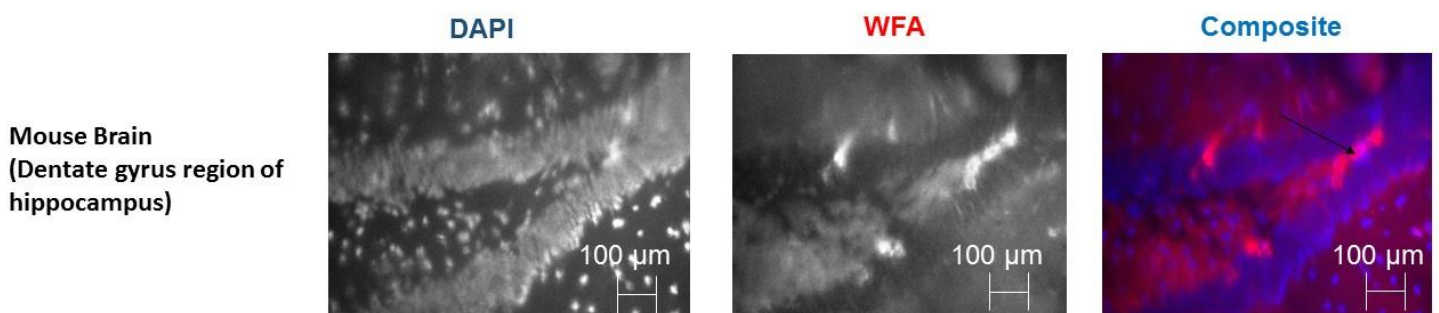
Figure 3.1 Successful staining of PNN-positive neurons in the mouse brain using WFA. In this figure, the dentate gyrus region of the hippocampus is shown with its granule cell layer displaying the typical '>' anatomy visible in coronal sections. The majority of staining is shown in the projections towards the CA3 region and in isolated neurons, predominantly within the sub granular region. X40 magnification, Scale bar=100μm

To determine whether SH-SY5Y cells express WFA-interacting proteins/modification, I carried out WFA staining of paraformaldehyde-fixed SH-SY5Y cells. SH-SY5Y cells were sourced from previously prepared laboratory stocks (B. Pickard). Cells were recovered and grown to 50% confluence and then fixed. Fixed cells were stained overnight (4°C) with biotinylated WFA, then

streptavidin conjugated to a red fluorophore, and mounted under a coverslip with DAPI counterstain and antifade solution and imaged using an epifluorescence microscope and camera. Images were processed and colour composites created using ImageJ (Fig.3.2, Fig 3:3).
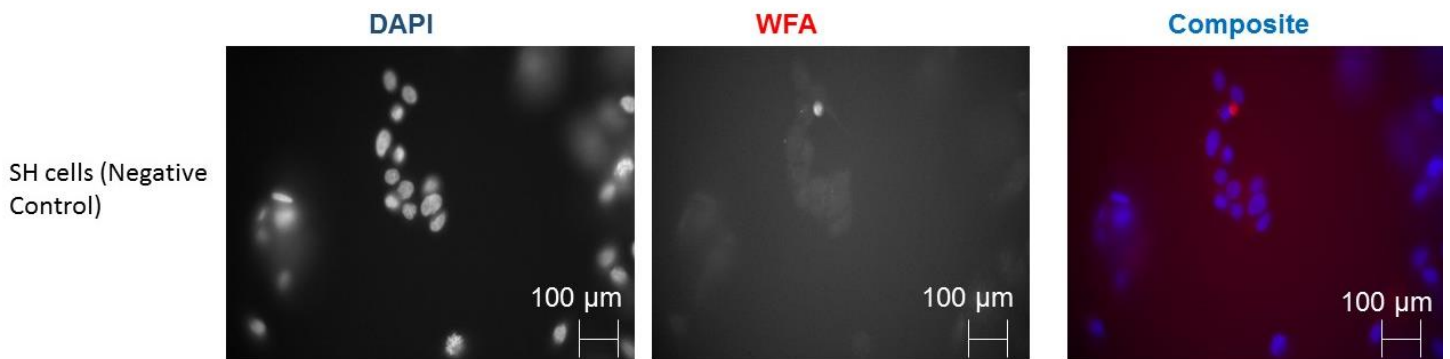
Figure 3.2 No WFA *staining of SH-SY5Y cells (Negative control)*. *Figure 3.2 shows the results obtained when SH-SY5Y cells are stained with* WFA *but no secondary (Streptavidin-fluorophore) which is part of the* WFA *biotin/Streptavidin system. As can be seen above, no red staining is observed in this negative in comparison with the positive control below (See figure 3.3). X40 magnification, Scale bar=100µm*
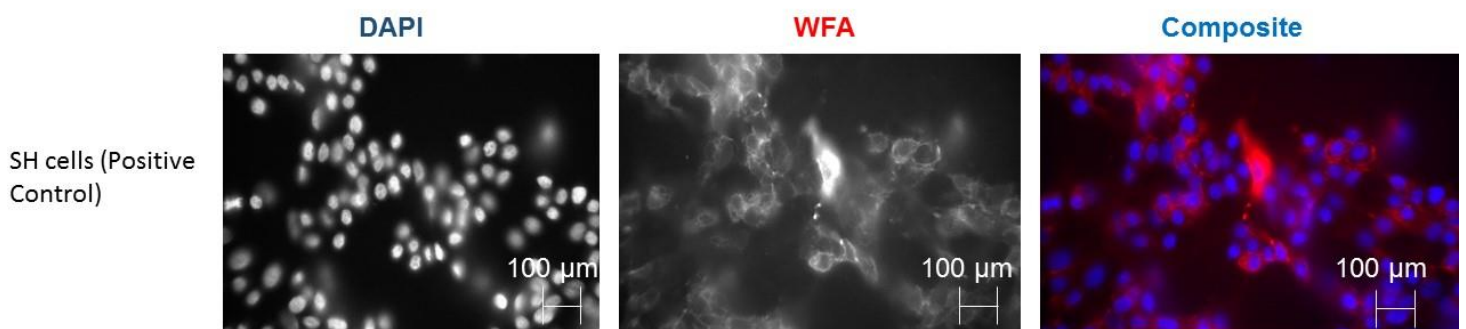
Figure 3.3 Successful staining of SH-SY5Y cells with WFA. *SH-SY5Y wild type cells were stained with* WFA.WFA *staining can be seen with the red and the blue (*DAPI*) indicating cell nuclei. In comparison with the negative control (no streptavidin-fluorophore), staining is strong and discrete, indicating the presence of perineuronal nets. X40 magnification, Scale bar=100µm*

The results obtained above indicate that the WFA staining is working and that *SH-SY5Y* cells do indeed express perineuronal nets. *SH-SY5Y* cells are a secondary cell line, and the results show that perineuronal nets are also expressed on secondary cell lines with neuronal properties. It is important note here that no primary antibody control was utilised, and the signal could potentially be as a result of non-specific binding of secondary antibody. The appearance of the perineuronal net is not a typical honeycomb-like structure as described in the literature. However, the results above

show that *SH-SY5Y* cells are a viable cell line for perineuronal net expression and can be further utilised to investigate the function and structure of perineuronal nets.

3.2 HEK293 and LAN5 cells lines, but not A549 cells, show positive staining with WFA

I determined whether perineuronal nets were also expressed on three other laboratory cell lines, *LAN 5*, *HEK293*, and *A549*. By undertaking this, it would further validate the use of *SH-SY5Y* cells as the best neuronal cell line for the subsequent experiments and also show that WFA staining is specific for neuronal cell lines. *LAN 5* is a human neuroblastoma cell line derived from the brain. *HEK293* (human embryonic kidney 293) is an immortalised cell line derived by viral transformation of kidney cells taken from an aborted foetus in 1973 (Shaw *et al.*, 2002). Despite being a kidney cell line, it has been shown to have properties of immature neurons, as shown by the expression of multiple neuronal markers (Shaw *et al.*, 2002). On the other hand, *A549* is an adenocarcinoma cell line derived human alveolar basal epithelial cell line with no expected neuronal properties. As seen below, WFA staining is seen on all neuronal-like cell lines (including in the literature it has been suggested that *HEK293* cells are derived from the peripheral nervous system though this is disputed (Madhusudana *et al.*, 2010). Since *A549* is definitively non-neuronal, it is reassuring to see that there is no WFA staining. Taking into consideration all the above, this shows that WFA staining is specific to 'neuronal' cell lines.

To further confirm that WFA staining was specific to neuronal cell lines, SDS-polyacrylamide gel electrophoresis and Western blotting were employed. *A549* cells were grown to confluence. Protein was extracted using cell lysis, scraping method, and then run on a 10 % percent gel. Samples were transferred to a nitrocellulose membrane using standard blotting and then incubated with biotinylated WFA and then secondary detection stain (streptavidin conjugated to horse radish peroxidase enzyme) using conventional antibody treatment protocols. Images were developed using ECL and exposure to X-ray film and scanned (See figure 3.4)
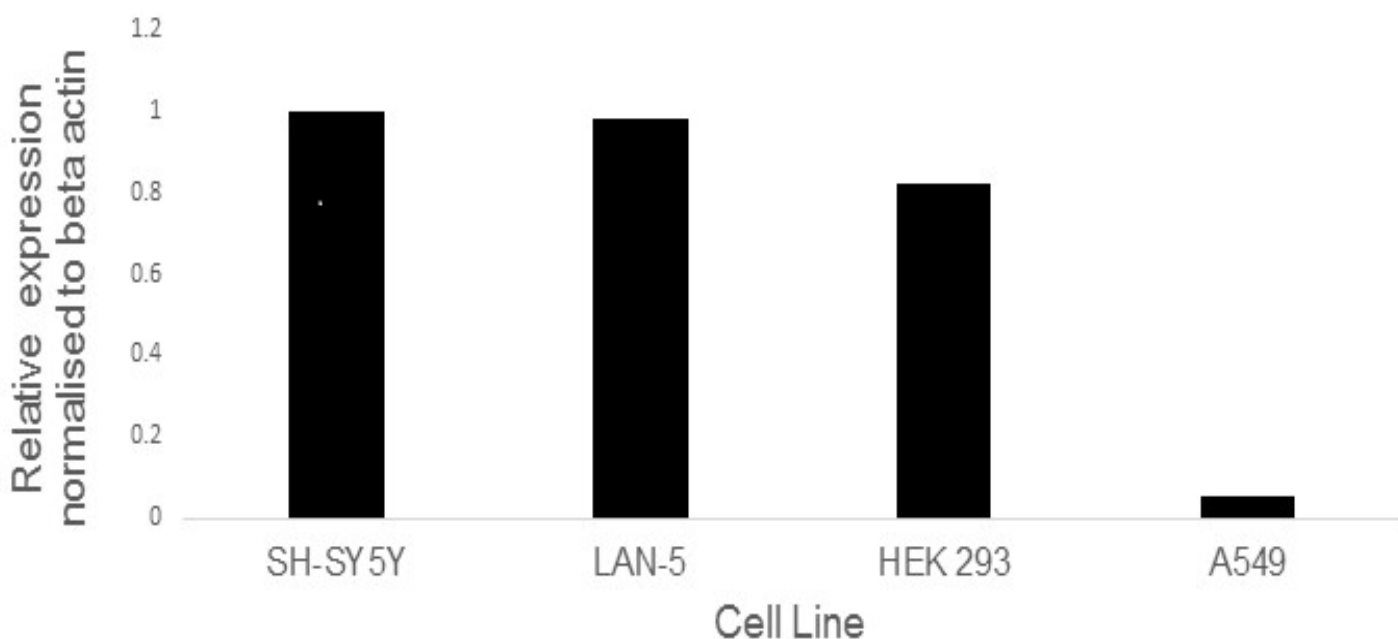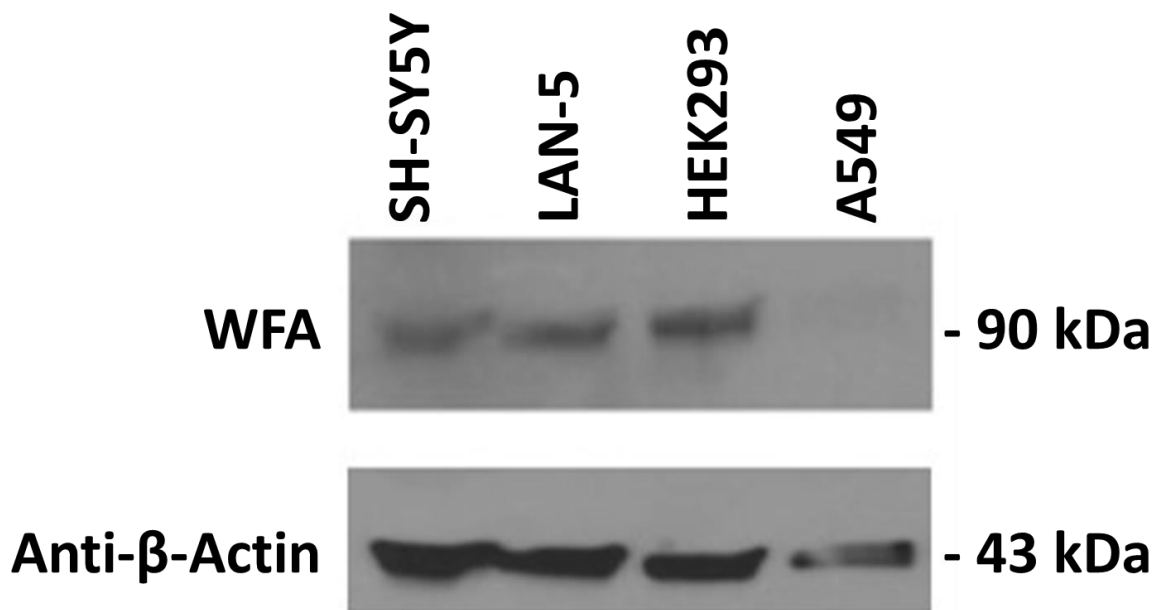
Figure 3.4 **WFA-binding glycoprotein is expressed in SH-SY5Y, LAN5 HEK293, but not A549,**
cells. *Figure 3.4 shows the results obtained when various secondary cell lines were stained with*
WFA. All cell lines except A549 show WFA staining and therefore have potential perineuronal nets.
A549 is a lung epithelial cell line used to contrast the expression of WFA targets within brain cell
lines. The WFA-stained band size is ~90 kDa but it is unknown which specific component of the

perineuronal net this corresponds to; an issue pursued later in this thesis. Beta actin, the loading control, is appearing at its known size of 43 kDa. No statistical analysis was undertaken as N=1.

The purpose of these experiments was to determine whether expression of glycoproteins that bind WFA occurs on other cell lines with neuronal properties such as *HEK-293*, *LAN5* and *A549* (lung epithelial cell line). Cells were monitored for WFA staining, and it was shown that WFA-binding glycoprotein expression occurred in all cell lines apart from *A549.* This is as expected as A549 is a lung epithelial cell line with no neuronal properties. Furthermore, the presence of WFA-binding glycoprotein expression indicates that perineuronal nets are present within the cells. Though our work is based on *SH-SY5Y* cells, there are other cell lines which can be utilised such as *LAN5* or *HEK-293.* Building on this, I have shown that perineuronal nets are not just expressed on *SH-SY5Y* cells but also other cell lines meaning that this is a viable cell line to progress with the studies. *SH-SY5Y* cells, as mentioned above, are the most commonly used secondary cell WFA-binding glycoprotein expression lines in neurological studies. Although other cell lines do indeed express perineuronal nets, the decision was taken to solely progress with *SH-SY5Y* cells though it is important to note that further potential experiments can occur on *LAN-5*, *HEK-293* and *PC12* cells which have also been used for neurological research studies.

3.3 Testing potential protein target(s) of WFA staining

In the previous section, it was demonstrated that *SH-SY5Y* express presumptive perineuronal nets through positive staining by WFA. WFA staining has been suggested to occur through its binding to the N-acetyl galactosamine residue of chondroitin sulphate proteoglycans or an unidentified sulphation motif on chondroitin sulphate proteoglycans. Interestingly, for WFA staining, the usual observation is for one band to be present. Occasionally, some blots would show two or more bands sometimes appearing at 90 kDa or 75 kDa which could be hypothesised as various isoforms of the specific chondroitin sulphate proteoglycans. The presence or absence of the extra bands might be due to cell growth conditions such as confluency. As a result, it was important to try to identify the protein(s) and their glycosylation state represented in Western blots. For example, *Aggrecan* was one candidate target as it is known to be a major component of perineuronal nets and is physically associated within nearly all types of perineuronal net structures located on parvalbumin-positive GABAergic interneurons, cortical neurons, basket cells and others. The band(s) could, alternatively,

represent one of the other common CSPGs such as *Versican* (known to have 4 isoforms: V0, V1, V2 and V3) or *Neurocan*. However, *Neurocan* (143 kDa), *Versican* (373 kDa), *Brevican* (140 kDa), *Aggrecan* (75 kDa), phosph*acan* (250 kDa), and their cross-linking protein, tenascin R (180 kDa), all show molecular weights very different from our observed WFA target and are unlikely to represent the WFA target detected.

To explore these aspects of WFA target characterisation in cell lines I carried out a number of exploratory studies. Firstly, mood stabilisers and anti-depressants such lithium, fluoxetine and venlafaxine previously implicated within the context of perineuronal net research were utilised. Lithium is a well-known drug used in the treatment of bipolar disorder. Fluoxetine has been shown to reduce perineuronal net staining in the brains of deceased patients with bipolar disorder (Ohira *et al.*, 2013) Finally, venlafaxine has been shown to exhibit its effect of degradation of perineuronal net components via MMP-9 proteolysis (Alaiyed *et al.*, 2019). Matrix metalloproteinases have long been implicated in the degradation of perineuronal net components. Protein was extracted using cell lysis, scraping method, and then run on 10 % percent agarose gel (Methods). Samples were transferred using the nitrocellulose method and then incubated with primary antibody (biotinylated WFA) and secondary antibody (streptavidin conjugated horse radish peroxidase). Images were developed using the ECL method and exposed to X-ray film and processed using ImageJ.

Furthermore, staining of *SH-SY5Y* cells with *Neurocan* and *Versican* were undertaken to determine the identity of the sole band appearing on WFA protein analysis. *SH-SY5Y* cells were sourced from previously prepared laboratory stocks (B. Pickard). After fixation sections were stained overnight (4°C) with primary antibodies such *Neurocan* and *Versican* respectively and the following day, washed, then blocked with PBS/Donkey serum and then incubated with secondary antibody (Mouse/Rabbit), then mounted under a coverslip with DAPI counterstain and antifade solution and imaged using epifluorescence microscope. Images were processed and colour composites created using ImageJ (Fig.3.5, Fig 3.6, Fig 3.7)
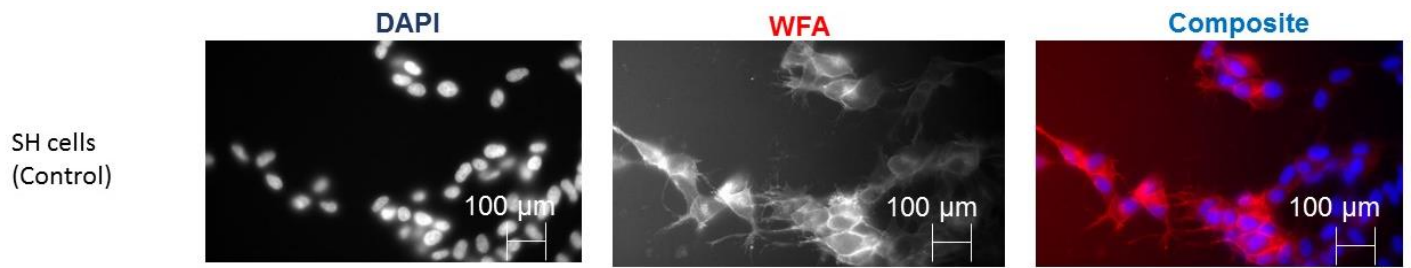
Figure 3.5. WFA *staining of SH-SY5Y cells shows the presence of perineuronal nets.* *Figure 3.5 shows the results obtained when SH-SY5Y wild-type cells are stained with WFA. As seen above, WFA staining can be seen with the red indicating WFA staining and the blue indicating DAPI. This was done as a positive control on the same biological sample to show with other staining that Neurocan and Versican are also present within perineuronal nets of SH-SY5Y cells. X40 magnification, Scale bar=100µm*
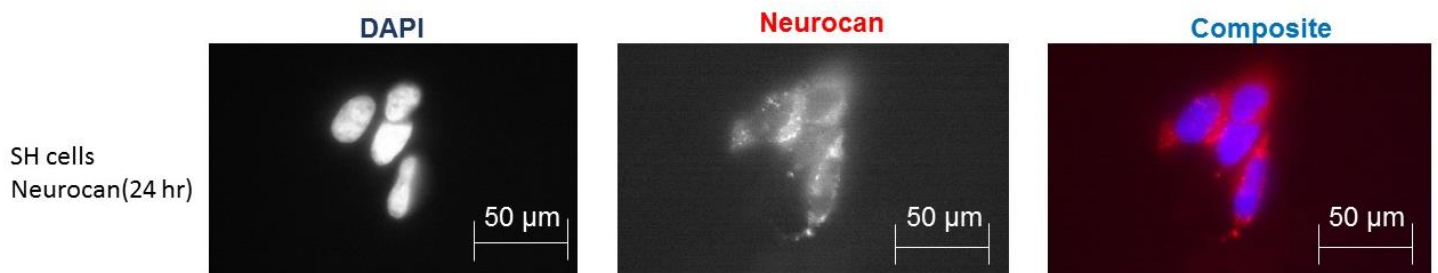
Figure 3.6. SH-SY5Y cells express Neurocan. *Figure 3.6 shows the results obtained when SH-SY5Y wild type cells are stained with Neurocan. left: DAPI centre: Neurocan right: Composite. As seen above, Neurocan staining can be seen with the red indicating Neurocan staining and the blue indicating DAPI. The fact that I have seen Neurocan staining here confirms that SH-SY5Y cells do express Neurocan. X40 magnification, Scale bar=50µm*
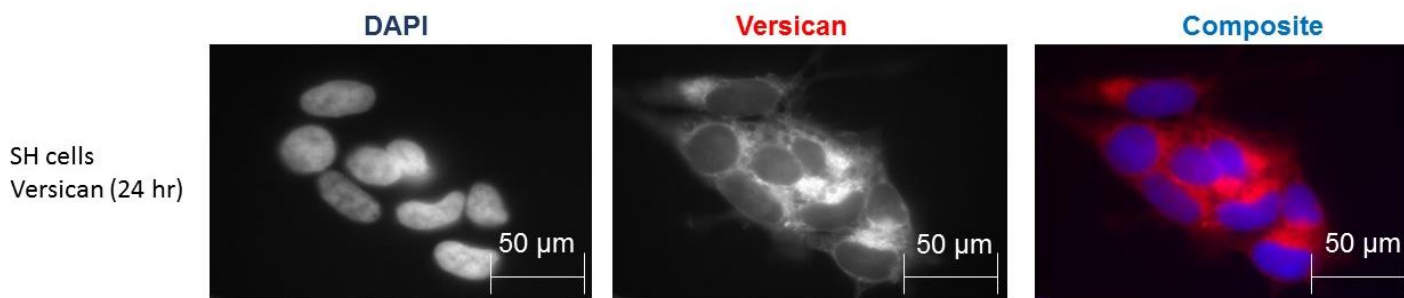
Figure 3.7. SH-SY5Y cells express Versican. *Figure 3.7 shows the results obtained when SH-SY5Y wild type cells are stained with Versican. left:* DAPI *centre: Versican right: Composite. As seen above, Versican staining can be seen with the red indicating Versican staining and the blue indicating* DAPI*. The fact that I have seen Versican staining here confirms that SH-SY5Y cells do express Versican. X100 magnification, Scale bar=50µm*

3.4 Does the WFA staining on SH-SY5Y cells respond to pharmacological inhibitors of the PNN that have been described in the literature?

Fluoxetine and venlafaxine are anti-depressants (Guirado *et al.*, 2014). Fluoxetine has been previously shown to decrease levels of PNN staining intensity in various brain regions such as the amygdala (Ohira *et al.*, 2013) whereas venlafaxine has been previously suggested to be involved in Matrix Metalloproteinase-9 (MMP-9) PNN proteolysis (Alaiyed *et al.*, 2019). Fundamentally, fluoxetine has been suggested to play a potential role in modulation of perineuronal nets. Moreover, chronic fluoxetine treatment reduces parvalbumin expression and perineuronal nets in gamma-aminobutyric acidergic interneurons of the frontal cortex in adult mice (Ohira *et al.*, 2013). Finally, chronic fluoxetine treatment alters the structure, connectivity, and plasticity of cortical interneurons (Guirado *et al.*,2014). Other pharmacological agents are also candidates for PNN modifiers. Lithium is a mood stabiliser used in the treatment of bipolar disorder and a recent gene trap screen undertaken by Pickard *et al.*, 2017 revealed that mutations in various perineuronal net components offered resistance to lithium treatment. Since lithium is directly and indirectly involved in regulation of Glycogen Synthase Kinase-3 (GSK-3) levels, I also decided to examine the GSK-3 inhibitor, 1-Azakenpaulone.1-Azakenpaullone acts as a potent and ATP-competitive inhibitor of GSK-3β.

SH-SY5Y cells were also treated with inhibitors 10µM fluoxetine and 10 µM venlafaxine for 24 hours. Protein was extracted and run on 10 % percent agarose gel. Samples were transferred using the nitrocellulose method and then incubated with biotinylated WFA and 'secondary' streptavidin

conjugated horseradish peroxidase. Images were developed using X ray film and processed using ImageJ (See figure 3.8).
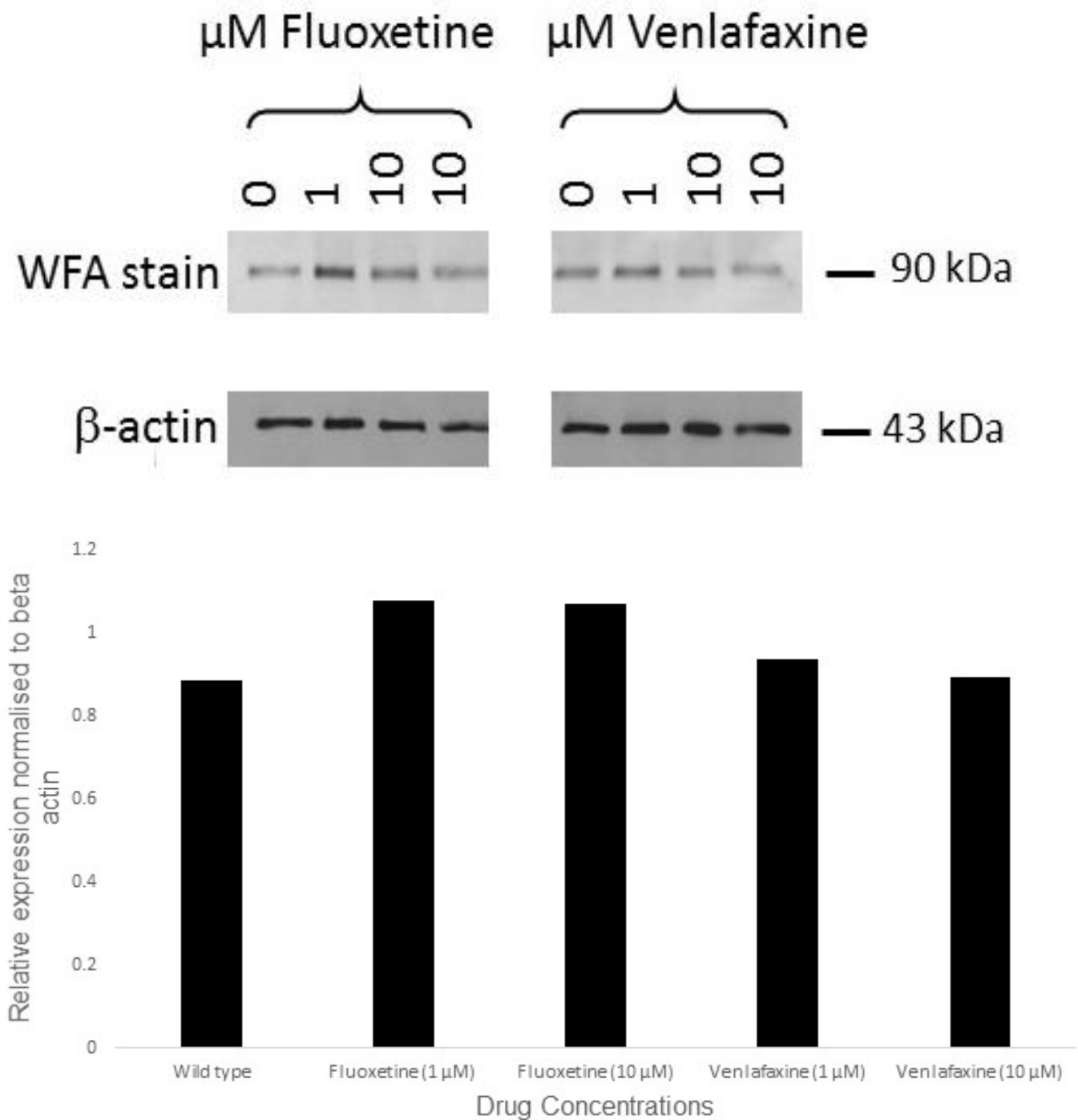
Figure 3.8 No effect on WFA *staining using inhibitors fluoxetine and venlafaxine in SH-SY5Y cells.* *Figure 3.8 above demonstrates the effect of these two anti-depressants on* WFA *staining.*

Through increasing levels of concentrations up to 10 µM, here the results display that there is no effect of both anti-depressants on WFA *staining on the wild type cells. This is in contrast in the literature where* WFA *staining is reduced in some primary cell lines and other secondary cell lines. No statistical analysis was undertaken as N=1.*

The aim of these experiments was to determine whether known inhibitors such as fluoxetine and venlafaxine decrease levels of WFA staining in *SH-SY5Y* cells. This was done by growing *SH-SY5Y* cells to confluence and treating them with respective drugs for 24-48 hours. The results above show that there is no change in WFA expression when treated with these drugs.

I next determined whether the cellular staining distribution with WFA was altered by fluoxetine, venlafaxine, lithium or 1-Azakenpaullone. As mentioned above in the literature, primary cell lines and other secondary cell lines had reduced WFA-binding glycoprotein expression and alterations of perineuronal nets when using certain inhibitors. Here, *SH-SY5Y* cells were sourced from previously prepared laboratory stocks (B. Pickard). Cells were recovered and grown to confluence and treated with respective inhibitors such as fluoxetine, venlafaxine, lithium and 1-Azakenpaullone for 24 to 48 hours, sections were stained overnight (4°C) with biotinylated WFA and mounted under a coverslip with DAPI counterstain and antifade solution and imaged using an epifluorescent microscope and camera. images were processed and colour composites created using ImageJ (Fig.3.9, Fig 3.10, Fig 3.11).

DAPI   **WFA**   **Composite**

SH Cells- No Fluoxetine treatment

100 μm   100 μm   100 μm

SH Cells- 10µM Fluoxetine (24hr)

100 μm   100 μm   100 μm

SH Cells- 10µM Fluoxetine (24 Hr)

100 μm   100 μm   100 μm

Mean fluorescence intensity (WFA)

350
300
250
200
150
100
50
0
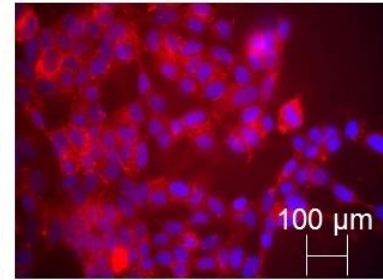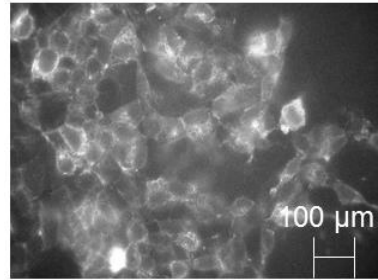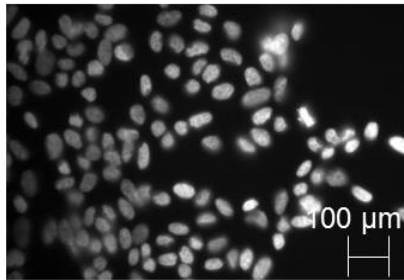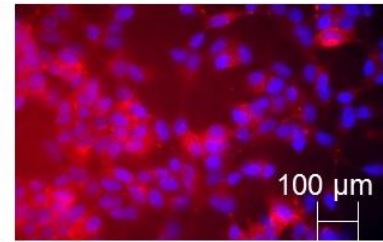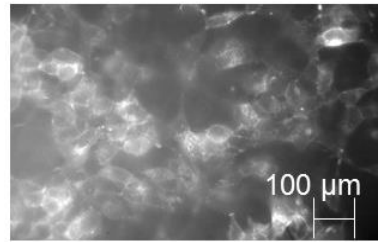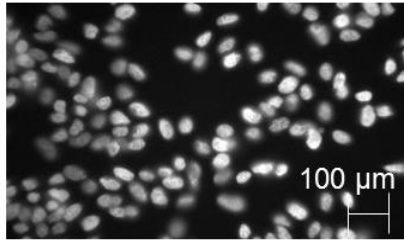
SHSY-5Y   SH-SY5Y with 10 µM Fluoxetine (24 H)
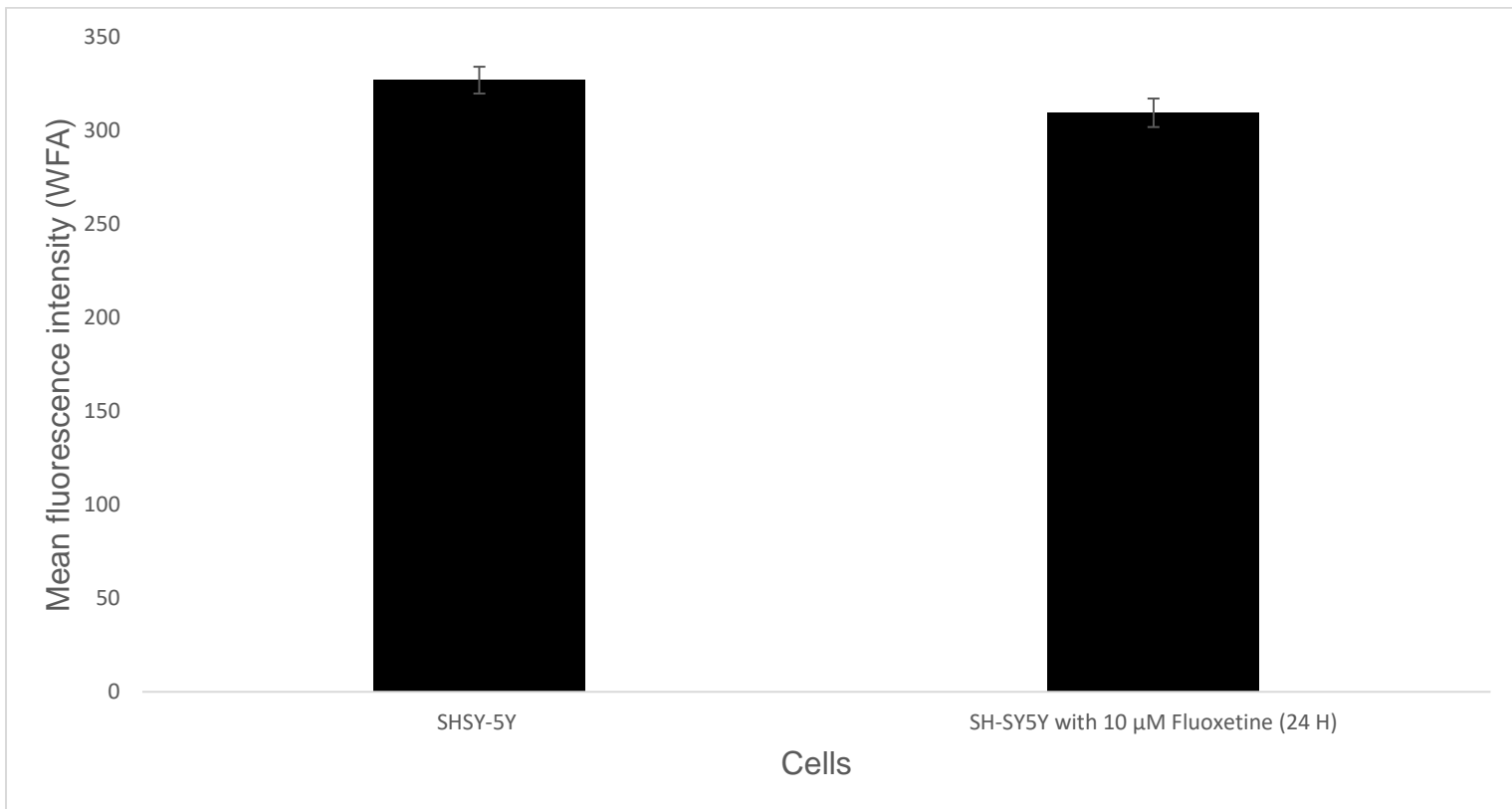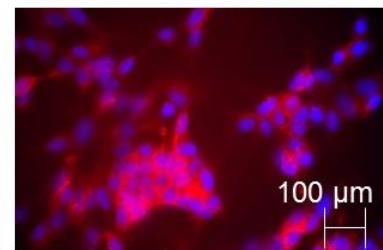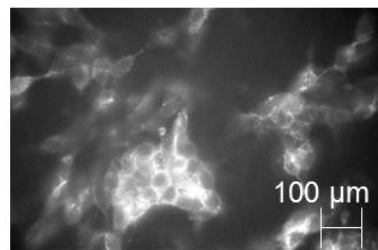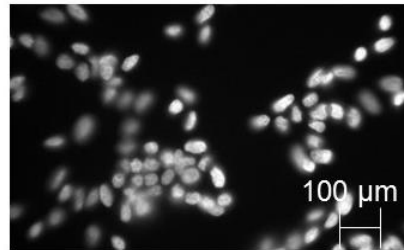
Cells

Figure 3.9. No effect on WFA staining when SH-SY5Y cells are treated with Fluoxetine. *Figure 3.9 shows the results obtained when SH-SY5Y cells are stained with WFA having also been treated with 10 μM Fluoxetine for 24 hours. As seen above, WFA staining can be seen with the red indicating WFA staining and the blue indicating DAPI. Fluoxetine did not decrease levels of WFA staining. In contrast with other studies, treatment of cells with fluoxetine has not decreased WFA staining. N=81 cells taken over two independent images for SH-SY5Y cells treated with fluoxetine for 24 hours so relevant statistical analysis was undertaken including two tail T-Testing and SEM. Analysis showed P>0.05. x 40 magnification, Scale bar = 100 μm.*
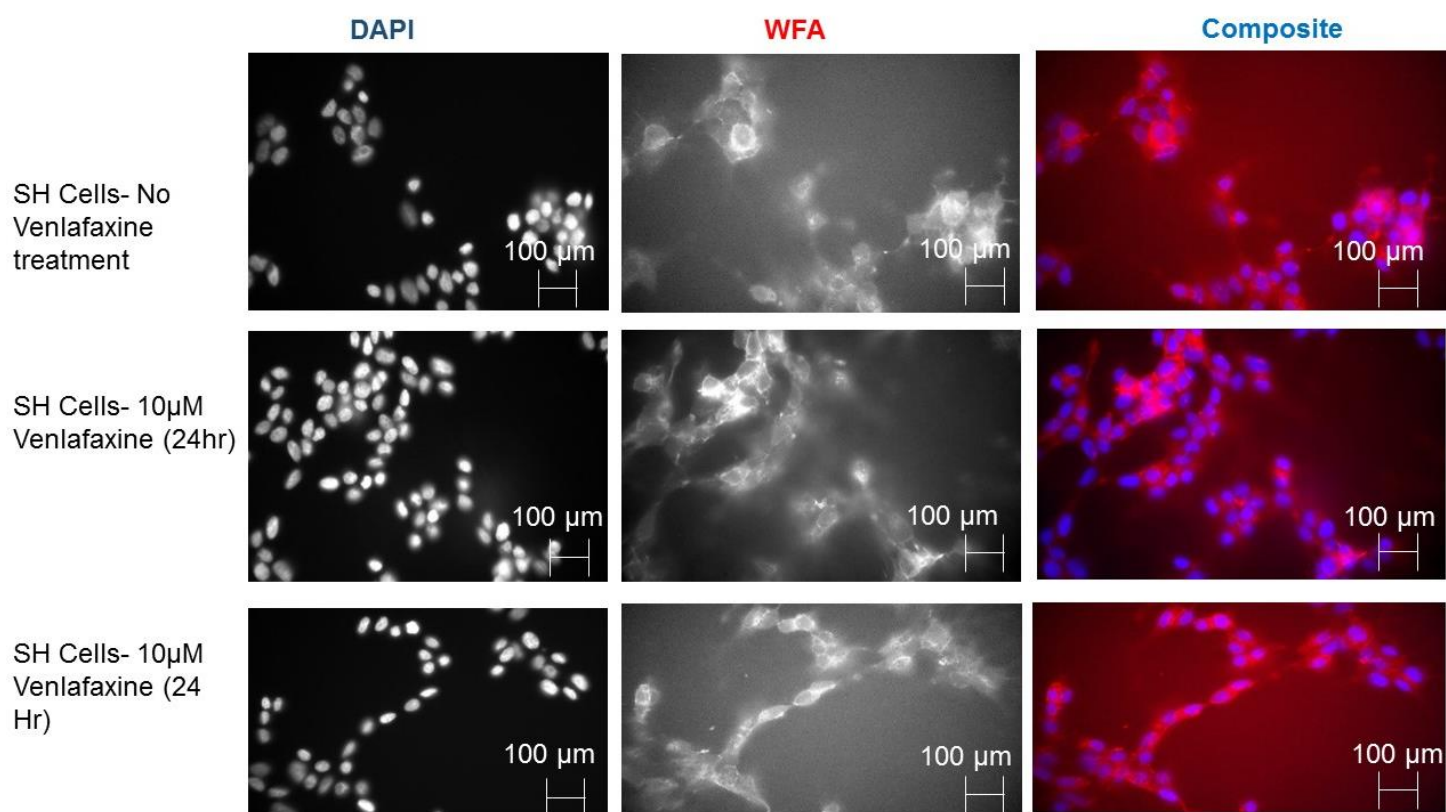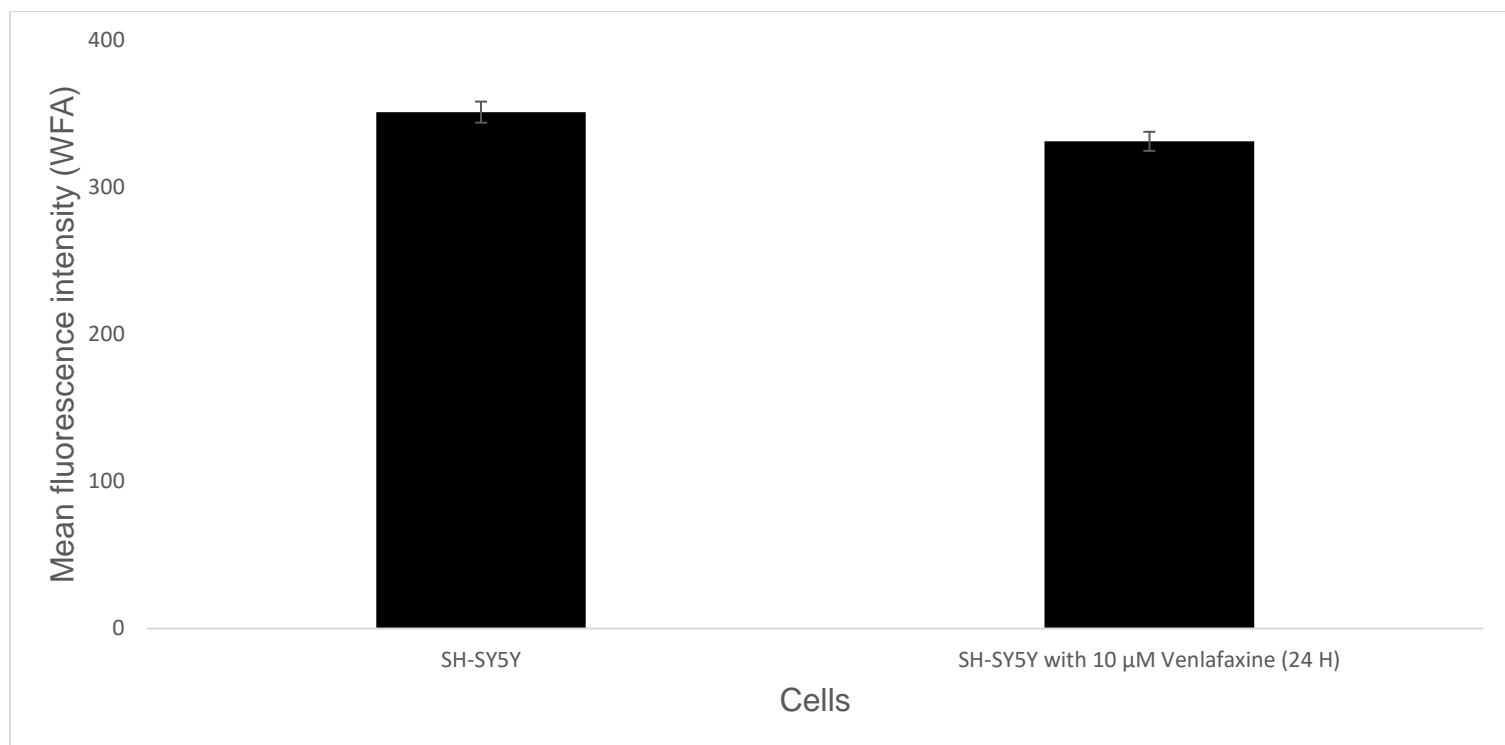
Figure 3.10 No effect on WFA staining when SH-SY5Y cells are treated with venlafaxine. *Figure 3.10 shows the results obtained when SH-SY5Y cells are stained with* WFA *having also been treated with venlafaxine. As seen above,* WFA *staining can be seen with the red indicating* WFA *staining and the blue indicating* DAPI*. Venlafaxine did not decrease levels of* WFA *staining. N=71 cells taken over two independent images for SH-SY5Y cells treated with Venlafaxine for 24 hours so relevant statistical analysis was undertaken including Two-tailed T-testing and SEM. Analysis showed P>0.05. x 40 magnification, Scale bar = 100 µm.*

	DAPI	**WFA**	**Composite**

SH Cells- No treatment (Control)

100 µm   100 µm   100 µm

SH Cells- 8.5 mM Lithium Chloride (24hr)

100 µm   100 µm   100 µm

SH Cells- 3µM 1-Azakenpaullone(24 Hr)

100 µm   100 µm   100 µm

Mean fluorescence intensity (WFA)

400
350
300
250
200
150
100
50
0

SH-SY5Y   Cells   SH-SY5Y with 8.5 mM lithium chloride (24 H)
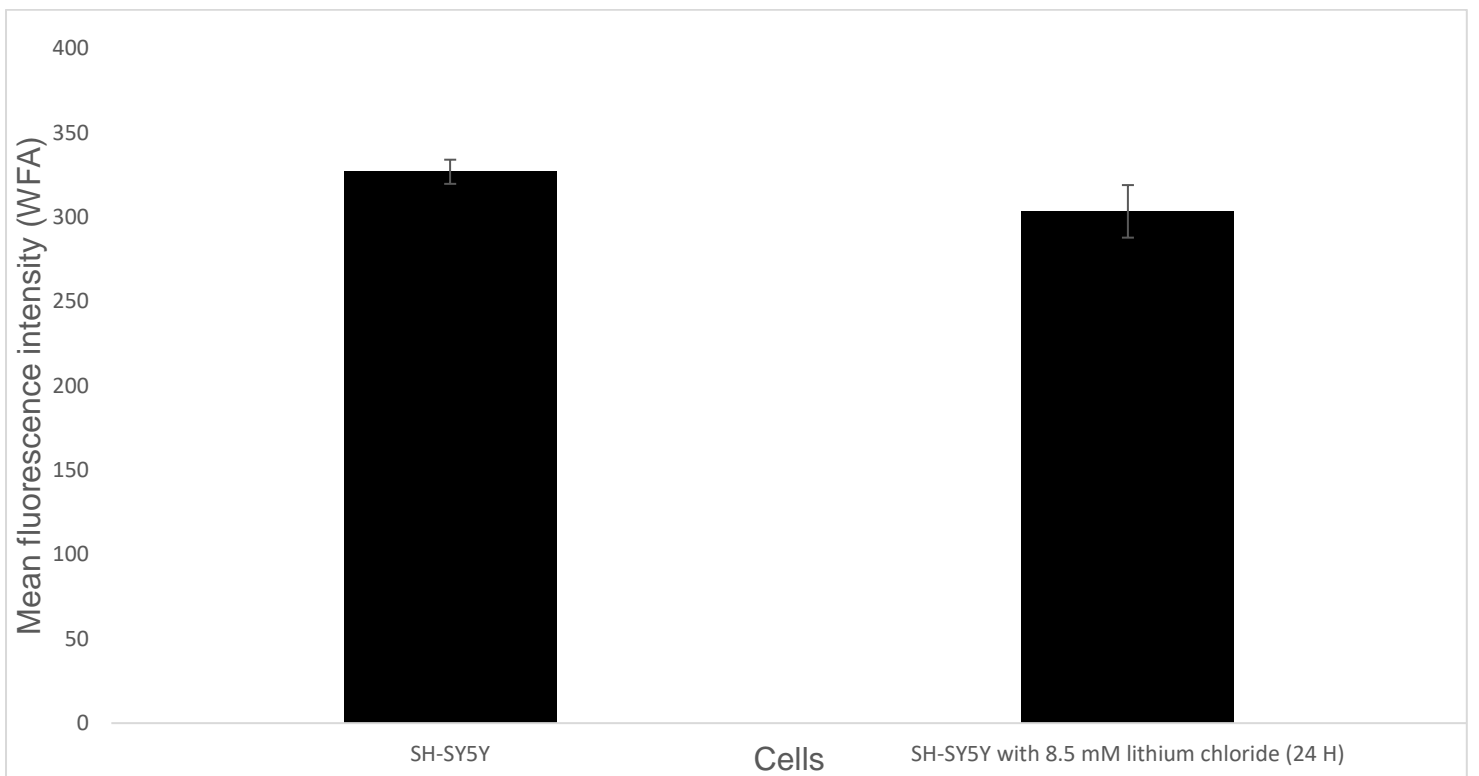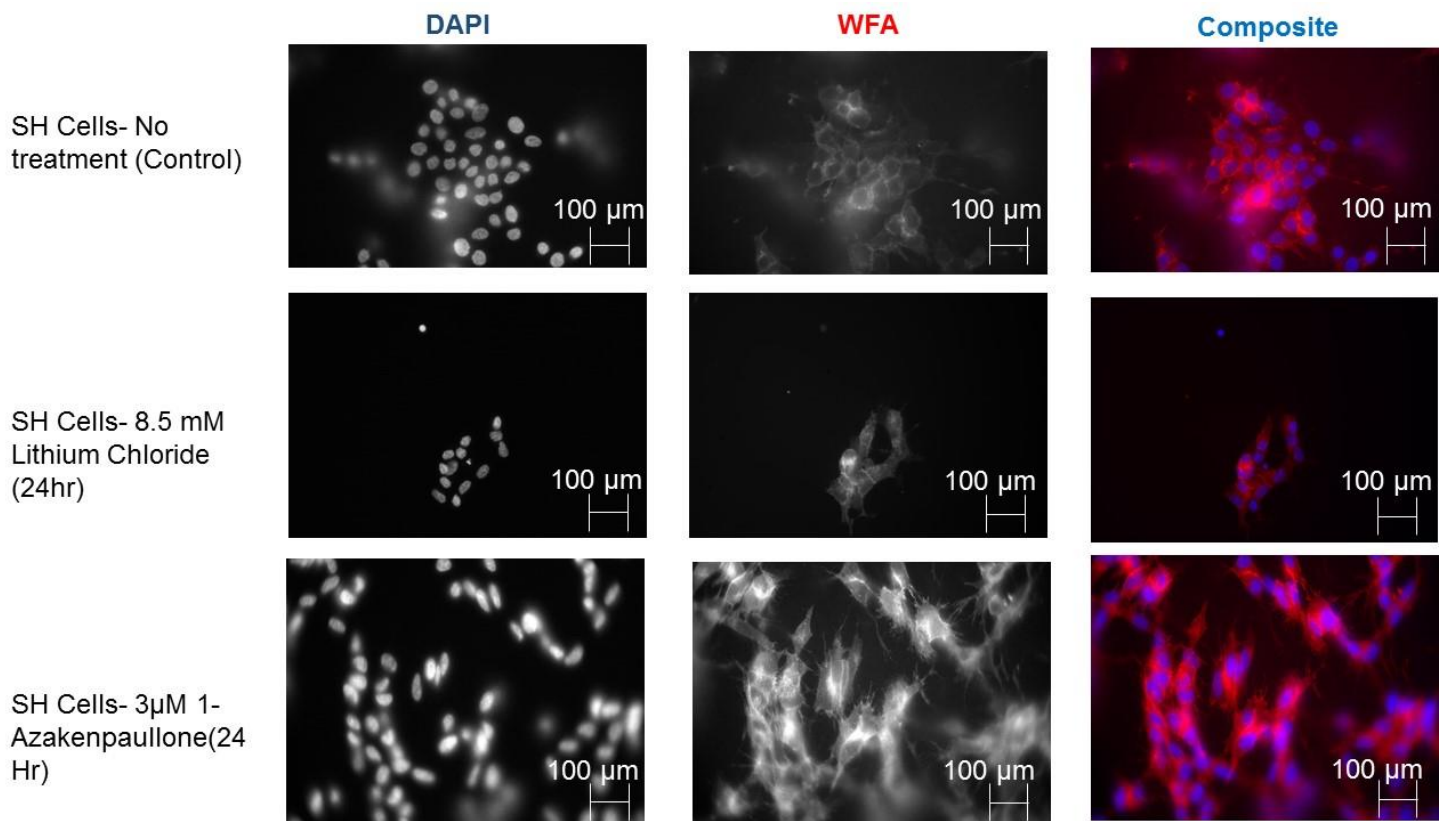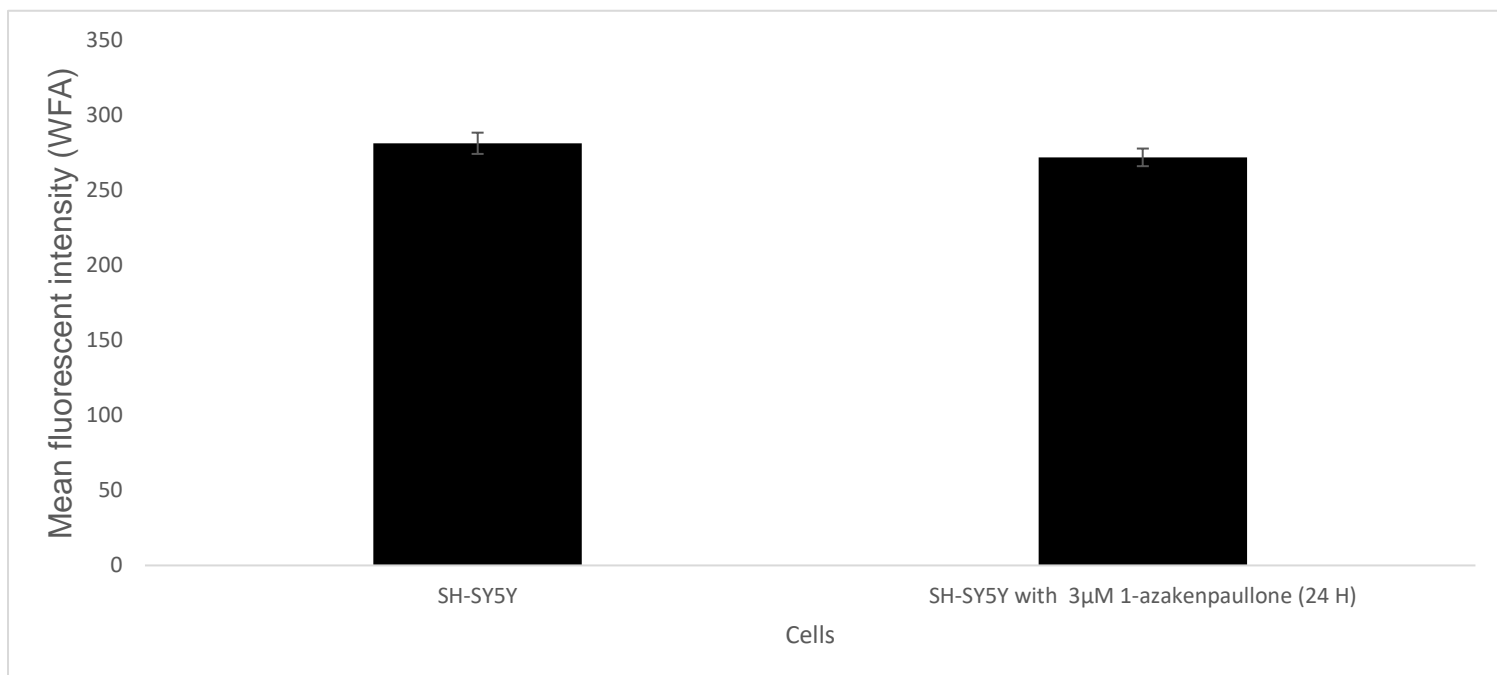
Figure 3.11 No effect on WFA staining when SH-SY5Y cells are treated with lithium or GSK 3 inhibitor (1-Azakenpaullone). *Figure 3.11 shows the results obtained when SH-SY5Y cells are stained with WFA having also been treated with Lithium and GSK 3 inhibitor (1-azakenpaulllone) for 24 hours. As seen above, WFA staining can be seen with the red indicating WFA staining and the blue indicating DAPI. Lithium did not decrease levels of WFA staining. 1-Azakenpaullone treatment of SH-SY5Y cells did not decrease levels of WFA staining. N=12 cells for lithium, 63 cells for 1-Azakenpaullone so relevant statistical analysis was undertaken including Two-tailed T-testing and SEM. Analysis showed P>0.05. x 40 magnification, Scale bar = 100 μm.*

The aim of these experiments was to determine whether pharmacological inhibitors influence WFA staining. Here, fluoxetine, Venlafaxine and lithium were utilised. Furthermore, 1-Azakenpaullone was also used as this is a GSK-3 inhibitor. Lithium has been long known to exert its effect via Gsk-3 in a direct or indirect manner. Cells were treated with respective drugs for 24-48 hours and then immunofluorescence microscopy was undertaken and western blotting. The results show that there was no effect on expression of glycoproteins that bind WFA using these inhibitors. Interestingly, the results I obtained here is in contrast to the literature where fluoxetine has been shown to decrease WFA staining in patients with bipolar disorder. However, those studies occurred on a primary cell line whereas the current studies were utilising secondary cell lines. Primary cell lines are more representative of the human body in contrast to secondary cell lines which may lose their neuronal

expression over time. Though there was no direct effect on WFA staining using GSK-3 inhibitor 1-Azakenpaullone as well as lithium.

3.5 Conclusion

In summary, *SH-SY5Y* cells do express a proteoglycan target(s) which can be recognised by WFA staining, and this is consistent with the presence of some form of perineuronal net staining on these cells. The staining appears to be a neuronal feature as it was absent in *A549* cells. However, while WFA staining clearly shows extracellular expression, the precise pattern and distribution of the presumptive PNN on *SH-SY5Y* cells differs from the classic image of PNNs on inhibitory interneurons in that it is not 'net-like' in its morphology. I failed to observe any effect of various pharmacological agents on WFA expression quantity or distribution on *SH-SY5Y* cells.

I still have no idea about the precise molecular target of WFA staining in *SH-SY5Y* cells or even *in vivo*. This prompted a research direction using WFA to 'pull down' potential proteoglycan constituents from lysed *SH-SY5Y* material for molecular analysis. This work is described in Chapter 7. However, the evidence suggests that *SH-SY5Y* cells are a viable cell model for the genetic dissection of perineuronal net formation using a WFA staining assay. The next question is whether the WFA staining protocol can be implemented on live cells to allow a genetic screen for phenotypic changes the PNN to take place. These questions are addressed in the next chapter.

CHAPTER 4

RESULTS: Using a gene trap screen to identify critical genes for PNN formation

4.1 Introduction and screening technology optimisation

In chapter 3, it was demonstrated that *SH-SY5Y* cells are a potential model cell line to investigate perineuronal nets due to their WFA staining profile. Following on from this, a gene trap screen was undertaken to identify genes critical for perineuronal net formation. For a successful gene trap screen to occur, a high-quality gene trap library must be used which has broad genome coverage. For these experiments, a SH-SY5Y gene trap library was provided by Dr Benjamin Pickard. Gene trap mutagenesis produces random insertional mutations via genomic integration of a gene trap plasmid vector. Originally used to generate mutant embryonic stem cells, gene trap mutagenesis has since undergone substantial development and found its usefulness in identification of novel gene functions and molecular mechanisms (Yap *et al.*, 2021) pGTIV3, an advanced poly(A) trap vector containing a human β-actin promoter upstream of neoR gene and a rabbit β-globin-derived splice donor (SD) sequence was employed (Yap *et al.*, 2021). This vector is unique, with the inclusion of a synthetic intron with a cis-acting mRNA destabilizing AU rich element (ARE) which degrades the transcribed Neomycin resistance (neoR) mRNA if expressed (Tsakiridis *et al.*, 2009). If the gene trap vector non-productively integrates into the genome outside of a gene, the synthetic intron is not removed resulting in the inclusion of the ARE which disintegrates the resulting neoR mRNA transcript, and the cell does not gain resistance to neomycin selection (Tsakiridis *et al.*, 2009) .Only true SD splicing events resulting from disruptive vector insertion into a gene intron permit the neoR to splice with the 3' end of the endogenous gene (thereby disrupting it) and generating neomycin resistance under selection. The fusion transcript between neoR and the 'trapped' endogenous gene can be analysed to identify it. To generate the library, pGTIV3 was introduced into the *SH-SY5Y* neuroblastoma cell line genome using electroporation to produce a library of cells which collectively represented approximately 15,000 different heterozygote gene mutations.
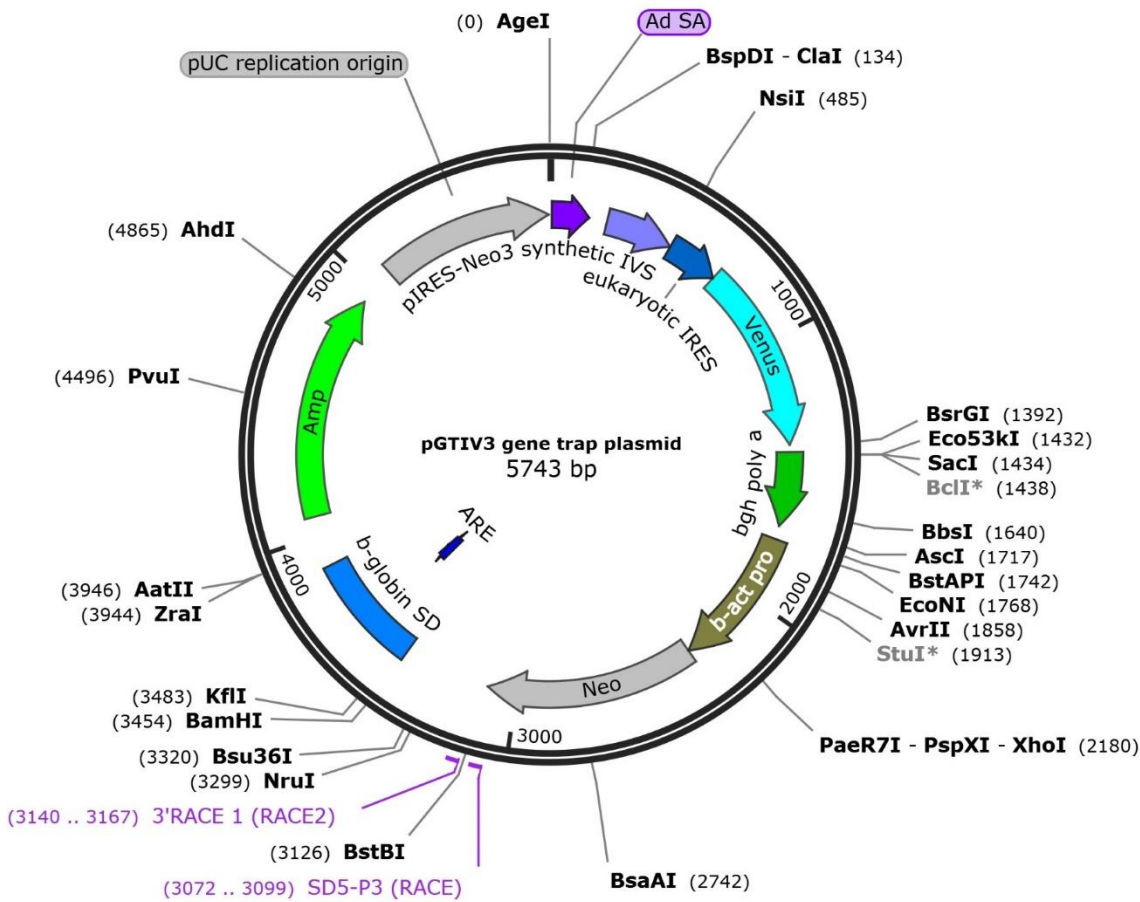
Figure 4.1 The pGTIV3 gene trap plasmid used in the creation of the mutant SH-SY5Y gene trap library (map created in SnapGene) as illustrated in Figure 2.1. For detailed explanation, please refer back to figure 2.1

One of the fundamental techniques required for the intended gene trap screen was live cell staining with WFA. This would allow the library cells to be kept alive and examined under the microscope to determine which colonies had WFA staining and which were showing reduced WFA staining. These negative colonies would then be picked, grown up to confluence, and RNA extracted, cDNA synthesised, and RACE-PCR performed, leading to mutated gene identification.

4.2 Optimising library plating and live staining procedures

A low plating density of library cells in 6 well plates enabled colonies to grow to a reasonable size for staining and picking purposes. This is illustrated in Figure 4.2 below.
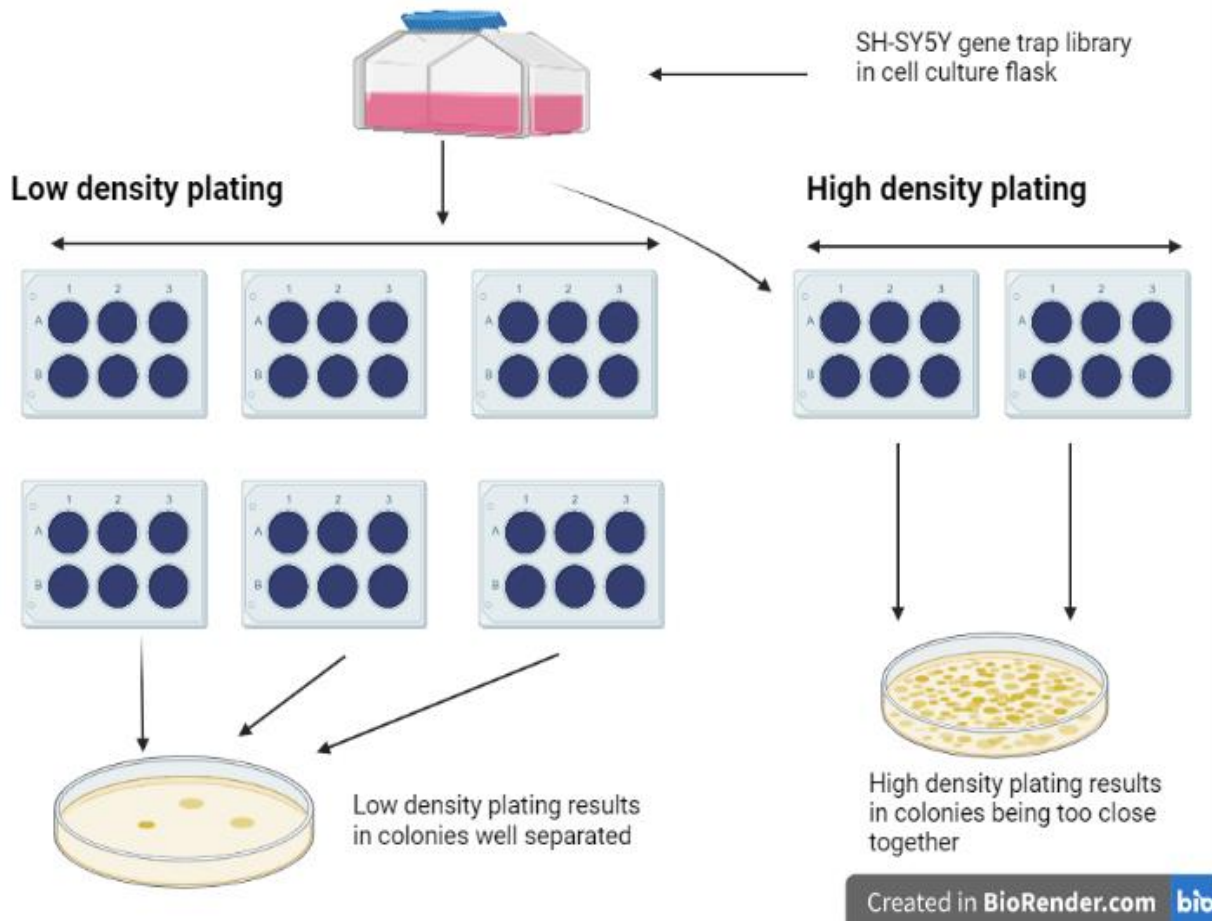
Figure 4.2 Plating out the SH-SY5Y mutant cell library to obtain larger, distinct colonies. *Figure 4.2 is a schematic produced in BioRender showing how the mutant gene trap library was plated out to obtain practical mutant colony sizes.*

These plates were initially stained with WFA streptavidin-green fluorophore to identify which colonies were producing a perineuronal net and which had no staining or reduced staining as examined under an inverted epifluorescence microscope. However, due to the way the gene trap vector was constructed, mutant *SH-SY5Y* cells also expressed Venus yellow fluorescent protein which overlapped in emission parameters with the green fluorophore conjugated to WFA (see figure 4.3).
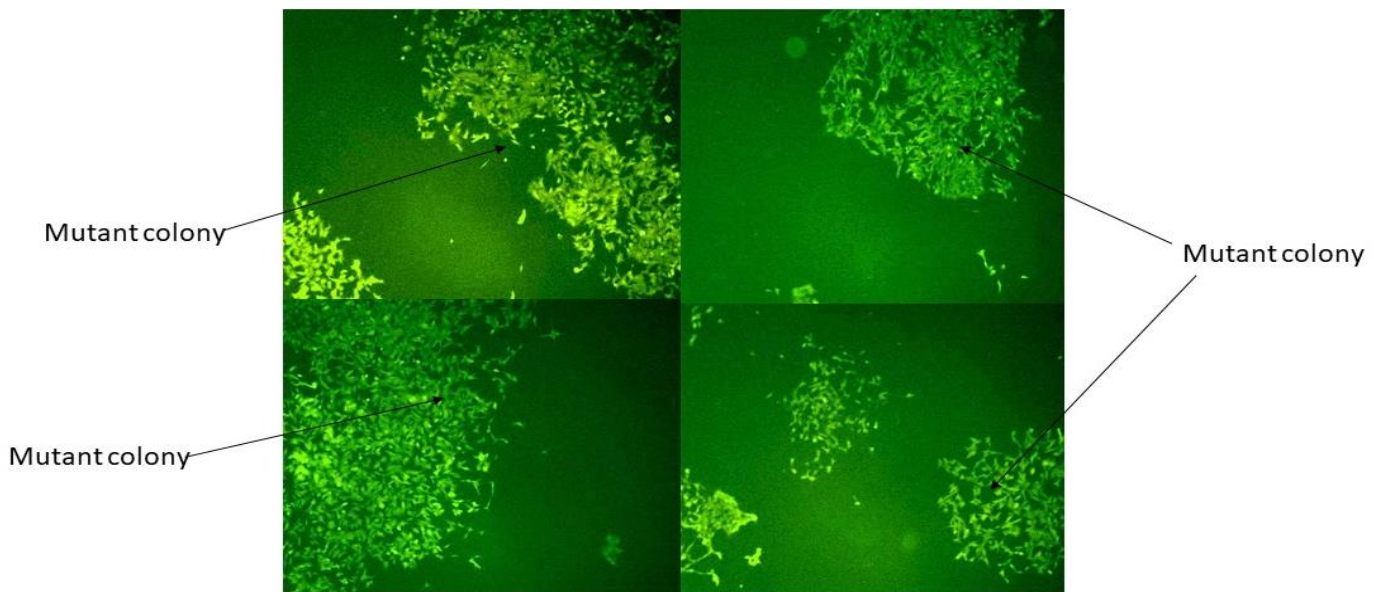
Figure 4.3 Exogenous venus fluorescent protein expression makes detection of PNN levels with a green probe impossible. Figure 4.3 above represents the live cell staining of SH-SY5Y mutant colonies with WFA conjugated to green fluorescent dye. However, since gene trap mutant colonies also contain a yellow (Venus) fluorescent protein which overlaps in its emission spectrum with the green dye, it was impossible to decipher which mutant colonies had reduced WFA staining.

To counter this issue, I ideally would have used WFA conjugated to a red fluorophore. Unfortunately, there is no commercially available red dye-conjugated WFA, so a composite [WFA-biotin]-[streptavidin-red fluorophore] staining approach was adopted to identify colonies with reduced WFA staining. Streptavidin is a protein that shows considerable affinity for biotin, a co-factor that plays a role in multiple eukaryotic biological processes (see Fig. 4.4).
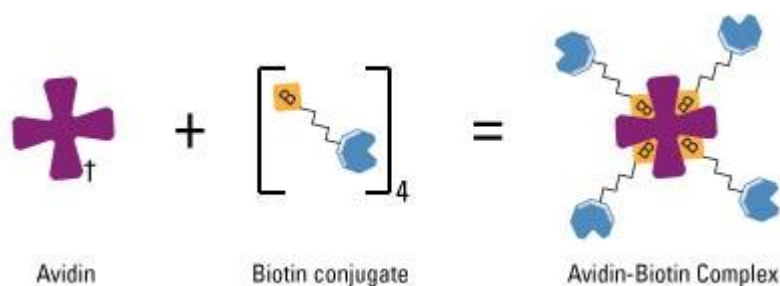
Figure 4.4 Schematic of the Avidin-biotin interaction. Avidin, Streptavidin or NeutrAvidin proteins can bind up to four biotin molecules, which are normally conjugated to an enzyme, antibody, or target protein to form an Avidin-biotin complex.

The streptavidin-biotin complex is the strongest known non-covalent interaction (K_{id} = 10^{-15} M) between a protein and ligand. The interaction between biotin and streptavidin is very rapid, and once formed, is unaffected by extremes of pH, temperature, organic solvents, and other denaturing agents. These features assisted the rapid live staining of the plated libraries, important as I wished to minimise the time that the cells spent outside of the incubator conditions.

This new live staining approach worked well, showing minimal background fluorescence in control experiments (see fig 4.5).
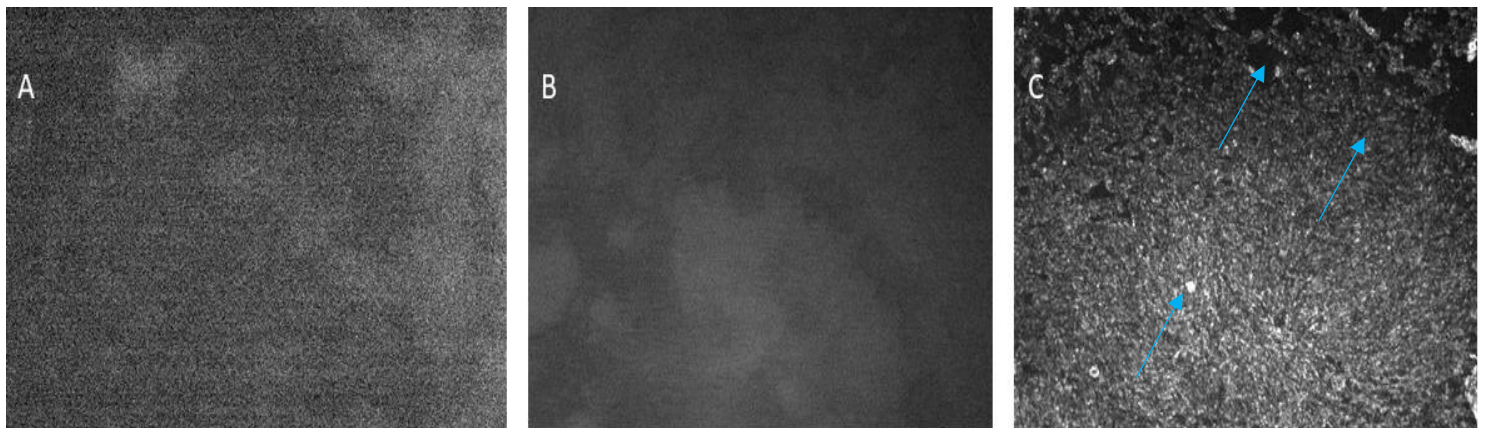
Figure 4.5 WFA-*biotin and streptavidin-red fluorophore complex testing*. *Live staining was undertaken of SH-SY5Y mutant colonies with the new composite probing protocol. I can clearly distinguish background from genuine PNN staining in the controls. A: No Streptavidin and No WFA. B: Streptavidin only. C: SH-SY5Y cells stained with biotinylated WFA and streptavidin-red. Panel C shows live-cell staining of fairly dense colonies of SHSY5Y with most cells showing reasonable amount of staining (grey), some with higher staining (white) and maybe some regions that are potential mutants with little staining (darker/black regions*

4.3 Results of the screen

The live cell screening process of mutant *SH-SY5Y* cells to identify colonies with no or reduced WFA staining was carried out with potentially interesting colonies marked by marker pen on plate lids and then picked in a laminar flow hood. Picked cells were grown up to confluence, taken through a secondary screen to isolate clonal mutants, and then frozen down as archived stocks. There were

nine mutant colonies chosen for analysis as these were deemed to have reduced WFA staining or abnormal shape.
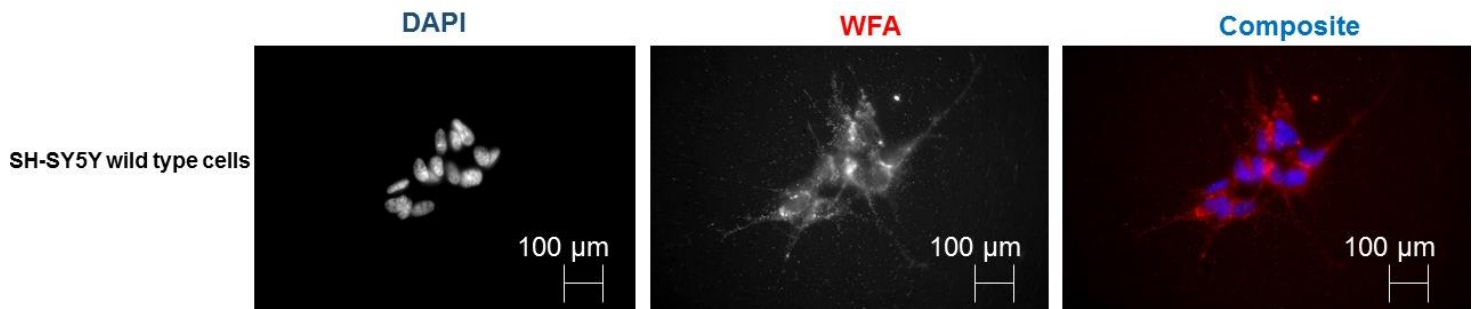
Figure 4.6 Successful WFA staining of SH-SY5Y cells. *Figure 4.6 above represents the results obtained during the fixation process with staining using biotinylated* WFA. *left:* DAPI *(Control). centre: Biotinylated* WFA *(Control), right: Composite (Control). As seen above, bright staining occurred identifying PNN's. This was done as a positive control to show that* WFA *staining of perineuronal nets was occurring in SH-SY5Y cells.* x40 magnification, scale bar= 100µm

Cells from the nine isolated colonies were plated out for further validation using a full fixation/immunofluorescence approach. Fixed cells were stained overnight (4°C) with WFA and mounted with DAPI counterstain and antifade solution and imaged using epifluorescence microscope and camera (Methods). Images were processed and colour composites created using ImageJ (Fig 4.7, 4.8, 4.9, 4.10, 4,11, 4.12, 4.13, 4.14)
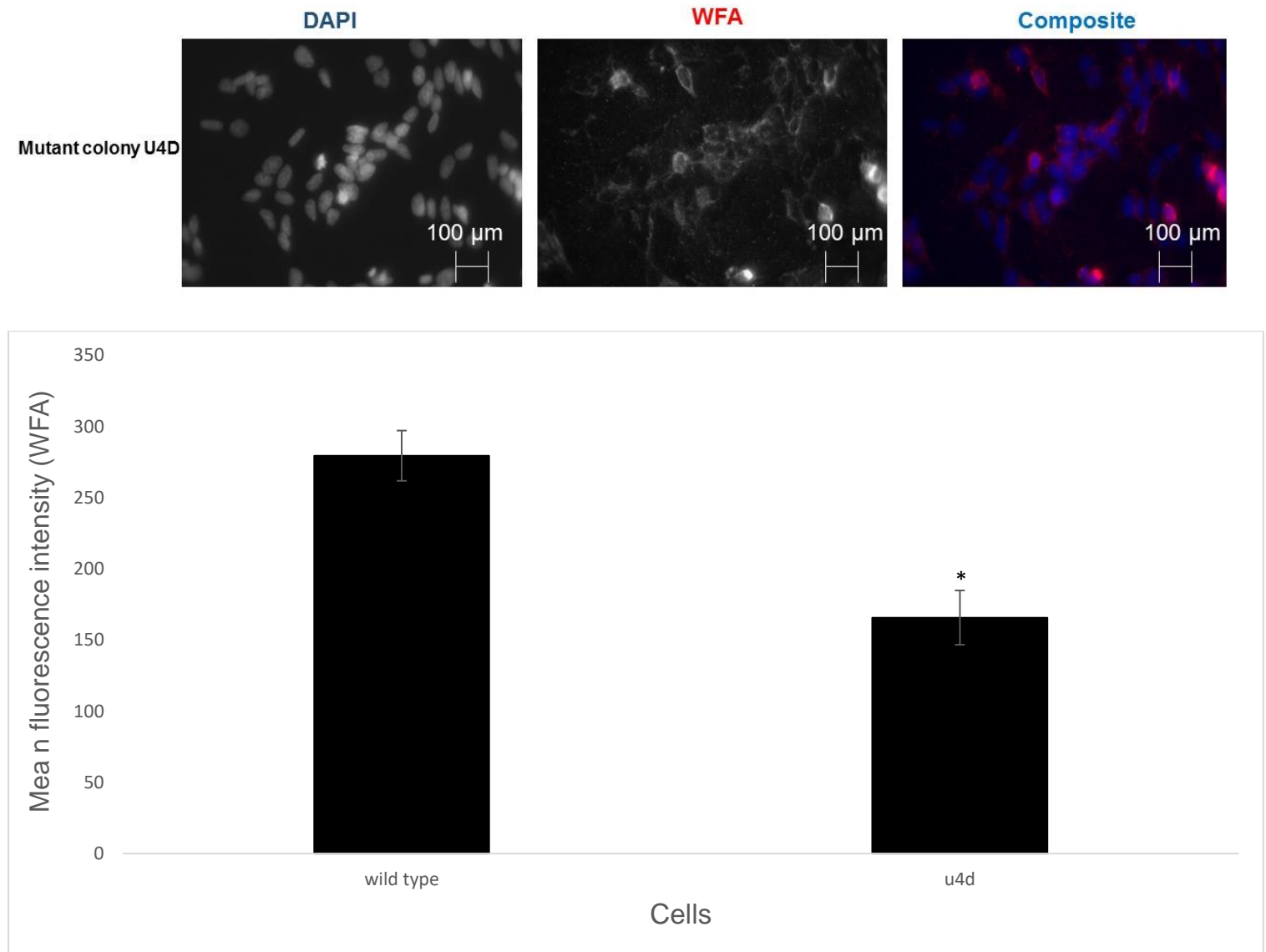
Figure 4.7 Reduced WFA *staining seen in mutant colony U4D.* *SH-SY5Y   mutant colony U4D stained with biotinylated* WFA*. Figure 4.7 above represents the results obtained during the fixation process with staining using biotinylated* WFA*. left:* DAPI *(U4D). centre: Biotinylated* WFA *(U4D). right: Composite (U4D). As seen above, reduced staining has occurred. Reduced staining is attributed to the mutant colony failing to produce a PNN or abnormal staining. Here, reduced staining can be seen and an abnormal perineuronal net shape. N=12 so statistical analysis was undertaken including two tail T-Testing and SEM. *P<0.05. X40 magnification, Scale Bar = 100µm*

4.3.2 Mutant colony P38A displays reduced WFA-binding glycoprotein expression.
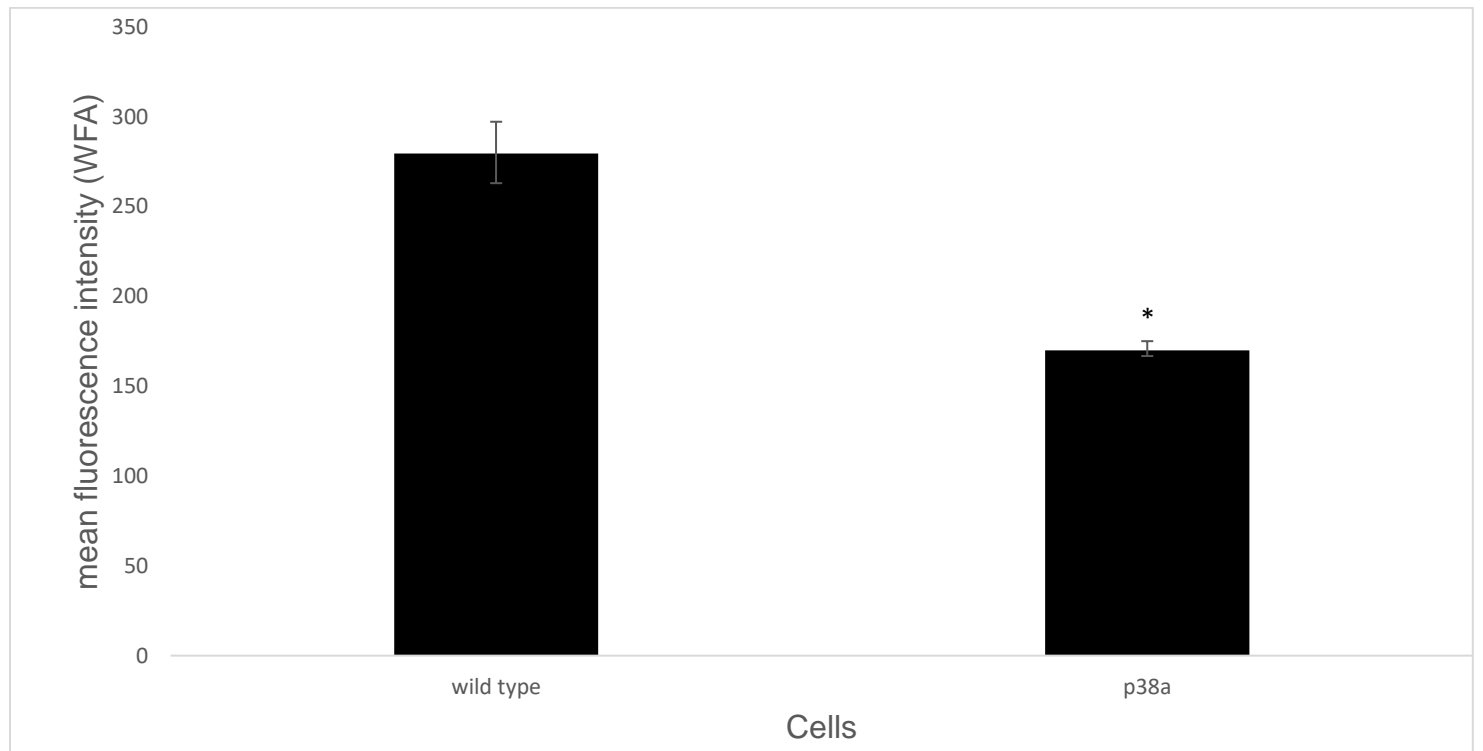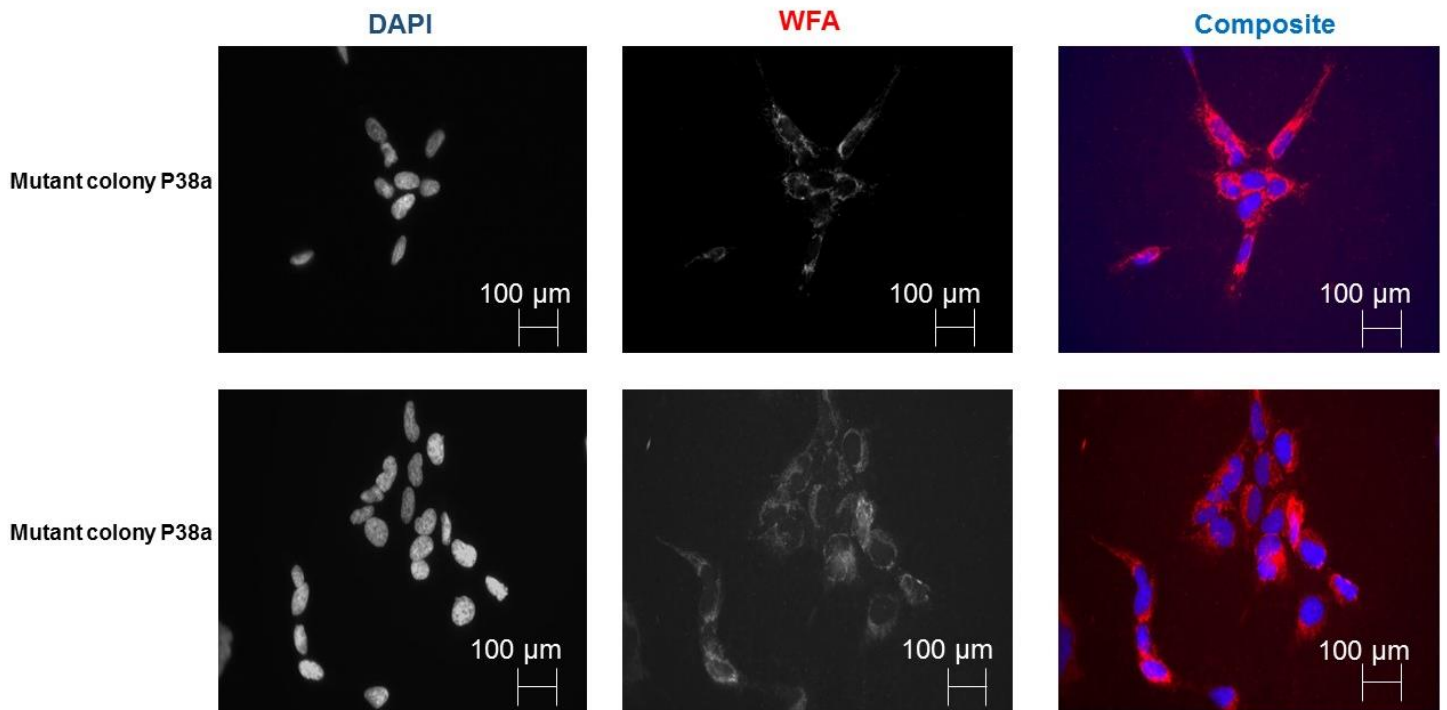
Figure 4.8 Mutant colony P38A has reduced** WFA **staining and an abnormal shape compared to wild type. *SH-SY5Y mutant colony P38A stained with biotinylated WFA. Figure 4.8 above*

represents the results obtained during the fixation process with staining using biotinylated WFA. As seen above, reduced staining has occurred. Reduced staining is attributed to the mutant colony failing to produce a PNN or abnormal staining. N=27 taken over two independent images so relevant statistical analysis was undertaken including two tail T-Testing and SEM *P<0.05. X40 magnification, Scale bar = 100µm.

4.3.3 Mutant colony U1B displays reduced WFA-binding glycoprotein expression
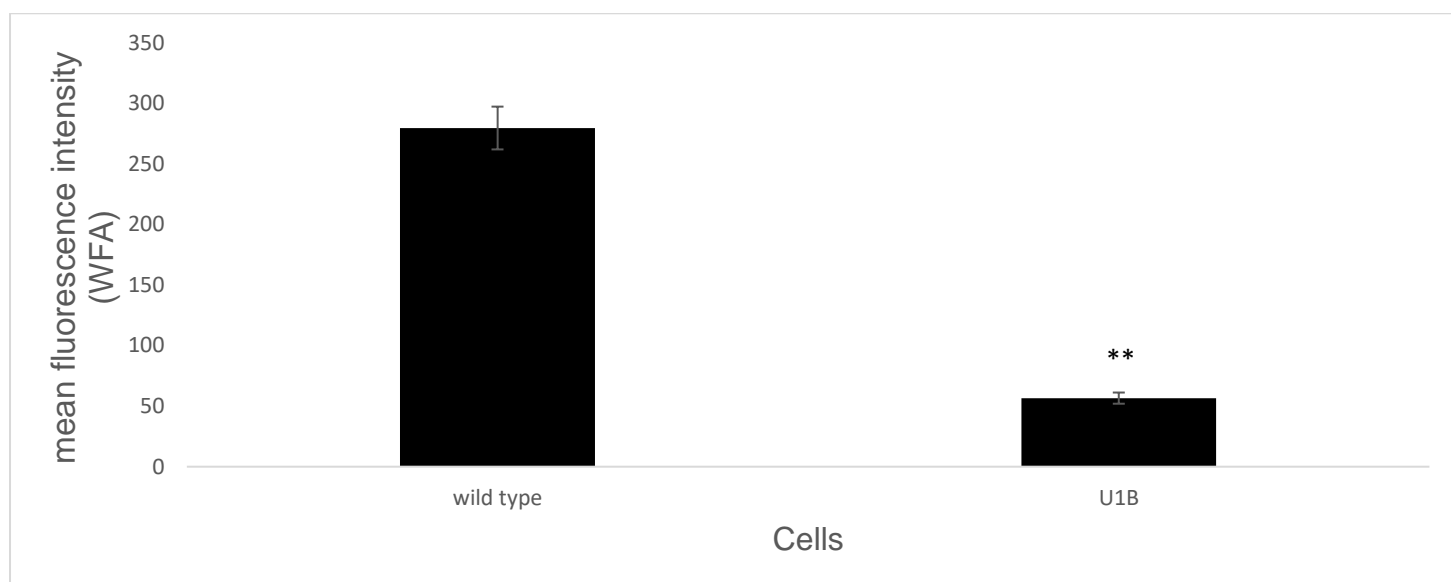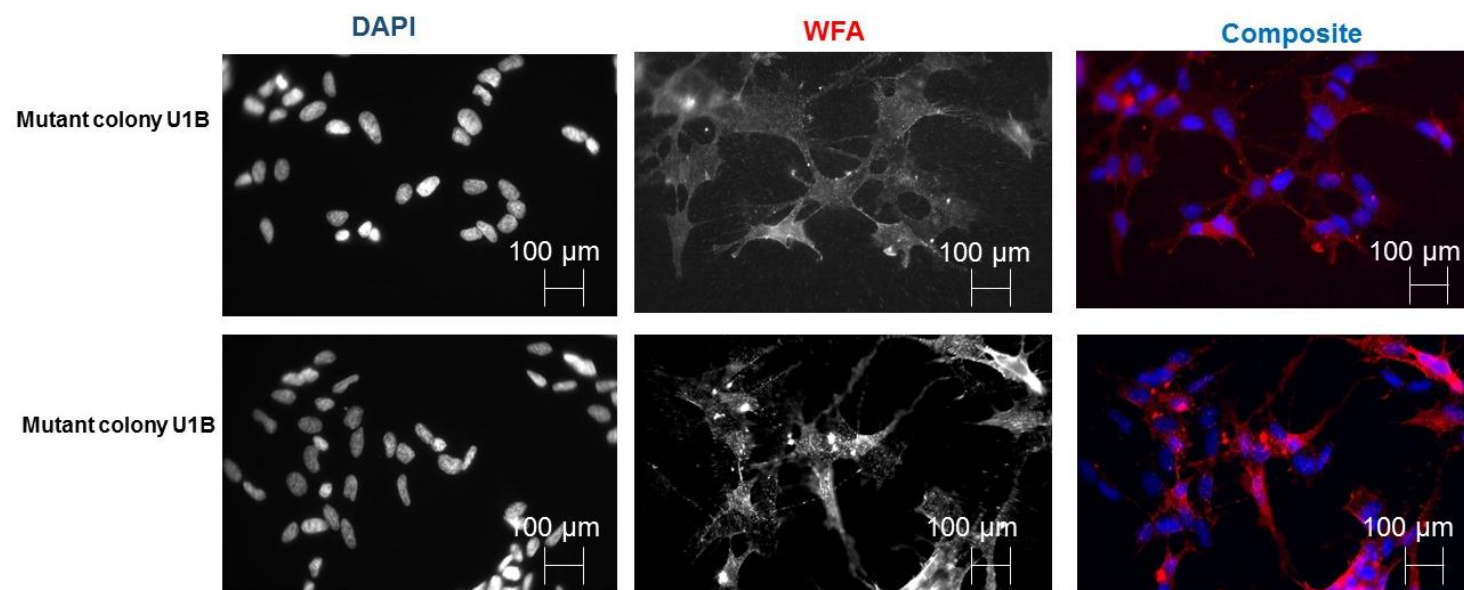
Figure 4.9. Reduced WFA *staining seen in mutant colony U1B SH-SY5Y mutant colony*. U1B stained with biotinylated WFA. Figure 4.9 above represents the results obtained during the fixation process with staining using biotinylated WFA. As seen above, reduced staining has occurred.

Reduced staining is attributed to the mutant colony failing to produce a PNN or abnormal staining. N=38 taken over two independent images so relevant statistical analysis was undertaken including two tail T-Testing and SEM **P<0.01. X40 magnification, Scale bar= 100μm.

4.3.4 Mutant colony P36b displays no reduced WFA staining.
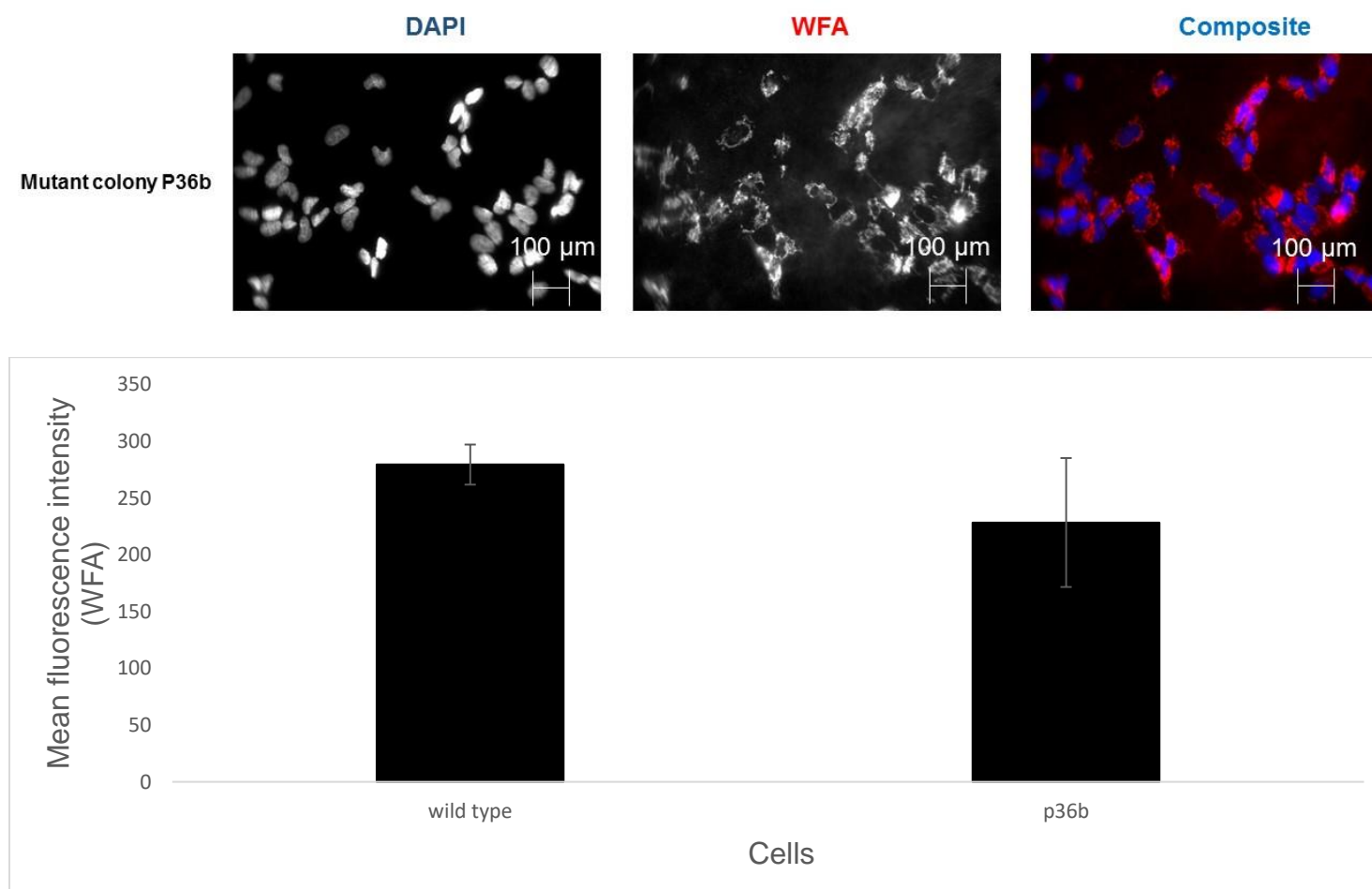
Figure 4.10 Mutant colony P36 b has no change in WFA staining. *SH-SY5Y mutant colony P36B stained with biotinylated WFA. Figure 4.10 above represents the results obtained during the fixation process with staining using biotinylated WFA. As seen above, reduced staining has occurred. Reduced staining is attributed to the mutant colony failing to produce a PNN or abnormal staining. N=12 so relevant statistical analysis was undertaken including two tail T-Testing and SEM. P>0.05. X40 magnification, Scale bar = 100μm*

4.3.5 Mutant colony P37b displays reduced WFA staining.
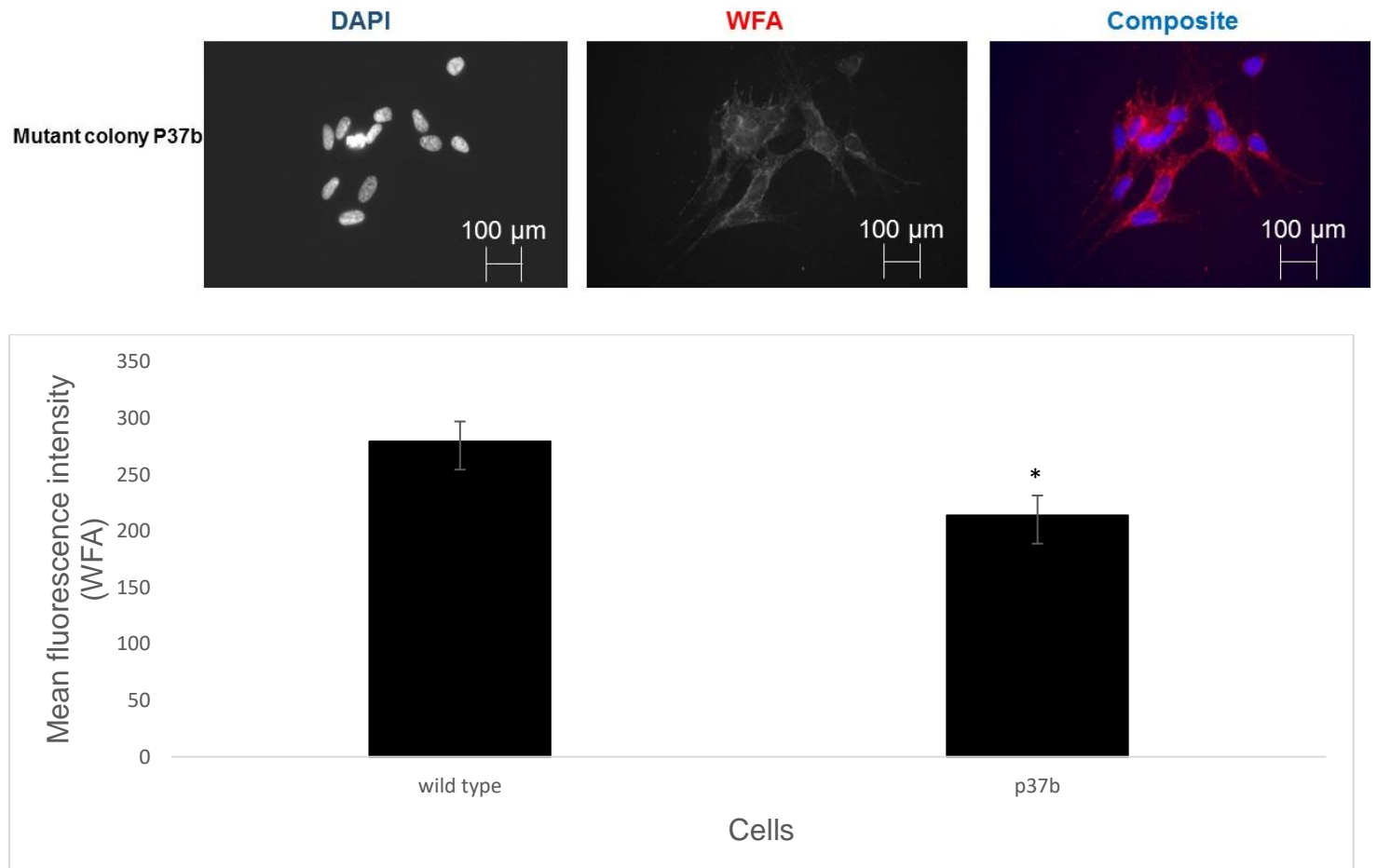
Figure 4.11 Mutant colony P37b has reduced WFA staining. *SH-SY5Y mutant colony P37b stained with biotinylated WFA. Figure 4.11 above represents the results obtained during the fixation process with staining using biotinylated WFA. As seen above, reduced staining has occurred. Reduced staining is attributed to the mutant colony failing to produce a PNN or abnormal staining. N=15 so relevant statistical analysis was undertaken including two tail T-Testing and SEM. *P<0.05. X40 magnification, Scale bar = 100μm*

4.3.6 Mutant colony P39a displays reduced WFA staining
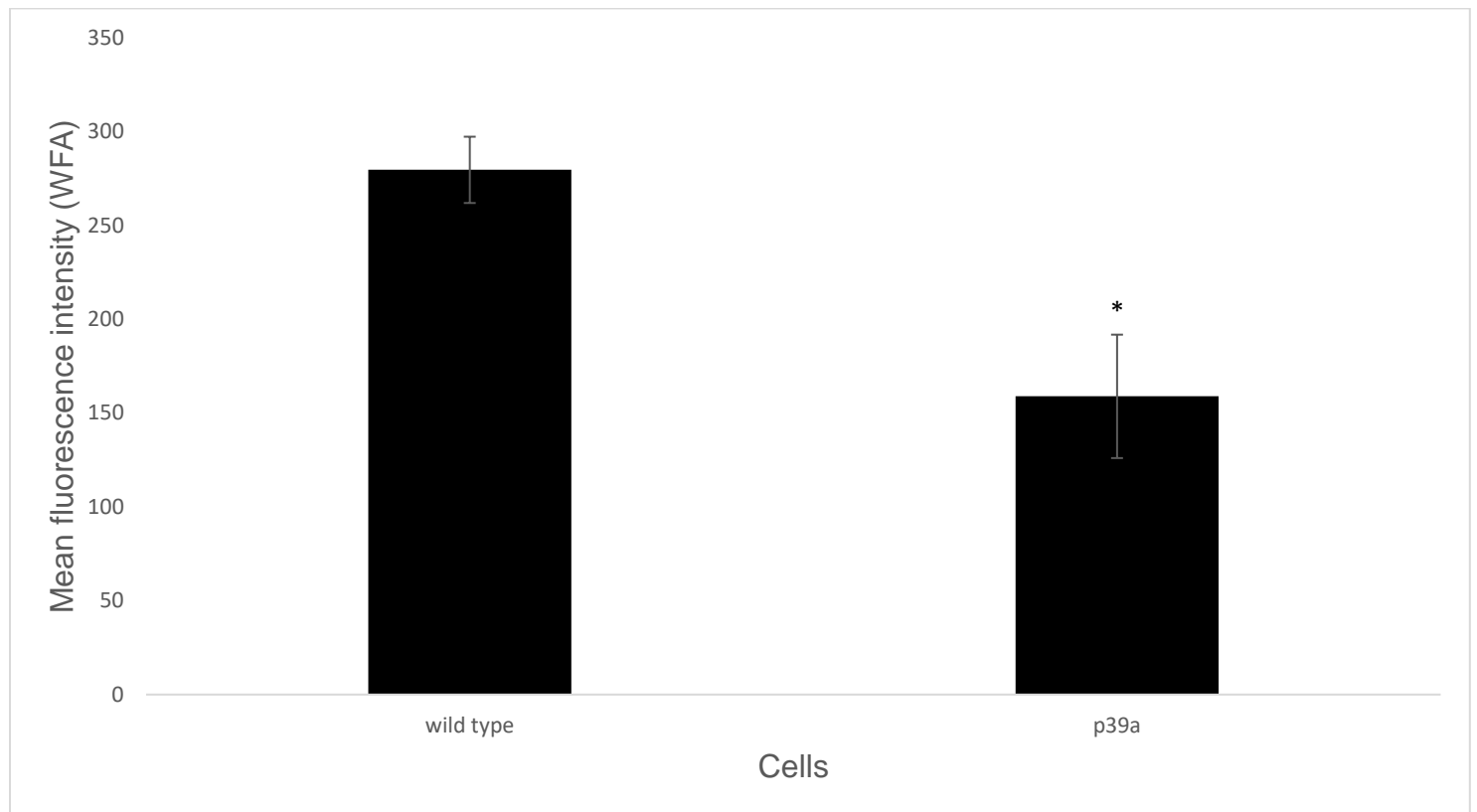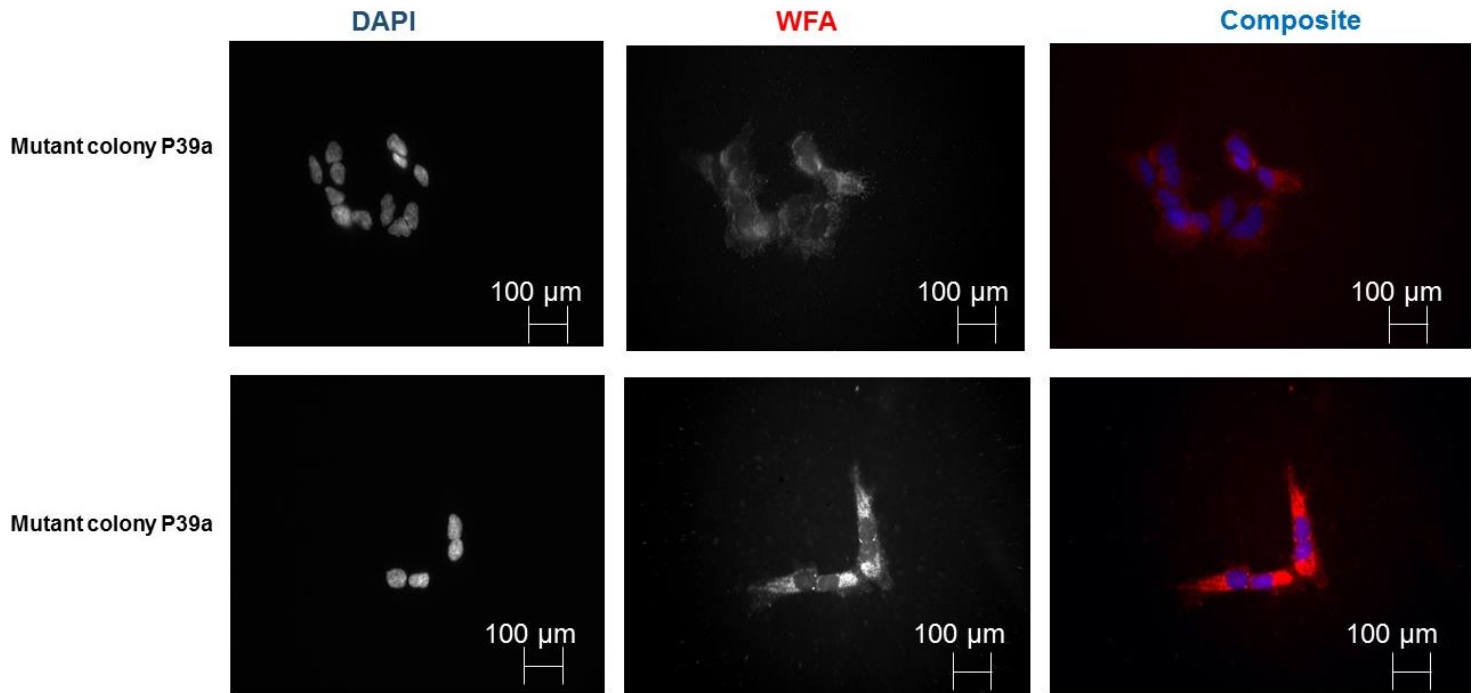
Figure 4.12 Mutant colony P39a has reduced WFA staining. *SH-SY5Y mutant colony P39a stained with biotinylated WFA. Figure 4.12 above represents the results obtained during the fixation process with staining using biotinylated WFA. As seen above, reduced staining has occurred. Reduced staining is attributed to the mutant colony failing to produce a PNN or abnormal staining.*

*N=21 taken over two independent images so relevant statistical analysis was undertaken including two tail T-Testing and SEM. *P<0.05. X40 magnification, Scale bar = 100µm*

4.3.7 Mutant colony u6a displays reduced WFA staining
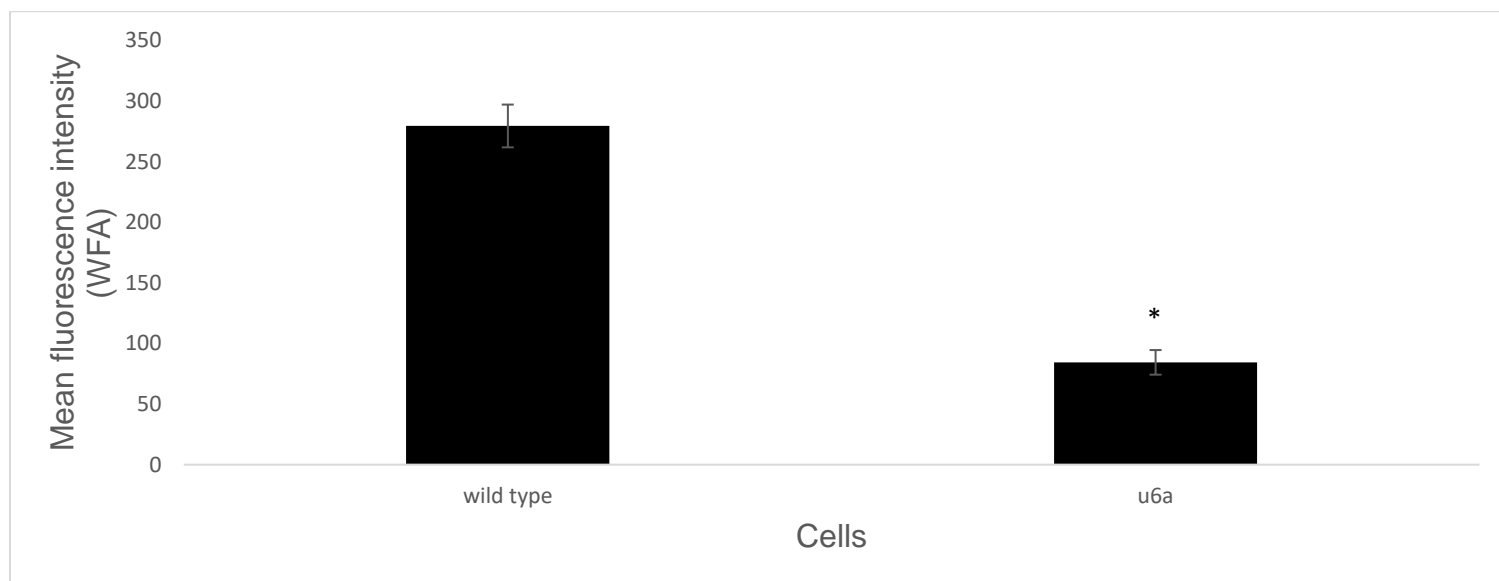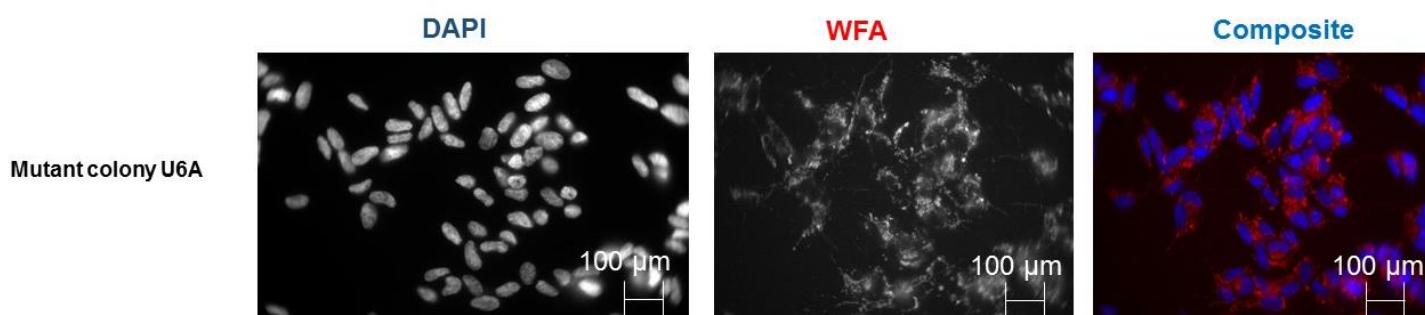
Figure 4.13 Reduced WFA staining seen in mutant colony U6a. *SH-SY5Y mutant colony U6A stained with biotinylated WFA. Figure 4.13 above represents the results obtained during the fixation process with staining using biotinylated WFA.As seen above, reduced WFA staining is seen in mutant colony U6A. N=90 cells so relevant statistical analysis was undertaken including two tail T-Testing and SEM *P<0.05. X40 magnification, Scale bar = 100µm*

4.3.8 Mutant colony U9B displays no change in WFA staining.
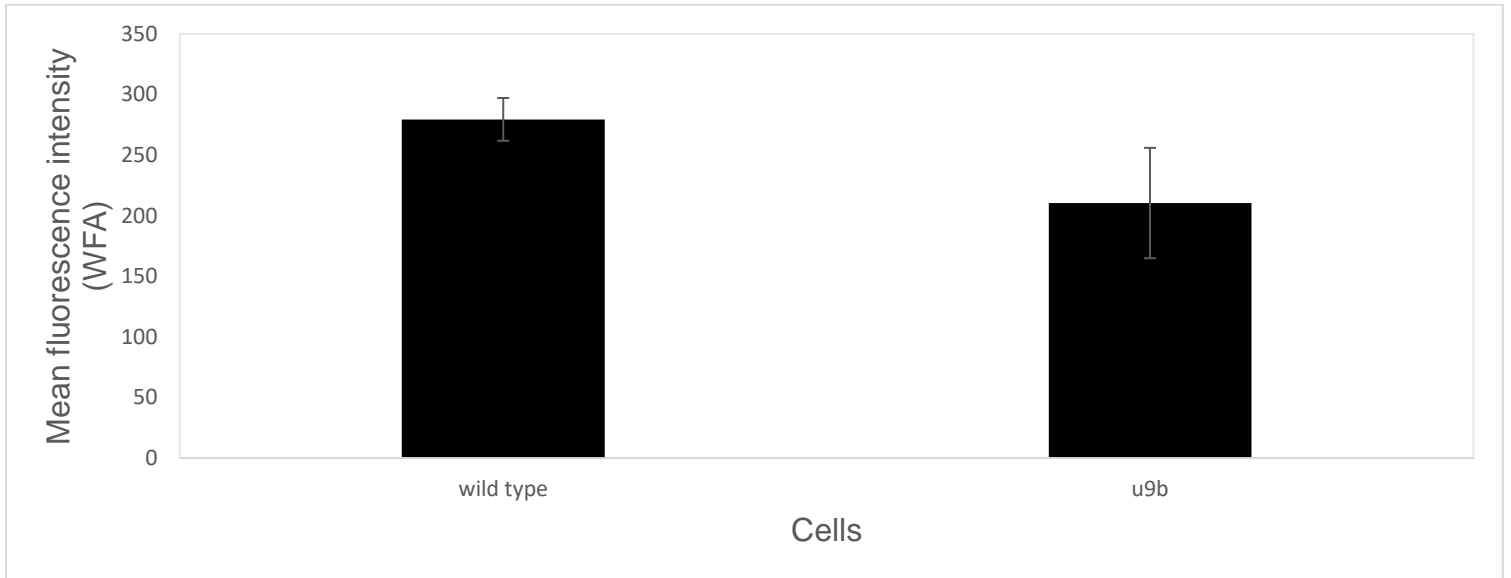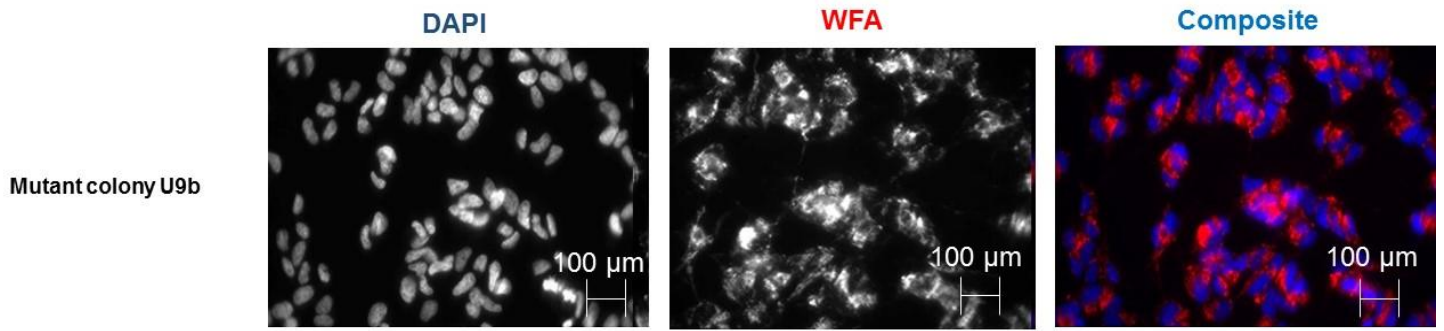
Figure 4.14 No change in WFA *staining seen in mutant colony U9B.* *SH-SY5Y mutant colony U9B stained with biotinylated* WFA*. Figure 4.14 above represents the results obtained during the fixation process with staining using biotinylated* WFA*. As seen above, reduced levels of staining are seen in mutant colony U9B. N=114 so relevant statistical analysis was undertaken including two tail T-Testing and SEM. P>0.05. X40 magnification, Scale bar = 100μm*

4.3.9 Analysing the expression of *Neurocan* and *Versican* in selected mutant colonies.

Any modification of the PNN by mutation would also be predicted to affect the distribution of known PNN components such as *Neurocan* and *Versican*. Selected mutant colonies P38A, U1B and U4D were chosen for standard immunofluorescence with antibodies against these two proteins. Images were processed, and colour composites created using ImageJ (Figure 4.15, Figure 4.16, Figure 4.17, Figure 4.18, Figure 4.19, Figure 4.20).
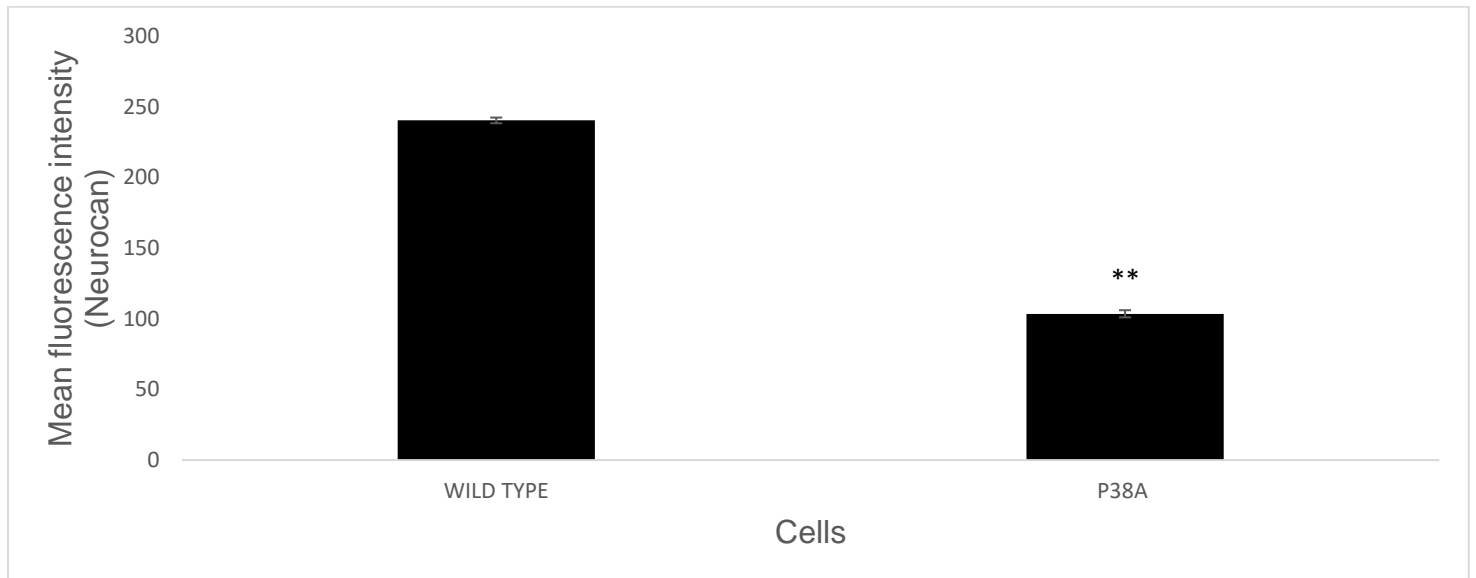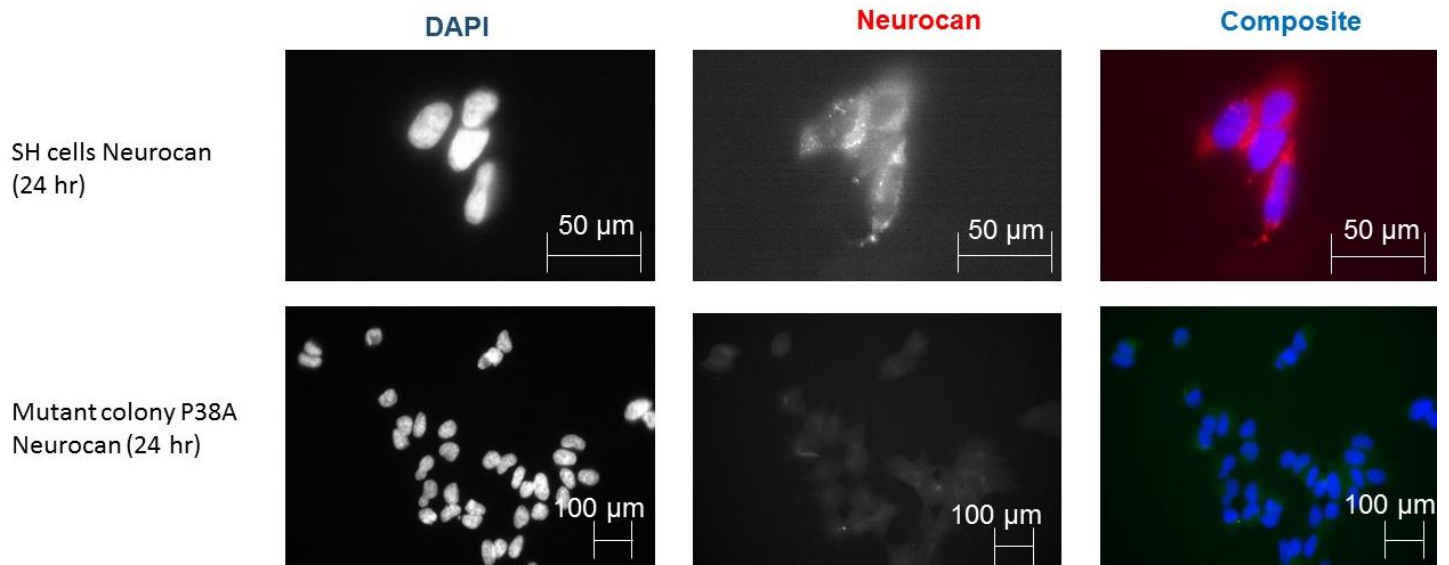
Figure 4.15 Reduced Neurocan levels seen in mutant colony P38A. *SH-SY5Y mutant (P38A) stained with Neurocan. above displays the results obtained through staining with Neurocan. As seen above, the mutant (P38A) identified earlier as a mutant failing to produce a PNN possessed decreased levels of staining with Neurocan. Neurocan is a component of the perineuronal net and a risk factor for bipolar disorder so it was important to understand how levels of Neurocan may be altered within this mutant. Here, the results indicate that levels of Neurocan staining was significantly reduced in mutant colony P38A. N=10 so relevant statistical analysis was undertaken two tail T-Testing and SEM. **P<0.01. X40 magnification, Scale bar = 100µm*
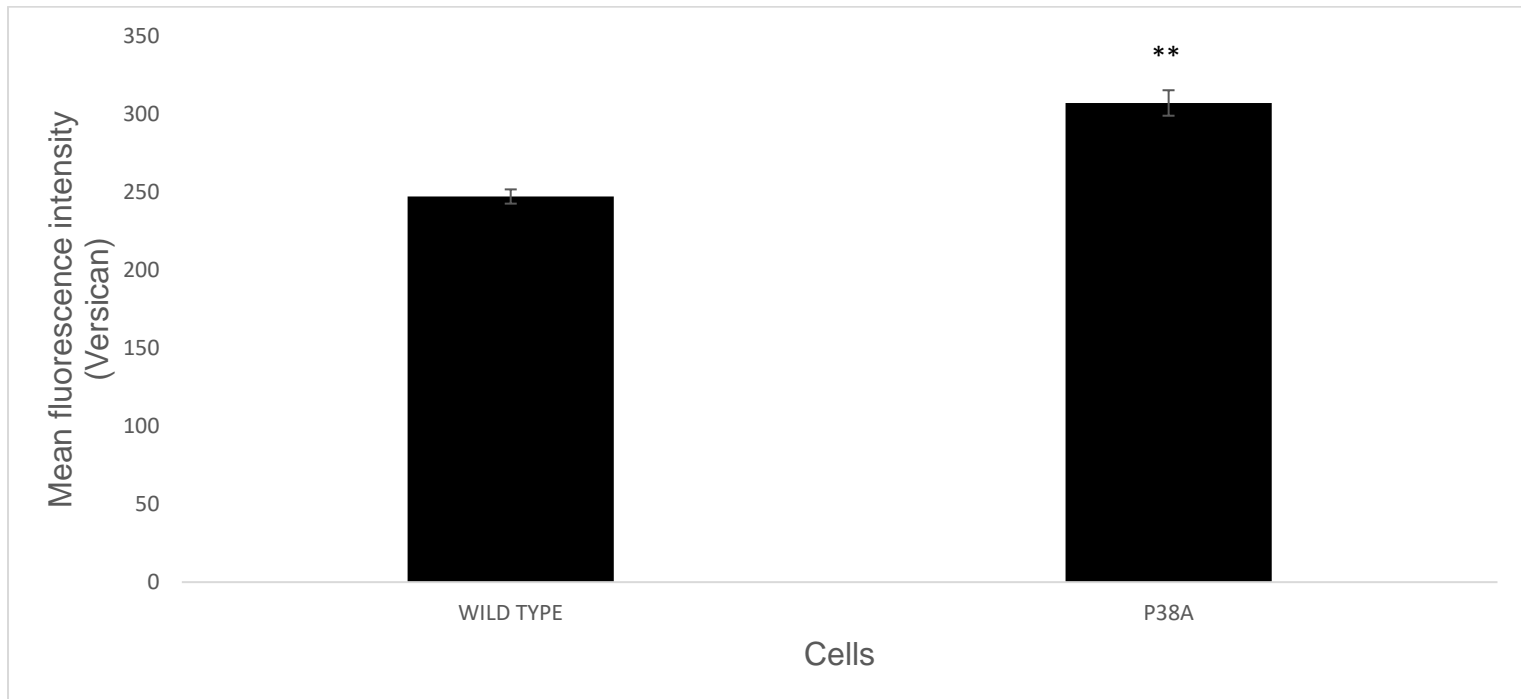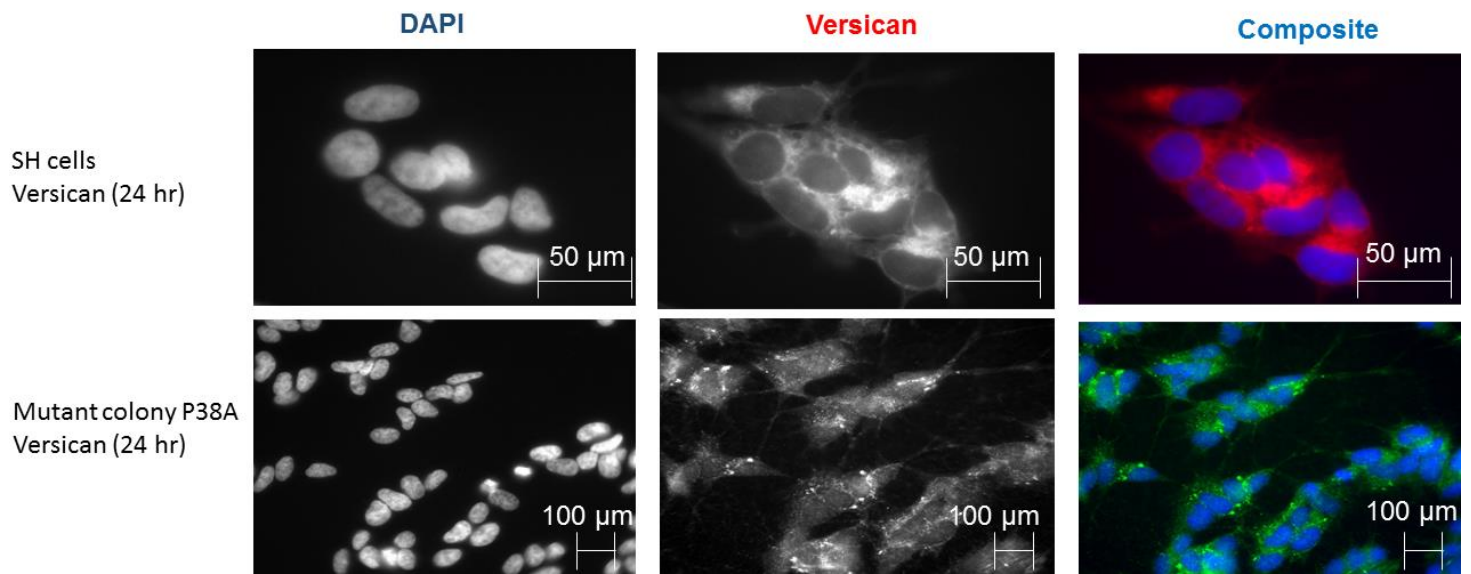
Figure 4.16. Increased Versican expression in mutant colony P38A. *SH-SY5Y mutant (P38A) stained with Versican. Figure 4.16 above displays the results obtained through staining with Versican. As seen above, the mutant (P38A) identified earlier as a mutant failing to produce a PNN possessed increased levels of staining with Versican in comparison with wild type cells. Versican is a key component of the perineuronal net so it was important to understand how levels of Versican may be altered within this mutant. Here, the results indicate that Versican staining was slightly increased in mutant colony P38A. N=24 cells so relevant statistical analysis was undertaken including two tail T-Testing and SEM. **P<0.01. X40 magnification, Scale bar = 100μm*
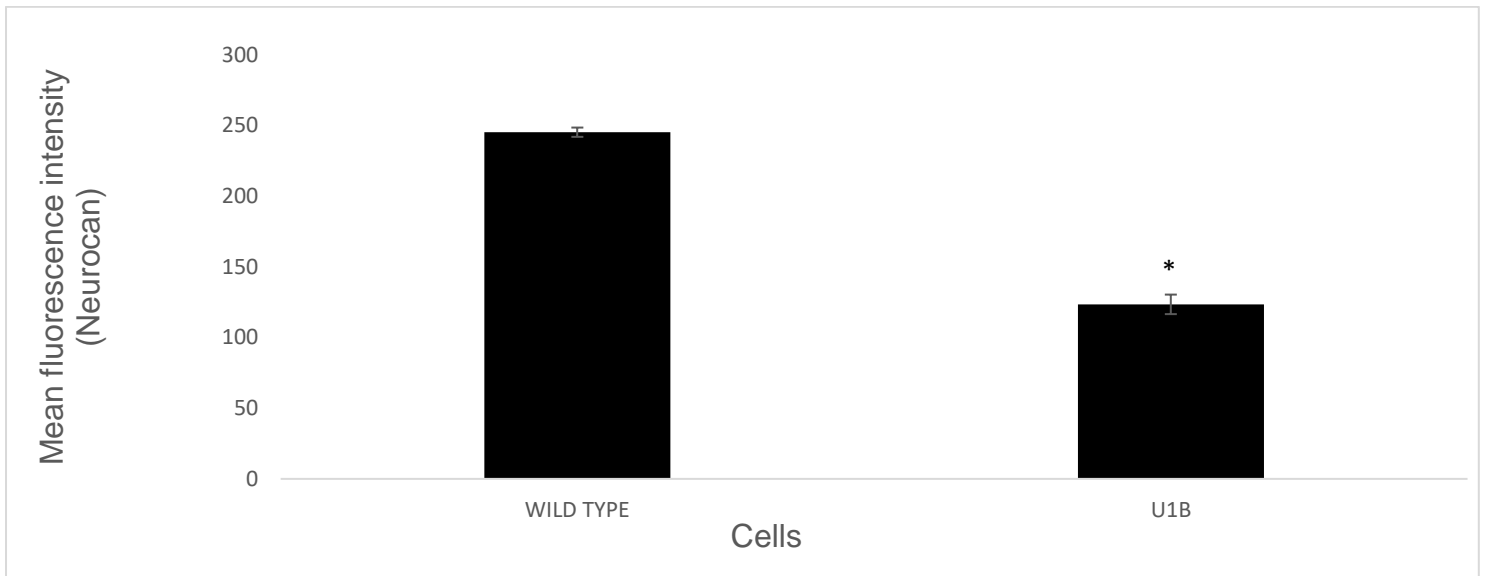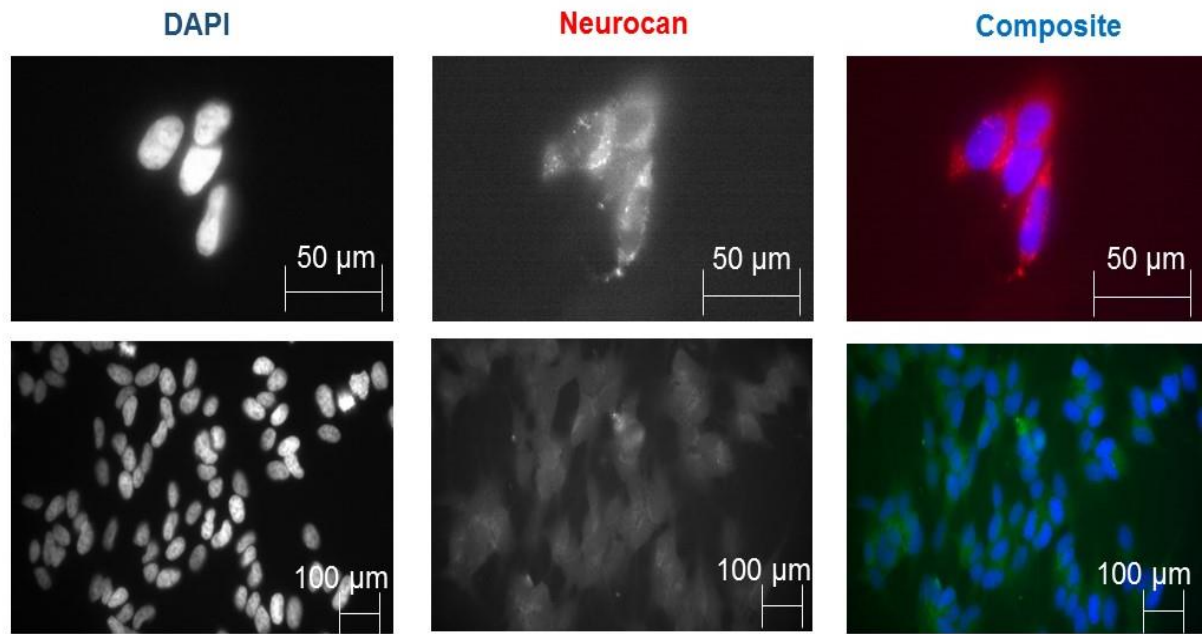
Figure 4.17 Reduced levels of Neurocan seen in mutant colony U1B. *SH-SY5Y mutant (U1B) stained with Neurocan. Figure 4.17 above displays the results obtained through staining with Neurocan. As seen above, the mutant (U1B) identified earlier as a mutant failing to produce a PNN possessed decreased levels of staining with Neurocan. Neurocan is a component of the perineuronal net and a risk factor for bipolar disorder so it was important to understand how levels of Neurocan may be altered within this mutant. Here, the results indicate that levels of Neurocan staining was significantly reduced in U1B. N=82 so relevant statistical analysis was undertaken including two tail T-Testing and SEM T-testing. *P<0.05. X40 magnification, Scale bar = 100µm*
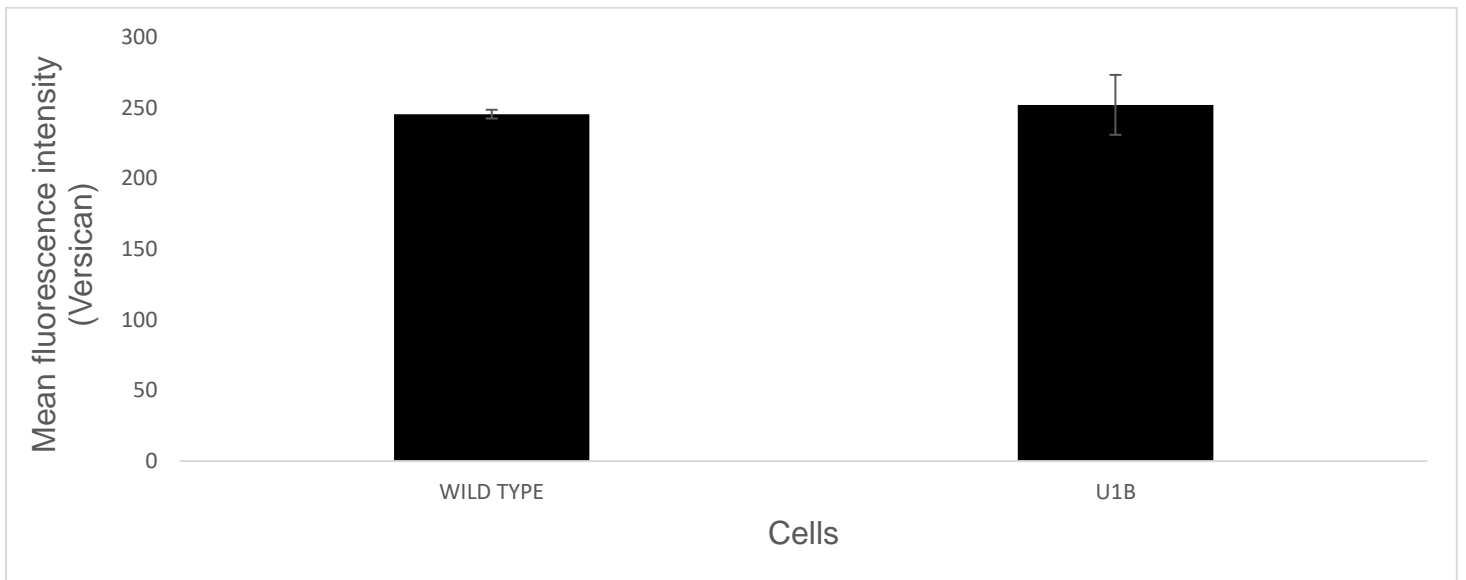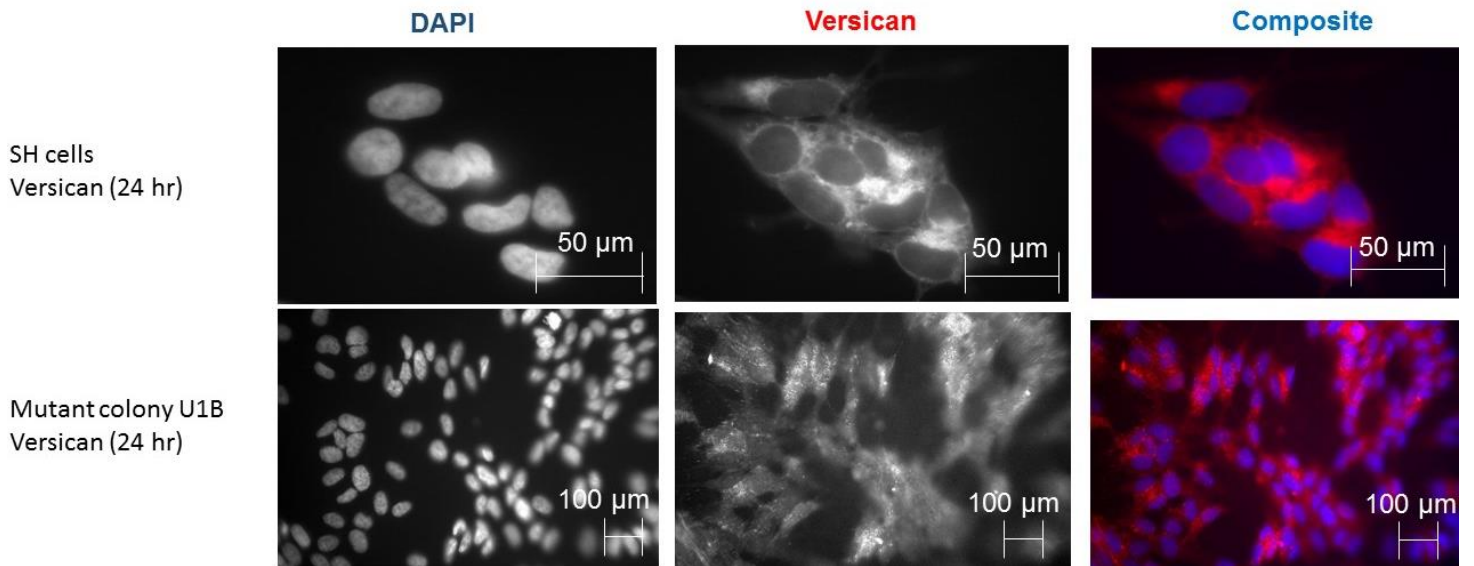
Figure 4.18. No change in Versican levels in mutant colony U1B. *SH-SY5Y mutant (U1B) stained with Versican. Figure 4.18 above displays the results obtained through staining with Versican. As seen above, the mutant (U1B) identified earlier as a mutant failing to produce a PNN possessed normal levels of staining with Versican. Versican is a key component of the perineuronal net so it was important to understand how levels of Versican may be altered within this mutant. Here, the results indicate that Versican staining was unaffected in U1B. N=71 so relevant statistical analysis was undertaken including two tail T-Testing and SEM. P>0.05. X40 magnification, Scale bar = 100µm*
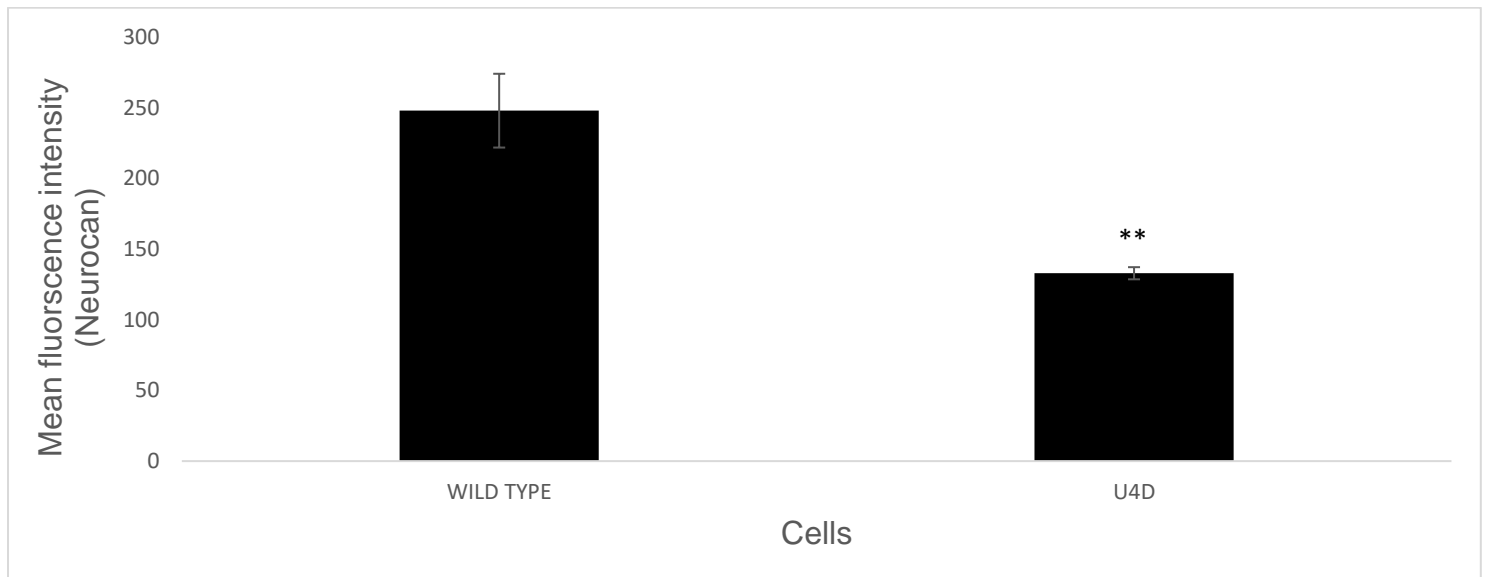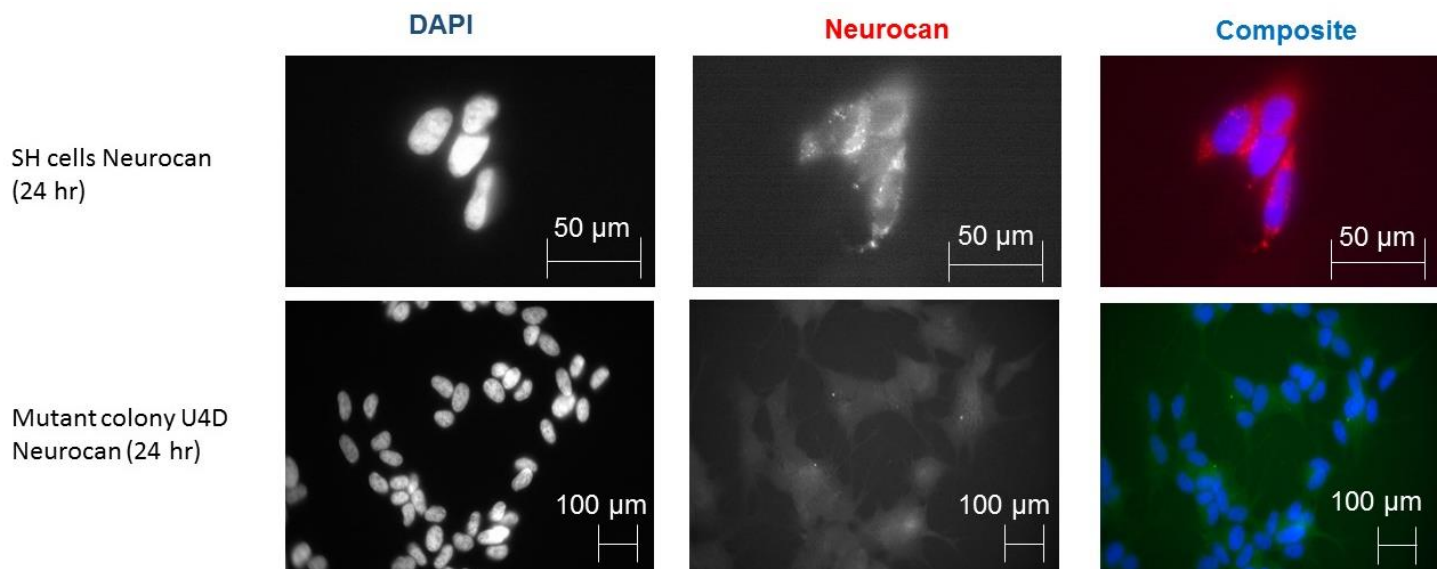
Figure 4.19 Reduced levels of Neurocan seen in mutant colony U4D. *SH-SY5Y mutant (U4D) stained with Neurocan. Figure 4.19 above displays the results obtained through staining with Neurocan. As seen above, the mutant (U4D) identified earlier as a mutant failing to produce a PNN possessed decreased levels of staining with Neurocan. Neurocan is a component of the perineuronal net and a risk factor for bipolar disorder so it was important to understand how levels of Neurocan may be altered within this mutant. Here, the results indicate that levels of Neurocan staining was significantly reduced in U4D. N=37 so relevant statistical analysis was undertaken including two tail T-Testing and SEM **P<0.01 X40 magnification, Scale bar = 100µm*

DAPI | Versican | Composite

SH cells
Versican (24 hr)

50 µm | 50 µm | 50 µm

Mutant colony U4D
Versican (24 hr)

100 µm | 100 µm | 100 µm
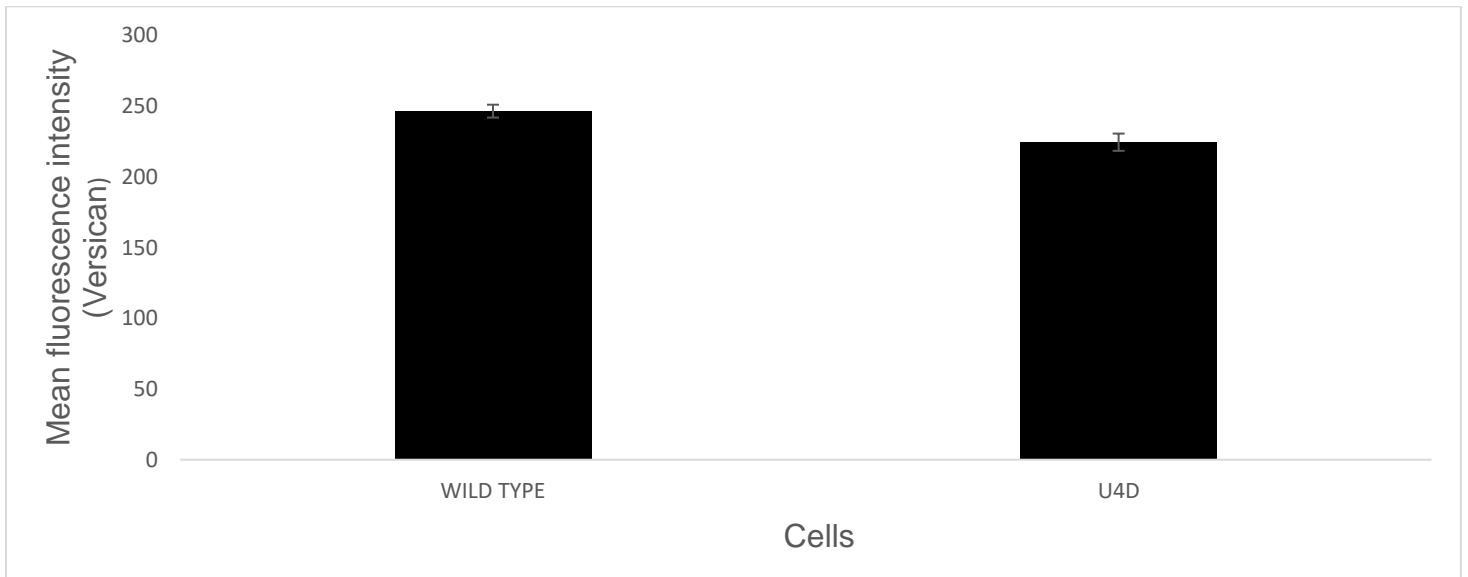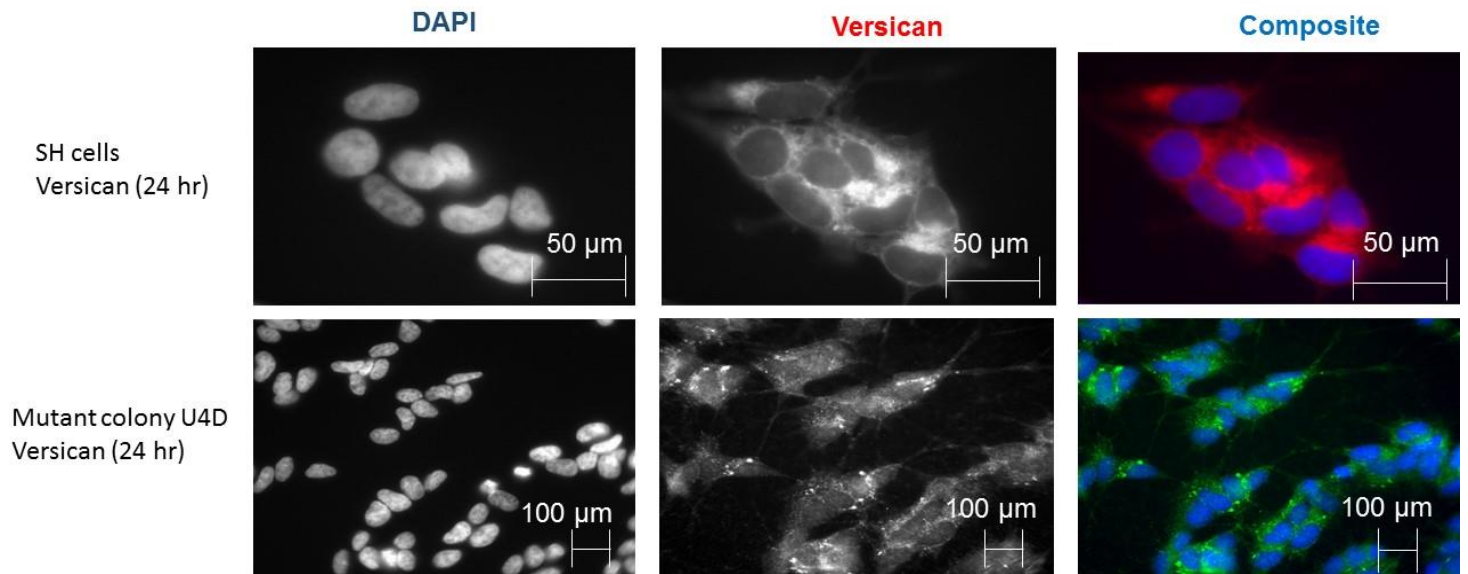
Figure 4.20 No change in Versican levels in mutant colony U4D.*SH-SY5Y mutant (U4D) stained with Versican. Figure 4.20 above displays the results obtained through staining with Versican. As seen above, the mutant (U4D) identified earlier as a mutant failing to produce a PNN possessed normal levels of staining with Versican. Versican is a key component of the perineuronal net so it was important to understand how levels of Versican may be altered within this mutant. Here, the results indicate that Versican staining was unaffected in U4D. N=64 so relevant statistical analysis was undertaken including two tail T-Testing and SEM. P>0.05. X40 magnification, Scale bar = 100µm*

4.3.10 Analysing the PNN protein expression of selected mutant colonies by Western blotting through staining with anti-*Neurocan* antibodies or WFA.

To verify imaging data at a quantifiable protein level, mutant colonies were analysed for their PNN component expression by WFA staining or use of anti-*Neurocan* antibodies *SH-SY5Y* mutant colonies P38A, U1B and U4D were grown to confluence and protein was extracted using the standard cell lysis method and then run on 10 % percent polyacrylamide gel and transferred to nitrocellulose membrane by electro blotting. Primary antibody, or biotinylated WFA, and secondary antibody, (or streptavidin), both conjugated horseradish peroxidase was used. Images were developed using X ray film and processed using ImageJ (Figure 4.21, Figure 4.22).
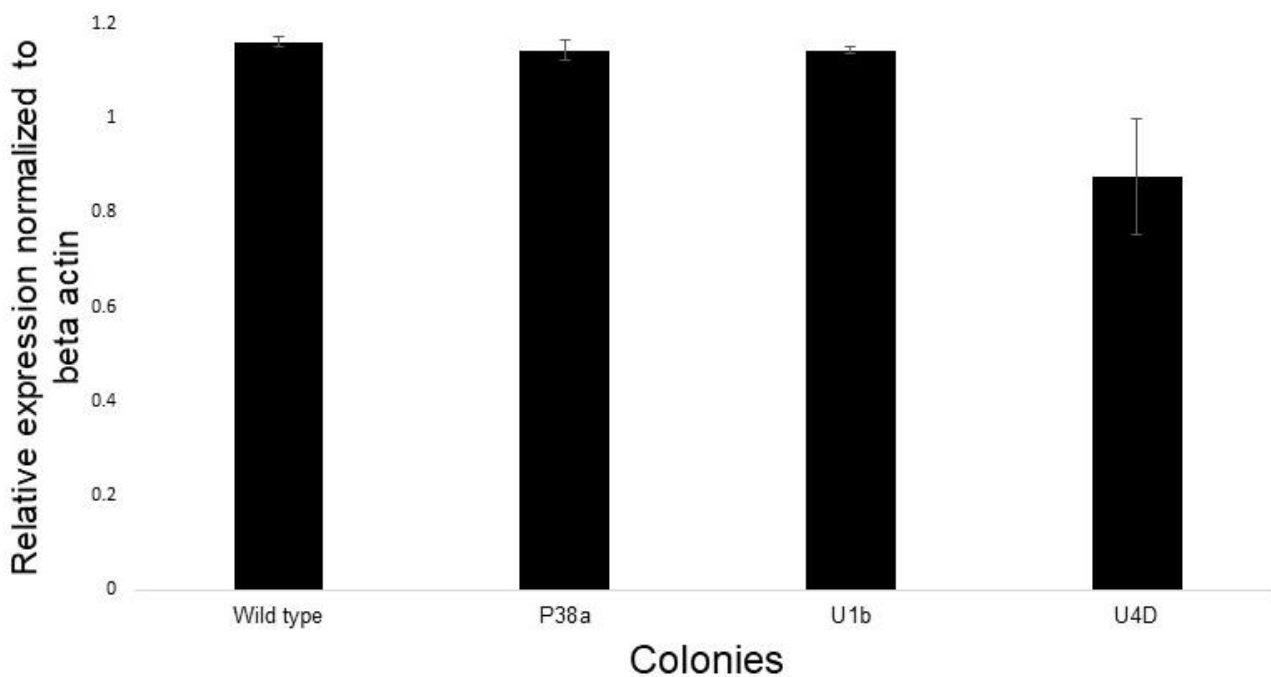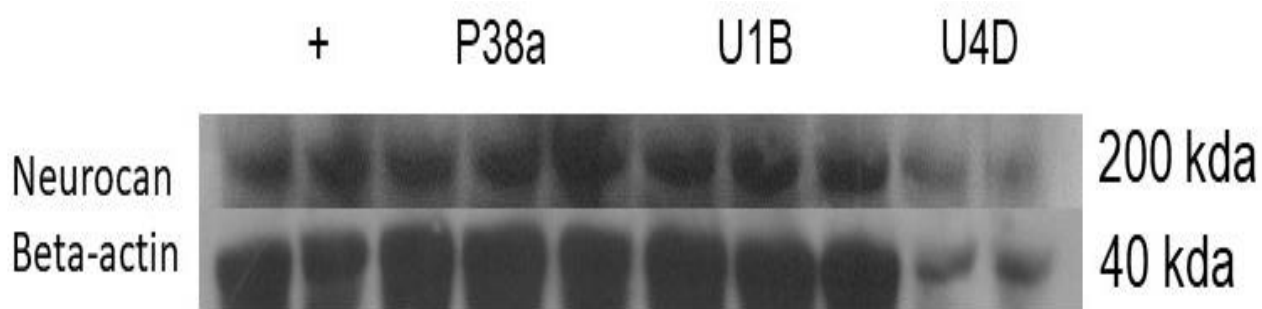
Figure 4.21 No significant change in Neurocan levels of mutant colonies during protein analysis. *Figure 4.21 shows that there is no significant change in Neurocan levels during protein analysis of mutant colonies P38A, U1B, U4D. Western blot analysis of Neurocan expression indicated little difference between wild type and mutant colonies. Beta actin loading control was used to normalise data. N=3, so relevant statistical analysis was undertaken including two tail T-Testing and SEM p>0.05*
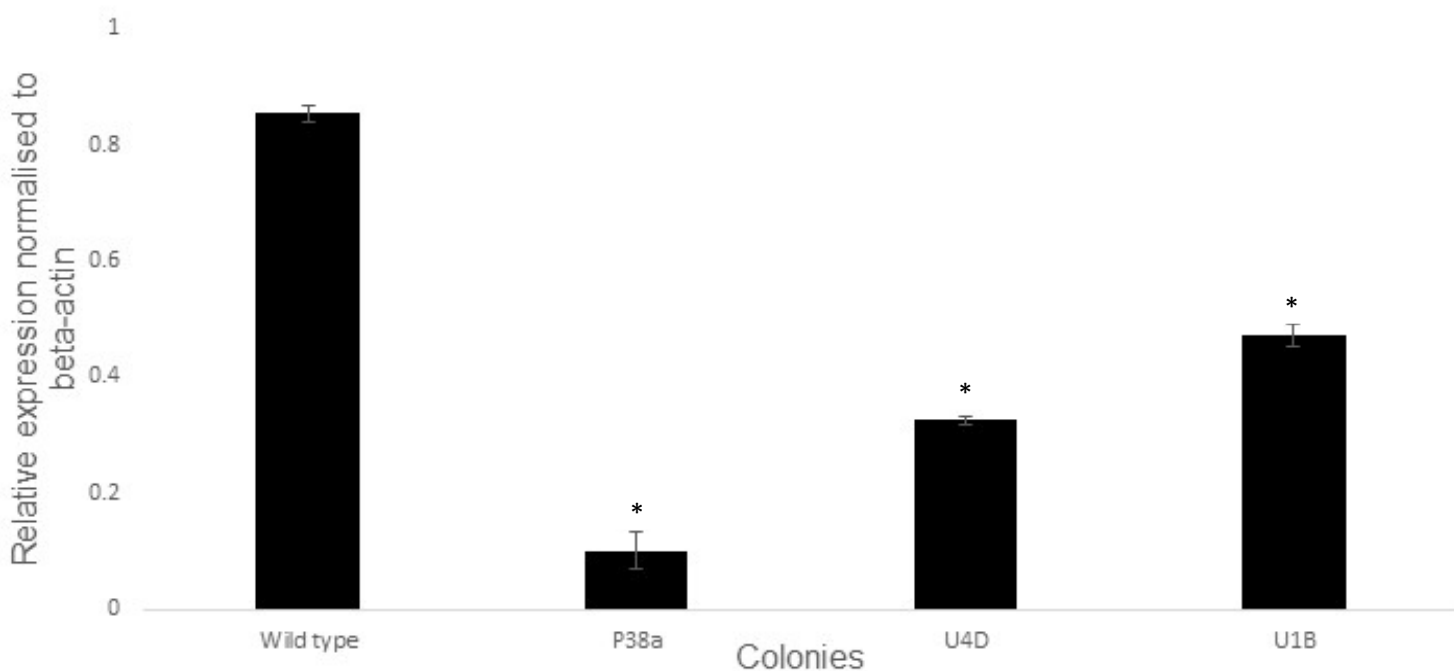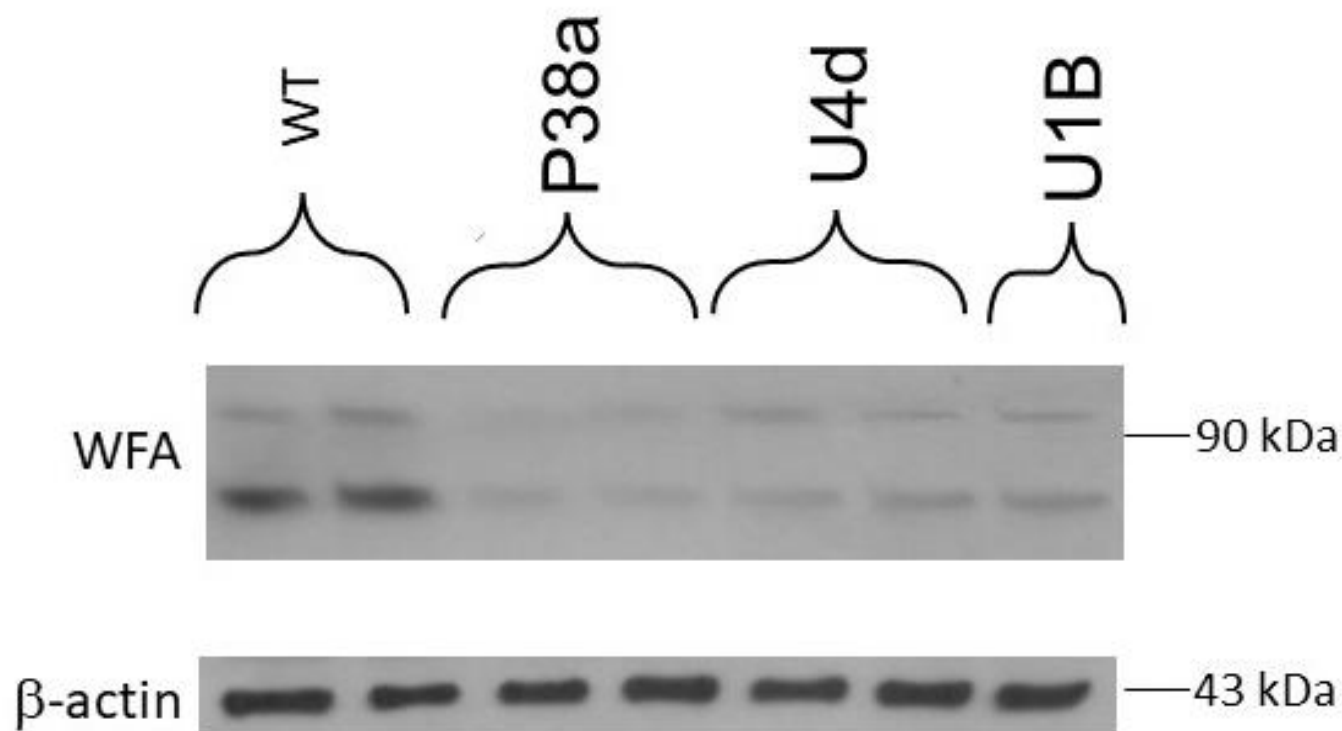
Figure 4.22. Reduced expression of glycoproteins stained by WFA seen in mutant colonies P38A, U1B, U4D compared to wild type. *Figure 4.22 shows that there is reduced WFA-binding glycoprotein expression of the mutant colonies during protein analysis. Western blot analysis shows that there is a significant reduction in WFA staining in the mutant colonies compared to wild type.*

114

Beta actin loading control was used to normalise the data N=3, so relevant statistical analysis was undertaken including two tail T-Testing and SEM. *P<0.05

The results of the sections above show that quantitative protein analysis appears to confirm that selected mutant colonies have reduced WFA staining (Table 4.1) in comparison with the wild type cells (Figure 4.6) as predicted from the purpose of the initial screen and the later immunofluorescence findings. In some colonies, such as U1B and U4D, levels of *Neurocan* expression were apparently reduced at the level of immunofluorescence, but this was not replicated in the protein analysis results. Finally, there was no change in *Versican* levels observed during immunofluorescence microscopy in mutant colonies U4D and U1B. However, with regards to P38a, there appeared to be a slight increase in Versican expression in comparison with wild type cells. The results above further indicate that *Neurocan* is not the 90 kDa band appearing in Western analysis and is functionally distinct from the PNN components that are altered in these mutant cells.

Colony picked	WFA staining using cell live staining	WFA staining using immunofluorescence microscopy	*Neurocan* staining	*Versican* staining	Protein analysis (*Neurocan*)	Protein analysis (WFA)
P36b	Reduced	No change	N/A	N/A	N/A	N/A
P37b	Reduced	Reduced	N/A	N/A	N/A	N/A
P38A	Reduced	Reduced	Reduced	Increased	No change	Reduced
P39a	Reduced	Reduced	N/A	N/A	N/A	N/A
U1B	Reduced	Reduced	Reduced	No change	No change	Reduced
U4D	Reduced	Reduced	Reduced	No change	No change	Reduced
U6A	Reduced	Reduced	N/A	N/A	N/A	N/A
U9B	Reduced	No change	N/A	N/A	N/A	N/A

Table 4.1 Colonies picked during the mutant gene trap screen with reduced* WFA *staining. *Table 4.1 shows the colonies obtained from the SH-SY5Y mutant gene trap library which have reduced* WFA *staining. I specifically utilised mutant colonies P38A, U1B and U4D as these had the best reduced* WFA *staining levels when visualised under the fluorescent microscope.*

4.4 Conclusion

In summary, a gene trap screen was undertaken to identify genes encoding proteins which have role in the production of a functional perineuronal net. Firstly, live cell staining was undertaken. Nine clones were noted as having reduced or no live WFA staining and were subsequently picked, isolated, and retested. Following this, immunofluorescence microscopy was undertaken as one validation of the live cell staining. The results suggested that various mutants had reduced WFA staining and some, such as P38A and U1B, had altered distribution of the PNN target(s) of WFA. In comparison with wild type *SH-SY5Y* perineuronal nets, mutated perineuronal nets often appeared to have reduced staining and altered distribution, which could be a result of protein expression/degradation and/or from mutations affecting the trafficking of WFA protein targets to full display on the cell surface. Furthermore, selected mutant colonies such as P38A, U1B, U4D had reduced WFA staining as indicated by both immunofluorescence and protein analysis. These colonies were also tested for *Versican* and *Neurocan* staining to see if their expression levels had been altered during mutation. Despite seeing no change in *Versican* expression levels in U4D and U1B during immunofluorescence and protein analysis, levels of *Neurocan* staining appeared to be reduced in colonies such as P38A, U1B and U4D. However, this was not verified by Western analysis. It is important to note however, with regards to mutant colony P38a, there was an increase in versican expression in comparison with wild type. Figure 4.23 depicts the potential mechanisms by which gene mutation could affect perineuronal net formation. The next step in the analytical process was to confirm the identity of the mutant genes using RACE-PCR and sequencing and to determine if they fall into any of these hypothetical functional categories.
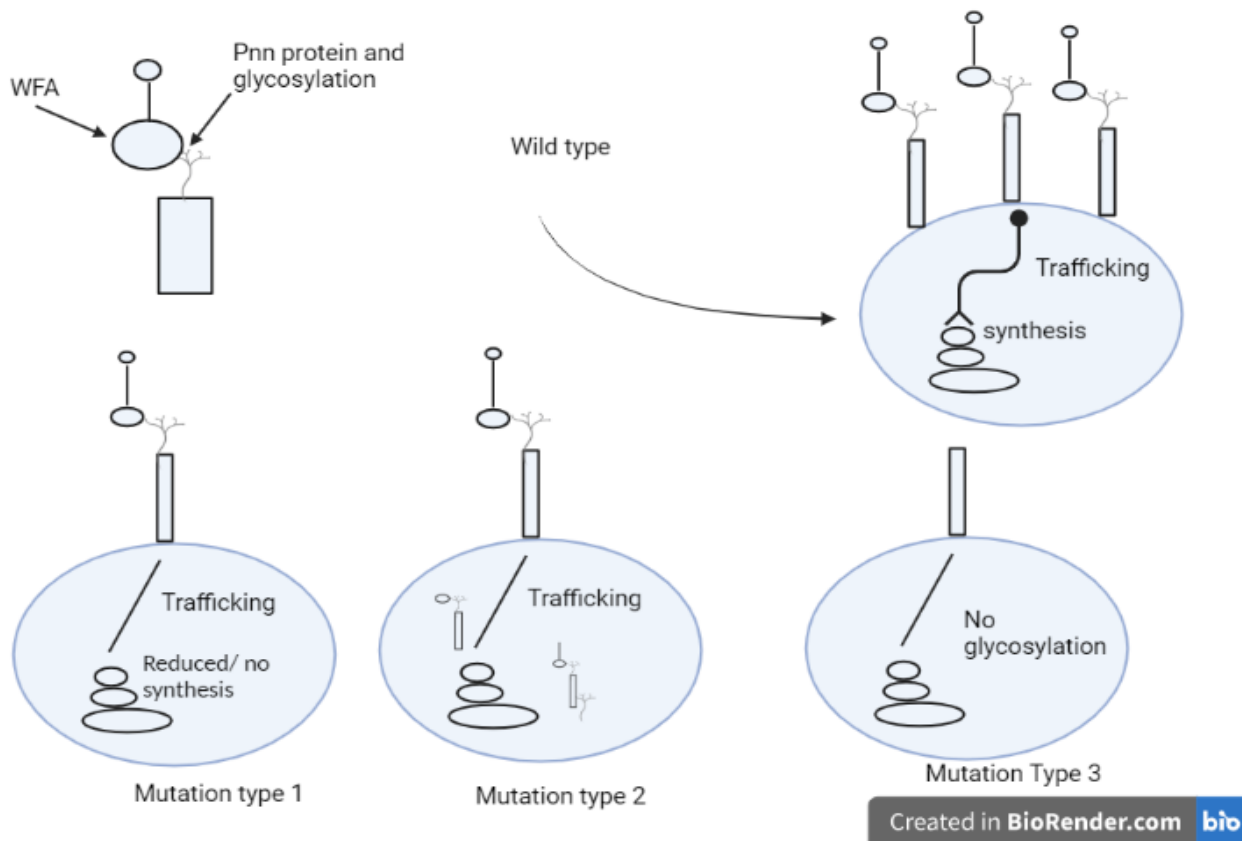
Figure 4.23 Schematic produced in BioRender depicting the various ways in which perineuronal net synthesis could be altered resulting in abnormal perineuronal nets. *The schematic above shows the three different ways in which perineuronal net synthesis could be altered by gene trap mutation, leading to production of abnormal perineuronal nets. Firstly, reduced protein levels or complete knockout could result in direct failure of the protein to be produced thus affecting the subsequent stages resulting in abnormal perineuronal nets. Secondly, the protein could be produced but will not be able be able to be trafficked to the cell meaning a mutational failure in trafficking leading to the subsequent stages being affected and thus affecting formation of the perineuronal net. Finally, the third mutation type would involve the protein being produced correctly but possessing no glycosylation because of a mutational event in a post translational modification enzyme, meaning that WFA would not detect the protein. Mutations along any of these steps would result in no detectable perineuronal net being formed and a positive genetic screen result.*

CHAPTER 5

RESULTS: Identification and analysis of the mutant genes from the selected screen colonies

5.1 Using RACE-PCR to determine the identity of mutant genes.

The following section focuses on identification and analysis of the mutant genes, which are failing to produce a functional perineuronal net. As previously described, mutant *SH-SY5Y* cells were stained with WFA through live staining to detect which cells are failing to produce perineuronal nets. This was then further validated via immunofluorescence microscopy and Western blotting. Here, to identify the mutants, a number of steps were undertaken. Firstly, the process of gene trap mutation generates a fusion mRNA transcript between the neoR gene and the trapped, mutated endogenous gene (Figure 5.1). Analysis consisted of mRNA extraction followed by cDNA synthesis, PCR, cloning, and finally sequencing. Rapid Amplification of cDNA Ends (RACE) is a PCR procedure for amplification of nucleic acid sequences from a messenger RNA template between a defined internal site (in this case, the NeoR gene) and an unknown 3´ end of the mRNA (the 3' end of the unknown trapped endogenous gene in this case). PCR requires two sequence-specific primers that flank the sequence to be amplified. However, to amplify and characterize regions of unknown sequences, this requirement imposes a limitation. The first step in RACE solves this by using reverse transcription to produce a cDNA copy of a region of the RNA transcript using a synthetic anchor sequence 5' to the standard oligodT primer. The cDNA is now bounded by known sequences at both ends. Two rounds of nested PCR are then carried out to amplify/capture the unknown 3´-mRNA sequences that lie between the neoR exon and the poly(A) tail.
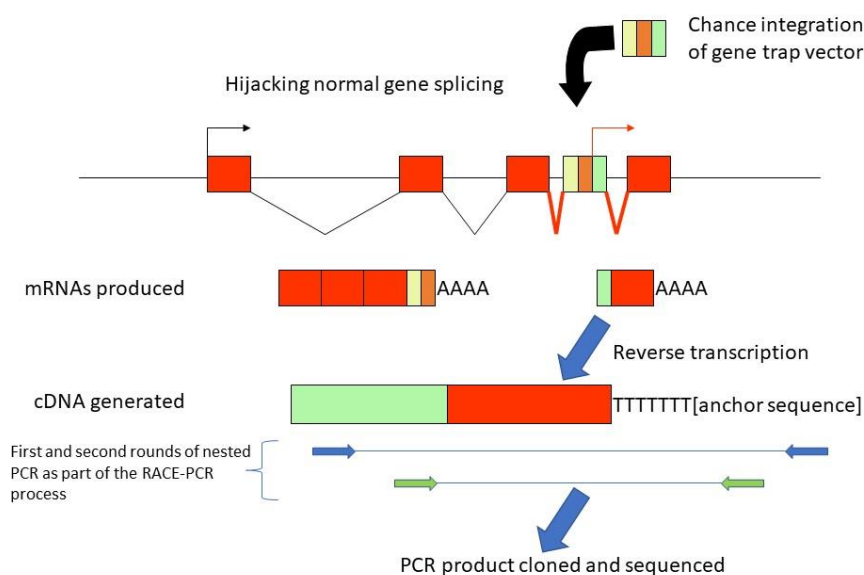
Figure 5.1 Gene trapping and RACE-PCR. *Figure 5.1 is a schematic produced showing how the gene trap vector integrates into a gene during the mutational process as the library is created. Following this, fusion mRNAs are produced and then cDNA is generated via reverse transcription. Two rounds of nested PCR are then undertaken as part of the RACE-PCR process and the PCR product is cloned and sequenced in order to identify the mutated gene in a cell clone of interest.*

To confirm the identity of the mutant genes with reduced WFA-binding glycoprotein expression, it was necessary, as described above, to carry out RNA extraction of the mutant colonies, cDNA synthesis and RACE-PCR. These procedures were undertaken and the resulting RACE-PCR products were electrophoresed on a 1% agarose gel (Figure 5.2 and 5.3).
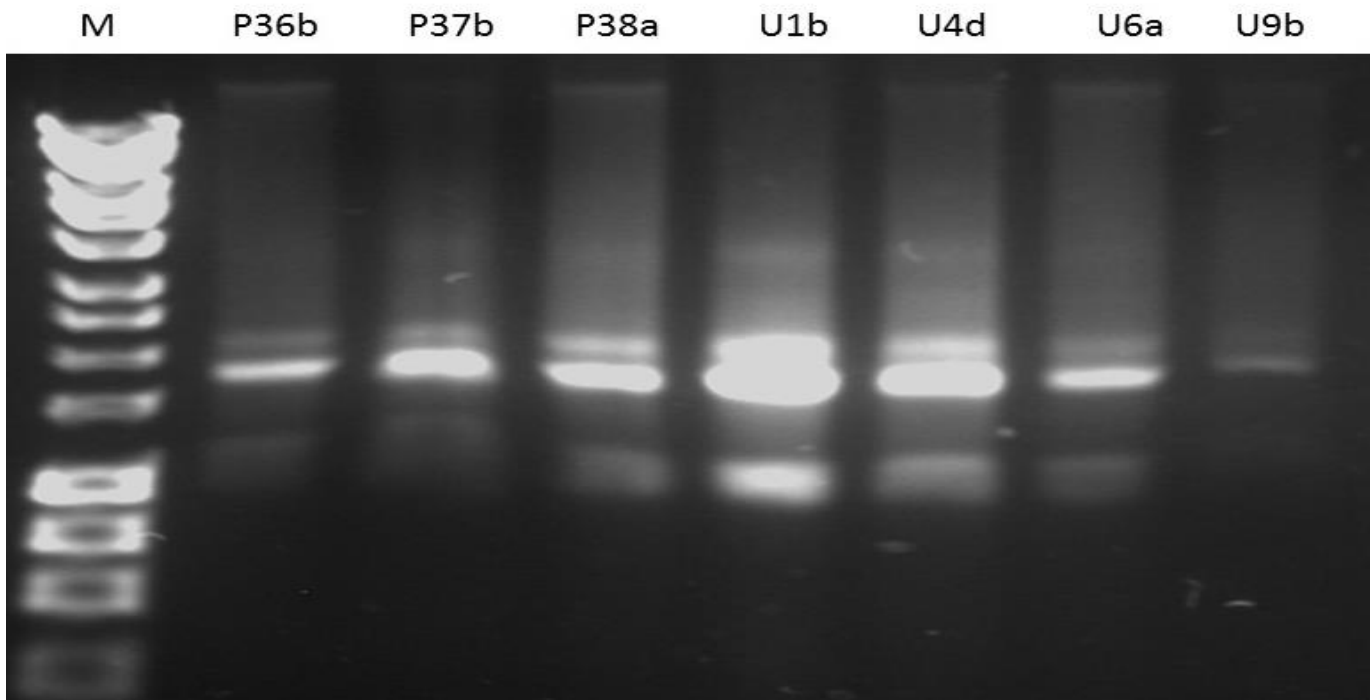
Figure 5.2 Successful RNA extraction of mutant colonies with reduced* WFA-binding glycoprotein *expression. *Gel electrophoresis undertaken at 100 V for 60 minutes on 1 % agarose gel. Figure 5.2 above displays the results obtained from the gel electrophoresis of RNA extraction of colonies, which were failing to produce or resulted in formation of an abnormal PNN. Two principal bands are seen representing undegraded 28S and 18S ribosomal RNA populations.*
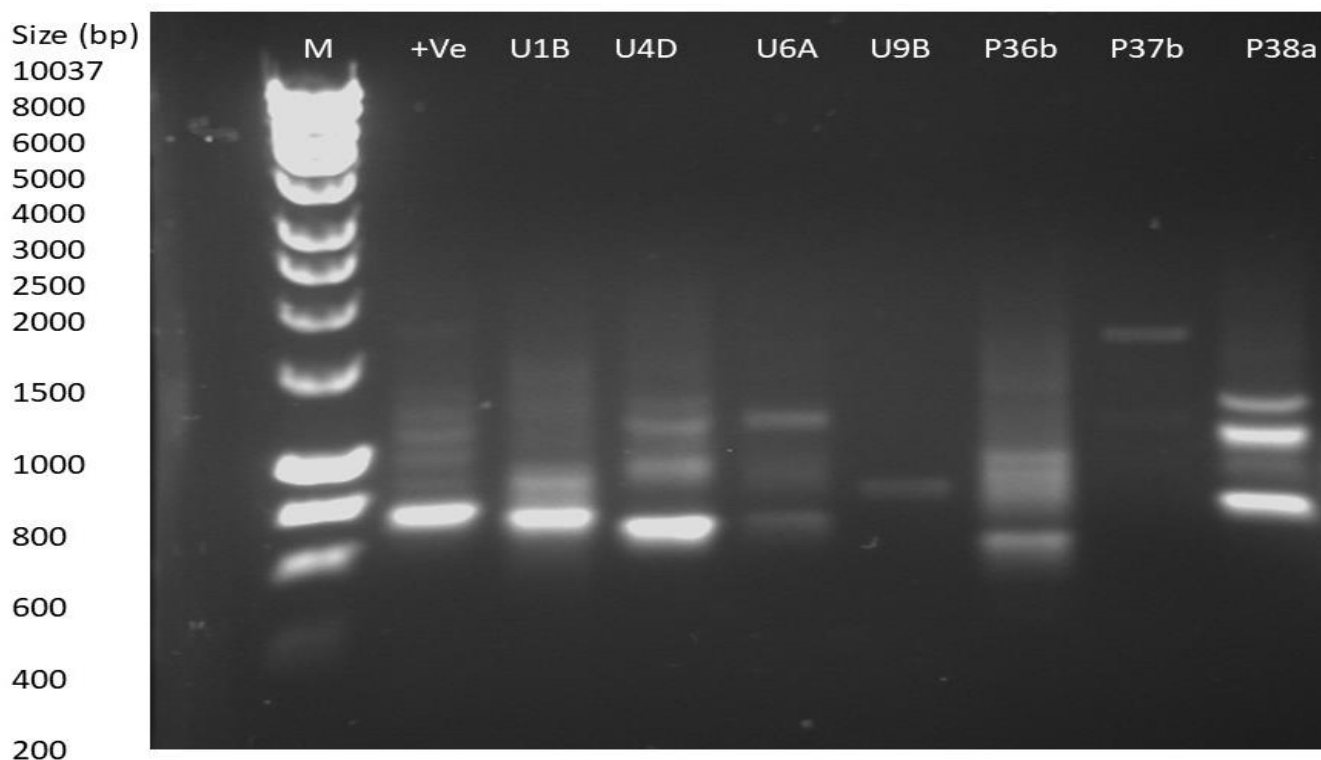
Figure 5.3. Gel electrophoresis of RACE- PCR products. *Gel electrophoresis undertaken at 100 V for 60 minutes on a 1 % agarose gel. RACE-PCR.* A positive control (+ve) was utilised to show that the RACE-PCR was working. The substrate for this reaction was cDNA from a colony isolated in a previous gene trap screen carried out in the lab. Interestingly, for P38a, there appears to be multiple bands which could indicate degradation, different genes amplified from a poorly isolated colony, or could reveal the presence of alternative splicing or cryptic splice acceptor sites.

5.2 Identification of the mutant genes using plasmid cloning and sequencing of the RACE-PCR products

RACE-PCR products were successfully purified and then ligated into the pGEM-T Vector, designed to efficiently clone PCR products. Ligations were transformed into chemically competent *E. coli* bacteria, plated and colonies grown in liquid broth for plasmid mini-prep purification of the cloned RACE-PCR products. Restriction digests of the plasmids were undertaken using EcoRI to determine which plasmid colonies contained inserts, and the size of the insert. Insert-containing plasmid DNA was then sent for sequencing (Source Bioscience, Nottingham) and Sequence electropherograms were analysed using Finch TV reader, and both NCBI Blast and UCSC Genome Browser BLAT were used for gene sequence identification. Table 5.1 below indicates the sequencing results identifying the 'trapped' genes in the colonies failing to produce a functional perineuronal net. The most

122

important of these are P38A, U4D and U1B due to their large sizes as well as U1B being exonic. The U1B clone sequence being exonic is a key criterion indicating the correct mutagenic event from the gene trap process. After transfection/electroporation of the gene trap construct into a cell, it stably integrates into the nuclear genomic DNA. If integration occurs within a gene intron, then the splice acceptor/donor sequences divert and block the normal processes of exon–exon splicing that create the mature and complete mRNA from the gene's pre-mRNA. This has three consequences. Firstly, mRNA from the trapped allele of the gene is generally truncated or unstable resulting in a loss-of-function mutation. Secondly, the endogenous gene and gene trap sequences produce a stable, hybrid mRNA: Neo^R (Neomycin/G418 resistance) fused to the endogenous gene 3' exons which permits antibiotic selection for productive gene trap events. Thirdly, these hybrid mRNAs comprising gene trap-derived and endogenous sequences can be readily amplified by the rapid amplification of cDNA ends RACE-PCR protocols described above to identify the gene that has been trapped. Taking into consideration the above, the expected observation should be an artificial splice event between Neo^R and exonic sequences of the trapped endogenous gene. U1B fulfilled that criterion and the endogenous gene exons (188 bp) were identified as belonging to the *GALNTL6* gene. Other candidate genes also prioritised for further description and analysis were *FAF1* (clone P38A) and *DCC* (clone U4D). Many other genes were not taken into consideration due to having incorrect splicing or no significant link with perineuronal nets and neuropsychiatric diseases (Table 5.1).

Colony	Gene name	Intronic/Exonic	Plasmid insert size (bp)	WFA live staining effect?	**Effect on *Neurocan*	**Effect on *Versican*	Comments	Properties
P36b b	*ADGRL2*	Intronic	108	Decreased	No effect	No effect		Latrophillin involved in cell signal and transduction, risk factor for depression and late onset Alzheimer's disease
P36 b e	*HBB*	Intronic	25	Decreased	No effect	No effect		Component of Haemoglobin
P37B	*PLA2G4*	Intronic	27	Decreased	No effect	No effect		Cell signalling, hydrolysis of lipids, risk factor for schizophrenia and epilepsy
P38 a	*FAF1*	Intronic	364	Decreased	Decreased	No effect	Very low levels of *Neurocan* staining	Parkinson's disease
P38 a c	*FAF1*	Intronic	366	Decreased	Decreased	No effect		Parkinson's disease
P38 a e	*FAF1*	Intronic	680	Decreased	Decreased	No effect		Parkinson's disease
U1B	*GALNTL6*	Exonic	188	Decreased	Decreased	No effect	Quite dim staining	Mucin type O-linked glycosylation
U4D b	*DCC*	Intronic	244	Decreased	Decreased	No effect	Very dim staining with *Neurocan*	Risk factor for schizrenia, axonal guidance
U6A	*EVI5*	Intronic	61	Decreased	No effect	No effect		Regulates GTPase activity, risk factor for multiple sclerosis and schizophrenia
U9b C	*SUGCT*	Exonic	353	Decreased	No effect	No effect		Mitochondrial enzyme, multiple SNPs show association with migraine

Table 5.1 Sequencing of mutant colonies. *Table 5.1 above represents the sequencing results obtained for the mutant colonies with reduced* WFA *staining. The table above indicates the identity of the mutant colonies which were deemed to have reduced WFA staining. Information related to*

these genes was obtained from GWAS catalogue as well as Gene Cards and Uniprot. As displayed above, the best candidate genes due to presence of non-intronic sequences are GALNTL6 and SUGCT indicating that the gene trap has worked in the way it is supposed to. GALNTL6 is involved in mucin type O-linked glycosylation and involved in the catalysis of the first step of O-linked glycosylation where it adds an N-Acetyl galactosamine residue to the proteoglycan component. SUGCT has been shown to have multiple SNPs associated with migraine. Other key genes taken forward for further analysis include FAF1 and DCC where FAF1 plays a role in oxidative stress and alpha synuclein regulation in parkinson's disease and DCC plays a role in axonal guidance and is a risk factor schizophrenia. With regards to the other genes identified, EVI5 is a risk factor for multiple sclerosis and schizophrenia. Other genes such as ADGRL2 (Risk factor for depression and late onset Alzheimer's disease) and PLA2G4 (risk factor for schizophrenia and epilepsy) were identified but not taken forward due to their lack of roles involved in extracellular matrix or neurological diseases at the time.
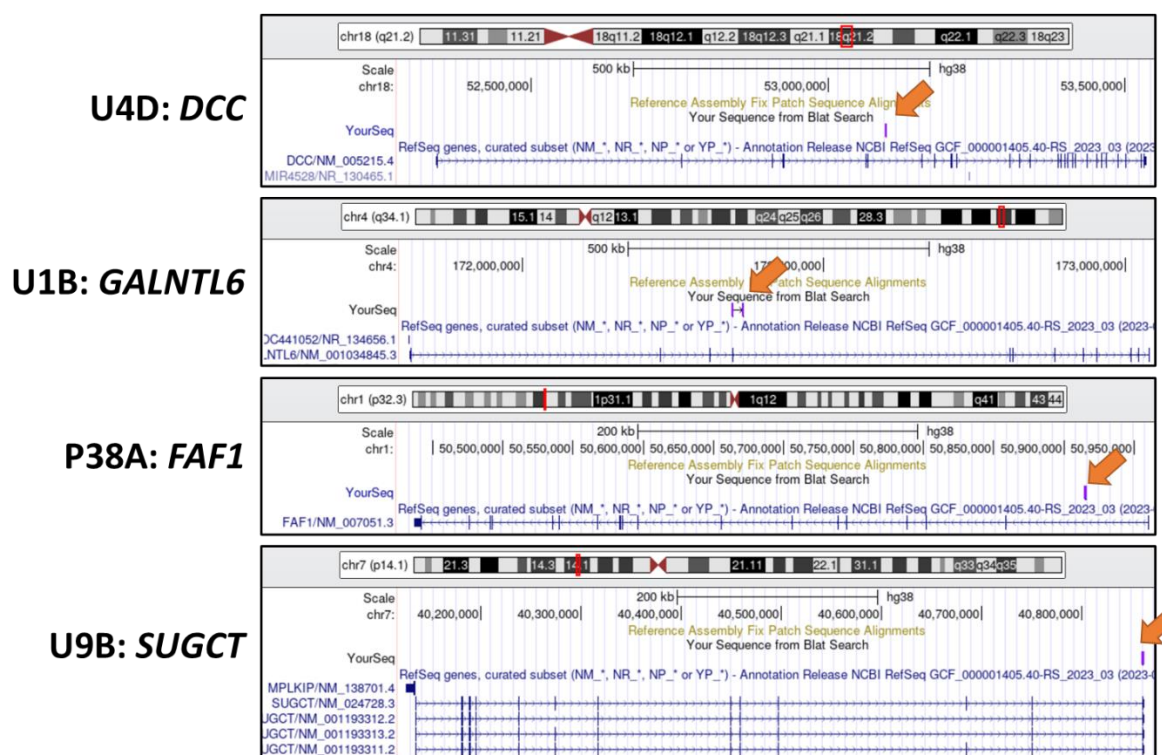
Figure 5.4 Where RACE-PCR products align within the genome and in relation to potentially 'trapped' genes. Sequences from plasmid cloned RACE-PCR products were aligned with the genome using the BLAT tool within the UCSC Genome Browser (https://genome.ucsc.edu/index.html). The orange arrows indicate the location of the matching

125

sequences. The expectation was that the actual genome insertion site of the gene trap vector would be 5'/upstream (with respect to the gene orientation) of the aligned sequence. Hence, the aligned sequence represents fusion mRNA downstream of the artificial splicing initiated from within the gene trap vector. Of importance is the presence of exonic RACE-PCR sequences within GALNTL6 and SUGCT, entirely as predicted by the model of gene trap action. However, the presence of cryptic splice-acceptors within the intron sequences of several trapped genes may still indicate that the gene trap insertion event could be deleterious by subverting the pattern of splicing across the gene.

5.3 U4D is identified as *DCC* using BLAT.

U4D, was sequenced and identified as *DCC* which is a GWAS risk factor for depression (Figure 5.4). *DCC* is *deleted in colorectal cancer* and is expressed throughout most of the nervous system during embryonic development and continues to be expressed in adulthood in various regions including the substantia nigra/ventral tegmental area, striatum, hippocampus, and cortex (Duman-Scheel, 2015). *DCC* was first identified via human colorectal cancers in which there was loss of heterozygosity at human chromosome 18q leading to the cloning of *DCC*. *DCC* encodes a cell surface receptor which was found to be altered in many colorectal cancers (Varadarajan and Butler, 2017). It has thus been hypothesised that *DCC* may function as a tumour suppressor gene. *DCC* has been established as a receptor for netrin 1 has been linked previously via GWAS catalogue to psychiatric wellness and a neuronal axon guidance cue which determines the direction and extent of cell migration and axonal outgrowth within the developing central nervous system (Varadarajan and Butler, 2017). Netrin-1 is classified as the founding member of the netrin family and is an axon guidance cue that has been characterized in both invertebrates and vertebrates (Varadarajan and Butler, 2017). This interaction is not only critical for neuronal development but plays a significant role in various cellular processes such as tissue organisation, cell adhesion, motility, proliferation, differentiation, cell survival and cancer (Duman-Scheel, 2015). Also, *DCC* has been functionally related to the dependence receptor family which are membrane receptors which can mediate or inhibit cellular apoptosis depending on the absence or presence of their corresponding ligand (Varadarajan and Butler, 2017). In the absence of netrin-1, the receptor does not stay inactive but stimulates an apoptotic signal through the activation of caspase-3 (Varadarajan and Butler, 2017). Consequently, cells expressing *DCC* receptors depend on ligands such as netrin-1 in the extracellular environment for survival. Crucially, when *DCC* is expressed in circumstances in which netrin-1 is not available, it induces cell death (Varadarajan and Butler, 2017).

Given that *DCC* was identified as the mutant in a cell line with reduced WFA-binding glycoprotein expression (U4D), it is important to examine the role of *DCC* in psychiatric diseases. *DCC* has been previously linked to schizophrenia as a genetic risk factor which shares many similar mechanism of pathophysiology with bipolar disorder (Vosberg *et al.*, 2018). Interestingly, chondroitin sulphate proteoglycan components of the perineuronal nets are also axon guidance cues, like *DCC*, (Vosberg *et al.*, 2018). *DCC* is a type 1 transmembrane receptor which belongs to the immunoglobulin superfamily (Vosberg *et al.*, 2018). *DCC* possesses a similar domain to its *Drosophila* Homologue Frazzled, the *C. elegans* homologue UNC40 and its vertebrate homologue neogenin (Vosberg *et al.*, 2018). The *DCC* receptor is composed of four Ig-like domains at its N terminus, followed by six fibronectin type III domains, an approximately 50-residue long membrane proximal stalk and a transmembrane segment (Vosberg *et al.*, 2018). This also possesses a very large cytoplasmic tail of approximately 350 residues without a defined domain structure. During the developing nervous system, guidance cues such as netrin 1 are bifunctional meaning they exhibit both attractive and repulsive effects (Vosberg *et al.*, 2018). Netrin 1 possesses the ability to bind to various cell surface receptors besides *DCC* (Vosberg *et al.*, 2018). This underlying mechanism of netrin-1 bifunctionality involves netrin-1 clustering different receptors together leading to alternative signalling outcomes. One example of a receptor Is UNC5. Crucially, *DCC* plays a significant role in the molecular switch from attraction to repulsion. *DCC* is expressed on the axonal surface and netrin-1 binding to *DCC* stimulates chemo attraction (Vosberg *et al.*, 2018). Association of netrin-1 with the extracellular portion of *DCC* leads to *DCC* homodimerization via its C-terminal cytoplasmic P3 motif but not the ecto-domains (Vosberg *et al.*, 2018). This recruits an intracellular signalling complex which leads to Src family kinase activation and eventually cytoskeleton rearrangement thus giving the attraction effect (Vosberg *et al.*, 2018). However, *DCC* co-expression of UNC5 on growth cones of neurons alters netrin mediated axon attraction to repulsion. Also, another study showed that a monoclonal antibody directed against the extracellular domains of *DCC* blocks attraction and repulsion thus displaying the critical role of *DCC* in both responses (Vosberg *et al.*, 2018). In the presence of netrin-1, UNC5 co immunoprecipitates with *DCC* thus suggesting formation of a ternary complex of netrin-1 with ecto domains of *DCC* and UNC5 (Vosberg *et al.*, 2018). Interestingly, the ternary complex also positions the cytoplasmic trail of two receptors in close proximity for interaction (Vosberg *et al.*, 2018). In hindsight, Netrin-1 binding to *DCC* alone results in axon attraction. More importantly, *DCC* may switch the netrin-1 mediated responses from attraction to repulsion when another receptor UNC5 co-exists (Vosberg *et al.*, 2018).

5.4 P38A is identified as possessing mutated *FAF1* using BLAT

The P38A clone contains potential mutation of the *FAF1* gene (Figure 5.4), otherwise known as *Fas-associated factor 1* is a fas-binding protein with a role in apoptosis (Sul *et al.*, 2013). *FAF1* can either stimulate or increase levels of Fas-mediated apoptotic cell death (Sul *et al.*, 2013). *FAF1* has been shown to play a role in various mechanisms which promote cell death and mediates caspase-8 activation via both intrinsic and extrinsic pathways (Yu *et al.*, 2016). Also, this suppresses NF-Kb activation by interrupting the IKK complex assembly(Yu *et al.*, 2016). *FAF1* also arrests the cell cycle by negatively regulating Aurora A thus inducing cell cycle arrest in the G2/M phase and cell death (Yu *et al.*, 2016). It also interacts with poly ubiquitinated proteins and valosin-containing protein thus inhibiting ubiquitin-dependent protein degradation. *FAF1* downregulation has also been shown in cervical and gastric carcinomas (Yu *et al.*, 2016). Finally, *FAF1* possesses domains with high homology to ubiquitin (Yu *et al.*, 2016). Since then, protein aggregation arising from ubiquitination has been implicated in neurodegenerative diseases.

FAF1 has been long known to possess a tumour suppressive role but has also been implicated in the pathogenesis of Parkinson's disease (Buddhala *et al.*, 2015). The human *FAF1* gene was localised to chromosome 1p32 at the PARK10 locus recently associated with late-onset Parkinson's disease (Sul *et al.*, 2013). *FAF1* expression has been seen to be significantly increased in the frontal cortex and midbrain of Parkinson's disease patients (Buddhala *et al.*, 2015). This potentiates the toxic effects of stressors which are associated with Parkinson's disease such as oxidative stress. Interestingly, perineuronal nets which this study is based on also play a key role in protecting neurons from oxidative stress (Buddhala *et al.*, 2015). *FAF1* is classified as a pathogenic substrate of parkin which is an ubiquitin E3 ligase. Inactivation of parkin via Parkinson disease linked mutations or by generic deletions results in *FAF1* accumulation and induction of *FAF1*-mediated biochemical events (Buddhala *et al.*, 2015). These include Caspase-3 activation, c-jun-N-terminal kinase activation and cell death occurring upon oxidative stress. This suggests that *FAF1* possesses a significant role in oxidative stress induced cell death and Parkinson's disease pathogenesis via its action on the apoptotic machinery (Sul *et al.*, 2013). As well as necrosis, apoptosis has also been implicated in the pathogenesis of Parkinson's disease. Various death promoting proteins such as p53 and JNK mediate both apoptosis and necrosis upon oxidative stress (Sul *et al.*, 2013). Previous studies have

also shown that *FAF1* acts as a positive modulator for Parkinson's disease and that *FAF1* deficiency disrupted Parkinson disease linked biochemical events such as caspase activation, reactive oxygen species generation (Yu, Kim and Kim, 2016). JNK activation and cell death. Also, *FAF1* has been shown to mediate regulated necrosis through PARP1 activation upon oxidative stress resulting in dopaminergic neurodegeneration (Yu, Kim and Kim, 2016). *FAF1* also possesses interactions with NGRYL1 which has been linked to congenital disorder of glycosylation thus making it important that I investigate the role of *FAF1* in PNNs (Buddhala *et al.*, 2015). *FAF1* has been shown to bind to NGLY1 which is an enzyme involved in congenital disorder of glycosylation. *FAF1* plays a regulatory role in NGLY1 function leading to potential removal of glycan groups from CS-GAG side chains on CSPGs, hyaluronan or tenascins resulting from partial regulatory loss due to decreased *FAF1* expression. This would then, in turn, alter PNN structural integrity due to deglycosylation of these key components and would reduce PNN density and neural plasticity. In addition to this, it is important to note the role of the ERAD complex which is involved in mediating the endoplasmic reticulum stress response also known as the 'unfolded protein response'. This is stimulated in order to degrade misfolded proteins, preventing their toxic aggregation (Hoozemans *et al.*,2012). NGLY1 is required for the ERAD complex function and various protein interactions such as between *FAF1* and NGLY1 and is required for efficient ERAD processing (Bertozzi *et al.*,2017). Clinical studies have shown that NGLY1 mutations results in neurological conditions including neurodevelopmental delay and neuropathy of the peripheral nervous system which occurs as a result of increased levels of misfolded proteins within the cell (Caglayan *et al.*,2014). It has been proposed that loss of *FAF1* as a critical factor for NGLY1 function could result in toxic build-up of misfolded proteins in Alzheimer's and Parkinson's diseases (Caglayan *et al.*,2014).

Furthermore, during Parkinson's disease, build-up of the synaptic protein α-synuclein occurs, forming into aggregates known as Lewy bodies. *FAF1* has been shown to restore autophagic flux for α-synuclein degradation in the brain of a Parkinson's disease mouse model. Moreover, *FAF1* has been known to play a role in oxidative stress and recently it has been shown that PNN populations are unaffected in Parkinson's disease brains but are involved in protecting neurons from developing α-synuclein pathology *in vitro* and in Parkinson diseased brains (Dickens, S.M, 2021).

5.5 U1B is identified as containing a mutation of the *GALNTL6* gene

U1B was the only gene trap mutation event which demonstrably occurred within an intron and caused splicing to an exon (Figure 5.4). As mentioned previously, WFA recognises proteoglycans with chains of N-linked glycans and O-linked glycans and so it was entirely logical that an enzyme, *GALNTL6*, responsible for O-linked glycosylation should emerge from the screen (Bennett *et al.*, 2014). *GALNTL6* is known by various names including GALNT17, UDP-N-Acetyl-Alpha-D-Galactosamine: Polypeptide N-Acetylgalactosaminyltransferase 20, GalNAc Transferase 17, and GALNACT20 (Bennett *et al.*, 2014). Though most protein glycosylation is controlled by one or two genes encoding the enzymes responsible for glycosylation initiation, mucin type O-glycosylation is controlled by a large family of up to 20 homologous genes classified as GalNAc-transferases (Bennett *et al.*, 2014). Mucin type O- glycosylation is stimulated by this family and these catalyse the first step in the biosynthesis thus forming the GalNAcα1-O-serine/threonine linkage in O-glycoproteins (Bennett *et al.*, 2014). These enzymes controlling the first step renders mucin type O-glycosylation unique compared to other protein glycosylation types (Bennett *et al.*, 2014). O-GalNac residues are processed further by the addition of various monosaccharides which are catalysed by more than 30 distinct glycosyltransferases, and this occurs in the Golgi apparatus after the protein folding stage. GalNac-Ts are classified as a subfamily of the glycosyltransferase family (Bennett *et al.*, 2014). A total of 20 human genes have already been identified with 17 being reported in the literature. This family is highly conserved throughout metazoan evolution and though the members vary, all completed genomes possess large families of highly homologous sequences (Bennett *et al.*, 2014). Members of this family share the common type II membrane structure of Golgi glycosyltransferases with a short N-terminal cytoplasmic tail, a hydrophobic non-cleaved signal sequence serving as a membrane spanning domain, a stem region of variable length and a luminal catalytic domain (Bennett *et al.*, 2014). These are also unique in the sense that they possess a C-terminal ricin-like domain of approximately 120 amino acids in addition to a catalytic unit. Their catalytic domains approximately 230 amino acids in length contain a GT-A structural motif which are characterized by two tightly interacting β-α-β Rossman-like folds (Bennett *et al.*, 2014).

Studies have shown that by blocking and inactivating mutations in the lectin domains, this affects the GalNAc-glycopeptide substrate specificities of the enzymes. These lectin domains function to regulate and enhance the catalytic efficiency of GalNAc-Ts with partially GalNAc-glycosylated substrates possessing a high density of acceptor sites as located within mucin tandem repeat sequences. It has been postulated that lectin domains could potentially enhance binding of GalNAc-

Ts to mucin substrates to stimulate initiation of O-glycosylation before O-glycans are elongated during the processing step. This is important as this would interfere with addition of GalNAc residues. The initiation process occurs simultaneously with the processing step in the Golgi meaning that the combined binding affinities of the catalytic and lectin domains may enhance competition as long as acceptor sites are available (Saito *et al.*, 2015).

GALNTL6 possesses an unusual glycine residue in the Gal/GalNAc-T motif (Bennett *et al.*, 2014). *GALNTL6* possesses a different acceptor substrate specificity from the other members of the family in that it transfers Gal to Xyl which is essential for the production of the link region of proteoglycans (Bennett *et al.*, 2014).

5.6 Conclusion

In this chapter, I identified genes which when mutated appeared to reduce live WFA staining indicating a dysfunctional perineuronal net. The three main genes identified were *FAF1*, *DCC* and *GALNTL6*. Both *FAF1* and *DCC* appeared to be intronic insertions/splicing from the gene trap vector, whereas *GALNTL6* demonstrated the expected exonic splicing process. Interestingly, all three have been previously implicated in brains diseases with varying modes and methods of disruption. For example, *FAF1* has been shown to play a key role in Parkinson's disease whereas *DCC* has been described as a risk factor for schizophrenia. However, perhaps, the most intriguing of all is *GALNTL6*, which is a part of the glycosyl transferases family and a well-known glycosylation enzyme playing a significant role in mucin type O-linked glycosylation. Although various genes were identified, these were considered the three most important candidates due to their roles in neuropsychiatric diseases and or glycosylation. Other genes were not pursued due to have no known link with the extracellular matrix or neuropsychiatric diseases such as *ADGRL2* (a latrophilin) or *SUGCT* (involved in lysine degradation). The gene trap screen has been shown to be relatively successful. However, with caution, the gene trap screen only identifies genes which have introns and will not identify genes which have no introns or very small introns. The next steps to be undertaken relate to validation of these genes - that they are indeed failing to produce a functional perineuronal net when mutated via alternative methods such as CRISPR and RNAi. In the next chapter, I will examine the results of producing *FAF1*, *DCC* and *GALNTL6* CRISPR knockouts. Furthermore, use of siRNA knockdown and pharmacological inhibition will also be utilised to determine the effect of the mutated genes on WFA-binding glycoprotein expression and hence perineuronal net formation.

CHAPTER 6

RESULTS: Applying CRISPR mutation, siRNA knockdown, and pharmacological inhibition to examine candidate protein function.

In previous chapters, a number of genes were identified which, when mutated, had reduced expression of WFA-binding glycoprotein and therefore were putatively failing to produce a functional perineuronal net. This screen was undertaken using live cell staining, immunofluorescence microscopy followed by RNA extraction, cDNA synthesis, RACE-PCR and sequencing. Candidate prioritisation led to a focus on three candidate genes; *FAF1*, *DCC* and *GALNTL6*. Gene trapping produces heterozygous loss-of-function mutations, rather than completely homozygous deletions. The advantages of this approach are that cellular lethality caused by mutation is less likely, and that many human and mouse mutations have heterozygote phenotypes. However, the full effect of mutations is often only felt in the homozygous state.

Therefore, in this chapter, in order to validate our findings, I explored what happens to WFA staining when a full homozygous knock-out of the genes was attempted. In CRISPR mutagenesis, both copies of the gene will be knocked out. In siRNA interference and pharmacological inhibition, the percentage loss-of-function could be anywhere in a continuous distribution from 0-100%. CRISPR is a cutting-edge technique which permits researchers to alter parts of the genome by removal, addition, or alteration of the DNA sequence. The CRISPR-Cas9 system is composed of two key molecules which introduce mutations into the DNA. This is an enzyme called Cas9 which acts as a pair of molecular scissors which can cut two strands of DNA at a specific location within the genome so that parts of the DNA can be added or removed. The second component is single guide RNA which consists of a small piece of predesigned RNA sequence of up to 20 bases long which is located within a longer RNA scaffold. This sgRNA guides Cas9 to the right part of the genome. This ensures that the Cas9 enzyme cuts at a specific, desired position within the genome. During the particular process of DNA repair that follows this cut (non-homologous end-joining (NHEJ)), deletions or insertions are introduced generally producing a non-functional allele of the gene.

RNA interference is a natural process with a role in the regulation of protein synthesis and in immunity. This is also a key tool for the exploration and manipulation of gene expression. Small pieces of RNA which permit RNA interference come in two forms: small interfering RNA (siRNA) and microRNA (miRNA). Both are approximately 22 nucleotides long but differ in their specificity, role and how they are synthesised. siRNAs are highly specific and are usually synthesised to decrease

the translation of specific messenger RNAs. siRNA molecules connect to and activate protein complexes such as the RNA-induced silencing complex. Once they are bound, they can bind to their target mRNAs and physically hinder ribosome's from continuing to produce the protein and mark that mRNA for destruction. This process is significant in regulating protein synthesis by acting as a layer of control separate and downstream from the various genes which regulate transcription itself. RNA interference prevents mRNAs from outlasting their need by removal before natural degradation.

6.2 Crispr construct design and purchase.

Initially, CRISPR constructs were created using sgRNAs designed in-house using the online resource, CHOPCHOP (https://chopchop.cbu.uib.no/) (see Materials and Methods Chapter). The synthesised sgRNAs were cloned into a plasmid vector allowing co-expression of sgRNA, CAS9, and antibiotic resistance. The last of these gene components allowed us to select for stably transfected *SH-SY5Y* cells expressing the CAS9 system, potentially maximising the chance of target gene disruption at the cellular and population level. Those cells that survived the antibiotic selection process would essentially become a pool of antibiotic resistant and CRISPR-mutated cells. The pools of resistant cells were then sub-cloned to allow growth of single colonies (potentially genetically pure) for further analysis. This led to experiments being conducted with cells *DCC* A, *DCC* B, *FAF1* E, *GALNTL6* E as well as importantly pool cells; *FAF1* pool, *GALNTL6* pool, and *DCC* pool though no s

For protein analysis by western blot and immunofluorescence, all CRISPR cell lines were individually stained with their corresponding anti-protein antibody as well as with biotinylated WFA for PNN level assessment. Live cell staining was also undertaken with all putative CRISPR knockouts. Furthermore, with regards to *FAF1*, two additional experiments were carried out. Firstly, with the hypothesis that *FAF1* disruption might only affect the correct trafficking of PNN proteins to the cell surface rather than reduce the total expression of PNN proteins (and hence produce an apparent PNN deficit only in live staining), enzymatic digestion of external/membrane bound proteins with trypsin was carried out to assess the location of immunoreactivity. Secondly, pharmacological inhibition of *FAF1* was carried out using KR-33493, a known potent *FAF1* inhibitor.

6.3 In-house designed CRISPR construct results.

CRIPSR constructs were designed in house for each candidate protein, and this was then subsequently tested via Western blotting and immunofluorescence to confirm whether gene expression of the candidate proteins had been decreased. Below, *DCC* knockout constructs had been produced and were then analysed for *DCC* expression using protein analysis (Fig 6.1). No *DCC* CRISPR KO's were produced, so I was unable to examine the effect on WFA-binding glycoprotein expression.
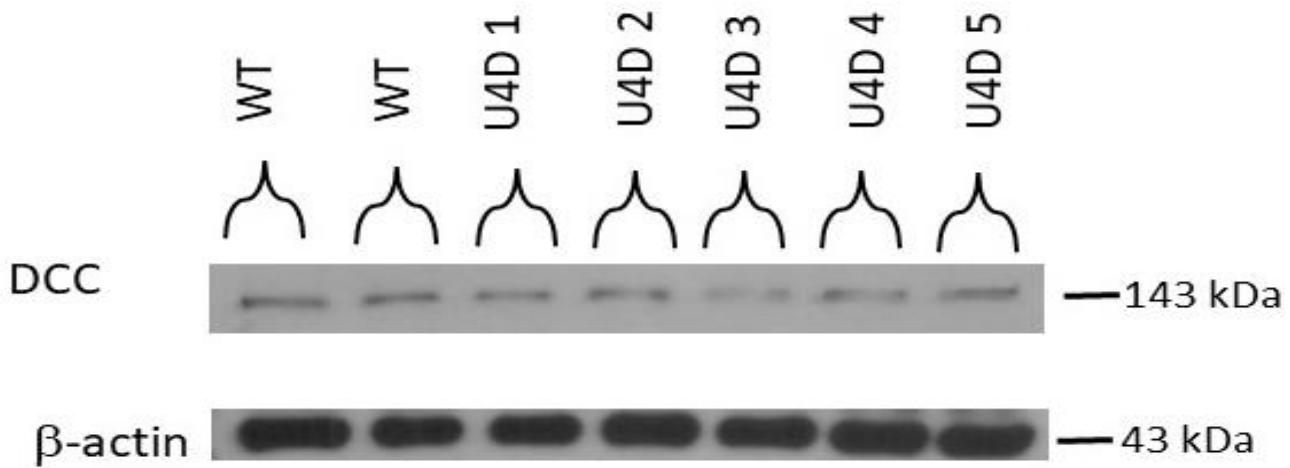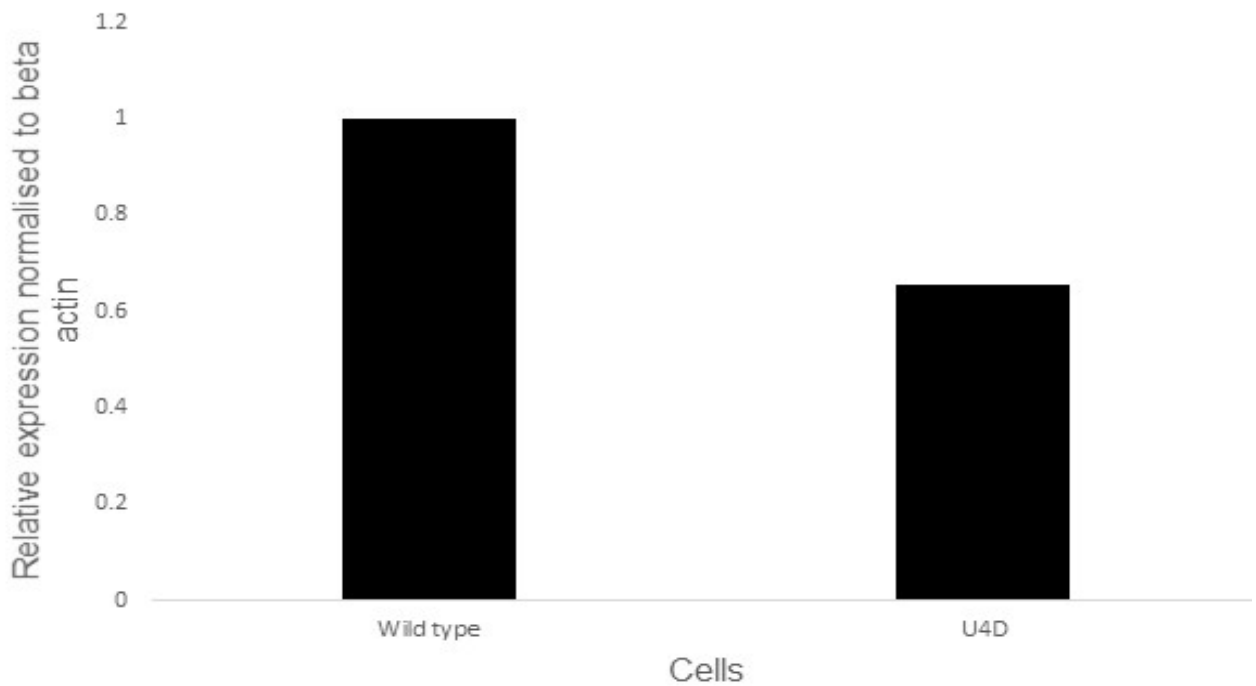
Figure 6.1 DCC expression still detected after attempted CRISPR knockout. *Figure 6.1 shows that there is of DCC expression detected during protein analysis of mutant gene trap colony U4D. Western blot analysis of DCC expression indicated some difference between wild type and mutant colony U4D. Beta actin loading control was used to normalise data. N=1 so no statistical analysis was undertaken.*

CRIPSR constructs were designed in house for each candidate protein, and this was then subsequently tested via Western blotting and immunofluorescence to confirm whether gene expression of the candidate proteins had been decreased. Below, *GALNTL6* knockout constructs had been produced and were then analysed for *GALNTL6* using protein analysis (Fig 6.2). No *GALNTL6* CRISPR KO's had been produced so I was unable to analyse WFA-binding glycoprotein expression.
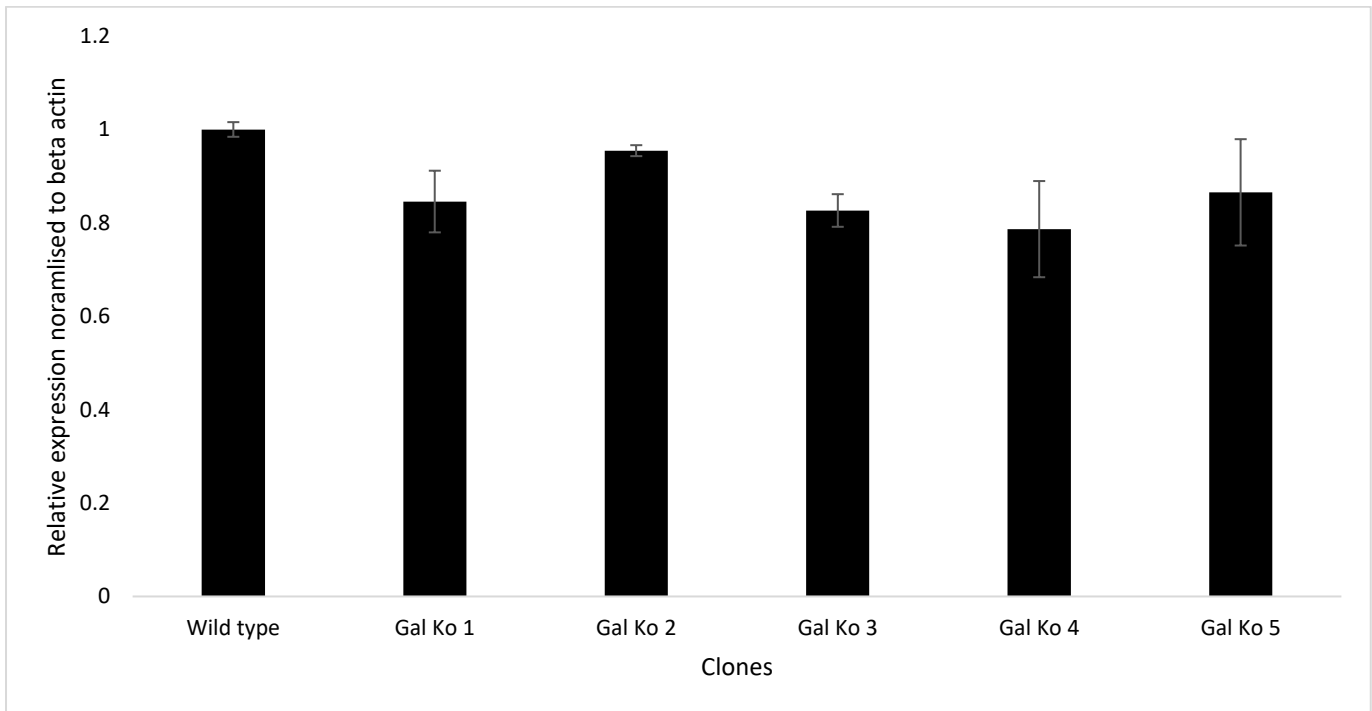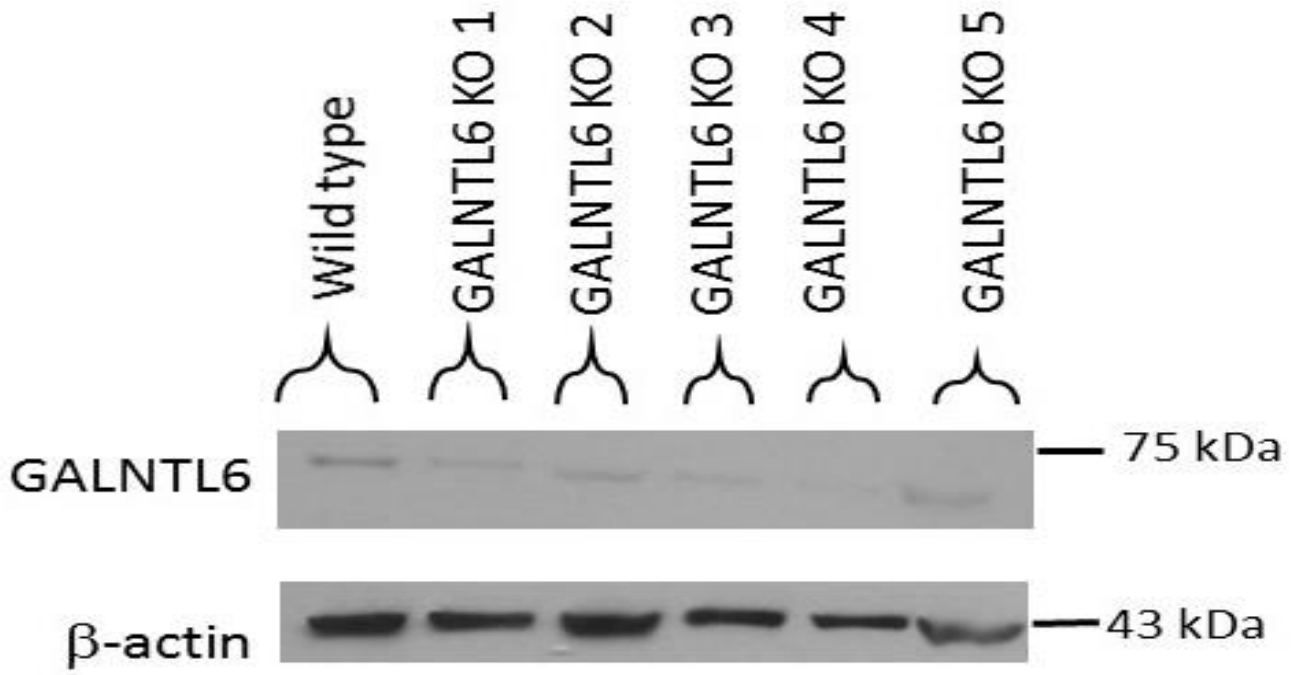
Figure 6.2 No significant change seen in GALNTL6 expression of attempted CRISPR knockout of GALNTL6 during protein analysis. *Figure 6.2 shows that there is no change in GALNTL6 expression levels during protein analysis of GALNTL6 CRISPR mutants. Beta actin loading control was used to normalise data. N=3. Relevant statistical analysis was undertaken including Two-tailed T-testing and SEM. P>0.05*

CRIPSR constructs were designed in house for each candidate protein, and this was then subsequently tested via western blotting and immunofluorescence to confirm whether gene expression of the candidate proteins had been decreased. *FAF1* mutant knockout constructs had been produced and were then analysed for *FAF1* using protein analysis. Although no successful FAF 1 CRISPR KOs had been produced due to technical issues, I was unable to examine for any subsequent effect on WFA-binding glycoprotein expression. Furthermore, mutant colony P38a was also analysed for *FAF1* expression (Figure 6.3).
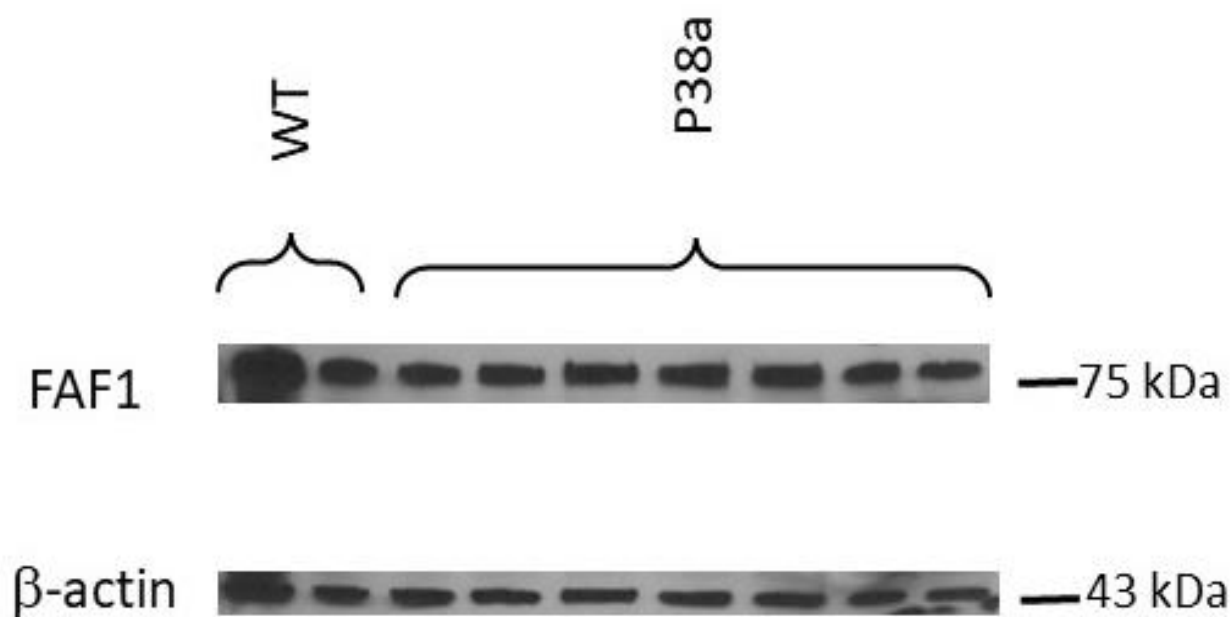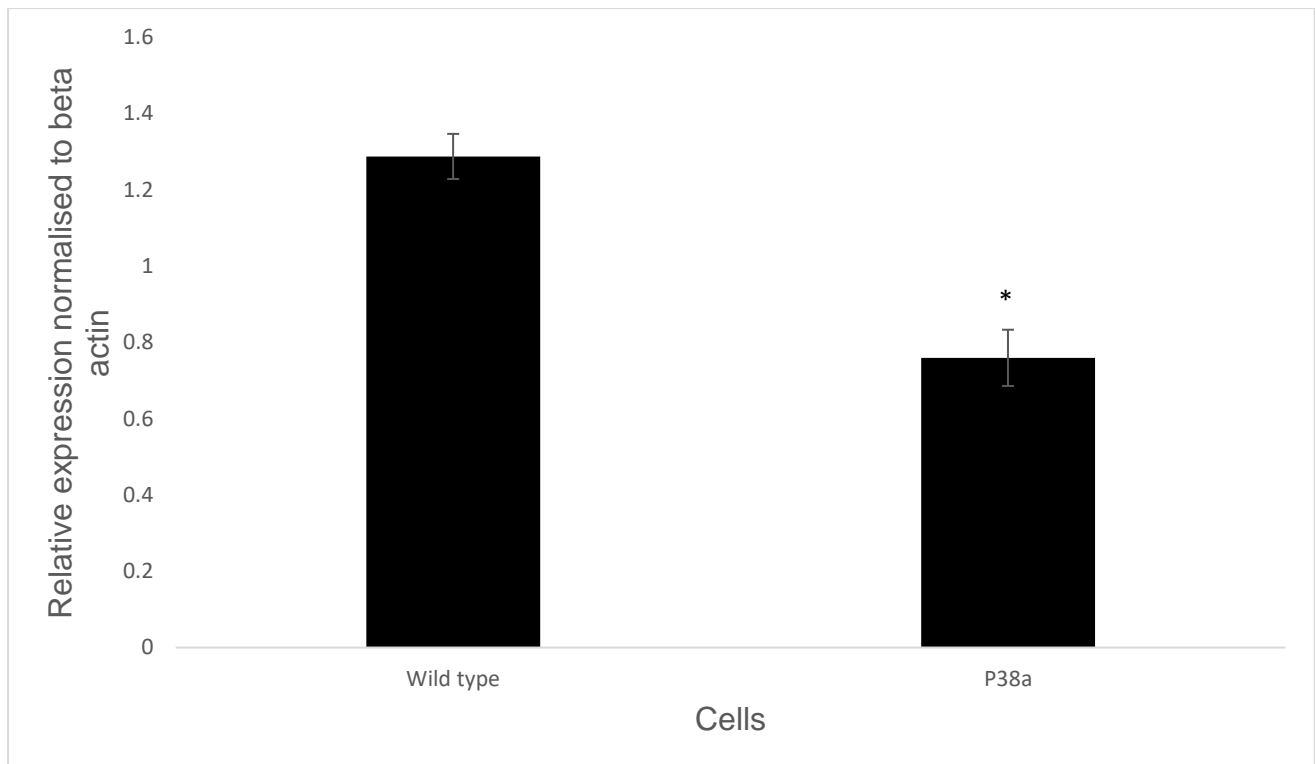
Figure 6.3 Reduced FAF1 levels seen in mutant colony P38A during protein analysis. *Figure 6.3 shows that there is reduced expression in FAF1 expression levels during protein analysis of mutant colony P38A. Western blot analysis of FAF1 expression indicated significant difference between wild type and mutant colonies. Since P38A is a gene trap mutant colony, it would be expected that it would have 50 % expression in comparison with wild type. Beta actin loading control was used to normalise data N=3. Relevant statistical analysis was undertaken including Two-tailed T-testing and SEM.*p<0.05*

A trypsinisation experiment was also undertaken to determine whether any effect of *FAF1* disruption is mediated by a trafficking failure rather than absolute production of the PNN. Trypsin was used to digest and remove the extracellular matrix/PNN from cells before analysis by Western, but would be unable to digest any matrix that was still inside the cell because of a failure to traffick it to the surface. It was predicted that WT cells would lose the majority of PNN/WFA staining on Western blots, whereas a trafficking mutant would still have staining because the PNN components recognised by WFA would have been protected within the cell. Another enzymatic option that could have been used was ChABC or MMP-9. Two flasks each of WT cells and *FAF1* CRISPR pool cells were prepared. One of each had protein extracted using the normal lysis/scraping approach and samples were labelled WT and *FAF1*, respectively. The other two were digested for 15 minutes at 37ºC with trypsin

to remove the PNN/ECM then, after washing these suspended cells with PBS and centrifuging, the pelleted cells were lysed to produce sample WT(tryp) and *FAF1*(tryp), respectively. Protein analysis was then undertaken, and Images were developed using X ray film (Methods) and processed using ImageJ (Figure 6.4).
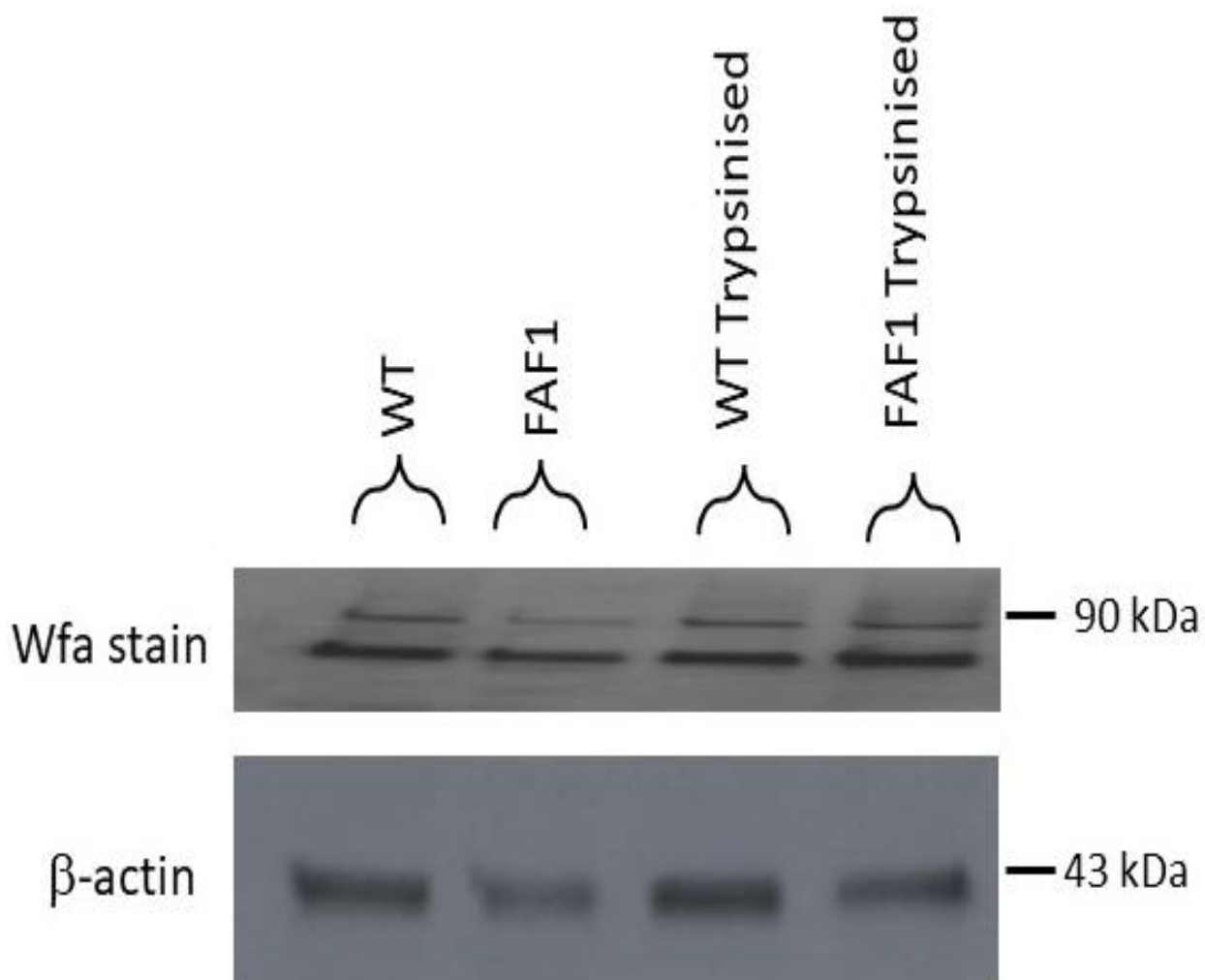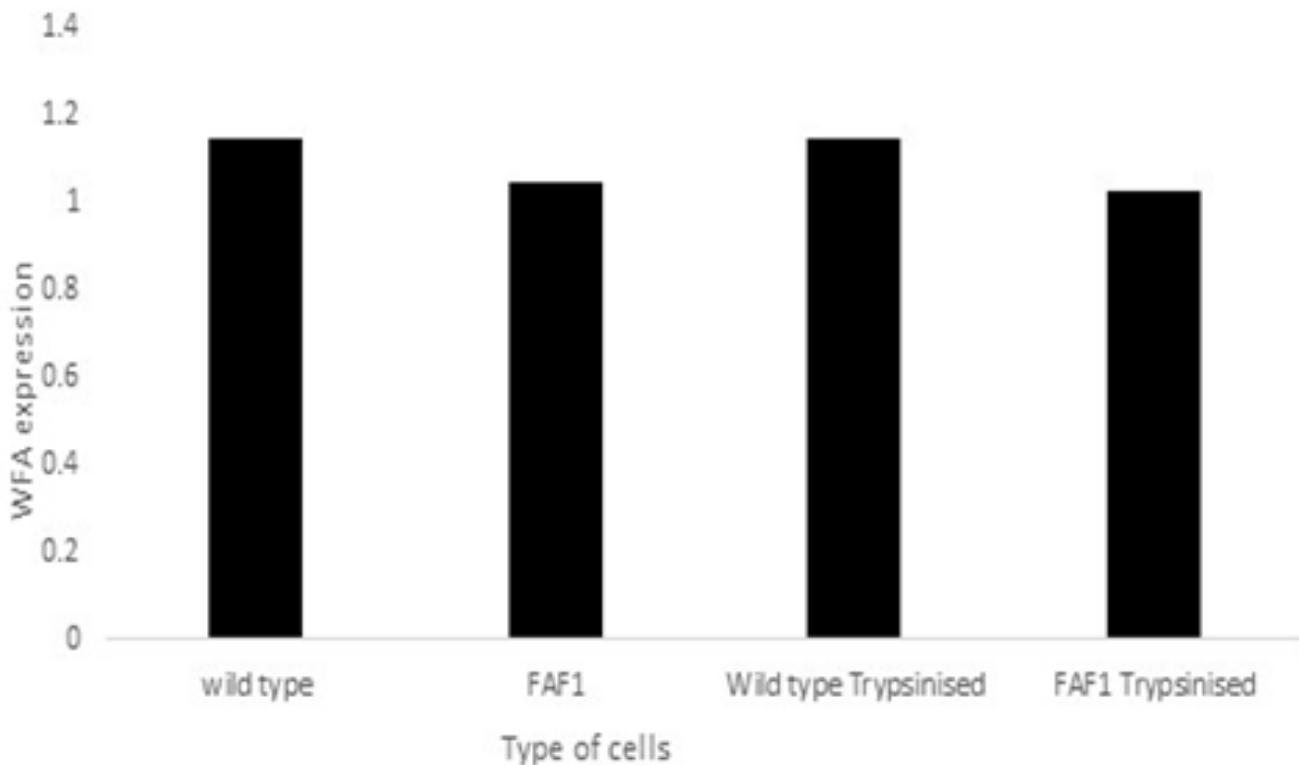
Figure 6.4 No reduced WFA *staining seen in wild type or FAF1 pool cells when trypsinised.*
Figure 6.4 above shows the results of protein analysis of WFA-binding glycoprotein *expression of wild type and trypsinised FAF1 pool cells. Western blot analysis of* WFA *staining indicated little difference between wild type cells and trypsinised FAF1 pool cells. Beta actin loading control was used to normalise data. N=1 so no statistical analysis was undertaken.*

If all the PNN proteins in the *FAF1* mutant had been locked up internally because of a trafficking error preventing them from being expressed on the surface, then trypsinisation would have had no effect on the WFA protein quantity in the *FAF1*(tryp) sample because the PNN proteins would not have been exposed to the enzyme. In fact, I can suggest that trypsin is not perhaps the best enzyme for this kind of experiment because I did not see evidence for the WT(tryp) showing reduced WFA staining which *would* have been expected because it has PNN expressed on the surface as demonstrated by the live staining. Better enzymes to have used would have been MMP9 or Chondroitinase.

141

6.4 siRNA inhibition of GALNTL6

Previously, I utilised CRISPR to knock out the candidate genes and see if there was any reduction in WFA-binding glycoprotein expression. However, despite some extensive research, I was not fully convinced that the CRISPR was working correctly to reduce the expression of the target genes. I then decided to try another alternative approach using siRNA. By transiently downregulating expression by degrading mRNAs, I could then see if there was any reduction in WFA-binding glycoprotein expression. I chose to focus solely on *GALNTL6* since it was the best candidate gene and undertook siRNA interference of the *GALNTL6* gene. Analysis was undertaken using protein analysis (Fig 6.5). The results showed that despite interference and attempted downregulation of the *GALNTL6* gene, there was no reduction in WFA-binding glycoprotein expression.
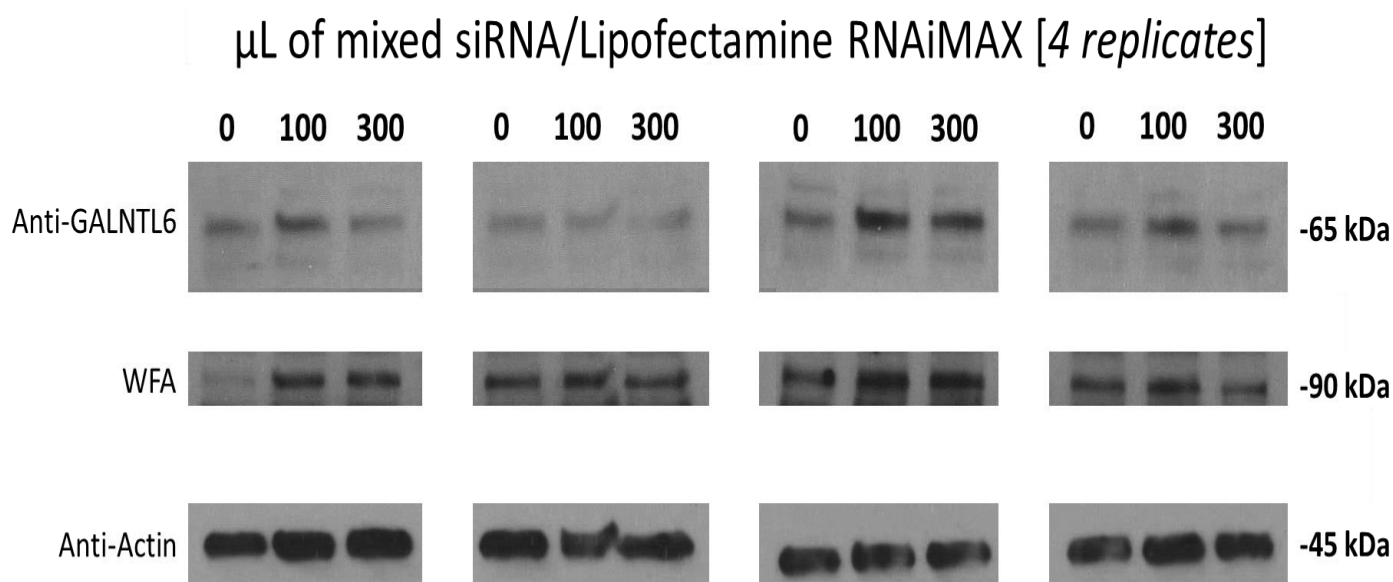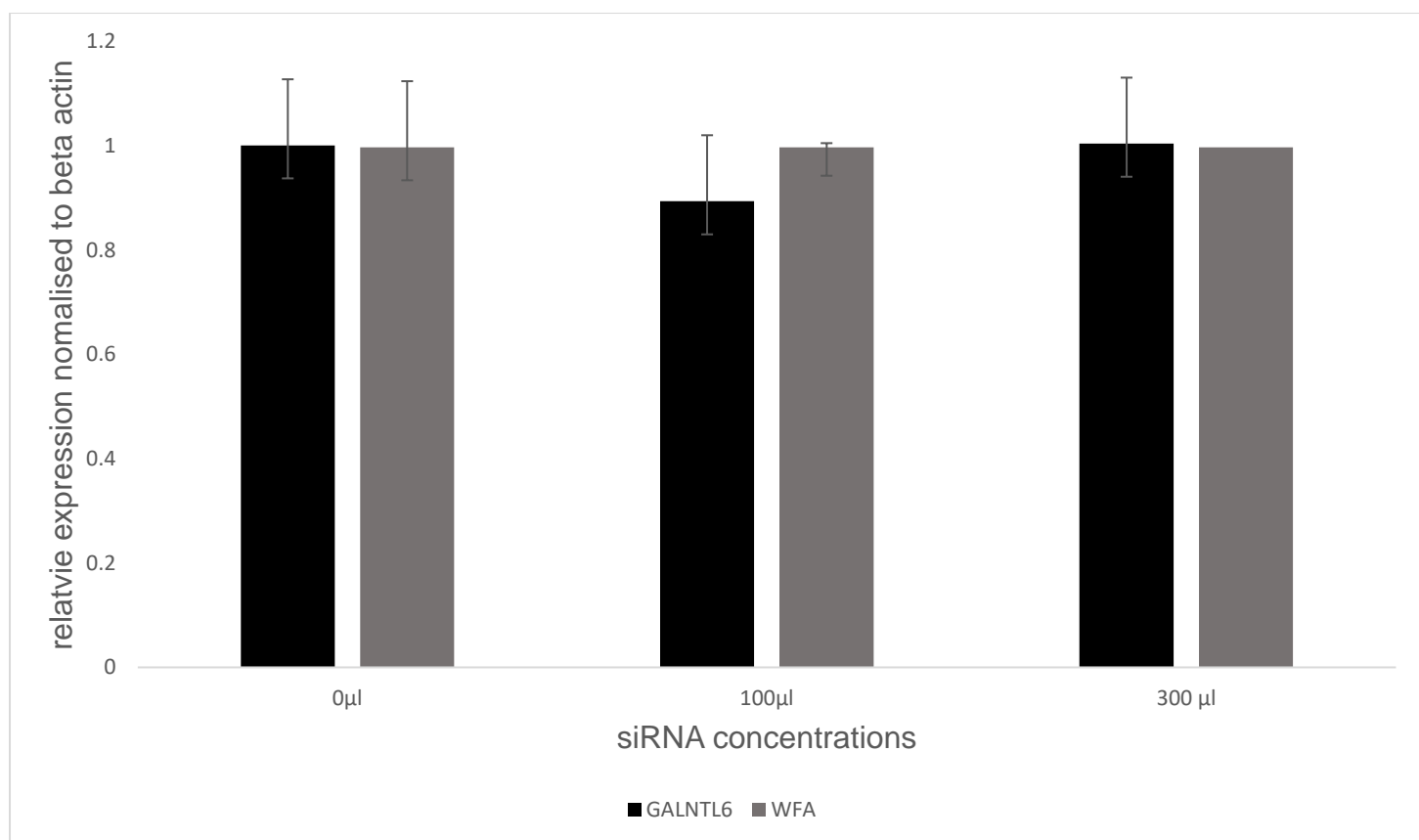
Figure 6.5 Attempted siRNA silencing of *GALNTL6* did not decrease GALNTL6 protein expression or alter WFA staining. *Figure 6.5 shows the results obtained when siRNA interference of GALNTL6 occurs. As you can see above, despite increasing the concentration of GALNTL6 siRNA to 300 µl, there is no reduction in WFA staining. Here, I utilised protein analysis to determine any alteration in WFA-binding glycoprotein expression. It can be seen that despite there is no reduction in WFA staining but there is no clear evidence of GALNTL6 being downregulated. N=4 so relevant statistical analysis was undertaken including T testing. Relevant statistical analysis was undertaken including Two-tailed T-testing and SEM. P>0.05*

6.5 Pharmacological inhibition of *FAF1* protein

Despite seeing reduced WFA staining in the initial gene trap screen, the results here show that there is no reduction in WFA staining when these genes are knocked out or silence via CRISPR or siRNA. Unfortunately, I seen no clear evidence that any of the candidate's protein expression was reduced using CRISPR or siRNA. As a result, I cannot say whether these candidate genes have alterations

in their WFA-binding glycoprotein expression since I have been unable to fully knock out or silence the genes. The biological understanding of the system is hampered by the technological inefficiencies of the genetic ablation techniques I tried to use. Here, I decided to utilise a *FAF1* pharmacological approach which is much more direct because I can say that the drug either inhibits the protein or it doesn't. In the previous results obtained, it was shown that no *FAF1* CRISPR knockouts had been produced and it was difficult to state whether there is any reduced WFA staining in both the pools and mutant cells. Here, I utilised protein analysis and a *FAF1* inhibitor to see whether there was any alteration in WFA-binding glycoprotein expression. Cells were grown to confluence and treated with various concentrations of the *Faf1* protein inhibitor, KR-33493 for 48 hours. Analysis was then undertaken using western blotting. The results show that varying concentration of *FAF1* inhibitor (KR-33493) did not alter WFA-binding glycoprotein expression (Fig 6.6).
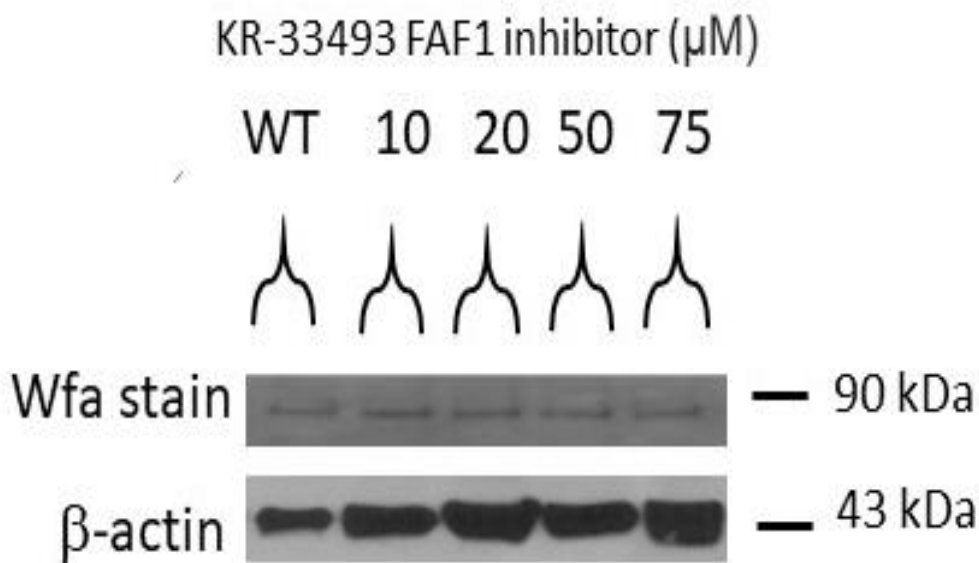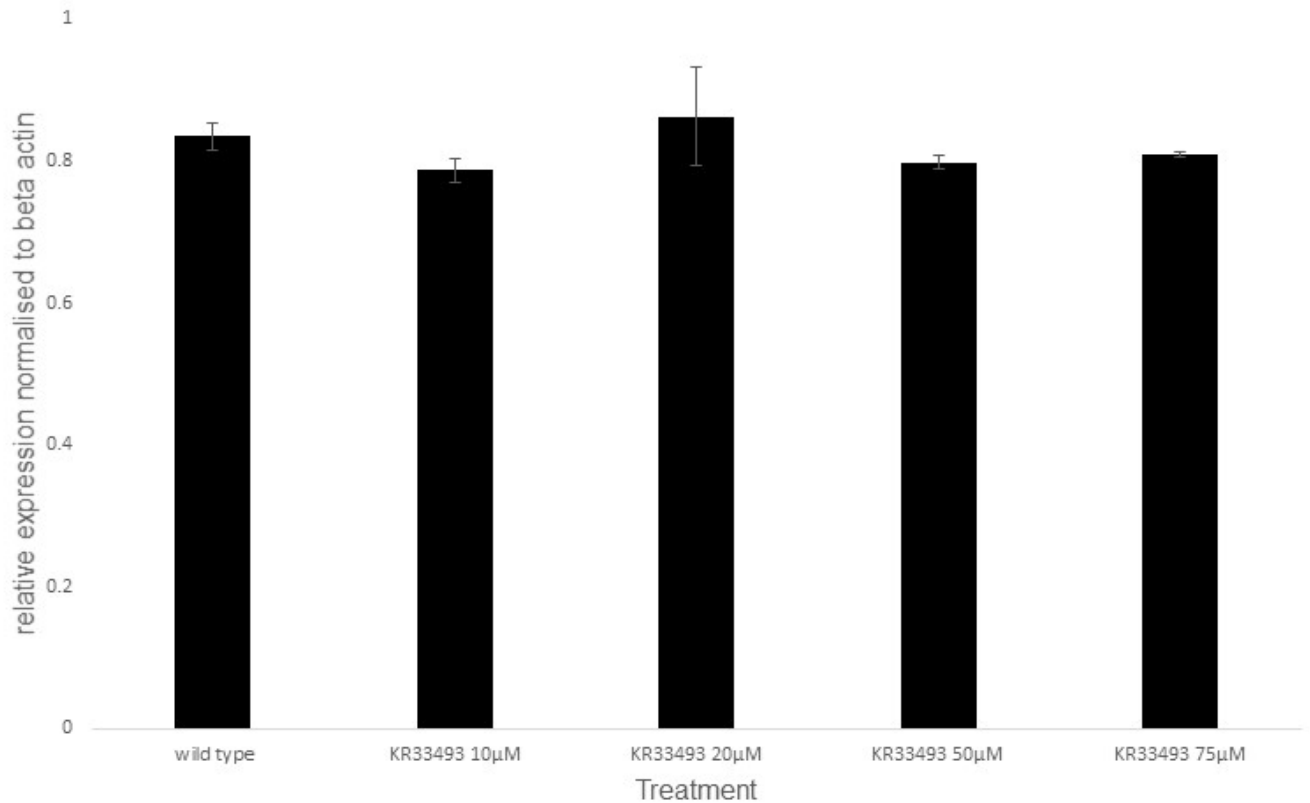
Figure 6.6 Use of FAF1 inhibitor KR-33493 does not reduce WFA *staining in wild type cells.*
Figure 6.6 shows the results obtained when wild type cells treated with increasing concentrations of
FAF1 inhibitor KR-33493 over a period of 48 hours. Western blot analysis of WFA-binding
glycoprotein *expression indicated little difference between wild type cells and cells treated with the*
FAF1 inhibitor. N=3 so relevant statistical analysis was undertaken including Two-tailed T-testing
and SEM P>0.05

The results above show that use of *FAF1* inhibitors have no effect on WFA-binding glycoprotein
expression. Although I identified *FAF1* in the initial gene trap screen as a mutant gene with reduced
WFA staining, the results conclude that inhibition of *FAF1* does not have any effect on WFA-binding
glycoprotein expression.

Chapter 6 focused on producing CRISPR knockouts of the 3 genes identified in the gene trap screen, *FAF1*, *DCC*, and *GALNTL6*, that were considered the strongest candidates for a role in the formation of the PNN. Furthermore, siRNA interference was also undertaken with regards to *GALNTL6* and pharmacological inhibition of *FAF1* activity as alternative ablation strategies. Protein analysis and immunofluorescence microscopy were undertaken to determine if there were any changes in WFA staining when these genes are either knocked out fully or silenced. The results showed that there was no reduction in WFA staining or any of the candidate genes within the attempted CRISPR KOs suggesting that there has been a failure to knock out the genes. This means that it cannot be confirmed whether there is reduced WFA-binding glycoprotein expression when these genes were knocked out. There was no clear evidence that the genes were fully knocked out during the CRISPR process. With respect to siRNA interference of *GALNTL6*, it was also shown that there was no reduction in WFA staining but importantly, I failed to downregulate expression of the *GALNTL6* gene. This is in contrast to the gene trap screen where there three genes were identified and sequenced as having reduced WFA staining or an abnormal perineuronal net shape. CRISPR is a well-documented technique which has shown to be effective at knocking out genes homozygous though also known for its off-target effects.   The same is also known for siRNA interference in which a gene is essentially silenced heterozygously. Also, a *FAF1* Inhibitor (KR-33493) was utilised to see whether inhibiting *FAF1* alters WFA-binding glycoprotein expression. This was also shown to be negative and a trypsinisation experiment of *FAF1* was also undertaken to determine whether trypsinising the cells could affect WFA staining. This also yielded no positive change in WFA-binding glycoprotein expression. The results obtained here show that despite identifying three candidate genes which have altered WFA-binding glycoprotein expression or perineuronal nets shapes when mutated during the gene trap screen, this was not reflected in the CRISPR or siRNA process due to the failure to knock out or downregulate *GALNTL6*. Looking at both the immunofluorescence microscopy and the protein analysis via western blotting, no significant change in WFA-binding glycoprotein expression was seen as no knockouts were produced. However, all 3 genes have been previously implicated in neuropsychiatric disease or processes. For example, *FAF1* has been previously implicated in Parkinson's disease, *DCC* has been identified as risk factor for schizophrenia in conjunction with its binding partner netrin 1. Finally, *GALNTL6* has been associated with mucin type O-linked glycosylation and glycosylation is a well-known process in the production of perineuronal

nets and chondroitin sulphate proteoglycans. Further examination of these genes is warranted in their potential roles and how they are involved in perineuronal net formation and what role do they play in chondroitin sulphate proteoglycans.

Chapter 7

RESULTS: Identifying the PNN protein component in SH-SH5Y cells which interacts with *Wisteria floribunda* (Japanese wisteria) agglutinin (WFA)

Chapter 3 described the staining pattern in *SH-SY5Y* cells observed with WFA. While WFA cellular immunoreactivity was obtained, and backed up by the detection of a specific reactive band(s) in Western blotting, the distribution of the staining was not directly comparable to the PNN morphology displayed by inhibitory interneurons *post mortem*. Two potential explanations exist: that the *SH-SY5Y* cells are so 'immature' (through ongoing proliferation) and non-neuronal that PNN formation is rudimentary OR that the WFA-reactive protein target is not the same as that observed in brain PNNs.

In this chapter, a pull-down assay was carried out to determine which glycoprotein(s) WFA binds to. Research has shown that all perineuronal nets contain *Aggrecan* even if they do not contain all of the other proteoglycans such as *Neurocan*, *Versican* etc. WFA is believed to bind to an unidentified sulphation motif or the N-acetyl galactosamine residues of chondroitin sulphate proteoglycans. In previous chapters, I have seen in protein analysis with WFA staining that sometimes there are one or two bands of WFA reactivity. The investigation here is to identify it/them to gain a better insight into PNN constitution and to see whether these might represent different isoforms of the same molecular entity.

The full methodology employed is detailed in the Methods Chapter. Briefly, *SH-SY5Y* cells were lysed under standard conditions (including protease inhibitor cocktail) and resulting proteins incubated overnight at 4°C in 50 mLs PBS with biotinylated WFA. Subsequently, streptavidin-conjugated resin beads were added to bind the biotin-WFA-protein target(s), and these were captured, washed with PBS, and finally eluted within a column plugged with glass wool. The resulting purified protein was analysed by Western blotting and by mass spectrometry-based identified at the 'FingerPrints' proteomics laboratory at the University of Dundee.

This process was carried out twice. In the first validation trial, cells from just one T25 flask of confluent *SH-SY5Y* cells were taken through the procedure described in the Materials and Methods Chapter 2 except that elution was either performed with hot CelLytic protein extraction buffer or, alternatively, hot 0.1% Sodium Dodecyl Sulphate (SDS) solution to determine the best elution strategy. Both approaches produced a similar yield of protein as depicted in a WFA-stained Western blot (fig. 7.1). The WFA-reactive band size which usually appears in our Western blotting of *SH-SY5Y* cells is 90 kDa. Two important statements can be made from this figure. Firstly, the lack of actin loading control

detected in the affinity-purified eluates indicates that the purification process has been relatively efficient at removing the majority of irrelevant proteins. Secondly, there is a drop from ~90 to ~30 kDa (figure 7.1) in detected band size after affinity purification. This does not appear to be the result of generalised degradation of the original protein (e.g., through indiscriminate protease action as the protease inhibitor cocktail concentration is reduced in the affinity binding stage) because the detected bands are sharp and discrete in nature. I suggest that this may represent a specific cleavage or dissociation event. For example, one potential PNN protein that might be captured by this protocol might be *Aggrecan*. Two members of the ADAMTS protease family exists called *Aggrecan*ase-1 and -2 are known to cleave this PNN component resulting in smaller polypeptides. I note that the FA binding step will occur in a large liquid volume that will have diluted the active concentration of the protease inhibitors. However, the published molecular light of *Aggrecan* core protein is 210-250 kDa, and much more when glycosylated, making this an unlikely candidate for this hypothesis.
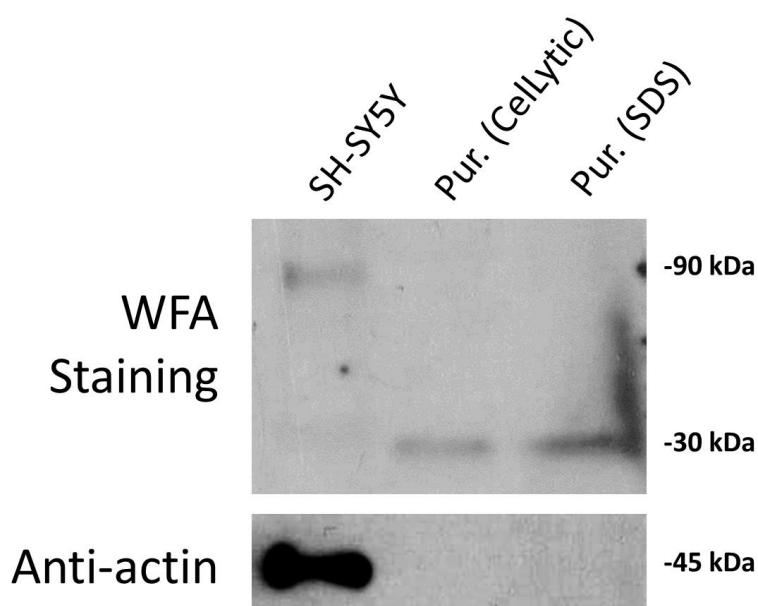
Figure 7.1. Successful pull-down of WFA-binding protein from SH-SY5Y cells. *Three protein samples were assessed by SDS-PAGE and Western blotting: protein lysate of standard SH-SY5Y cells, SH-SY5Y lysate that has been affinity purified and eluted from WFA/Sepharose beads using CelLytic agent at 60ºC (Pur. CelLytic), and SH-SY5Y lysate that has been affinity purified and eluted from WFA/Sepharose beads using 0.1% SDS at 60ºC (Pur. SDS). A band of 90 kDa can be seen for the first sample (consistent with previous experiments) but both the purified products show a drop in size of 60 kDa to ~30 kDa. This does not appear to be the result of generalised degradation of the original protein (e.g., through indiscriminate protease action) but may represent a specific cleavage event that occurred during the overnight incubation in PBS. Importantly, there is no Beta-actin visible in the purified samples indicating that the purification process has removed a considerable portion of the total proteome.*

In a second, larger-scale (2 x confluent T75 flasks), preparation eluate from the preparative process detailed in the Methods was fully loaded onto a polyacrylamide gel, briefly run into the gel, and a gel slice taken, fixed in methanol/acetic acid, dried, and sent for proteomic analysis at the FingerPrints Proteomics Laboratory at the University of Dundee. Results were returned in a spreadsheet (Appendix 1) in which candidate proteins were ranked according to the cumulative instances of each identified peptide fragment sequence from each protein (the Mascot Score; Mascot being the software package used to convert mass spectrometry m/z values into identified protein fragments). A number of 'FingerPrints' bespoke quality control qualifiers were also applied such that certain proteins were annotated as 'contamination', principally members of the keratin family. As keratin is a skin protein, the assumption made was that this represents handling issues. I am not convinced by this categorisation because PPE usage will have prevented this.

Regardless, the list of identified proteins was surprisingly extensive (803 proteins: approximately 4% of all proteins). However, as can be seen in Fig 7.2, the majority of these may represent rare 'carry-over' from the purification process, determined by the low number of different peptide fragments identified (Y-axis) and their low cumulative abundance (X-axis, Mascot Score). Additionally, a number of high-abundance cellular proteins were identified such as HNRP proteins, ribonucleoproteins, and cytoskeleton components like tubulin. I propose that these failed to be completely washed out of the column during the pull-down, perhaps due to their abundance or non-specific association with WFA or biotin.

I reasoned that the true WFA-binding protein would have several specific properties that might give us confidence of true identification. These were:

- Being a secreted or membrane-bound protein
- Having known or potential glycosylation sites, specifically the O-linked glycosylation sites that form the post-translational modification known to be the target for WFA binding.
- Being of approximately 90 or 30 kDa molecular light as determined by Western blotting.
- Having prior evidence for a role in extracellular matrix formation/function.

In Table 7.1, the top candidates, excluding proteins deemed contamination, are ranked according to the Mascot Score. Vimentin (VIM), in fourth place, is the closest fit to our criteria. If being nominally extracellular is the most important consideration, then Annexin 6 (ANXA67) becomes the most

favourable protein. Both are displayed in a plot of Mascot Score against total number of peptides identified in Figure 7.2. Only ANXA6 (Annexin A6) came somewhat close to fulfilling the criteria as it can be extracellular in some instances but has very low scores in the other molecular criteria as indicated by its position in the scatterplot. Annexin 6 is part of a family of calcium dependent membrane and phospholipid binding proteins (Takagi *et al.*, 2002). Their functions are still not clearly defined and various members of the annexin family are known to be involved in exocytic and endocytic pathways (Takagi *et al.*, 2002). Annexin 6 is a protein involved in mediating the endosome aggregation and vesicle fusion in secreting epithelia during exocytosis (Takagi *et al.*, 2002). Annexin 6 has also been previously reported to be a candidate receptor for chondroitin sulphate chains in chondroitin sulphate proteoglycans (Takagi *et al.*, 2002). Importantly, there are no possible O-linked glycosylation sites on ANXA6 Annexin 6 is not classified as a good candidate because WFA would never be able to bind to it via glycosylation (Takagi *et al.*, 2002).

Score Mascot: A4 Mascot	Accession	Description	Coverage [%]	# Peptides	# PSMs	# Unique Peptides	# AAs	MW [kDa]	# Peptides
5149	P22626	Heterogeneous nuclear ribonucleoproteins A2/B1 OS=Homo sapiens OX=9606 GN=HNRNPA2B1 PE=1 SV=2	72	28	87	24	353	37.4	28
3852	Q08211	ATP-dependent RNA helicase A OS=Homo sapiens OX=9606 GN=DHX9 PE=1 SV=4	47	55	92	55	1270	140.9	55
3463	P09651	Heterogeneous nuclear ribonucleoprotein A1 OS=Homo sapiens OX=9606 GN=HNRNPA1 PE=1 SV=5	63	26	72	13	372	38.7	26
2957	**P08670**	**Vimentin OS=Homo sapiens OX=9606 GN=VIM PE=1 SV=4**	**73**	**41**	**74**	**37**	**466**	**53.6**	**41**
2943	A0A0U1RRM4	Polypyrimidine tract-binding protein 1 OS=Homo sapiens OX=9606 GN=PTBP1 PE=1 SV=1	64	27	84	23	588	62.4	27
2879	P07437	Tubulin beta chain OS=Homo sapiens OX=9606 GN=TUBB PE=1 SV=2	72	26	73	5	444	49.6	26
2617	B2R5W2	Heterogeneous nuclear ribonucleoproteins C1/C2 OS=Homo sapiens OX=9606 GN=HNRNPC PE=1 SV=1	59	26	67	3	290	31.9	26
2587	P68371	Tubulin beta-4B chain OS=Homo sapiens OX=9606 GN=TUBB4B PE=1 SV=1	72	26	68	1	445	49.8	26
2538	P14866	Heterogeneous nuclear ribonucleoprotein L OS=Homo sapiens OX=9606 GN=HNRNPL PE=1 SV=2	52	29	54	5	589	64.1	29
2537	Q12906	Interleukin enhancer-binding factor 3 OS=Homo sapiens OX=9606 GN=ILF3 PE=1 SV=3	59	39	82	34	894	95.3	39

Table 7.1 Top ten proteins identified that were not annotated as 'contaminants' by the FingerPrints Laboratory*. The protein which comes out of this pull-down assay with the strongest coverage and match to our criteria is Vimentin. As displayed in the table above, Vimentin has 73 % coverage along its 466 amino acids and a molecular weight of 53.6 kDa.*
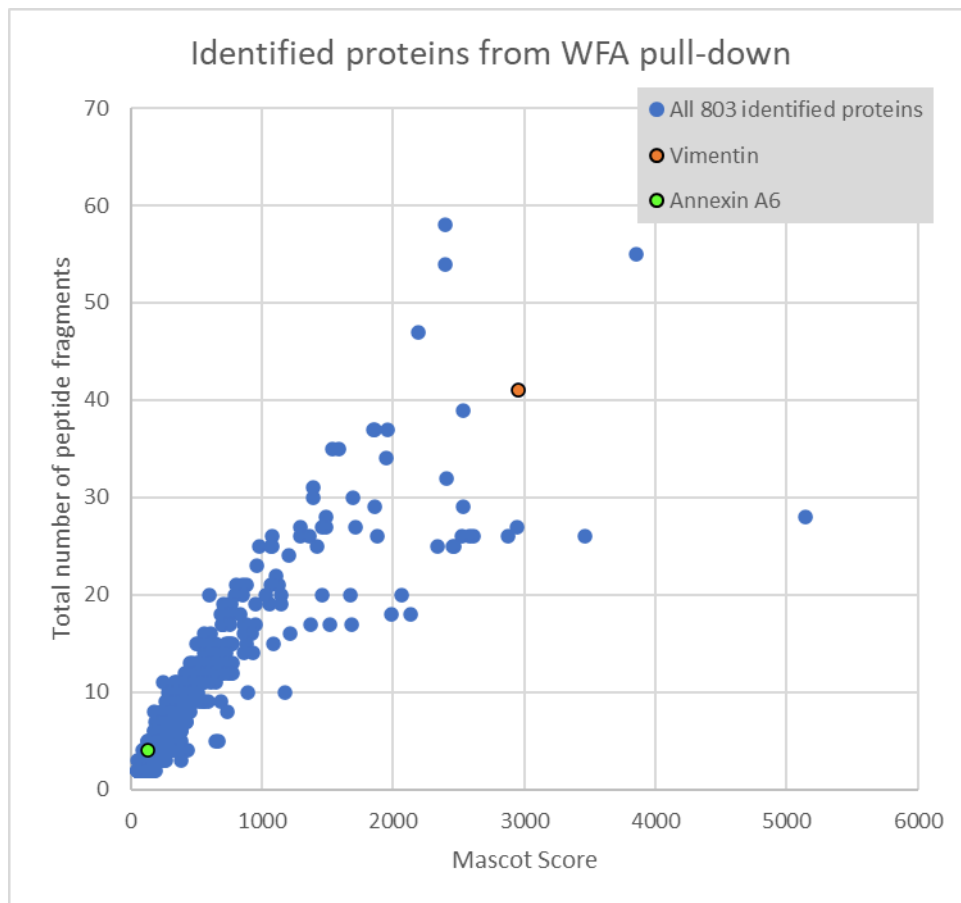
Figure 7.2 The full list of identified proteins is to be found in Appendix 1, but the top ten proteins (excluding potential contaminants) are shown as above in figure 7.1. *Most fall into the highly abundant category and do not meet the criteria listed above, suggesting a failure to wash out of the column. However, in fourth position, vimentin (VIM), an intermediate filament cytoskeletal protein and Annexin A6 (much further down the list of proteins) are perhaps the best candidates identified in the study. These are highlighted in the image as coloured circles.*

If Vimentin is the best candidate, then I must address the size difference between the calculated mass of the protein based on sequence (~54 kDa) and the sizes seen in our Western analysis (90 kDa) and ~30 kDa after purification. In Fig 7.3, the sequence of the Vimentin protein is shown, followed by domain and post-translational modification mapping. It can be seen that Vimentin has three N-terminal regions potential O-linked glycosylation sites. This would suggest that the protein has an extracellular role (glycosylation is only found on extracellular proteins). If these sites were to be modified, there is the potential for the observed mass to be increased. As an example of this effect, the growth factor erythropoietin (EPO) has a baseline molecular light of 18 kDa but this

increases to ~30 kDa after glycosylation. By definition, any WFA binding target will be glycosylated and so subject to mass addition.
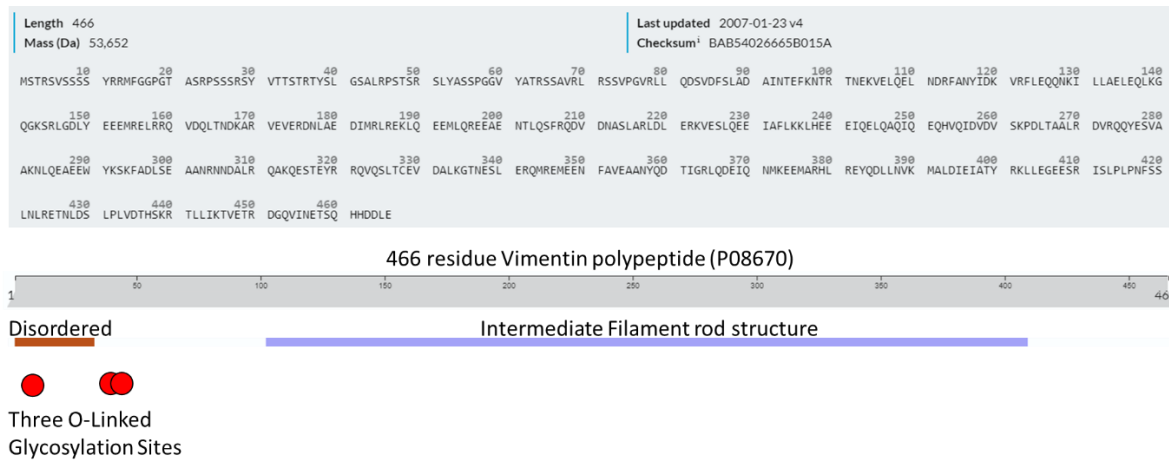
Fig 7.3 Protein sequence of Vimentin. *Figure 7.3 shows the protein sequence of vimentin followed by domain and post-translational modification mapping. Vimentin appears to have three N-terminal regions potential O-linked glycosylation sites at Ser-7, Thr-33, and Ser-34, a requirement for a protein to be potentially detected by WFA.*

7.3 The structure and role of Vimentin

Vimentin is a class III intermediate filament protein with high degree of evolutionary conservation among vertebrates (Ostrowska-Podhorodecka & McCulloch, 2021). All intermediate filament proteins possess a central coiled-coil rod domain of 310 amino acids (Ostrowska-Podhorodecka & McCulloch, 2021). The N-terminal part of the domain is a coil 1A motif (Ostrowska-Podhorodecka & McCulloch, 2021) separated from the coil 1B motif by a rigid alpha helical linker L1 structure which contributes to the final filament structure (Ostrowska-Podhorodecka & McCulloch, 2021). These combined N-terminal and C-terminal domains are produced into dimers which possess coiled-coil 2A and 2B domain regions (Ostrowska-Podhorodecka & McCulloch, 2021). Vimentin dimers are arranged in an anti-parallel manner to produce tetramers (Ostrowska-Podhorodecka & McCulloch, 2021). The formation of vimentin filaments is dynamic which regulates protein-protein interactions and can alter influence certain signalling networks (Ostrowska-Podhorodecka & McCulloch, 2021). The most common post-translational modification of phosphorylation and possesses at least 35 sites phosphorylation sites are in the head and tail domains of vimentin (Ostrowska-Podhorodecka &

McCulloch, 2021). Intermediate filaments are classified in various types based on similarities in sequence which also display similarities in tissue origin (Ostrowska-Podhorodecka & McCulloch, 2021). Keratin is defined as the main intermediate filament protein which is expressed in epithelial cells whilst vimentin is expressed in mesenchymal cells such as fibroblasts, endothelial cells, and leukocytes (Ostrowska-Podhorodecka & McCulloch, 2021). Whilst vimentin is not expressed fully in epithelial cells, it can be expressed within transformed cells associated with cancer, fibrosis, or immortalized cell lines (Ostrowska-Podhorodecka & McCulloch, 2021).

Vimentin has been expressed in a wide range of mesenchymal cells and tissues of various organisms (Ostrowska-Podhorodecka & McCulloch, 2021). Vimentin has been linked to a small number of pathophysiological conditions. Vimentin has been shown to be linked with various types of cancer invasion and can serve as a potential target for cancer therapy (Ostrowska-Podhorodecka & McCulloch, 2021). Vimentin has also been linked to effective wound healing and tissue regeneration due to contributions to cell motility and adhesion (Ostrowska-Podhorodecka & McCulloch, 2021).

Despite being ostensibly internal in nature (as a cytoskeletal intermediate filament), there is substantial evidence that vimentin can occupy the extracellular space. It has been shown that certain cell types have active mechanisms to release vimentin into the extracellular space such as covalent modification by either phosphorylation or citrullination (Suprewicz *et al*., 2021). These include neutrophils, macrophages, and endothelial cells to provide positive signals for wound healing and act as a cofactor for pathogen infection (Suprewicz *et al*., 2021). Studies have shown that cell surface vimentin acts as a biochemical signal between various cell types and also as an attachment factor through which various types of bacteria and viruses infect cells (Suprewicz *et al*., 2021). As a result of these modifications, cytoskeletal vimentin intermediate filaments are disassembled leading to vimentin release on the external surface of the same cell (Suprewicz *et al*., 2021). Furthermore, this could occur in soluble form or on the surface of exosomes where it can target cells including epithelial cells or neurons which do not express vimentin endogenously (Suprewicz *et al*., 2021).

Caspases are known to be key mediators of apoptosis. Vimentin has been shown to be cleaved by multiple caspases at distinct sites *in vitro* such as asparagine 85 by caspases 3 and 7 and Asp 259 by caspase 6 to produce multiple proteolytic fragments (Byun *et al*., 2001). Vimentin Caspase cleavage of vimentin alters its cytoplasmic network of intermediate filaments and occurs with nuclear

fragmentation (Byun *et al.*, 2001). These studies indicate that caspase proteolysis of vimentin stimulates apoptosis by altering intermediate filaments and by breaking down intermediate filaments and by amplifying the cell death signal via a pro apoptotic cleavage product (Byun *et al.*, 2001).

In the extracellular space, vimentin can bind to surfaces of other cells and the extracellular matrix, and the interaction between extracellular vimentin and other cell types can result in changes in cellular functions, such as activation of fibroblasts to a fibrotic phenotype (Bucki *et al.*, 2022). Extracellular vimentin binds external cell membranes, and it is unknown whether vimentin can act as an adhesive anchor independently for cells is largely uncharacterized (Bucki *et al.*, 2022). Some studies have utilised traction force microscopy and spheroid expansion assays to characterize how various cell types respond to extracellular vimentin (Bucki *et al.*, 2022). Attachment of cells and spreading vimentin coated surfaces is decreased by hyaluronic acid, degrading enzymes, hyaluronan synthase inhibitors, soluble heparin and N-acetyl glucosamine that have little or no effect on the similar cell types binding to collagen-coated hydrogels (Bucki *et al.*, 2022). These studies indicate the effectiveness of substrate- bound vimentin as a cell ligand and indicates that carbohydrate structures, including the glycocalyx and glycosylated cell surface proteins possess N-acetyl glucosamine which is part of a novel class of adhesion receptors for extracellular vimentin (Bucki *et al.*, 2022).

Vimentin also binds to glycosaminoglycans such as hyaluronic acid and heparin in which one of the two carbohydrate units is either N-acetylglucosamine or another closely related structure (Bucki *et al.*, 2022). Vimentin has a high affinity for N-acetylglucosamine containing cell surface structures and the fact that many or perhaps all of the proposed vimentin binding cell surface proteins are themselves glycosylated, indicates a key role for hyaluronic acid (Bucki *et al.*, 2022). This suggests that either hyaluronic acid and heparin rich like glycocalyx or transmembrane proteins are heavily glycosylated are important elements in the mechanism by which extracellular vimentin binds and stimulates eukaryotic cells (Bucki *et al.*, 2022)

Vimentin has been shown to be overexpressed after spinal cord injury and stroke resulting in glial formation. Various studies have displayed that glial scar formation alters neurogenesis (Menet *et al.*, 2003, Aswendt *et al.*,2022). Vimentin has been shown to play a potential biomarker for stroke progression and brain tumours and as a possible therapeutic target in various nervous system disorders. Vimentin has been reported to be involved in scar formation, axonal regeneration, inflammatory response and apoptosis activation.

In the majority of tumours, vimentin is overexpressed. For instance, in brain tumours, high vimentin expression is regarded as an important marker of poor prognosis (Zhao *et al.*, 2018). Interestingly, brain tumour-related and meningitis-related studies have mostly addressed the functions of cell surface vimentin, while the functions of intracellular or extracellular-associated vimentin remain unclear. Additionally, vimentin not only promotes the migration of SCs but also inhibits myelination. There is a possibility that SC migration might inhibit myelination (Triolo *et al.*, 2012). Therefore, understanding the mechanism of vimentin regulation may contribute to a better understanding of various nervous system injuries and diseases.

Multiple sclerosis (MS) is classified to be an autoimmune disease of CNS in which T lymphocytes cross the BBB leading to demyelination and axonal degeneration (Lassmann, 2018). Vimentin is present in reactive astrocytes located in the demyelinating lesions of MS, and vimentin is one of the 14-3-3 protein-interacting proteins found in cultured human astrocytes (Satoh *et al.*, 2004). With regards to Alzheimer's disease (AD), a neurodegenerative disease, neuronal vimentin expression is positively correlated with amyloid deposition in AD brains. Initially, damage in neurons causes synaptic disruption and dendrite retraction. After several hours or several days, the neuron expresses and transports vimentin to the damaged dendrite where it participates in neuron repair (Levin *et al.*, 2009).

Upregulated vimentin expression increases the ability of Schwann cells to guide and promote axon regeneration after sciatic nerve injury (Perlson *et al.*, 2005; Berg *et al.*, 2013). Schwann cells are the main glial cells of the Peripheral nervous system and play a significant role in guiding peripheral nerve regeneration. Following injury, Schwann cells and macrophages begin to clean debris at the injured site and Schwann cells from distal sites proliferate and migrate to the injured site and form a framework to guide nerve regeneration. The results in the regenerated nerve fibre reinnervating its targets, and Schwann cells remyelinating the regenerated axon (Abe and Cavalli, 2008). Increase in miR-138-5p decreases vimentin expression in Schwann cells and the 3′UTR of vimentin is a defect target of miR-138-5p. One study also found vimentin to be a negative regulator of myelination (Triolo *et al.*, 2012). Further evidence has shown that extracellular vimentin which is secreted by macrophages and reactive astrocytes is a neurotrophic factor which could stimulate axonal regrowth and facilitate motor function rehabilitation following SCI (Shigyo and Tohda, 2016). Denosomin a compound has been shown to increase concentration of astrocyte secreted vimentin which is closely linked to axonal regeneration in spinal cord traumatic mice (Teshigawara *et al.*,2013). Finally, one

study indicated that recombinant vimentin treatment increases axonal growth and enhances performance in motor function in spinal cord injury mice (Shigyo and Tohda, 2016). Recombinant vimentin has also been associated with neurite outgrowth. Interestingly, intracellular and extracellular vimentin have been shown to play alternating roles in axonal regrowth (Shigyo *et al.*, 2015). Further evidence has shown that extracellular vimentin which is secreted by macrophages and reactive astrocytes is a neurotrophic factor which could stimulate axonal regrowth and facilitate motor function rehabilitation following SCI (Shigyo and Tohda, 2016). Denosomin a compound has been shown to increase concentration of astrocyte secreted vimentin which is closely linked to axonal regeneration in spinal cord traumatic mice (Teshigawara *et al.*,2013). Finally, one study indicated that recombinant vimentin treatment increases axonal growth and enhances performance in motor function in spinal cord injury mice (Shigyo and Tohda, 2016). Recombinant vimentin has also been associated with neurite outgrowth. Interestingly, intracellular and extracellular vimentin have been shown to play alternating roles in axonal regrowth (Shigyo *et al.*, 2015). Further studies have shown that vimentin inhibition along with Chondroitinase ABC plays a significant role in initiating axon regeneration and locomotor function recovery (Xia *et al.*, 2015). Using this combined treatment of targeting vimentin suggested a significant role in SCI repair and the importance of using vimentin inhibition and Chondroitinase ABC in decreased glial scar and degrading chondroitin sulphate proteoglycans which are inhibitory molecules for axonal sprouting.

Vimentin has also been shown to be a central meningitis factors which mediates the penetration and destruction of the BBB and colonization of the brain by multiple bacterial pathogens. Studies have also shown that host cell vimentin interacts with the group B streptococcal surface antigen I/II protein, BspC, to enable colonization in the brain endothelium and CNS inflammation during the pathogenesis of Group B Streptococcus (GBS) meningitis. Studies displayed that in a mouse model of haematogenous meningitis, vimentin knockout mice were significantly less susceptible to GBS infection, resulting in a decreased inflammatory response (Deng *et al.*,2019). Blocking this receptor ligand interaction could provide an effective technique in preventing bacterial meningitis. Further evidence has shown that extracellular vimentin which is secreted by macrophages and reactive astrocytes is a neurotrophic factor which could stimulate axonal regrowth and facilitate motor function rehabilitation following SCI (Shigyo and Tohda, 2016). Denosomin a compound has been shown to increase concentration of astrocyte secreted vimentin which is closely linked to axonal regeneration in spinal cord traumatic mice (Teshigawara *et al.*,2013). Finally, one study indicated that recombinant vimentin treatment increases axonal growth and enhances performance in motor function in spinal

cord injury mice (Shigyo and Tohda, 2016). Recombinant vimentin has also been associated with neurite outgrowth. Interestingly, intracellular and extracellular vimentin have been shown to play alternating roles in axonal regrowth (Shigyo *et al.*, 2015). Further studies have shown that vimentin inhibition along with Chondroitinase ABC plays a significant role in initiating axon regeneration and locomotor function recovery (Xia *et al.*, 2015). Using this combined treatment of targeting vimentin suggested a significant role in SCI repair and the importance of using vimentin inhibition and Chondroitinase ABC in decreased glial scar and degrading chondroitin sulphate proteoglycans which are inhibitory molecules for axonal sprouting. Finally, extracellular vimentin has been shown to be a novel ligand of IGF1R that promotes axonal growth in a similar manner to IGF1 (Shigyo *et al.*,2015).

7.4 Conclusion

In previous chapters, I have seen in protein analysis of WFA-binding glycoprotein expression that sometimes there are one or two bands of WFA. The investigation here is to see whether these are specific proteoglycans or different isoforms. To determine this, a pull-down assay was conducted to determine what proteins WFA is binding to and to identify these single or double bands which are appearing on WFA-binding glycoprotein expression analysis through Western blotting. The band size which usually appears is 75-90 kDa which is produced on Western blots of *SH-SY5Y* cells. Eluate from the preparative process detailed in the Methods was fully loaded onto a polyacrylamide gel, a gel slice taken, fixed, and sent to the Dundee Fingerprints service for identification. The results of the pulldown assay indicate that the purification technique is working but I also have a lot of other proteins coming through. Looking at the data above, of most interest within the proteins being pulled down was vimentin.

CHAPTER 8

Discussion

8.1 Brief summary of findings

During the work set out in this thesis, it was shown that *SH-SY5Y* cells possess perineuronal nets and have a strong neuronal profile. With regard to perineuronal nets, there is plenty of evidence within the literature that perineuronal nets are important contributors to the function of specific neurons in the brain. The perineuronal net is a specialized form of the extracellular matrix and is composed of various components such as chondroitin sulphate proteoglycans, hyaluronan, hyaluronan synthases and tenascin R. Studies have shown that a malformed perineuronal net is associated with neuropsychiatric disorders. Therefore, my hypothesis was that by understanding the molecular synthesis of the PNN, I might gain further insights into its function and ways in which it might be modulated or repaired in wellness.

I first established the presence of WFA staining in brain tissue indicating the presence of perineuronal nets. WFA staining was detected on *SH-SY5Y* cells using immunofluorescence microscopy and also by Western blot analysis. Staining was also observed in *Lan-5* and *Hek-293* cell lines with neuronal properties, but not *A549*, a lung epithelial cell line. To date, there has been no known literature or research investigating WFA-binding glycoprotein expression on *SH-SY5Y* cells. Furthermore, to characterize WFA staining, *SH-SY5Y* cells were treated with fluoxetine and venlafaxine for 48 hours and then WFA staining analysed using Western blotting and immunofluorescence microscopy. The results did not show any significant change in WFA staining despite published studies suggesting that fluoxetine and venlafaxine decrease WFA staining. Based on earlier in-house research findings on the molecular mechanisms of lithium action, cells were also treated with lithium and 1-Azakenpaullone (GSK-3 inhibitor) to determine any changes in WFA-binding glycoprotein expression, but none were observed. However, it was hypothesized that gene trap mutants identified with reduced PNN staining would help us better understand the function and maturation of the perineuronal net and act as potentially important therapeutic targets for neuropsychiatric diseases. Applying gene trapping to *SH-SY5Y* cells, live cell staining was undertaken using fluorescently labelled WFA to identify which colonies of the mutant gene trap library were failing to produce a functioning perineuronal net. Those colonies with reduced WFA staining as well abnormal shapes were then isolated using picking technique and expanded for analysis.

At this point, I had between 3-7 colonies all with either reduced WFA staining, or abnormal expression patterns as shown in the Results. RACE-PCR revealed the identity of the genes. The genes identified included *FAF1*, *DCC* and *GALNTL6*. *FAF1* has been previously shown to play a key role in the progression of Parkinson's disease. *DCC* has been reported to be a risk factor for

schizophrenia, and *GALNTL6* belongs to a family of glycosyl transferases which are involved in mucin-type O-linked glycosylation. CRISPR KO constructs were then attempted to be produced for each of the candidate genes though it is important to note that no sufficient knockout had occurred of any candidate gene and was analysed for downregulated candidate protein expression and effect on WFA-binding glycoprotein expression. Similarly, siRNA interference was also utilised to in essence silence on part of the gene to monitor WFA-binding glycoprotein expression and see if there is any disruption. Unfortunately, technical problems with the CRISPR and siRNA approaches prevented us from creating new mutated cell lines for these genes, and validating their roles in PNN function. It is important to note that other genes were also identified but at the time were not taken forward due to their limited link with the extracellular matrix, perineuronal net or neurological diseases. However, examination of the genes via GWAS catalogue displayed that *SUGCT* possesses multiple SNPs associated with migraine. Furthermore, *EVI5* has recently been associated as a risk factor for multiple sclerosis and schizophrenia (Hoppenbrouwers *et al.*, 2008). *ADGRL2* according to the GWAS catalogue has been shown as a risk factor for depression and late onset *Alzheimer's* disease whereas *PLA2G4* is a risk factor for schizophrenia and epilepsy (Tao *et al.*, 2005). *EVI5* was one of the genes identified within the gene trap screen and has been shown to be a risk factor for multiple sclerosis. Though no direct link has been revealed between EVI5 and perineuronal nets, the compound Fingolimod has been widely used for the treatment of multiple sclerosis and has also been shown to restore neuroplasticity (Ueno *et al.*,2022). One recent study showed that use of fingolimod resulted in an increase of parvalbumin positive neurons within various regions of the brain such as the hippocampus and prefrontal cortex (Ueno *et al.*,2022). An increase in WFA positive PNNs were also confirmed in mice treated with fingolimod within the somatosensory cortex only (Ueno *et al.*,2022). It was also shown that fingolimod increased the density of PV-positive neurons within the brain of mature mice (Ueno *et al.*, 2022).

As a final piece of work, I further explored the nature of WFA action by identifying a potential target of this stain, vimentin. Future work should test its expression and molecular weight correlation with WFA staining using immunofluorescence and Western blotting.

8.2 Critical analysis of the research: staining pattern

During the studies described here, in *SH-SY5Y* cells, the distribution of the perineuronal net was abnormal compared to *in vivo* cells. The classic publication WFA/PNN staining pattern on parvalbumin positive interneurons is very distinctive and different from the *SH-SY5Y* pattern. Interneurons show an entirely extracellular staining arranged in a 'honeycomb-like' pattern around the cell soma. *SH-SY5Y* cells, by contrast, should a pattern of distribution consistent with some endoplasmic reticulum retention while also having a diffuse extracellular distribution (evident from the live staining in the screen). This incomplete secretion and failure to adopt a precise extracellular pattern is perhaps not surprising when comparing an hours-old proliferating cell which is incompletely differentiated, with a years-old, terminally differentiated neuron. Although not carried out in this investigation, it would be interesting to observe the effects of *SH-SY5Y* differentiation protocols on the WFA/PNN staining pattern and also investigate staining in other, ostensibly more neuronal cell lines.

8.3 Critical analysis of the research: Pharmacological effects contrasted with the literature

With regards to the treatment of the *SH-SY5Y* cells with lithium, 1-azakepaullone, fluoxetine and venlafaxine, there was no observed change in WFA staining. Aside from the laboratory's previous gene trap screen for gene mutations found to be resistant to lithium treatment, other studies have investigated lithium's effect on the perineuronal net. For example, Biphosphate nucleotidase 2 (*BPNT2*) is part of a family of phosphatases which are directly inhibited by lithium and is localized to the Golgi apparatus where it metabolizes the by-products of glycosaminoglycan sulphation reactions (Eisele *et al.*,2022). Recent studies involved production of a conditional neuronal-specific *BPNT2* knockout mice where decrease levels of chondroitin 4-sulphation were seen in these mice but there was no change in the WFA staining of perineuronal nets. Decreased levels of total glycosaminoglycan sulphation across brain regions showed decreases in chondroitin 4-sulphation as well as an increase in chondroitin 6-sulphation (Eisele *et al.*,2022). However, these changes were independent of gross alterations within perineuronal nets (Eisele *et al.*,2022). These studies demonstrated that BPNT2, a known target of lithium, is essential for glycosaminoglycan sulphation within the brain indicating that investigation of BPNT2 effects on the PNN is of the utmost importance (Eisele *et al.*,2022). Furthermore, it also showed that chondroitin-4 sulphate may be associated with

a looser extracellular matrix which does not stain with WFA. With regards to the previous lithium gene trap screen conducted within the laboratory, 35 genes from that previous lithium function screen, six were related to perineuronal net components. *SH-SY5Y* cells were also treated with fluoxetine and venlafaxine for 48 hours. Other studies have shown that post-natal fluoxetine treatment alters perineuronal net formation and maintenance in the hippocampus (Alaiyed *et al.*, 2019) In addition, chronic fluoxetine treatment alters the structure, connectivity and plasticity of cortical interneurons (Ohira *et al.*,2013). Furthermore, studies with mice deficient in MMP-9, a protease known to degrade perineuronal nets, should that venlafaxine enhanced gamma power and increased neuronal population activity dynamics linked to memory processes (Alayed *et al.*,2019). Similarly, matrix metalloprotease-9 has been shown to increase branching of excitatory neurons and attenuating the perineuronal net to decrease inhibitory input to these neurons (Alayed *et al.*,2019).They have the potential to increase the overall excitatory, inhibitory balance and neuronal population dynamics which are significant in mood and memory. It is important to note that all these results and studies showing decreased WFA staining and alteration of perineuronal nets were conducted in primary cell lines. Primary cell lines are more representative of the human brain. Also, secondary cell lines will lose their neuronal profile over time. In summary, fluoxetine and venlafaxine treatment do not appear to decrease WFA-binding glycoprotein expression in *SH-SY5Y* cells.

8.4 Critical analysis of the research

The live cell staining of the *SH-SY5Y* mutant gene trap library displayed various colonies with reduced WFA staining or an altered perineuronal net distribution. However, with the gene trapping screen used here comes several drawbacks. Firstly, this was rather subjective and based on the human eye discernment of reduced staining. Issues can arise when trying to accurately "pick" mutant patches of cells and then running them through all the stages for molecular analysis. Colonies once picked would need to be grown up fully to confluence and in some cases isolated again due to picking multiple mutant patches. A more objective approach that has actually been applied in other in-house screens would have been the use of fluorescence-activated cell sorting (FACS) whereby library cells could have been removed from the culture vessel, stained with WFA, and then sorted at the cellular level according to staining intensity. Low-staining cells would have then been subjected to further rounds of selection or genetic analysis. The issue at the time was that enzymatic or physical removal of these adherent cells from the culture vessel would have destroyed the ECM/PNN and our ability

to detect the very thing I was interested in. However, the later Trypsin experiment suggests that the PNN is quite resilient to digestion.

Gene trapping is defined as a high-throughput approach of producing mutation vectors which can simultaneously disrupt and report the expression of the endogenous gene at the point of insertion. Vectors can be classed as either promoter trap vectors or gene trap vectors depending on the areas they integrate into. Promoter trap vectors possess promoter less reporter regions such as βgeo (a fusion of neomycin phosphotransferase and β-galactosidase). Therefore, they must be integrated into an exon of a transcriptionally active locus for the cell to be selected for neomycin resistance or by *LacZ* staining. Gene trap vectors also have the ability to integrate into an intron and these vectors possess a splice acceptor site positioned at the 5′-end of the reporter gene, allowing the vector to be spliced to the endogenous gene to form a fusion transcript (and also disrupting the gene). The advantage of using gene trapping is that a large number of mutations can be produced with relative ease. One drawback of using gene trapping is that some genes (e.g. with small or no introns) will not be captured. Therefore, I may have identified genes which when mutated have reduced WFA staining but there may well be others out there which cannot be mutated but which warrant investigation. A second drawback of gene trapping is that the rarity of the insertion events means that heterozygous gene disruption is only ever possible in a given cell. The particular biological process or pathway affected must be susceptible to 'loss-of-function' effects before a phenotype could be observed. It may well be that some of the gene mutations will not have that severity to be detectable in our phenotypic screen. Some cellular screens have employed CRISPR or siRNA, but these also suffers from drawbacks. siRNA screens can be highly variable and hard to replicate due to each individual siRNA's stochastic effect on expression. CRISPR libraries, like gene trapping create a permanent change in gene function and CAN be homozygous. However, as with animal experiments, there is the possibility that some of these homozygous changes may be incompatible with cell survival, or will have a dramatic effect on proliferation, resulting in loss of representation in the library as culture progresses.

Interestingly, many mutations produced intronic fusion sequences during the analysis, whilst *GALNTL6* produced a true exonic mutation. *GALNTL6* showed the correct pattern of splicing indicating an INTRONIC vector insertion yielding EXONIC trapped sequences as determined by RACE-PCR. The way the gene trap works is that splicing occurs resulting in formation of a truncated protein. Through the mRNA splicing, and insertion of the "fake" exon, I should have only seen fusions between the gene trap and endogenous exon sequences: this unfortunately only occurred rarely,

167

e.g., with *GALNTL6*, making this the strongest and best possible candidate mutant gene producing reduced WFA staining.

8.5 Critical analysis of the research: Issues with CRISPR validation

Having used gene trapping to identify mutant genes with reduced WFA staining or abnormal perineuronal net distribution, CRISPR validation and siRNA silencing was undertaken. Gene trapping, although effective, produces just one form of mutation as described above. Techniques such as CRISPR can provide further validation in entirely independently generated mutant cell lines. CRISPR KO constructs were produced for *DCC*, *FAF1* and *GALNTL6*. Unfortunately, in comparison with the gene trapping showing reduced WFA staining, the Western blot analysis of cells treated with KO constructs yielded little difference in WFA staining in comparison to wild type. Possibly, this could be due to incorrect picking of the colony when being identified with reduced WFA staining meaning that the colony picked during the live cell staining process was actually showing no reduced WFA staining. Despite colonies being plated out at low densities and the *SH-SY5Y* mutant gene trap library contains 1000s of mutated genes, they can still be quite close to one another. Puromycin was used to kill all wild type cells which did not possess the antibiotic resistance gene which was present within the CRISPR plasmids for the constructs. Thus, our intention was always to make stable cell lines with candidate gene ablation. It may be that the lower efficiency of stable line Cas9/sgRNA activity compared to high-efficiency transient transfection hindered the effectiveness of the mutation process. Our home-designed sgRNAs may not have been 100 % efficient meaning that even cells which take in the CRISPR/Cas9 may not have the correct genome editing activity. However, commercial CRISPR plasmids (with nominal 'guarantees') were also utilised but still there was no effective gene ablation as determined by Western blotting and immunofluorescence microscopy.

8.6 Critical analysis of the research: Pharmacological downregulation as an alternative

FAF1 appeared to be the strongest candidate gene with one attempted crispr colony showing decreased expression of WFA-binding glycoproteins during the CRISPR process. Therefore, I further utilised a *FAF1* inhibitor KR-33493 to determine whether this may result in reduced WFA staining. Our results showed that there was no reduction in expression of WFA-binding glycoproteins during protein analysis, strongly suggesting that *FAF1* has no simple role in PNN formation.

8.7 Critical analysis of the research: Exploring the functions of the candidates

In the gene trap screen, all three genes which were identified (*FAF1*, *DCC*, *GALNTL6*) named as colonies P38a, U4D and U1B during the screening process, had reduced WFA staining and/or abnormal perineuronal net distributions. These genes also have their respective roles in neuropsychiatric/neurological diseases where *FAF1* is involved in the progression of Parkinson's disease, *DCC* is a risk factor for schizophrenia and *GALNTL6* is involved in a type of O-linked glycosylation known as mucin type O-linked glycosylation. *GALNTL6*, being part of the glycosyl transferases family and having been an exonic mutation, would have been the best candidate to further study. Production of perineuronal net components, chondroitin sulphate proteoglycans, requires O-linked glycosylation reactions where carbohydrate units are added.

8.8 Critical analysis of the research: What does WFA bind to?

Finally, during this research, I observed that WFA-based protein analysis of both wild type cells and *SH-SY5Y* mutant genes, there were sometimes one or two bands on blots. Determining the identity of this band/these bands was key to our studies because it could show us an important component of the perineuronal net and further define the target of WFA staining. For example, it is universally accepted that all perineuronal nets have *Aggrecan*. It might be assumed that this band(s) was *Aggrecan*. However, the sizes of these bands were either 90 kDa or 75 kDa meaning that the larger *Aggrecan* protein should be ruled out.

Our pull-down assay many proteins in the eluted material but the protein that most closely met our criteria for being a WFA target was the intermediate filament component, Vimentin. Intermediate filaments are classified as a major component of the cytoskeleton and are essential for normal cell morphology, motility and signal transduction (Tarbet *et al*., 2018). Dysregulation of intermediate filaments results in a wide range of human diseases such as skin disorders and neuropathy (Tarbet *et al*., 2018). For production of an intermediate filament, vimentin molecules produce dimers which then assemble to produce tetramers which then associate laterally and longitudinally to assemble into mature 10 nm-wide filaments of varying lengths (Snider *et al*., 2018). Many cells possess vimentin, and it is found commonly in cancer cells which have undergone metastasis.

Recent evidence has shown that post-translational modifications are an important mode of intermediate filament regulation, with all intermediate filaments able to undergo phosphorylation, ubiquitination, acetylation and glycosylation (Snider and Omary.,2014). Interestingly, perineuronal nets contain proteins with extensive N-linked and O-linked glycosylation. During glycosylation, cells can reversibly attach a sugar modification called O-GlcNAc to vimentin (Tarbet *et al.*, 2018). O-GlcNAc can be attached to several different parts of vimentin and each location may have a different effect. How cells control their vimentin filaments or what role O-GlcNAc plays in this process is currently poorly understood (Tarbet *et al.*, 2018). Vimentin is heavily O-GlcNAcylated on several sites particularly its head domain (Wang *et al.*, 2007).

Vimentin was originally classified as an intracellular intermediate filament protein (Shigyo & Tohda, 2016). This is a problem when I consider it as a component of the ECM and target for WFA binding. However, more recent studies have also reported that vimentin is located in the extracellular space and displays novel protein activity there (Shigyo & Tohda, 2016). Previous studies reported that the drug denosomin improved motor dysfunction in mice with spinal cord injury (Shigyo & Tohda, 2016). At the site of injury, astrocytes which expressed and secreted vimentin were increased in number and axonal growth occurred in an extracellular vimentin-dependent manner in denosomin-treated mice (Shigyo & Tohda, 2016). However, these studies had limitations in the sense that extracellular vimentin was investigated *in vitro* (Shigyo & Tohda, 2016). Therefore, further studies sought to explore whether extracellular vimentin stimulates axonal extension related to motor improvement after spinal cord injury *in vivo* (Shigyo & Tohda, 2016). These studies concluded that extracellular vimentin treatment in spinal cord injury significantly improved motor dysfunction (Shigyo & Tohda, 2016). Furthermore, this should that extracellular vimentin could be a novel neurotrophic factor which stimulates axonal growth activity and motor function recovery after spinal cord injury (Shigyo & Tohda, 2016). Interestingly, during spinal cord injury, other studies have shown that chondroitin sulphate proteoglycans, a key component of perineuronal nets, are also upregulated in spinal cord injury (Shigyo & Tohda, 2016).

In the extracellular space, vimentin can also bind to surfaces of other cells and the extracellular matrix, and the interaction between extracellular vimentin and other cell types can result in changes in cellular functions, such as activation of fibroblasts to a fibrotic phenotype (Bucki *et al.*, 2022).

Extracellular vimentin binds external cell membranes, and it is unknown whether vimentin can act as an adhesive anchor independently for cells is largely uncharacterized (Bucki *et al.*, 2022). Some studies have utilized traction force microscopy and spheroid expansion assays to characterize how various cell types respond to extracellular vimentin (Bucki *et al.*, 2022). Attachment of cells and spreading vimentin coated surfaces is decreased by hyaluronic acid, degrading enzymes, hyaluronan synthase inhibitors, soluble heparin and N-acetyl glucosamine that have little or no effect on the similar cell types binding to collagen-coated hydrogels (Bucki *et al.*, 2022). These studies indicate the effectiveness of substrate- bound vimentin as a cell ligand and indicates that carbohydrate structures, including the glycocalyx and glycosylated cell surface proteins possess N-acetyl glucosamine which is part of a novel class of adhesion receptors for extracellular vimentin (Bucki *et al.*, 2022). Vimentin does not have a signal peptide or other features of conventionally secreted protein; it has been shown that vimentin has been shown to selectively released into the extracellular by active processes rather than appearing in the extracellular environment solely resulting from mechanical damage to the cell membrane permeability barrier (Bucki *et al.*, 2022). The extracellular expression of vimentin requires at least two active processes. The first is stimulation of protein arginine deaminases or protein kinases which either succinate or phosphorylate key residues which are essential for vimentin to assemble into filaments (Bucki *et al.*, 2022). The activation of these processes results in solubilization of vimentin into small oligomeric units (Bucki *et al.*, 2022). The second route in which Vimentin release occurs into the extracellular space or localized to the exterior surface of the cell membrane and involves the unconventional type 3 secretion pathway (Bucki *et al.*, 2022). It has been postulated that vimentin binds the cell surface due to its affinity for polysaccharides (Bucki *et al.*, 2022). One study indicates that vimentin binds selectively to polymers with multiple copies of N-acetylglucosamine but no other sugar types (Bucki *et al.*, 2022). Vimentin also binds to glycosaminoglycans such as hyaluronic acid and heparin in which one of the two carbohydrate units is either N-acetylglucosamine or another closely related structure (Bucki *et al.*, 2022). Vimentin has a high affinity for N-acetylglucosamine containing cell surface structures and the fact that many or perhaps all of the proposed vimentin binding cell surface proteins are themselves glycosylated, indicates a key role for hyaluronic acid (Bucki *et al.*, 2022). This suggests that either hyaluronic acid and heparin rich like glycocalyx or transmembrane proteins are heavily glycosylated are important elements in the mechanism by which extracellular vimentin binds and stimulates eukaryotic cells (Bucki *et al.*, 2022).

The cellular distributions, molecular actions and post-translational modifications described above provide some supportive evidence that vimentin could still be the PNN component that is bound by WFA. There are clearly some key experiments that would need to be conducted to prove this: notably, anti-vimentin antibodies and WFA recognising the same molecular light band on Western blots and co-localising in the extracellular matrix of cells. These experiments were not possible in the time-frame of my studies.

8.9 Future of PNN research and final thoughts

Perineuronal nets control synaptic stabilization in both the developing and adult central nervous system and the disruption of perineuronal nets has been shown to stimulate neuroplasticity. Studies have investigated the possibility of memory prolongation by attenuating perineuronal net formation using 4-methylbelliferone (4-mu), an inhibitor of hyaluronan synthesis (Dubisova *et al.*, 2022). The studies should that oral administration of 4-mu decreased perineuronal net formation and increased memory retention in mice (Dubisova *et al.*, 2022). Their results suggested that 4-mu treatment could potentially offer routes for perineuronal net modulation in memory enhancement (Dubisova *et al.*, 2022). Other studies have also looked at the expression of OTX2, MMP3 and MMP9 in the case of sleep deprivation and trauma (Fang *et al.*, 2020). This has led to researchers targeting these specific perineuronal net components as therapeutic targets (Fang *et al.*, 2020).

Other studies have shown the importance of TrkB dependent plasticity and targeting PTP sigma perineuronal net interactions. This research could lead to the ability of the perineuronal nets to restrict TRKB dependent plasticity (Browne *et al.*, 2022). PTP sigma mimetics have been produced and have displayed efficacy in pre-clinical models of spinal cord injury (Browne *et al.*, 2022). Further research of perineuronal receptor interactions with perineuronal nets in the context of memory should be undertaken to understand these interactions.

Moreover, growing evidence to support alterations in ECM components in the context of multiple sclerosis. It has been shown that oligodendrocyte progenitors are enriched for perineuronal components including *Aggrecan*, *Neurocan*, *Versican*, phosph*acan*, *Brevican* and tenascin R in a pathological state where perineuronal net levels are increased (Browne *et al.*, 2022). Perineuronal nets can also act as a scaffold for inhibitors of synapse formation such as semaphorin 3A (Browne *et al.*, 2022). Interestingly, Semaphorin 3A was one of the genes identified in the earlier lithium gene

trap screen resulting in our research doing a WFA gene trap screen. With regards to therapeutic development, inhibiting Sema3A which is mainly found in the adult cortical perineuronal nets could provide us with the most compelling results in treatment of multiple sclerosis. Semaphorins and Plexin A1 are upregulated in human brains of individuals diagnosed with multiple sclerosis (Browne *et al.*, 2022). These changes are important as sempahorins are known to decrease axonal regeneration, oligodendrocyte progenitor cell differentiation and oligodendrocyte migration (Browne *et al.*, 2022). Further studies also support a role for semaphorins in the pathophysiology of schizophrenia. CSPGs, key components of perineuronal nets, are known to be decreased in schizophrenia subjects (Browne *et al.*, 2022).

Several limitations remain with our understanding of PNN physiology and function. Optimization of PNN visualization remains a concern since not all *Aggrecan* containing perineuronal nets are labelled with WFA. When designing future experiments for future perineuronal networks, the circadian rhythmicity of perineuronal net density and composition are significant factors which should be taken into consideration. Strategies to degrade perineuronal nets currently rely on Ch-ABC, a polysaccharide lyase derived from the bacterium *Proteus vulgaris* (Browne *et al.*, 2022). Levels of CSPG degradation is limited by Ch-ABCs profile of thermal instability, short half-life and repeated dosing requirements to maintain therapeutically relevant knockdown of perineuronal nets (Browne *et al.*, 2022). Numerous studies have addressed this issue stabilizing the protein by site-directed mutagenesis or by covalent molecules such as glycerol, sorbitol or polyethene glycol (Browne *et al.*, 2022). Using local delivery of stabilized Ch-ABC has provided the greatest success in pre-clinical models of spinal cord injury (Browne *et al.*, 2022). Viral delivery of Ch-ABC has also been utilised for spinal cord injury associated pathology *ex vivo* and i*n vivo* (Browne *et al.*, 2022). Other strategies have utilised Ch-ABC with scaffolds to improve long-term targeted knockdown. Furthermore, utilizing tamoxifen-inducible selective Ch-ABC in hippocampal CA2 neurons in a conditional CA2 Cre-expressing mouse line resulted in sustained knockdown of perineuronal nets (Browne *et al.*, 2022). The knockdown was more evident in CA1 and CA3 with more widespread knockdown occurring with repeated tamoxifen injections (Browne *et al.*, 2022). Research in the perineuronal net field is moving towards the use of targeted knockdowns of perineuronal components by pharmacological or genetic means and away from the use of non-selective knockdown of perineuronal nets by Ch-ABC administration. By doing this, this will determine the level of contribution, PNN subcomponents have with perineuronal net function and synaptic plasticity in specific disease models and lead to production of small molecule inhibitors or novel drug classes which can be produced clinically.

In summary, the research that has been conducted has started the process of a deeper investigation of the processes and pathways that regulation the perineuronal net. Perineuronal nets develop in the juvenile brain and become stabilized in the adult brain but become dysregulated during periods of mental wellness. Investigating these genes, their binding partners and mechanisms of action in relation to perineuronal nets could unlock a future of potential therapeutic treatment. Though I used gene trapping mainly to identify these genes, this is not always reliable and further research using CRISPR or siRNA libraries in not just SH-SY5Y cells but other secondary and primary cell lines, and within the mouse brain could provide further insight into beneficial therapeutic treatment for perineuronal net-related neuropsychiatric diseases.

Chapter 9

References

A.advancedbrain.com. (2018). *Which Brain Areas Are Most Involved in Music Listening?* [online] Available at: http://a.advancedbrain.com/news/brain_areas.jsp [Accessed 30 Aug. 2018].

Alaiyed, S., Bozzelli, P., Caccavano, A., Wu, J. and Conant, K. (2019). Venlafaxine stimulates PNN proteolysis and MMP-9-dependent enhancement of gamma polr; relevance to antidepressant efficacy. *Journal of Neurochemistry*, 148(6), pp.810-821.

Allen, N. J., and Barres, B. A. (2009) Neuroscience: Glia - more than just brain glue. Nature 457, 675−677.

Alterations in BDNF (brain derived neurotrophic factor) and GDNF (glial cell line-derived neurotrophic factor) serum levels in bipolar disorder: The role of lithium. Journal of Affective Disorders, 166, pp.193-200.

Alto, L. T. & Terman, J. R. Semaphorins and their Signaling Mechanisms. *Methods Mol Biol* 1493**,** 1–25 (2017).

Anderson, E., Katunga, L. and Willis, M. (2012). Mitochondria as a source and target of lipid peroxidation products in healthy and diseased heart. *Clinical and Experimental Pharmacology and Physiology*, 39(2), pp.179-193.

Anlar, B. and Gunel-Ozcan, A. (2012). Tenascin-R: Role in the central nervous system. *The International Journal of Biochemistry & Cell Biology*, 44(9), pp.1385-1389.

Aswendt, M. *et al.* (2022) 'Reactive astrocytes prevent maladaptive plasticity after ischemic stroke', *Progress in Neurobiology*, 209, p. 102199. doi: 10.1016/j.pneurobio.2021.102199.

Airaksinen, M. and Saarma, M. (2002). THE GDNF FAMILY: SIGNALLING, BIOLOGICAL FUNCTIONS AND THERAPEUTIC VALUE. *Nature Reviews Neuroscience*, 3(5), pp.383-394.

Barros, C. S., Franco, S. J. & Müller, U. Extracellular matrix: functions in the nervous system. *Cold Spring Harb. Perspect. Biol.* **3,** a005108 (2011).

Barros, C. S. *et al.* 1 integrins are required for normal CNS myelination and promote AKT-dependent myelin outgrowth. *Development* 136, 2717–2724 (2009).

Basselin, M., kim, H. W., Chen, M., Ma, K., Rapoport, S. I., Murphy, R. C., and Farias, S. E. (2010) Lithium modifies brain arachidonic and docosahexaenoic metabolism in rat lipopolysaccharide model of neuroinflammation. J. Lipid. Res. 51, 1049−1056.

Bayer, T., Buslei, R., Havas, L. and Falkai, P. (1999). Evidence for activation of microglia in patients with psychiatric wellnesses. *Neuroscience Letters*, 271(2), pp.126-128.

Beeson, D., Cossins, J., Rodriguez-Cruz, P., MaxWell, S., Liu, W. and Palace, J. (2018). Myasthenic syndromes due to defects in COL13A1 and in the N-linked glycosylation pathway. *Annals of the New York Academy of Sciences*, 1413(1), pp.163-169.

Bekku, Y. *et al.* Bral2 is Indispensable for the Proper Localization of *Brevican* and the Structural Integrity of the Perineuronal Net in the Brainstem and Cerebellum. *J. Comp. Neurol* 520**,** 1721–1736 (2012).

Bendz, H., Aurell, M. and Lanke, J. (2001). A historical cohort study of kidney damage in long-term lithium patients: continued survewellance needed. *European Psychiatry*, 16(4), pp.199-206.

Benes, F., Kwok, E., Vincent, S. and Todtenkopf, M. (1998). A reduction of nonpyramidal cells in sector CA2 of schizophrenics and manic depressives. *Biological Psychiatry*, 44(2), pp.88-97.

Beaulieu, J. (2012). A role for Akt and glycogen synthase kinase-3 as integrators of dopamine and serotonin neurotransmission in mental health. *Journal of Psychiatry & Neuroscience*, 37(1), pp.7-16.

Beaulieu, J. and Caron, M. (2008). Looking at Lithium: Molecular Moods and Complex Behaviour. *Molecular Interventions*, 8(5), pp.230-241.

Beaulieu, J. (2011). Beyond cAMP: the regulation of Akt and GSK3 by dopamine receptors. *Frontiers in Molecular Neuroscience*, 4.

Beaulieu, J., Sotnikova, T., Marion, S., Lefkowitz, R., Gainetdinov, R. and Caron, M. (2005). An Akt/β-Arrestin 2/PP2A Signaling Complex Mediates Dopaminergic Neurotransmission and Behavior. *Cell*, 122(2), pp.261-273.

Beurdeley, M. *et al.* Otx2 binding to perineuronal nets persistently regulates plasticity in the mature visual cortex. *J. Neurosci.* 32, 9429–37 (2012).

Belmaker, R. H. (2004) Bipolar disorder. N. Engl. J. Med. 351, 476− 486. (4) Gershon, S., Chengappa, K. N., and Malhi, G. S. (2009) Lithium specificity in bipolar wellness: a classic agent for the classic disorder. Bipolar Disord. 11, 34−44.

Berretta, S., Pantazopoulos, H., Markota, M., Brown, C. and Batzianouli, E. (2015). Losing the sugar coating: Potential impact of perineuronal net abnormalities on interneurons in schizophrenia. *Schizophrenia Research*, 167(1-3), pp.18-27.

Benarroch, E. E. Extracellular matrix in the CNS. *Neurology* 85, 1417–1427 (2015).

Bennett, E., Mandel, U., Clausen, H., Gerken, T., Fritz, T. and Tabak, L. (2014). Control of mucin-type O-glycosylation: A classification of the polypeptide GalNAc-transferase gene family. *Glycobiology*, 22(6), pp.736-756.

Beroun, Anna; Mitra, Shiladitya; Michaluk, Piotr; u. a. (2019): „MMPs in learning and memory and neuropsychiatric disorders". In: *Cellular and Molecular Life Sciences*. 76 (16), S. 3207–3228, DOI: 10.1007/s00018-019-03180-8.

Bertozzi, C. *et al.* (2017) *Inhibition of NGLY1 inactivates the transcription factor NRF1 and Potentiates Proteasome inhibitor cytotoxicity* [Preprint]. doi:10.26434/chemrxiv.5388046.v1.

Beurdeley, M., Spatazza, J., Lee, H., Sugiyama, S., Bernard, C., Di Nardo, A., Hensch, T. and Prochiantz, A. (2012). Otx2 Binding to Perineuronal Nets Persistently Regulates Plasticity in the Mature Visual Cortex. *Journal of Neuroscience*, 32(27), pp.9429-9437.

Beurel, E., and Jope, R. S. (2009) Lipopolysaccharide-induced interleukin-6 production is controlled by glycogen synthase kinase-3 and STAT3 in the brain. J. Neuroinflammation, DOI: 10.1186/1742-2094-6- 9

Biscaro, B., Lindvall, O., Tesco, G., Ekdahl, C. and Nitsch, R. (2012). Inhibition of Microglial Activation Protects Hippocampal Neurogenesis and Improves Cognitive Deficits in a Transgenic Mouse Model for Alzheimer's Disease. *Neurodegenerative Diseases*, 9(4), pp.187-198.

Bitanihirwe, Byron K.Y.; Woo, Tsung-Ung W. (2014): „Perineuronal nets and schizophrenia: The importance of neuronal coatings". In: *Neuroscience & Biobehavioral Reviews*. 45, S. 85–99, DOI: 10.1016/j.neubiorev.2014.03.018.

Biunno, I. and Cattaneo, M. (2011). SEL1L (sel-1 suppressor of lin-12-like (C. elegans)). *Atlas of Genetics and Cytogenetics in Oncology and Haematology*, (2).

Blond, B., Fredericks, C. and Blumberg, H. (2012). Functional neuroanatomy of bipolar disorder: structure, function, and connectivity in an amygdala-anterior paralimbic neural system. *Bipolar Disorders*, 14(4), pp.340-355.

Bonneh-Barkay, D. & Wiley, C. A. Brain extracellular matrix in neurodegeneration. *Brain Pathology* 19**,** 573–585 (2009)

Bosetti, F., Rintala, J., Seemann, R., Rosenberger, T. A., Contreras, M. A., Rapoport, S. I., and Chang, M. C. (2002) Chronic lithium downregulates cyclooxygenase-2 activity and prostaglandin E(2) concentration in rat brain. Mol. Psychiatry 7, 845−850.

Bosetti, F., Seemann, R., Bell, J., Zahorchak, R., Friedman, E., Rapoport, S. and Manickam, P. (2002). Analysis of gene expression with cDNA microarrays in rat brain after 7 and 42 days of oral lithium administration. *Brain Research Bulletin*, 57(2), pp.205-209.

Bolr, N. and Johnston, I. (2010). Targeted rapid amplification of cDNA ends (T-RACE)--an improved RACE reaction through degradation of non-target sequences. *Nucleic Acids Research*, 38(21), pp.e194-e194.

Brown, J. M. *et al.* A sulphated carbohydrate epitope inhibits axon regeneration after injury. *Proc. Natl. Acad. Sci.* 109**,** 4768–4773 (2012).

Browne, C.A. *et al.* (2022) "Perineuronal nets as therapeutic targets for the treatment of neuropsychiatric disorders," Frontiers in Synaptic Neuroscience, 14. Available at: https://doi.org/10.3389/fnsyn.2022.889800.

Bucki, R. (2022) Extracellular vimentin is sufficient to promote cell attachment, spreading, and motility by a mechanism involving N-acetyl glucosamine-containing structures [Preprint]. doi:10.1101/2022.11.28.518249.

Bucki, R. *et al.* (2022) "Extracellular vimentin is sufficient to promote cell attachment, spreading, and motility by a mechanism involving N-acetyl glucosamine-containing structures." Available at: https://doi.org/10.1101/2022.11.28.518249.

Buddhala, C., Campbell, M., Perlmutter, J. and Kotzbauer, P. (2015). Correlation between decreased CSF α-synuclein and Aβ1–42 in Parkinson disease. *Neurobiology of Aging*, 36(1), pp.476-484.

Burchell, J., Beatson, R., Graham, R., Taylor-Papadimitriou, J. and Tajadura-Ortega, V. (2018). O-linked mucin-type glycosylation in breast cancer. *Biochemical Society Transactions*, 46(4), pp.779-788.

Burgess, N., Maguwere, E. and O'Keefe, J. (2002). The Human Hippocampus and Spatial and Episodic Memory. *Neuron*, 35(4), pp.625-641.

Byun, Y. *et al.* (2001) "Caspase cleavage of vimentin disrupts intermediate filaments and promotes apoptosis," Cell Death & Differentiation, 8(5), pp. 443–450. Available at: https://doi.org/10.1038/sj.cdd.4400840.

Caglayan, S. *et al.* (2014) 'Lysosomal sorting of amyloid-β by the SORLA receptor is impaired by a familial alzheimer's disease mutation', *Science Translational Medicine*, 6(223). doi:10.1126/scitranslmed.3007747.

Calabrese, J., Bowden, C., Sachs, G., Yatham, L., Behnke, K., Mehtonen, O., Montgomery, P., Ascher, J., Paska, W., Earl, N. and DeVeaugh-Geiss, J. (2003).

A Placebo-Controlled 18-Month Trial of Lamotrigine and Lithium Maintenance Treatment in Recently Depressed Patients with Bipolar I Disorder. *The Journal of Clinical Psychiatry*, 64(9), pp.1013-1024.

Calker, D. and Belmaker, R. (2000). The high affinity inositol transport system - implications for the pathophysiology and treatment of bipolar disorder. *Bipolar Disorders*, 2(2), pp.102-107.

Carstens, K. E., Phwellips, M. L., Pozzo-Mweller, L., Iinberg, R. J. & Dudek, S. M. Perineuronal Nets Suppress Plasticity of Excitatory Synapses on CA2 Pyramidal Neurons. *J. Neurosci.* 36, 6312–6320 (2016).

Carulli, D., de Winter, F. and Verhaagen, J. (2021) 'Semaphorins in adult nervous system plasticity and disease', *Frontiers in Synaptic Neuroscience*, 13. doi:10.3389/fnsyn.2021.672891.

Connell, B. J. & Lortat-Jacob, H. Human Immunodeficiency Virus and Heparan Sulphate: From Attachment to Entry Inhibition. *Front. Immunol.* 4, 385 (2013).

Carulli, D., Foscarin, S., Faralli, A., Pajaj, E. and Rossi, F. (2013). Modulation of semaphorin3A in perineuronal nets during structural plasticity in the adult cerebellum. *Molecular and Cellular Neuroscience*, 57, pp.10-22.

Carulli, D., Kwok, J. and Pizzorusso, T. (2016). Perineuronal Nets and CNS Plasticity and Repair. *Neural Plasticity*, 2016, pp.1-2.

Carulli, D., Kwok, J. and Pizzorusso, T. (2016). Perineuronal Nets and CNS Plasticity and Repair. *Neural Plasticity*, 2016, pp.1-2.

Carulli, D. and Verhaagen, J. (2021) 'An extracellular perspective on CNS maturation: Perineuronal nets and the control of plasticity', *International Journal of Molecular Sciences*, 22(5), p. 2434. doi:10.3390/ijms22052434

Cassidy, F. (2016). Antidepressant treatment response in bipolar II disorder. *Bipolar Disorders*, 18(8), pp.706-707.

Chaunsali, Lata; Tewari, Bhanu P.; Sontheimer, Harald (2021): „Perineuronal Net Dynamics in the pathophysiology of epilepsy". In: *Epilepsy Currents*. 21 (4), S. 273–281, DOI: 10.1177/15357597211018688.

Cheung, W.D. and Hart, G.W. (2008) "AMP-activated protein kinase and p38 MAPK activate O-glcnacylation of neuronal proteins during glucose deprivation," Journal of Biological Chemistry, 283(19), pp. 13009–13020. Available at: https://doi.org/10.1074/jbc.m801222200.

Chaunsali, L., Tewari, B.P. and Sontheimer, H. (2021) 'Perineuronal Net Dynamics in the pathophysiology of epilepsy', *Epilepsy Currents*, 21(4), pp. 273–281. doi:10.1177/15357597211018688.

Colla, M., Schubert, F., Bubner, M., Heidenreich, J., Bajbouj, M., Seifert, F., Luborzewski, A., Heuser, I. and Kronenberg, G. (2008). Glutamate as a spectroscopic marker of hippocampal structural plasticity is elevated in long-term

euthymic bipolar patients on chronic lithium therapy and correlates inversely with diurnal cortisol. *Molecular Psychiatry*, 14(7), pp.696-704.

Colton, C. (2009). Heterogeneity of Microglial Activation in the Innate Immune Response in the Brain. *Journal of Neuroimmune Pharmacology*, 4(4), pp.399-418.

Condomitti, G. & de Wit, J. Heparan Sulphate Proteoglycans as Emerging Players in Synaptic Specificity.
Front. Mol. Neurosci. 11**,** (2018).

Cotter, D., Mackay, D., Landau, S., Kerwin, R., and Everall, I. (2001) Reduced glial cell density and neuronal size in the anterior cingulate cortex in major depressive disorder. Arch. Gen. Psychiatry 58, 545−553

Cotter, D., Pariante, C. and Everall, I. (2001). Glial cell abnormalities in major psychiatric disorders: the evidence and implications. *Brain Research Bulletin*, 55(5), pp.585-595.

Coulson-Thomas, V., Lauer, M., Soleman, S., Zhao, C., Hascall, V., Day, A. and Fawcett, J. (2016). Tumor Necrosis Factor-stimulated Gene-6 (TSG-6) Is Constitutively Expressed in Adult Central Nervous System (CNS) and Associated with Astrocyte-mediated Glial Scar Formation following Spinal Cord Injury. *Journal of Biological Chemistry*, 291(38), pp.19939-19952.

Cowansage, K., LeDoux, J. and Monfils, M. (2010). Brain-Derived Neurotrophic Factor: A Dynamic Gatekeeper of Neural Plasticity. *Current Molecular Pharmacology*, 3(1), pp.12-29.

Cui, H., Freeman, C., Jacobson, G. A. & Small, D. H. Proteoglycans in the Central Nervous System: Role in Development, Neural Repair, and Alzheimer's Disease. *Int. Union Biochem. Mol. Biol.* 65**,** 108– 120 (2013).

David, L. S., Schachner, M. & Saghatelyan, A. The Extracellular Matrix

Glycoprotein Tenascin-R Affects Adult But Not Developmental Neurogenesis in the Olfactory Bulb. *J. Neurosci.* 33**,** 10324– 10339 (2013).

Dear, T. and Boehm, T. (2009). Diverse mRNA exprssion patterns of the mouse calpain genes Capn5, Capn6 and Capn11 during development. *Mechanisms of Development*, 89(1-2), pp.201-209.

de Ramon Francàs, G., Zuñiga, N. R. & Stoeckli, E. T. The spinal cord shows the way – How axons navigate intermediate targets. *Dev. Biol.* 432**,** 43–52 (2017).

Dick, G., Tan, C., Alves, J., Ehlert, E., Mweller, G., Hsieh-Wilson, L., Sugahara, K., Oosterhof, A., van Kuppevelt, T., Verhaagen, J., Fawcett, J. and Kwok, J. (2013). *Semaphorin 3A* Binds to the Perineuronal Nets via Chondroitin Sulphate Type E Motifs in Rodent Brains. *Journal of Biological Chemistry*, 288(38), pp.27384-27395.

Dick, G. *et al.* Semaphorin 3A binds to the perineuronal nets via chondroitin sulphate type E motifs in rodent brains. *J. Biol. Chem.* 288**,** 27384–27395 (2013).

Dickens, Stuart-Mark (2021). Establishing the perineuronal net as a neuroprotective barrier in Parkinson's disease, Unpublished PHD thesis, University of Leeds

Dityatev, A., Seidenbecher, C. I. & Schachner, M. Compartmentalization from the outside: The extracellular matrix and functional microdomains in the brain. *Trends in Neurosciences* 33**,** 503–512 (2010).

Dewald, O. (2005). CCL2/Monocyte Chemoattractant Protein-1 Regulates Inflammatory Responses Critical to Healing Myocardial Infarcts. *Circulation Research*, 96(8), pp.881-889.

de Winter, F., Kwok, J., Fawcett, J., Vo, T., Carulli, D. and Verhaagen, J. (2016). The Chemorepulsive Protein *Semaphorin 3A* and Perineuronal Net-Mediated Plasticity. *Neural Plasticity*, 2016, pp.1-14.

Djerbal, L., Lortat-Jacob, H. & Kwok, J. Chondroitin sulphates and their binding molecules in the central nervous system. *Glycoconjugate Journal* 34**,** 363–376 (2017).

Donegan, J. and Lodge, D. (2016). Hippocampal Perineuronal Nets Are Required for the Sustained Antidepressant Effect of Ketamine. *International Journal of Neuropsychopharmacology*, p.pyw095.

Dubacheva, G. V *et al.* Controlling Multivalent Binding through Surface Chemistry: Model Study on Streptavidin. *J. Am. Chem. Soc.* 139**,** 4157–4167 (2017).

Dubisova, J. *et al.* (2022) "Oral treatment of 4-methylumbelliferone reduced perineuronal nets and improved recognition memory in mice," Brain Research Bulletin, 181, pp. 144–156. Available at: https://doi.org/10.1016/j.brainresbull.2022.01.011.

Duman-Scheel, M. (2015). Deleted in Colorectal Cancer (*DCC*) Pathfinding: Axon Guidance Gene Finally Turned Tumor Suppressor. *Current Drug Targets*, 13(11), pp.1445-1453.

Drug Treatments for Geriatric Bipolar Disorder: A Perspective from the ISBD Geriatric Bipolar Taskforce. (2015). *Bipolar Disorders*, 17, pp.31-31.

Escudero, D. (2011) 'Has2 (hyaluronan synthase 2)', Atlas of Genetics and Cytogenetics in Oncology and Haematology [Preprint], (2). doi:10.4267/2042/44682.

Eisele, B.S. *et al.* (2022) 'Bisphosphate nucleotidase 2 (BPNT2), a molecular target of lithium, regulates chondroitin sulphation patterns in the cerebral cortex and

Hippocampus', *Advances in Biological Regulation*, 83, p. 100858. doi:10.1016/j.jbior.2021.100858.

Enwright, John F; Sanapala, Sowmya; Foglio, Aaron; u. a. (2016): Reduced labeling of parvalbumin neurons and perineuronal nets in the dorsolateral prefrontal cortex of subjects with schizophrenia. In: *Neuropsychopharmacology*. 41 (9), S. 2206–2214, DOI: 10.1038/npp.2016.24.

Eskici, N., Erdem-Ozdamar, S. and Dayangac-Erden, D. (2018). The altered expression of perineuronal net elements during neural differentiation. *Cellular & Molecular Biology Letters*, 23(1).

Elvsåshagen, T., Zuzarte, P., Istlye, L., Bøen, E., Josefsen, D., Boye, B., Hol, P., Malt, U., Young, L. and Andreazza, A. (2016). Dentate gyrus−cornu ammonis (CA) 4 volume is decreased and associated with depressive episodes and lipid peroxidation in bipolar II disorder: Longitudinal and cross-sectional analyses. *Bipolar Disorders*, 18(8), pp.657-668.

Fang, X. *et al.* (2020) "Matrix metalloproteinase 9 (MMP9) level and MMP9 - 1562C>T in patients with obstructive sleep apnea: A systematic review and meta-analysis of case-control studies," Sleep Medicine, 67, pp. 110–119. Available at: https://doi.org/10.1016/j.sleep.2019.11.1247.

Farrokhi, M. (2017). *Sema3a* and multiple sclerosis. *Gene*, 615, p.41.

Fawcett, James W.; Fyhn, Marianne; Jendelova, Pavla; u. a. (2022): „The extracellular matrix and perineuronal nets in memory". In: *Molecular Psychiatry*. 27 (8), S. 3192–3203, DOI: 10.1038/s41380-022-01634-3.

Femenía, T., Gómez-Galán, M., Lindskog, M. and Magara, S. (2012). Dysfunctional hippocampal activity affects emotion and cognition in mood disorders. *Brain Research*, 1476, pp.58-70.

Fornai, F., Longone, P., Ferrucci, M., Lenzi, P., Isidoro, C., Ruggieri, S. and Paparelli, A. (2008). Autophagy and amyotrophic lateral sclerosis: The multiple roles of lithium. *Autophagy*, 4(4), pp.527-530.

Fausther, M., Lavoie, E., Goree, J., Baldini, G. and Dranoff, J. (2014). NT5E Mutations That Cause Human Disease Are Associated with Intracellular Mistrafficking of NT5E Protein. *PLoS ONE*, 9(6), p.e98568.

Favuzzi, E., Marques-Smith, A., Deogracias, R., Winterflood, C., Sánchez-Aguilera, A., Mantoan, L., Maeso, P., Fernandes, C., Elrs, H. and Rico, B. (2017). Activity-Dependent Gating of Parvalbumin Interneuron Function by the Perineuronal Net Protein *Brevican. Neuron*, 95(3), pp.639-655.e10.

Francis, L., Francis, V. and Venuthurupalli, S. (2013). Proliferative glomerulonephritis with monoclonal IGG deposits on a background of chronic lithium nephrotoxicity – a case report. *Pathology*, 45, p.S68.

Freland, L. and Beaulieu, J. (2012). Inhibition of GSK3 by lithium, from single molecules to signaling networks. *Frontiers in Molecular Neuroscience*, 5.

Frischknecht, R. *et al.* (2009) 'Brain extracellular matrix affects AMPA receptor lateral mobility and short-term synaptic plasticity', *e-Neuroforum*, 15(3), pp. 94–95. doi:10.1515/nf-2009-0304.

Foscarin, S., Raha-Chowdhury, R., Fawcett, J. W. & Kwok, J. C. F. Brain ageing changes proteoglycan sulphation, rendering perineuronal nets more inhibitory. *Aging (Albany. NY).* 9**,** 1607–1622 (2017).

Fountoulakis, K., Kontis, D., Gonda, X. and Yatham, L. (2013). A systematic review of the evidence on the treatment of rapid cycling bipolar disorder. *Bipolar Disorders*, 15(2), pp.115-137.

Gama, M., Houle, G., Noreau, A., Dionne-Laporte, A., Dion, P., Rouleau, G., Barsottini, O. and Pedroso, J. (2016). SYNE1 mutations cause autosomal-

recessive ataxia with retained reflexes in Brazilian patients. *Movement Disorders*, 31(11), pp.1754-1756.

Gamboa, N. T. *et al.* Neurovascular patterning cues and implications for central and peripheral neurological disease. *Surg. Neurol. Int.* 8**,** 208 (2017).

Galtrey, C. M. & Fawcett, J. W. The role of chondroitin sulphate proteoglycans in regeneration and plasticity in the central nervous system. *Brain Res. Rev.* 54**,** 1–18 (2007).

Garrett, A. and Chang, K. (2008). The role of the amygdala in bipolar disorder development. *Development and Psychopathology*, 20(04), p.1285.

Garrido, J., Simón, D., Varea, O. and Wandosell, F. (2007). GSK3 alpha and GSK3 beta are necessary for axon formation. *FEBS Letters*, 581(8), pp.1579-1586.

Gershon, S., Chengappa, K. and Malhi, G. (2009). Lithium specificity in bipolar wellness: a classic agent for the classic disorder. *Bipolar Disorders*, 11, pp.34-44.

George, N. & Geller, H. M. Extracellular matrix and traumatic brain injury. *J. Neurosci. Res.* 96**,** 573– 588 (2018).

Ghosh, A. and Giese, K. (2015). Calcium/calmodulin-dependent kinase II and Alzheimer's disease. *Molecular Brain*, 8(1).

Giamanco, K., Morawski, M. and Matthews, R. (2010). Perineuronal net formation and structure in *Aggrecan* knockout mice. *Neuroscience*, 170(4), pp.1314-1327.

Gigante, A., Bond, D., Lafer, B., Lam, R., Young, L. and Yatham, L. (2012). Brain glutamate levels measured by magnetic resonance spectroscopy in patients with bipolar disorder: a meta-analysis. *Bipolar Disorders*, 14(5), pp.478-487.

Gitlin, M. (2016). Lithium side effects and toxicity: prevalence and management strategies. *International Journal of Bipolar Disorders*, 4(1).

Gilad, G. M., and Gilad, V. H. (2007) Astroglia growth retardation and increased microglia proliferation by lithium and ornithine decarboxylase inhibitor in rat cerebellar cultures: Cytotoxicity by combined lithium and polyamine inhibition. J. Neurosci. Res. 85, 594− 601.

Gow, Matthew; Mirembe, Dora; Longwe, Zaomba; u. a. (2013): „A gene trap mutagenesis screen for genes underlying cellular response to the mood stabilizer lithium". In: *Journal of Cellular and Molecular Medicine*. 17 (5), S. 657–663, DOI: 10.1111/jcmm.12048.

Grover, S., Ghosh, A., Sarkar, S., Chakrabarti, S. and Avasthi, A. (2014). Sexual Dysfunction in Clinically Stable Patients with Bipolar Disorder Receiving Lithium. *Journal of Clinical Psychopharmacology*, 34(4), pp.475-482.

Guloksuz, S., Cetin, E. A., Cetin, T., Deniz, G., Oral, E. T., and Nutt, D. J. (2010) Cytokine levels in euthymic bipolar patients. J. Affective Disord. 126, 458−462

Hariri, A. and Shin, L. (2011). Ilcome to Biology of Mood & Anxiety Disorders. *Biology of Mood & Anxiety Disorders*, 1(1), p.1.

Härtig, Wolfgang; Brückner, Gert; Brauer, Kurt; u. a. (1995): „Allocation of perineuronal nets and parvalbumin-, Calbindin-D28K- and glutamic acid decarboxylase-immunoreactivity in the amygdala of the rhesus monkey". In: *Brain Research*. 698 (1–2), S. 265–269, DOI: 10.1016/0006-8993(95)01016-o.

Hoppenbrouwers, I.A. *et al.* (2008) 'EVI5 is a risk gene for multiple sclerosis', *Genes & Immunity,* 9(4), pp. 334–337. doi:10.1038/gene.2008.22.

Hosp, J., Strüber, M., Yanagawa, Y., Obata, K., Vida, I., Jonas, P. and Bartos, M. (2013). Morpho-physiological criteria divide dentate gyrus interneurons into classes. *Hippocampus*, 24(2), pp.189-203.

Hoozemans, J.J.M. *et al.* (2012) 'Activation of the unfolded protein response is an early event in alzheimer's and parkinson's disease', *Neurodegenerative Diseases*, 10(1–4), pp. 212–215. doi:10.1159/000334536.

Huang, H. and Akbarian, S. (2007). GAD1 mRNA Expression and DNA Methylation in Prefrontal Cortex of Subjects with Schizophrenia. *PLoS ONE*, 2(8), p.e809.

Huang, Y., Coupland, N., Lebel, R., Carter, R., Seres, P., Wilman, A. and Malykhin, N. (2013). Structural Changes in Hippocampal Subfields in Major Depressive Disorder: A High-Field Magnetic Resonance Imaging Study. *Biological Psychiatry*, 74(1), pp.62-68.

Huang, W. C., Lin, Y. S., Wang, C. Y., Tsai, C. C., Tseng, H. C., Chen, C. L., Lu, P. J., Chen, P. S., Qian, L., Hong, J. S., and Lin, C. F. (2008) Glycogen synthase kinase-3 negatively regulates anti-inflammatory interleukin-10 for lipopolysaccharide-induced iNOS/NO biosynthesis and RANTES production in microglial cells. Immunology. 128, e275−286

Hull, M., Lee, E., Lee, T., Anand, N., LaLone, V., and Parameswaran, N. (2014) Lithium chloride induces TNFα in mouse macrophages via MEK-ERK-dependent pathway. J. Cell. Biochem. 115, 71−80.

Hussaini, S., Choi, C., Cho, C., Kim, H., Jun, H. and Jang, M. (2014). Wnt signaling in neuropsychiatric disorders: Ties with adult hippocampal neurogenesis and behavior. *Neuroscience & Biobehavioral Reviews*, 47, pp.369-383.

Irvine, S. F. & Kwok, J. C. F. Perineuronal nets in spinal motoneurones: Chondroitin sulphate proteoglycan around alpha motoneurones. *Int. J. Mol. Sci.* 19, (2018).

Iwashkiw, J., Vozza, N., Kinsella, R. and Feldman, M. (2017). Pour some sugar on it: the expanding world of bacterial proteinO-linked glycosylation. *Molecular Microbiology*, 89(1), pp.14-28.

Jakovcevski, I., Miljkovic, D., Schachner, M. and Andjus, P. (2012). Tenascins and inflammation in disorders of the nervous system. *Amino Acids*, 44(4), pp.1115-1127.

Jacquinet, J.-C. & Lopin-Bon, C. Stereocontrolled preparation of biotinylated chondroitin sulphate E di-, tetra-, and hexasaccharide conjugates. *Carbohydr. Res.* 402, 35–43 (2015).

Janssen, B. J. C. *et al.* Structural basis of semaphorin-plexin signalling. *Nature* 467, (2010).

Jakovljević, A. *et al.* (2021) 'Structural and functional modulation of perineuronal nets: In search of important players with highlight on tenascins', *Cells*, 10(6), p. 1345. doi:10.3390/cells10061345.

Javadapour, A., Malhi, G., Ivanovski, B., Chen, X., In, W. and Sachdev, P. (2010). Hippocampal Volumes in Adults with Bipolar Disorder. *Journal of Neuropsychiatry*, 22(1), pp.55-62.

Jetsonen, E. *et al.* (2023) 'Activation of trkb in parvalbumin interneurons is required for the promotion of reversal learning in spatial and fear memory by antidepressants', *Neuropsychopharmacology*, 48(7), pp. 1021–1030. doi:10.1038/s41386-023-01562-y.

Jia, M., Jiang, L., Wang, Y., Huang, J., Yu, M. and Xue, H. (2016). lincRNA-p21 inhibits invasion and metastasis of hepatocellular carcinoma through Notch signaling-induced epithelial-mesenchymal transition. *Hepatology Research*, 46(11), pp.1137-1144.

Jin, G., Long, C., Liu, W., Tang, Y., Zhu, Y., Zhou, X., Ai, Y., Zhang, Q. and Shen, H. (2013). Identification and characterization of novel alternative splice variants of human SAMD11. *Gene*, 530(2), pp.215-221.

John, Urmwella; Patro, Nisha; Patro, Ishan (2022): „Perineuronal nets: Cruise from a honeycomb to the safety nets". In: *Brain Research Bulletin*. 190, S. 179–194, DOI: 10.1016/j.brainresbull.2022.10.004.

Jun, I., Park, H., Piao, H., Han, J., An, M., Yun, B., Zhang, X., Cha, Y., Shin, Y., Yook, J., Jung, J., Gee, H., Park, J., Yoon, D., Jeung, H. and Lee, M. (2017). ANO9/TMEM16J promotes tumourigenesis via EGFR and is a novel therapeutic target for pancreatic cancer. *British Journal of Cancer*, 117(12), pp.1798-1809.

Kaidanovich-Beilin, O. and Woodgett, J. (2011). GSK-3: Functional Insights from Cell Biology and Animal Models. *Frontiers in Molecular Neuroscience*, 4.

Kaneda, T., Makino, S., Nishiyama, M., Asaba, K. and Hashimoto, K. (2008). Differential Neuropeptide Responses to Starvation with Ageing. *Journal of Neuroendocrinology*, 13(12), pp.1066-1075.

Kanekiyo, T. *et al.* Heparan Sulphate Proteoglycan and the Low-Density Lipoprotein Receptor-Related Protein 1 Constitute Major Pathways for Neuronal Amyloid- Uptake. *J. Neurosci.* 31, 1644–1651 (2011).

Kang, K., Kim, Y. J., Kim, Y. H., Roh, J. N., Nam, J. M., Kim, P. Y., Ryu, W. S., Lee, S. H., and Yoon, B. W. (2012) Lithium pretreatment reduces brain injury after intracerebral hemorrhage in rats. Neurol. Res. 34, 447−454.

Kele, J. (2006). Neurogenin 2 is required for the development of ventral midbrain dopaminergic neurons. *Development*, 133(3), pp.495-505.

Keswani, A., Chustz, R., Suh, L., Carter, R., Peters, A., Tan, B., Chandra, R., Kim, S., Azam, T., Dinarello, C., Kern, R., Schleimer, R. and Kato, A. (2011). Differential expression of interleukin-32 in chronic rhinosinusitis with and without nasal polyps. *Allergy*, 67(1), pp.25-32.

Kerner, B. (2014). Genetics of bipolar disorder. *The Application of Clinical Genetics*, p.33.

Khairallah, W., Fawaz, A., Brown, E. and El-Hajj Fuleihan, G. (2007). Hypercalcemia and diabetes insipidus in a patient previously treated with lithium. *Nature Clinical Practice Nephrology*, 3(7), pp.397-404.

Kim, B., Park, Y., Libermann, T. and Cho, J. (2011). PTH regulates myleoid ELF-1-like factor (MEF)-induced MAB-21-like-1 (MAB21L1) expression through the JNK1 pathway. *Journal of Cellular Biochemistry*, 112(8), pp.2051-2061.

Kim, S., Lee, H. and Kim, Y. (2013). Neural stem cell-based treatment for neurodegenerative diseases. *Neuropathology*, p.n/a-n/a.

Knijff, E. M., Breunis, M. N., Kupka, R. W., de Wit, H. J., Ruwhof, C., Akkerhuis, G. W., Nolen, W. A., and Drexhage, H. A. (2007) An imbalance in the production of IL-1beta and IL-6 by monocytes of bipolar patients: restoration by lithium treatment. Bipolar Disord. 9, 743−753

Körner, S., Böselt, S., Wichmann, K., Thau-Habermann, N., Zapf, A., Knippenberg, S., Dengler, R. and Petri, S. (2016). The Axon Guidance Protein *Semaphorin 3A* Is Increased in the Motor Cortex of Patients With Amyotrophic Lateral Sclerosis. *Journal of Neuropathology & Experimental Neurology*, 75(4), pp.326-333.

Kovalevich and Langford (2016). Considerations for the use of SH-SY5Y neuroblastoma cells in neurobiology. *Methods Molecular Biology*, 1078, pp.9-21.

Kovalevich, Jane; Langford, Dianne (2013): „Considerations for the use of SH-SY5Y neuroblastoma cells in neurobiology". In: *Neuronal Cell Culture*., S. 9–21, DOI: 10.1007/978-1-62703-640-5_2.

Kraszewska, A., Chlopocka-Wozniak, M., Abramowicz, M., Sowinski, J. and Rybakowski, J. (2014). A cross-sectional study of thyroid function in 66 patients with bipolar disorder receiving lithium for 10-44 years. *Bipolar Disorders*, 17(4), pp.375-380.

Kremer, A. (2011). GSK3 and Alzheimer's disease: facts and fiction…. *Frontiers in Molecular Neuroscience*, 4.

Kucharz, E. J., Sierakowski, S. J., and Goodwin, J. S. (1993) Lithium *in vitro* enhances interleukin-2 production by T cells from patients with systemic lupus erythematosus. Immunopharmacol. Immunotoxicol. 15, 515−523.

Kurihara, D. & Yamashita, T. Chondroitin sulphate proteoglycans down-regulate spine formation in cortical neurons by targeting tropomyosin-related kinase B (TrkB) protein. *J. Biol. Chem.* 287**,** 13822– 13828 (2012).

Kwok, J., Dick, G., Wang, D. and Fawcett, J. (2011). Extracellular matrix and perineuronal nets in CNS repair. *Developmental Neurobiology*, 71(11), pp.1073-1089.

Kwok, J. C. F., Foscarin, S. & Fawcett, J. W. *Extracellular Matrix, Neuromethods.* 93**,** (2015).

Lau, L. W., Cua, R., Keough, M. B., Haylock-Jacobs, S. & Yong, V. W. Pathophysiology of the brain extracellular matrix: A new target for remyelination. *Nature Reviews Neuroscience* 14**,** 722–729 (2013).

Lee, Dongmin; Hyun, Jung Ho; Jung, Kanghoon; u. a. (2017): „A calcium- and light-gated switch to induce gene expression in activated neurons". In: *Nature Biotechnology*. 35 (9), S. 858–863, DOI: 10.1038/nbt.3902.

Lemarchant, S., Wojciechowski, S. and Koistinaho, J. (2016). Perineuronal nets in neurodegeneration. *Oncotarget*, 7(48).

Lendvai, D. *et al.* Neurochemical mapping of the human hippocampus reveals perisynaptic matrix around functional synapses in Alzheimer's disease. *Acta Neuropathol* 125**,** 215–229 (2013).

Lepkifker, E., Sverdlik, A., Iancu, I., Ziv, R., Segev, S. and Kotler, M. (2004). Renal Insufficiency in Long-Term Lithium Treatment. *The Journal of Clinical Psychiatry*, 65(6), pp.850-856.

Logsdon, A.F. *et al.* (2021) 'Decoding perineuronal net glycan sulphation patterns in the alzheimer's disease brain', *Alzheimer's & Dementia*, 18(5), pp. 942–954. doi:10.1002/alz.12451.

Leighton, S.P. *et al.* (2017) 'Chemokines in depression in health and in inflammatory wellness: A systematic review and meta-analysis', *Molecular Psychiatry*, 23(1), pp. 48–58. doi:10.1038/mp.2017.205.

Li, Z., Su, D., Ying, L., Yu, G. and Mao, W. (2017). Study on expression of CDH4 in lung cancer. *World Journal of Surgical Oncology*, 15(1).

Liang, W. G. *et al.* Structural basis for oligomerization and glycosaminoglycan binding of CCL5 and CCL3. *Proc. Natl. Acad. Sci.* 113**,** 5000–5005 (2016).

Li, B., Yamamori, H., Tatebayashi, Y., Shafit-Zagardo, B., Tanimukai, H., Chen, S., Iqbal, K. and Grundke-Iqbal, I. (2008). Failure of Neuronal Maturation in Alzheimer Disease Dentate Gyrus. *Journal of Neuropathology & Experimental Neurology*, 67(1), pp.78-84.

Li, Y., Jin, H., Yan, C., Ren, C., Jiang, C., Jin, C., Seo, K. and Jin, X. (2014). Molecular cloning, sequence identification, and gene expression analysis of bovine ADCY2 gene. *Molecular Biology Reports*, 41(6), pp.3561-3568.

Liberman, Z., Plotkin, B., Tennenbaum, T. and Eldar-Finkelman, H. (2008). Coordinated phosphorylation of insulin receptor substrate-1 by glycogen synthase kinase-3 and protein kinase CβII in the diabetic fat tissue. *American Journal of Physiology-Endocrinology and Metabolism*, 294(6), pp.E1169-E1177.

Licht, R. (2011). Lithium: Still a Major Option in the Management of Bipolar Disorder. *CNS Neuroscience & Therapeutics*, 18(3), pp.219-226.

Lisman, J. (2017). Glutamatergic synapses are structurally and biochemically complex because of multiple plasticity processes: long-term potentiation, long-term depression, short-term potentiation and scaling. *Philosophical Transactions of the Royal Society B: Biological Sciences*, 372(1715),

Liu, C. C. *et al.* Neuronal heparan sulphates promote amyloid pathology by modulating brain amyloid-β clearance and aggregation in Alzheimer's disease. *Sci. Transl. Med.* **8,** 332ra44 (2016).

Looyenga, B. and Brundin, P. (2013). Silencing synuclein at the synapse with PLK2. *Proceedings of the National Academy of Sciences*, 110(41), pp.16293-16294.

Luscher, C. and Malenka, R. (2012). NMDA Receptor-Dependent Long-Term Potentiation and Long-Term Depression (LTP/LTD). *Cold Spring Harbor Perspectives in Biology*, 4(6), pp.a005710-a005710.

Ly, P. and Song, W. (2011). Loss of activated CaMKII at the synapse underlies Alzheimer's disease memory loss. *Journal of Neurochemistry*, 119(4), pp.673-675.

Maeda, N., Ishii, M., Nishimura, K. & Kamimura, K. Functions of chondroitin sulphate and heparan sulphate in the developing brain. *Neurochem. Res.* 36**,** 1228–1240 (2011).

Malinauskas, T., Janssen, B., Iir, G., Cader, M., Siebold, C. and Jones, E. (2013). Neuropilins Lock Secreted Semaphorins onto Plexins in a Ternary Signalling Complex. *Biophysical Journal*, 104(2), p.613a.

Mann, L., Heldman, E., Bersudsky, Y., Vatner, S., Ishikawa, Y., Almog, O., Belmaker, R. and Agam, G. (2009). Inhibition of specific adenylyl cyclase isoforms by lithium and carbamazepine, but not valproate, may be related to their antidepressant effect. *Bipolar Disorders*, 11(8), pp.885-896.

Mann-Wrobel, M., Carreno, J. and Dickinson, D. (2011). Meta-analysis of neuropsychological functioning in euthymic bipolar disorder: an update and investigation of moderator variables. *Bipolar Disorders*, 13(4), pp.334-342.

Massey, J. (2006). Chondroitinase ABC Digestion of the Perineuronal Net Promotes Functional Collateral Sprouting in the Cuneate Nucleus after Cervical Spinal Cord Injury. *Journal of Neuroscience,* 26(16), pp.4406-4414.

Mao, Y., Francis-Ist, P. and Irvine, K. (2015). Fat4/Dchs1 signaling between stromal and cap mesenchyme cells influences nephrogenesis and ureteric bud branching. *Development*, 142(15), pp.2574-2585.

Malhi, G., Ivanovski, B., Hadzi-Pavlovic, D., Mitchell, P., Vieta, E. and Sachdev, P. (2007). Neuropsychological deficits and functional impairment in bipolar depression, hypomania and euthymia. *Bipolar Disorders*, 9(1-2), pp.114-125.

Maki, Y. and Kadara, H. (2013). GPRC5A (G protein-coupled receptor, family C, group 5, member C). *Atlas of Genetics and Cytogenetics in Oncology and Haematology*, (8).

Mao, L. (2002). Glutamate Cascade to cAMP Response Element-Binding Protein Phosphorylation in Cultured Striatal Neurons through Calcium-Coupled Group I Metabotropic Glutamate Receptors. *Molecular Pharmacology*, 62(3), pp.473-484.

Mathivanan, S. (2017). Extracellular Matrix and the Extracellular Environment. *Proteomics*, 17(23-24), p.7700185.

Matsebatlela, T., Gallicchio, V., and Becker, R. (2012) Lithium modulates cancer cell growth, apoptosis, gene expression and cytokine production in HL-60 promyelocytic leukaemia cells and their drugresistant sub-clones. Biol. Trace Elem. Res. 149, 323−330.

McKnight, R., Adida, M., Budge, K., Stockton, S., Goodwin, G. and Geddes, J. (2012). Lithium toxicity profile: a systematic review and meta-analysis. The Lancet, 379(9817), pp.721-728.

Ménager, C., Arimura, N., Fukata, Y. and Kaibuchi, K. (2004). PIP3 is involved in neuronal polarization and axon formation. *Journal of Neurochemistry*, 89(1), pp.109-118.

Menko, A.S. *et al.* (2014) "A central role for vimentin in regulating repair function during healing of the lens epithelium," Molecular Biology of the Cell, 25(6), pp. 776–790. Available at: https://doi.org/10.1091/mbc.e12-12-0900.

Merrwell, J. E., Murphy, S. P., Mitrovic, B., Mackenzie-Graham, A., Dopp, J. C., Ding, M., Griscavage, J., Ignarro, L. J., and LoInstein, C. J. (1997) Inducible nitric oxide synthase and nitric oxide production by oligodendrocytes. J. Neurosci. Res. 48, 372−384

Merendino, R. A., Mancuso, G., Tomasello, F., Gazzara, D., Cusumano, V., Chwellemi, S., Spadaro, P., and Mesiti, M. (1994) Effects of lithium carbonate on cytokine production in patients affected by breast cancer. J. Biol. Regul. Homeostatic Agents 8, 88−91

Miranda, J.M. *et al.* (2022) 'Hippocampal parvalbumin interneurons play a critical role in memory development', Cell Reports, 41(7), p. 111643. doi:10.1016/j.celrep.2022.111643.

Monneau, Y., Arenzana-Seisdedos, F. & Lortat-Jacob, H. The slet spot: how GAGs help chemokines guide migrating cells. *J. Leukoc. Biol.* 99**,** 935–953 (2016).

Mie Nishimura, Nobuyuki Miyamoto, Jun Nishihira. Daily Oral Chondroitin Sulphate Oligosaccharides for Knee Joint Pain in Healthy Subjects: A Randomized, Blinded, Placebo-Controlled Study. *Open Nutr. J.* 12**,** (2018).

Mikles, D., Bhat, V., Schuchardt, B., McDonald, C. and Farooq, A. (2014). Enthalpic factors override the polyelectrolyte effect in the binding of EGR1 transcription factor to DNA. *Journal of Molecular Recognition*, 27(2), pp.82-91.

Miyata, S., Nadanaka, S., Igarashi, M. and Kitagawa, H. (2018). Structural Variation of Chondroitin Sulphate Chains Contributes to the Molecular Heterogeneity of Perineuronal Nets. *Frontiers in Integrative Neuroscience*, 12.

Miyata, S., Komatsu, Y., Yoshimura, Y., Taya, C. & Kitagawa, H. Persistent cortical plasticity by upregulation of chondroitin 6-sulphation. *Nat. Neurosci.* 15, 414–422 (2012).

Miyata, S., Nishimura, Y. & Nakashima, T. Perineuronal nets protect against amyloid β-protein neurotoxicity in cultured cortical neurons. *Brain Res.* 1150, 200–206 (2007).

Miyata, Shinji; Kitagawa, Hiroshi (2017): „Formation and remodeling of the brain extracellular matrix in neural plasticity: Roles of chondroitin sulfate and hyaluronan". In: *Biochimica et Biophysica Acta (BBA) - General Subjects*. 1861 (10), S. 2420–2434, DOI: 10.1016/j.bbagen.2017.06.010.

Mjg, R., García Medrano, B. & Bravo, J. The Role of the Basal Lamina in Nerve Regeneration. J Cytol Histol 7, 438 (2016).

Modabbernia, A., Taslimi, S., Brietzke, E., and Ashrafi, M. (2013) Cytokine alterations in bipolar disorder: a meta-analysis of 30 studies. Biol. Psychiatry 74, 15−25.

Morton, D. (2014). Id4 acts as a tumor suppressor by inducing apoptosis and senescence in p53-dependent manner. *Cancer Research*, 74(19 Supplement), pp.599-599.

Moncada, S., and Bolanos, J. P. (2006) Nitric oxide, cell bioenergetics and neurodegeneration. J. Neurochem. 97, 1676−1689

Morikawa, S., Ikegaya, Y., Narita, M. & Tamura, H. Activation of perineuronal net-expressing excitatory neurons during associative memory encoding and retrieval. *Sci. Rep.* 7, (2017).

Morawski, M. *et al.* Ion exchanger in the brain: Quantitative analysis of

perineuronally fixed anionic binding sites suggests diffusion barriers with ion sorting properties. *Sci. Rep.* 5**,** 16471 (2015).

Muller, H. (2003). Is lithium still the gold standard in the treatment of bipolar disorders?. *European Archives of Psychiatry and Clinical Neuroscience*, 253(3), pp.113-114.

Munkholm, K., Braüner, J., Kessing, L. and Vinberg, M. (2013). Cytokines in bipolar disorder vs. healthy control subjects: A systematic review and meta-analysis. *Journal of Psychiatric Research*, 47(9), pp.1119-1133.

Munkholm, K., Braü ner, J. V., Kessing, L. V., and Vinberg, M. (2013) Cytokines in bipolar disorder vs. healthy control subjects: a systematic review and meta-analysis. J. Psychiatr. Res. 47, 1119−1133.

Murase, Sachiko; Robertson, Sarah E.; Lantz, Crystal L.; u. a. (2022): „Chronic monocular deprivation reveals MMP9-dependent and -independent aspects of murine visual system plasticity". In: *International Journal of Molecular Sciences*. 23 (5), S. 2438, DOI: 10.3390/ijms23052438.

Nahman, S., Belmaker, R. H., and Azab, A. N. (2012) Effects of lithium on lipopolysaccharide-induced inflammation in rat primary glia cells. Innate Immun. 18, 447−458

Nakamura, Hiroyuki; Fujii, Yutaka; Inoki, Isao; u. a. (2000): „*Brevican* is degraded by matrix metalloproteinases and *Aggrecan*ase-1 (ADAMTS4) at different sites". In: *Journal of Biological Chemistry*. 275 (49), S. 38885–38890, DOI: 10.1074/jbc.m003875200.

National Academy of Sciences. Perineuronal nets and recall of distant fear memories. *PNA* 115, 433–434 (2018).

Nasarre, P., Gemmwell, R. M. & Drabkin, H. A. The emerging role of class-3 semaphorins and their neuropilin receptors in oncology. *OncoTargets and*

Therapy 7**,** 1663–1687 (2014).

Natsume, H., Tokuda, H., Adachi, S., Matsushima-Nishiwaki, R., Kato, K., Minamitani, C., Otsuka, T., and Kozawa, O. (2011) Wnt3a regulates tumor necrosis factor-α-stimulated interleukin-6 release in osteoblasts. Mol. Cell. Endocrinol. 331, 66−72

Nery, F., Norris, M., Eliassen, J., Iber, W., Blom, T., Ilge, J., Barzman, D., Strawn, J., Adler, C., Strakowski, S. and DelBello, M. (2017). White matter volumes in youth offspring of bipolar parents. *Journal of Affective Disorders*, 209, pp.246-253.

Netrin-1 overexpression in bone marrow mesenchymal stem cellspromotes functional recovery in a rat model of peripheral nerve injury. (2015). *Journal of Biomedical Research*.

Niisato, K. Age-Dependent Enhancement of Hippocampal Long-Term Potentiation and Impairment of Spatial Learning through the Rho-Associated Kinase Pathway in Protein Tyrosine Phosphatase Receptor Type Z-Deficient Mice. *J. Neurosci.* 25**,** 1081–1088 (2005).

Nithianantharajah, J. and Hannan, A. (2006). Enriched environments, experience-dependent plasticity and disorders of the nervous system. *Nature Reviews Neuroscience*, 7(9), pp.697-709.

Nolen, W. and Iisler, R. (2012). The association of the effect of lithium in the maintenance treatment of bipolar disorder with lithium plasma levels: a post hoc analysis of a double-blind study comparing switching to lithium or placebo in patients who responded to quetiapine (Trial 144). *Bipolar Disorders*, 15(1), pp.100-109.

Nurnberg, H. (2008). Sildenafil as Treatment for Antidepressant-Induced Sexual Dysfunction- A randomized controlled trial. *JAMA*, 300(20), p.2365.

Ohira, K., Takeuchi, R., Iwanaga, T. and Miyakawa, T. (2013). Chronic fluoxetine treatment reduces parvalbumin expression and perineuronal nets in gamma-aminobutyric acidergic interneurons of the frontal cortex in adult mice. *Molecular Brain*, 6(1), p.43.

Öngür, D., Jensen, J., Prescot, A., Stork, C., Lundy, M., Cohen, B. and Renshaw, P. (2008). Abnormal Glutamatergic Neurotransmission and Neuronal-Glial Interactions in Acute Mania. *Biological Psychiatry*, 64(8), pp.718-726.

Orrù, G. and Carta, M. (2018). Genetic Variants Involved in Bipolar Disorder, a Rough Road Ahead. *Clinical Practice & Epidemiology in Mental Health*, 14(1), pp.37-45.

Oruč, L., Kapur-Pojskić, L., Ramić, J., Pojskić, N. and Bajrović, K. (2012). Assessment of relatedness between *Neurocan* gene as bipolar disorder susceptibility locus and schizophrenia. *Bosnian Journal of Basic Medical Sciences*, 12(4), p.245.

Ostrowska-Podhorodecka, Z. and McCulloch, C.A. (2021) "Vimentin regulates the assembly and function of matrix adhesions," Wound Repair and Regeneration [Preprint]. Available at: https://doi.org/10.1111/wrr.12920.

Özerdem, A., Tunca, Z., Çımrın, D., Hıdıroğlu, C. and Ergör, G. (2013). Female vulnerability for thyroid function abnormality in bipolar disorder: role of lithium treatment. *Bipolar Disorders*, 16(1), pp.72-82.

Pantazopoulos, H. and Berretta, S. (2016). In Sickness and in Health: Perineuronal Nets and Synaptic Plasticity in Psychiatric Disorders. *Neural Plasticity*, 2016, pp.1-23.

Pantazopoulos, H., Markota, M., Jaquet, F., Ghosh, D., Wallin, A., Santos, A., Caterson, B. and Berretta, S. (2015). *Aggrecan* and chondroitin-6-sulphate

abnormalities in schizophrenia and bipolar disorder: a postmortem study on the amygdala. *Translational Psychiatry*, 5(1), pp.e496-e496.

Pantazopoulos, H. *et al.* A Slet Talk: The Molecular Systems of Perineuronal Nets in Controlling Neuronal Communication. *Front. Integr. Neurosci* 11**,** 33 (2017).

Papaioannou, V. (2014). The T-box gene family: emerging roles in development, stem cells and cancer. *Development*, 141(20), pp.3819-3833.

Pape, H. (2016). Fear and Fear Memory. *German Research*, 38(2), pp.12-15.

Petersen, J. and Douglas, J. (2013). Tenascin-X, collagen, and Ehlers–Danlos syndrome: Tenascin-X gene defects can protect against adverse cardiovascular events. *Medical Hypotheses*, 81(3), pp.443-447.

Pickard, Benjamin S. (2017): „Genomics of Lithium Action and response". In: *Neurotherapeutics*. 14 (3), S. 582–587, DOI: 10.1007/s13311-017-0554-7.

Pintér, P. and Alpár, A. (2022) 'The role of extracellular matrix in human neurodegenerative diseases', *International Journal of Molecular Sciences*, 23(19), p. 11085. doi:10.3390/ijms231911085

Pomin, V. and Mulloy, B. (2018). Glycosaminoglycans and Proteoglycans. *Pharmaceuticals*, 11(1), p.27.

Pomin, V. and Mulloy, B. (2018). Glycosaminoglycans and Proteoglycans. *Pharmaceuticals*, 11(1), p.27.

Quinn, E., Hwell, M., Anney, R., Gwell, M., Corvin, A. and Morris, D. (2010). Evidence for cis-acting regulation of ANK3 and CACNA1C gene expression. *Bipolar Disorders*, 12(4), pp.440-445.

Qureshi, H., Ahmad, R., Sylvester, J. and Zafarullah, M. (2007). Requwerement of phosphatidylinositol 3-kinase/Akt signaling pathway for regulation of tissue inhibitor of metalloproteinases-3 gene expression by TGF-β in human chondrocytes. *Cellular Signalling*, 19(8), pp.1643-1651.

Rajkowska, G., Halaris, A., and Selemon, L. D. (2001) Reductions in neuronal and glial density characterize the dorsolateral prefrontal cortex in bipolar disorder. Biol. Psychiatry 49, 741−752.

Rachel K. Okolicsanyi, Lotta E. Oikari, Chieh Yu, L. R. G. and L. M. H. Heparan Sulphate Proteoglycans as Drivers of Neural Progenitors Derived From Human Mesenchymal Stem Cells. *Front. Neurosci.* 11, (2018).

Rao, J., Harry, G., Rapoport, S. and Kim, H. (2009). Increased excitotoxicity and neuroinflammatory markers in postmortem frontal cortex from bipolar disorder patients. *Molecular Psychiatry*, 15(4), pp.384-392.

Rao, J. S., Lee, H. J., Rapoport, S. I., and Bazinet, R. P. (2008) Mode of action of mood stabilizers: is the arachidonic acid cascade a common target? Mol. Psychiatry 13, 585−596.

Reichardt and Prokop. Introduction: The Role of Extracellular Matrix in Nervous System Development and Maintenance. *Dev. Neurobiol.* (2011). doi:10.1002/dneu.20975

Reinhard, J., Roll, L. & Faissner, A. Tenascins in Retinal and Optic Nerve Neurodegeneration. *Front. Integr. Neurosci.* 11, 30 (2017).

Ricken, R., Bopp, S., Schlattmann, P., Himmerich, H., Bschor, T., Richter, C., Stamm, T., Bauer, F., Heinz, A., HellIg, R., Lang, U. and Adli, M. (2016). Leptin serum concentrations are associated with light gain during lithium augmentation. *Psychoneuroendocrinology*, 71, pp.31-35.

Richter, R. P., Baranova, N. S., Day, A. J. & Kwok, J. C. Glycosaminoglycans in extracellular matrix organisation: are concepts from soft matter physics key to understanding the formation of perineuronal nets? *Curr. Opin. Struct. Biol.* 50**,** 65–74 (2018).

Robert, L. Éditorial Matrix biology: past, present and future. *Pathol Biol* 49**,** 279–83 (2001).

Rogel, M.R. *et al.* (2011) "Vimentin is sufficient and required for wound repair and remodeling in alveolar epithelial cells," The FASEB Journal, 25(11), pp. 3873–3883. Available at: https://doi.org/10.1096/fj.10-170795.

Romberg, C. *et al.* Depletion of perineuronal nets enhances recognition memory and long-term depression in the perirhinal cortex. *J. Neurosci.* 33**,** 7057–7065 (2013).

Ruzicka, J. *et al.* (2022) 'Perineuronal nets affect memory and learning after synapse withdrawal', *Translational Psychiatry*, 12(1). doi:10.1038/s41398-022-02226-z.

Rybakowski, J. (2013). Genetic Influences on Response to Mood Stabilizers in Bipolar Disorder. *CNS Drugs*, 27(3), pp.165-173.

Rybakowski, J., Permoda-Osip, A., Skibinska, M., Adamski, R. and Bartkowska-Sniatkowska, A. (2012). Single ketamine infusion in bipolar depression resistant to antidepressants: are neurotrophins involved? *Human Psychopharmacology: Clinical and Experimental*, 28(1), pp.87-90.

Sade, Y., Toker, L., Kara, N., Einat, H., Rapoport, S., Moechars, D., Berry, G., Bersudsky, Y. and Agam, G. (2016). IP3 accumulation and/or inositol depletion:

two downstream lithium's effects that may mediate its behavioral and cellular changes. *Translational Psychiatry*, 6(12), pp.e968-e968.

Saito, S., Fujii, K., Ozeki, Y., Ohmori, K., Honda, G., Mori, H., Kato, K., Kuroda, J., Aoki, A., Asahi, H., Sato, H., Shimoda, K. and Akiyama, K. (2017). Cognitive function, treatment response to lithium, and social functioning in Japanese patients with bipolar disorder. *Bipolar Disorders*, 19(7), pp.552-562.

Saito, M., Wu, G., Hui, M., Masiello, K., Dobrenis, K., Ledeen, R. and Saito, M. (2015). Ganglioside accumulation in activated glia in the developing brain: comparison between WT and GalNAcT KO mice. *Journal of Lipid Research*, 56(8), pp.1434-1448.

Sällman Almén, M., Bringeland, N., Fredriksson, R. and Schiöth, H. (2012). The Dispanins: A Novel Gene Family of Ancient Origin That Contains 14 Human Members. *PLoS ONE*, 7(2), p.e31961.

Sánchez-Ventura, J., Lane, M.A. and Udina, E. (2022) 'The role and modulation of spinal perineuronal nets in the healthy and injured spinal cord', *Frontiers in Cellular Neuroscience*, 16. doi:10.3389/fncel.2022.893857.

Saroukhani, S., Emami-Parsa, M., Modabbernia, A., Ashrafi, M., Farokhnia, M., Hajiaghaee, R. and Akhondzadeh, S. (2013). Aspirin for treatment of lithium-associated sexual dysfunction in men: randomized double-blind placebo-controlled study. *Bipolar Disorders*, 15(6), pp.650-656.

Schenkel, L., Ist, A., Jacobs, R., SIeney, J. and Pavuluri, M. (2012). Cognitive dysfunction is worse among pediatric patients with bipolar disorder Type I than Type II. *Journal of Child Psychology and Psychiatry*, 53(7), pp.775-781.

Schloesser, R., Huang, J., Klein, P. and Manji, H. (2007). Cellular Plasticity Cascades in the Pathophysiology and Treatment of Bipolar Disorder. *Neuropsychopharmacology*, 33(1), pp.110-133.

Schneider, C.A., Rasband, W.S. and Eliceiri, K.W. (2012) 'NIH image to imagej: 25 years of image analysis', *Nature Methods*, 9(7), pp. 671–675. doi:10.1038/nmeth.2089.

Schultz, C., Mühleisen, T., Nenadic, I., Koch, K., Wagner, G., Schachtzabel, C., Siedek, F., Nöthen, M., Rietschel, M., Deufel, T., Kiehntopf, M., Cichon, S., Reichenbach, J., Sauer, H. and Schlösser, R. (2013). Common variation in *NCAN*, a risk factor for bipolar disorder and schizophrenia, influences local cortical folding in schizophrenia. *Psychological Medicine*, 44(04), pp.811-820.

Scola, G. and Andreazza, A. (2015). The role of neurotrophins in bipolar disorder. *Progress in Neuro-Psychopharmacology and Biological Psychiatry*, 56, pp.122-128.

Shaw, G. *et al.* (2002) 'Preferential transformation of human neuronal cells by human adenoviruses and the origin of HEK 293 cells', *The FASEB Journal*, 16(8), pp. 869–871. doi:10.1096/fj.01-0995fje.

Shemi, D., Azab, A. N., and Kaplanski, J. (2001) Timedependent effect of LPS on PGE2 and TNF-α production by rat glial brain culture: influence of COX and cytokine inhibitors. J. Endotoxin Res. 6, 377−381.

Shine, B., McKnight, R., Leaver, L. and Geddes, J. (2015). Long-term effects of lithium on renal, thyroid, and parathyroid function: a retrospective analysis of laboratory data. *The Lancet*, 386(9992), pp.461-468.

Shigyo, M. and Tohda, C. (2016) 'Extracellular Vimentin is a novel axonal growth facilitator for functional recovery in spinal cord-injured mice', Scientific Reports, 6(1). doi:10.1038/srep28293.

Shigyo, M. *et al.* (2015) 'Extracellular vimentin interacts with insulin-like growth factor 1 receptor to promote axonal growth', Scientific Reports, 5(1). doi:10.1038/srep12055.

Shi, Q., Liu, H., Han, P., Li, C., Wang, Y., Wu, W., Zhu, D., Amos, C., Fang, S., Lee, J., Han, J. and Ii, Q. (2017). Genetic Variants in WNT2B and BTRC Predict Melanoma Survival. *Journal of Investigative Dermatology*, 137(8), pp.1749-1756.

Shi, X. and Habecker, B. (2011). gp130 cytokines stimulate proteasomal degradation of tyrosine hydroxylase via extracellular signal regulated kinases 1 and 2. *Journal of Neurochemistry*, 120(2), pp.239-247.

Shoeman, R.L. *et al.* (2002) "Deletion mutagenesis of the amino-terminal head domain of vimentin reveals dispensability of large internal regions for intermediate filament assembly and stability," Experimental Cell Research, 279(2), pp. 344–353. Available at: https://doi.org/10.1006/excr.2002.5618.

Siebert, J., Conta Steencken, A. and Osterhout, D. (2014). Chondroitin Sulphate Proteoglycans in the Nervous System: Inhibitors to Repair. *BioMed Research International*, 2014, pp.1-15.

Siebold, C. & Jones, E. Y. Structural insights into semaphorins and their receptors. Semin. Cell Dev. Biol. 24, 139–145 (2013).

Sinha, A. *et al.* (2023) 'Protein–protein interactions between tenascin-R and rptpζ/phosph*ACAN* are critical to maintain the architecture of perineuronal nets', *Journal of Biological Chemistry*, 299(8), p. 104952. doi:10.1016/j.jbc.2023.104952.

Slaker, M., Blacktop, J. and Sorg, B. (2016). Caught in the Net: Perineuronal Nets and Addiction. *Neural Plasticity*, 2016, pp.1-8.

Slaker, M., Harkness, J. and Sorg, B. (2016). A standardized and automated method of perineuronal net analysis using Wisteria floribunda agglutinin staining intensity. *IBRO Reports*, 1, pp.54-60.

Smith, C. C. *et al.* Differential regulation of perineuronal nets in the brain and spinal cord with exercise training. *Brain Res. Bull.* **111,** 20–26 (2015)

Snider, N.T., Ku, N.-O. and Omary, M.B. (2018) 'The sIet side of vimentin', eLife, 7. doi:10.7554/elife.35336.

Soares da Costa, D., Reis, R. L. & Pashkuleva, I. Sulphation of

Glycosaminoglycans and Its Implications in Human Health and Disorders. *Annu. Rev. Biomed. Eng.* 19**,** annurev–bioeng–071516–044610 (2017).

Sood, D. *et al.* Fetal brain extracellular matrix boosts neuronal network formation in 3D bioengineered model of cortical brain tissue. *ACS Biomater Sci Eng* 2**,** 131–140 (2016).

Soles, A. *et al.* (2023) 'Extracellular matrix regulation in physiology and in brain disease', *International Journal of Molecular Sciences*, 24(8), p. 7049. doi:10.3390/ijms24087049.

Song, H., Stevens, C. and Gage, F. (2002). Astroglia induce neurogenesis from adult neural stem cells. *Nature*, 417(6884), pp.39-44.

Sheng, M. and Hyoung Lee, S. (2003). AMPA receptor trafficking and synaptic plasticity: major unansWered questions. *Neuroscience Research*, 46(2), pp.127-134.

Sorg, B., Berretta, S., Blacktop, J., Fawcett, J., Kitagawa, H., Kwok, J. and Miquel, M. (2016). Casting a Wide Net: Role of Perineuronal Nets in Neural Plasticity. *The Journal of Neuroscience*, 36(45), pp.11459-11468.

Steiner, J., Bielau, H., Brisch, R., Danos, P., Ullrich, O., Mawrin, C., Bernstein, H. and Bogerts, B. (2008). Immunological aspects in the neurobiology of suicide: Elevated microglial density in schizophrenia and depression is associated with suicide. *Journal of Psychiatric Research*, 42(2), pp.151-157.

Steullet, P; Cabungcal, J-H; Bukhari, S A; u. a. (2017): „The thalamic reticular nucleus in schizophrenia and bipolar disorder: Role of parvalbumin-expressing neuron networks and oxidative stress". In: *Molecular Psychiatry*. 23 (10), S. 2057–2065, DOI: 10.1038/mp.2017.230.

Stoeckli, E. T. Understanding axon guidance: are I nearly there yet? Development 145, dev151415 (2018).

Study of Various Human Traits in accordance to Hardy-Iinberg. (2016). *International Journal of Science and Research (IJSR)*, 5(1), pp.166-167.

Sul, J., Park, M., Shin, J., Kim, Y., Yoo, S., Kong, Y., Kwon, K., Lee, Y. and Kim, E. (2013). Accumulation of the parkin substrate, *FAF1*, plays a key role in the dopaminergic neurodegeneration. *Human Molecular Genetics*, 22(8), pp.1558-1573.

Sun, G., Horrocks, L. and Farooqui, A. (2007). The roles of NADPH oxidase and phospholipases A2in oxidative and inflammatory responses in neurodegenerative diseases. *Journal of Neurochemistry*, 0(0), p.070611013409004

Suprewicz, Ł. *et al.* (2021) "Extracellular Vimentin as a target against SARS-COV-2 host cell invasion." Available at: https://doi.org/10.1101/2021.01.08.425793

Suttkus, A. *et al. Aggrecan*, link protein and tenascin-R are essential components of the perineuronal net to protect neurons against iron-induced oxidative stress. 5**,** (2014).

Suttkus, A., Holzer, M., Morawski, M. & Arendt, T. The neuronal extracellular matrix restricts distribution and internalization of aggregated Tau-protein. *Neuroscience* 313**,** 225–235 (2016).

Suttkus, A., Morawski, M. & Arendt, T. Protective Properties of Neural Extracellular Matrix. *Mol. Neurobiol.* 53**,** 73–82 (2016).

Swarup, V. P. *et al.* Exploiting Differential Surface Display of Chondroitin Sulphate Variants for Dwerecting Neuronal Outgrowth NIH Public Access. *J Am Chem Soc* 135**,** 13488–13494 (2013).

Szmulewicz, A., Samamé, C., Caravotta, P., Martino, D., Igoa, A., Hidalgo-Mazzei, D., Colom, F. and Strejilevich, S. (2016). Behavioral and emotional adverse events of drugs frequently used in the treatment of bipolar disorders: clinical and theoretical implications. *International Journal of Bipolar Disorders*, 4(1).

Takeda, A., Shuto, M. & Funakoshi, K. Chondroitin Sulphate Expression in Perineuronal Nets After Goldfish Spinal Cord Lesion. *Front. Cell. Neurosci.* 12, 63 (2018).

Tao, R., Yu, Y., Zhang, Xiaojuan, Shi, J., *et al.* (2005) 'A family based study of the genetic association between the PLA2G4D gene and schizophrenia', *Prostaglandins, Leukotrienes and Essential Fatty Acids*, 73(6), pp. 419–422. doi:10.1016/j.plefa.2005.08.008.

Tao, R., Yu, Y., Zhang, Xiaojuan, Guo, Y., *et al.* (2005) 'Cytosolic PLA2 genes possibly contribute to the etiology of schizophrenia', *American Journal of Medical Genetics Part B: Neuropsychiatric Genetics*, 137B(1), pp. 56–58. doi:10.1002/ajmg.b.30210.

Tansley, S.; Gu, N.; Guzmán, A.U.; Cai, W.; Wong, C.; Lister, K.C.; Muñoz-Pino, E.; Yousefpour, N.; Roome, R.B.; Heal, J.; *et al.* Microglia-mediated degradation of perineuronal nets promotes pain. *Science* **2022**, *377*, 80–86.

Tarbet, H.J. *et al.* (2018) "Site-specific glycosylation regulates the form and function of the intermediate filament cytoskeleton," eLife, 7. Available at: https://doi.org/10.7554/elife.31807.

Tajtakova, M., Pidanicova, A., Valansky, L., Lachvac, L., Nagy, V., Sivonova, M., Dobrota, D., Kliment, J. and Petrovicova, J. (2010). Serum level of IGFBP3 and IGF1/IGFBP3 molar ratio in addition to PSA and single nucleotide polymorphism in PSA and CYP17 gene may contribute to early diagnostics of prostate cancer. *Neoplasma*, 57(2), pp.118-122.

Themedicalbiochemistrypage.org. (2018). *Glycosaminoglycans and Proteoglycans.* [online] Available at: https://themedicalbiochemistrypage.org/glycans.php [Accessed 3 Sep. 2018].

Tewari, B.P. *et al.* (2022) 'A glial perspective on the extracellular matrix and perineuronal net remodeling in the central nervous system', *Frontiers in Cellular Neuroscience*, 16. doi:10.3389/fncel.2022.1022754.

Thériault, S., Gaudreault, N., Lamontagne, M., Rosa, M., Boulanger, M., Messika-Zeitoun, D., Clavel, M., Capoulade, R., Dagenais, F., Pibarot, P., Mathieu, P. and Bossé, Y. (2018). A transcriptome-wide association study identifies PALMD as a susceptibility gene for calcific aortic valve stenosis. *Nature Communications*, 9(1).

Takagi, H. *et al.* (2002) "Annexin 6 is a putative cell surface receptor for chondroitin sulphate chains," Journal of Cell Science, 115(16), pp. 3309–3318. Available at: https://doi.org/10.1242/jcs.115.16.3309.

Thomas, M., Pelleieux, S., Vitale, N. and Olivier, J. (2016). Dietary arachidonic acid as a risk factor for age-associated neurodegenerative diseases: Potential mechanisms. *Biochimie*, 130, pp.168-177.

Tian, N., Kanno, T., Jin, Y. and Nishizaki, T. (2014). Lithium potentiates GSK-3β activity by inhibiting phosphoinositide 3-kinase-mediated Akt phosphorylation. *Biochemical and Biophysical Research Communications*, 450(1), pp.746-749.

Tseng, P., Chen, Y., Tu, K., Wang, H., Chung, W., Wu, C., Hsu, S., Kuo, H. and Lin, P. (2016). State-dependent increase in the levels of neurotrophin-3 and

neurotrophin-4/5 in patients with bipolar disorder: A meta-analysis. *Journal of Psychiatric Research*, 79, pp.86-92.

Tucker, R., Peterson, C., Hendaoui, I., Bichet, S. and Chiquet-Ehrismann, R. (2016). The expression of tenascin-C and tenascin-W in human ossicles. *Journal of Anatomy*, 229(3), pp.416-421.

Tunca, Z., Ozerdem, A., Ceylan, D., Yalçın, Y., Can, G., Resmi, H., Akan, P., Ergör, G., Aydemir, Ö., Cengisiz, C. and Kerim, D. (2014).

Ueno, Hiroshi; Takahashi, Yu; Murakami, Shinji; u. a. (2022): FINGOLIMOD increases parvalbumin-positive neurons in adult mice. In: *IBRO Neuroscience Reports.* 13, S. 96–106, DOI: 10.1016/j.ibneur.2022.06.005.

Varadarajan, S. and Butler, S. (2017). Netrin1 establishes multiple boundaries for axon growth in the developing spinal cord. *Developmental Biology*, 430(1), pp.177-187.

van 't Spijker, H. and Kwok, J. (2017). A Slet Talk: The Molecular Systems of Perineuronal Nets in Controlling Neuronal Communication. *Frontiers in Integrative Neuroscience*, 11.

Végh, M. J. *et al.* Reducing hippocampal extracellular matrix reverses early memory deficits in a mouse model of Alzheimer's disease. *Acta Neuropathol. Commun.* 2, 76 (2014).

Vitellaro-Zuccarello, L., Bosisio, P., Mazzetti, S., Monti, C. & De Biasi, S. Differential expression of several molecules of the extracellular matrix in functionally and developmentally distinct regions of rat spinal cord. *Cell Tissue Res.* 327, 433–447 (2007).

Vo, T. *et al.* The chemorepulsive axon guidance protein semaphorin3A is a constituent of perineuronal nets in the adult rodent brain. *Mol. Cell. Neurosci.* 56, 186–200 (2013).

Vosberg, D., Zhang, Y., Menegaux, A., Chalupa, A., Manitt, C., Zehntner, S., Eng, C., DeDuck, K., Allard, D., Durand, F., Dagher, A., Benkelfat, C., Srour, M., Joober, R., Lepore, F., Rouleau, G., Théoret, H., Bedell, B., Flores, C. and Leyton, M. (2018). Mesocorticolimbic Connectivity and Volumetric Alterations in *DCC* Mutation Carriers. *The Journal of Neuroscience*, 38(20), pp.4655-4665.

Voutsinos-Porche, B., Koning, E., Kaplan, H., Ferrandon, A., Guenounou, M., Nehlig, A., and Motte, J. (2004) Temporal patterns of the cerebral inflammatory response in the rat lithium-pilocarpine model of temporal lobe epilepsy. Neurobiol. Dis. 17, 385−402

Wang, D. and Fawcett, J. (2012) 'The perineuronal net and the control of CNS plasticity', *Cell and Tissue Research*, 349(1), pp. 147–160. doi:10.1007/s00441-012-1375-y.

Wang, D., Ichiyama, R. M., Zhao, R., Andrews, M. R. & Fawcett, J. W. Chondroitinase Combined with Rehabilitation Promotes Recovery of Forelimb Function in Rats with Chronic Spinal Cord Injury. *J. Neurosci.* 31, 9332–9344 (2011).

Wang, F., McIntosh, A., He, Y., Gelernter, J. and Blumberg, H. (2011). The association of genetic variation in CACNA1C with structure and function of a frontotemporal system. *Bipolar Disorders*, 13(7-8), pp.696-700.

Wang, Z., Pandey, A. and Hart, G.W. (2007) "Dynamic interplay between O-linked N-acetylglucosaminylation and glycogen synthase kinase-3-dependent phosphorylation," Molecular & Cellular Proteomics, 6(8), pp. 1365–1379. Available at: https://doi.org/10.1074/mcp.m600453-mcp200.

Wang, J., Shao, L., Sun, X. and Young, L. (2009). Increased oxidative stress in the anterior cingulate cortex of subjects with bipolar disorder and schizophrenia. *Bipolar Disorders*, 11(5), pp.523-529.

Wang, H. M., Zhang, T., Li, Q., Huang, J. K., Chen, R. F., and Sun, X. J. (2013) Inhibition of glycogen synthase kinase-3β by lithium chloride suppresses 6-

hydroxydopamine-induced inflammatory response in primary cultured astrocytes. Neurochem. Int. 63, 345−353

Wang, T. *et al.* (2023) 'Vimentin as a potential target for diverse nervous system diseases', Neural Regeneration Research, 18(5), p. 969. doi:10.4103/1673-5374.355744.

Warren, P.M. *et al.* (2018) "Regulation of CNS plasticity through the extracellular matrix," *The Oxford Handbook of Developmental Neural Plasticity* [Preprint]. Available at: https://doi.org/10.1093/oxfordhb/9780190635374.013.11.

Watkins, C. C., Sawa, A., and Pomper, M. G. (2014) Glia and immune cell signaling in bipolar disorder: insights from neuropharmacology and molecular imaging to clinical application. Transl. Psychiatry 4, e350.

Waugh, M. (2012). Phosphatidylinositol 4-kinases, phosphatidylinositol 4-phosphate and cancer. *Cancer Letters*, 325(2), pp.125-131.

Wight, T.N. *et al.* (2020) '*Versican*—a critical extracellular matrix regulator of immunity and inflammation', *Frontiers in Immunology*, 11. doi:10.3389/fimmu.2020.00512.

Weiss, L. and Nieto, M. (2018). The crux of Cux genes in neuronal function and plasticity. *Brain Research*, S0006-8993(18), pp.30114-30118.

Wen, T., Binder, D., Ethell, I. and Razak, K. (2018). The Perineuronal 'Safety' Net? Perineuronal Net Abnormalities in Neurological Disorders. *Frontiers in Molecular Neuroscience*, 11.

Welge, J. and DelBello, M. (2013). Treatment of youth with bipolar disorder: long-term versus maintenance. *Bipolar Disorders*, 15(2), pp.150-152.

Wing, W. (2011). Large-scale genome-wide association analysis of bipolar disorder identifies a new susceptibility locus near ODZ4. *Nature Genetics*, 43(10), pp.977-983.

Wöhr, M; Orduz, D; Gregory, P; u. a. (2015): „Lack of parvalbumin in mice leads to behavioral deficits relevant to all human autism core symptoms and related neural morphofunctional abnormalities". In: *Translational Psychiatry*. 5 (3), DOI: 10.1038/tp.2015.19.

Xing, G., Russell, S., Hough, C., O'Grady, J., Zhang, L., Yang, S., Zhang, L. and Post, R. (2002). Decreased prefrontal CaMKII α mRNA in bipolar wellness. *Neuroreport*, 13(4), pp.501-505.

Xu, J.-C. *et al.* (2013) 'The extracellular matrix glycoprotein Tenascin-R regulates neurogenesis during development and in the adult dentate gyrus of Mice', *Journal of Cell Science* [Preprint]. doi:10.1242/jcs.137612.

Yamaguchi, Y. (2000) 'Lecticans: Organizers of the brain extracellular matrix', *Cellular and Molecular Life Sciences*, 57(2), pp. 276–289. doi:10.1007/pl00000690.

Yang, S., Cacquevel, M., Saksida, L., Bussey, T., Schneider, B., Aebischer, P., Melani, R., Pizzorusso, T., Fawcett, J. and Spwellantini, M. (2015). Perineuronal net digestion with chondroitinase restores memory in mice with tau pathology. *Experimental Neurology*, 265, pp.48-58.

Yang, L. *et al.* (2023) 'Extracellular matrix and Synapse Formation', *Bioscience Reports*, 43(1). doi:10.1042/bsr20212411.

Yang, S. *et al.* Perineuronal net digestion with chondroitinase restores memory in mice with tau pathology. *Exp. Neurol.* 265**,** 48–58 (2015).

Yang, S. *et al.* An Approach to Synthesize Chondroitin Sulphate-E (CS-E) Oligosaccharide Precursors. *J. Org. Chem.* 83**,** 5897–5908 (2018).

Yap, C., Digilio, L., McMahon, L. and Winckler, B. (2017). The endosomal neuronal proteins Nsg1/NEEP21 and Nsg2/P19 are itinerant, not resident proteins of dendritic endosomes. *Scientific Reports*, 7(1).

Ye, H., Wang, W., Cao, J. and Hu, X. (2017). SPARCL1 suppresses cell migration and invasion in renal cell carcinoma. *Molecular Medicine Reports*, 16(5), pp.7784-7790.

Yelland, T. & Djordjevic, S. Crystal Structure of the Neuropilin-1 MAM Domain: Completing the Neuropilin-1 Ectodomain Picture. *Structure* 24**,** 2008–2015 (2016).

Yu, C., Kim, B. and Kim, E. (2016). *FAF1* mediates regulated necrosis through PARP1 activation upon oxidative stress leading to dopaminergic neurodegeneration. *Cell Death & Differentiation*, 23(11), pp.1873-1885.

Yu, F., Wang, Z., Tanaka, M., Chiu, C. T., Leeds, P., Zhang, Y., and Chuang, D. M. (2012) Post trauma treatment with lithium and valproate: reduction of lesion volume, attenuation of blood-brain barrier disruption, and improvement in motor coordination in mice with traumatic brain injury. J. Neurosurgeon. 119, 766−773

Zhou, X.-H. *et al.* (2001) '*Neurocan* is dispensable for brain development', *Molecular and Cellular Biology*, 21(17), pp. 5970–5978. doi:10.1128/mcb.21.17.5970-5978.2001.

Zanetti, S. and Canalise, E. (2013). Hairy and Enhancer of Split-related with YRPW Motif (HEY)2 Regulates Bone Remodelling in Mice. *Journal of Biological Chemistry*, 288(30), pp.2154.

Appendix 1

Raw protein identification and quantification data produced from the WFA pull-down experiment described in Chapter 7.

Accession	Description	Coverage [%]	# AAs	MW [kDa]	Score Mascot	# Peptides
P22626	Heterogeneous nuclear ribonucleoproteins A2/B1 OS=Homo sapiens OX=9606 GN=HNRNPA2B1 PE=	72	353	37.4	5149	28
Q08211	ATP-dependent RNA helicase A OS=Homo sapiens OX=9606 GN=DHX9 PE=1 SV=4	47	1270	140.9	3852	55
P09651	Heterogeneous nuclear ribonucleoprotein A1 OS=Homo sapiens OX=9606 GN=HNRNPA1 PE=1 SV=5	63	372	38.7	3463	26
P08670	**Vimentin OS=Homo sapiens OX=9606 GN=VIM PE=1 SV=4**	**73**	**466**	**53.6**	**2957**	**41**
A0A0U1RRM4	Polypyrimidine tract-binding protein 1 OS=Homo sapiens OX=9606 GN=PTBP1 PE=1 SV=1	64	588	62.4	2943	27
P07437	Tubulin beta chain OS=Homo sapiens OX=9606 GN=TUBB PE=1 SV=2	72	444	49.6	2879	26
B2R5W2	Heterogeneous nuclear ribonucleoproteins C1/C2 OS=Homo sapiens OX=9606 GN=HNRNPC PE=1 SV	59	290	31.9	2617	26
P68371	Tubulin beta-4B chain OS=Homo sapiens OX=9606 GN=TUBB4B PE=1 SV=1	72	445	49.8	2587	26
P14866	Heterogeneous nuclear ribonucleoprotein L OS=Homo sapiens OX=9606 GN=HNRNPL PE=1 SV=2	52	589	64.1	2538	29
Q12906	Interleukin enhancer-binding factor 3 OS=Homo sapiens OX=9606 GN=ILF3 PE=1 SV=3	59	894	95.3	2537	39
A0A3B3ITJ4	Heterogeneous nuclear ribonucleoprotein L (Fragment) OS=Homo sapiens OX=9606 GN=HNRNPL PE	52	537	59.2	2530	26
Q9BVA1	Tubulin beta-2B chain OS=Homo sapiens OX=9606 GN=TUBB2B PE=1 SV=1	70	445	49.9	2465	25
Q13885	Tubulin beta-2A chain OS=Homo sapiens OX=9606 GN=TUBB2A PE=1 SV=1	70	445	49.9	2454	25
Q00839	Heterogeneous nuclear ribonucleoprotein U OS=Homo sapiens OX=9606 GN=HNRNPU PE=1 SV=6	41	825	90.5	2405	32
P78527	DNA-dependent protein kinase catalytic subunit OS=Homo sapiens OX=9606 GN=PRKDC PE=1 SV=3	19	4128	468.8	2401	58
Q6P2Q9	Pre-mRNA-processing-splicing factor 8 OS=Homo sapiens OX=9606 GN=PRPF8 PE=1 SV=2	29	2335	273.4	2401	54
P07910	Heterogeneous nuclear ribonucleoproteins C1/C2 OS=Homo sapiens OX=9606 GN=HNRNPC PE=1 SV	58	306	33.7	2342	25
O75643	U5 small nuclear ribonucleoprotein 200 kDa helicase OS=Homo sapiens OX=9606 GN=SNRNP200 PE=	32	2136	244.4	2192	47
Q71U36	Tubulin alpha-1A chain OS=Homo sapiens OX=9606 GN=TUBA1A PE=1 SV=1	63	451	50.1	2135	18
P04350	Tubulin beta-4A chain OS=Homo sapiens OX=9606 GN=TUBB4A PE=1 SV=2	60	444	49.6	2070	20
P68363	Tubulin alpha-1B chain OS=Homo sapiens OX=9606 GN=TUBA1B PE=1 SV=1	63	451	50.1	1985	18
A8MXP9	Matrin-3 OS=Homo sapiens OX=9606 GN=MATR3 PE=1 SV=1	60	895	99.9	1960	37
Q15393	Splicing factor 3B subunit 3 OS=Homo sapiens OX=9606 GN=SF3B3 PE=1 SV=4	38	1217	135.5	1946	34
P51991	Heterogeneous nuclear ribonucleoprotein A3 OS=Homo sapiens OX=9606 GN=HNRNPA3 PE=1 SV=2	49	378	39.6	1885	26
P52272	Heterogeneous nuclear ribonucleoprotein M OS=Homo sapiens OX=9606 GN=HNRNPM PE=1 SV=3	53	730	77.5	1863	37
P10809	60 kDa heat shock protein, mitochondrial OS=Homo sapiens OX=9606 GN=HSPD1 PE=1 SV=2	52	573	61	1858	29
O75533	Splicing factor 3B subunit 1 OS=Homo sapiens OX=9606 GN=SF3B1 PE=1 SV=3	38	1304	145.7	1853	37
P08238	Heat shock protein HSP 90-beta OS=Homo sapiens OX=9606 GN=HSP90AB1 PE=1 SV=4	42	724	83.2	1717	27
P55265	Double-stranded RNA-specific adenosine deaminase OS=Homo sapiens OX=9606 GN=ADAR PE=1 SV	31	1226	136	1695	30
Q9BQE3	Tubulin alpha-1C chain OS=Homo sapiens OX=9606 GN=TUBA1C PE=1 SV=1	58	449	49.9	1688	17
P61978	Heterogeneous nuclear ribonucleoprotein K OS=Homo sapiens OX=9606 GN=HNRNPK PE=1 SV=1	51	463	50.9	1674	20
Q15029	116 kDa U5 small nuclear ribonucleoprotein component OS=Homo sapiens OX=9606 GN=EFTUD2 PE	48	972	109.4	1583	35
A0A3B3IUD7	Programmed cell death 11, isoform CRA_a OS=Homo sapiens OX=9606 GN=PDCD11 PE=1 SV=1	25	1872	208.7	1534	35
G8JLB6	Heterogeneous nuclear ribonucleoprotein H OS=Homo sapiens OX=9606 GN=HNRNPH1 PE=1 SV=1	49	472	51.2	1519	17
P07900	Heat shock protein HSP 90-alpha OS=Homo sapiens OX=9606 GN=HSP90AA1 PE=1 SV=5	42	732	84.6	1492	28
O43390	Heterogeneous nuclear ribonucleoprotein R OS=Homo sapiens OX=9606 GN=HNRNPR PE=1 SV=1	46	633	70.9	1486	27
Q13509	Tubulin beta-3 chain OS=Homo sapiens OX=9606 GN=TUBB3 PE=1 SV=2	62	450	50.4	1460	20
P12270	Nucleoprotein TPR OS=Homo sapiens OX=9606 GN=TPR PE=1 SV=3	17	2363	267.1	1459	27
O60506	Heterogeneous nuclear ribonucleoprotein Q OS=Homo sapiens OX=9606 GN=SYNCRIP PE=1 SV=2	47	623	69.6	1425	25
Q9NR30	Nucleolar RNA helicase 2 OS=Homo sapiens OX=9606 GN=DDX21 PE=1 SV=5	50	783	87.3	1393	30
P02545	Prelamin-A/C OS=Homo sapiens OX=9606 GN=LMNA PE=1 SV=1	48	664	74.1	1392	31
Q12905	Interleukin enhancer-binding factor 2 OS=Homo sapiens OX=9606 GN=ILF2 PE=1 SV=2	53	390	43	1371	17
Q15233	Non-POU domain-containing octamer-binding protein OS=Homo sapiens OX=9606 GN=NONO PE=1	57	471	54.2	1365	26
Q9BQG0	Myb-binding protein 1A OS=Homo sapiens OX=9606 GN=MYBBP1A PE=1 SV=2	26	1328	148.8	1299	26
P14618	Pyruvate kinase PKM OS=Homo sapiens OX=9606 GN=PKM PE=1 SV=4	56	531	57.9	1299	27
Q5T6W2	Heterogeneous nuclear ribonucleoprotein K (Fragment) OS=Homo sapiens OX=9606 GN=HNRNPK PE	55	379	41.8	1212	16
P38159	RNA-binding motif protein, X chromosome OS=Homo sapiens OX=9606 GN=RBMX PE=1 SV=3	51	391	42.3	1206	24
H0YH80	Heterogeneous nuclear ribonucleoprotein A1 (Fragment) OS=Homo sapiens OX=9606 GN=HNRNPA1	71	191	19.5	1175	10
A0A0G2JIW1	Heat shock 70 kDa protein 1B OS=Homo sapiens OX=9606 GN=HSPA1B PE=1 SV=1	43	642	70.1	1148	20
Q14195	Dihydropyrimidinase-related protein 3 OS=Homo sapiens OX=9606 GN=DPYSL3 PE=1 SV=1	42	570	61.9	1147	19
Q14974	Importin subunit beta-1 OS=Homo sapiens OX=9606 GN=KPNB1 PE=1 SV=2	32	876	97.1	1133	21
Q1KMD3	Heterogeneous nuclear ribonucleoprotein U-like protein 2 OS=Homo sapiens OX=9606 GN=HNRNPU	38	747	85.1	1107	22
Q15424	Scaffold attachment factor B1 OS=Homo sapiens OX=9606 GN=SAFB PE=1 SV=4	21	915	102.6	1087	15
Q3BDU5	Prelamin-A/C OS=Homo sapiens OX=9606 GN=LMNA PE=1 SV=1	51	487	55.6	1083	26
Q7KZ85	Transcription elongation factor SPT6 OS=Homo sapiens OX=9606 GN=SUPT6H PE=1 SV=2	21	1726	198.9	1082	25
O00567	Nucleolar protein 56 OS=Homo sapiens OX=9606 GN=NOP56 PE=1 SV=4	53	594	66	1067	25
P13639	Elongation factor 2 OS=Homo sapiens OX=9606 GN=EEF2 PE=1 SV=4	30	858	95.3	1067	21
Q9UKM9	RNA-binding protein Raly OS=Homo sapiens OX=9606 GN=RALY PE=1 SV=1	74	306	32.4	1064	19
O43143	Pre-mRNA-splicing factor ATP-dependent RNA helicase DHX15 OS=Homo sapiens OX=9606 GN=DHX	37	795	90.9	1035	20
P20700	Lamin-B1 OS=Homo sapiens OX=9606 GN=LMNB1 PE=1 SV=2	45	586	66.4	977	25
Q16531	DNA damage-binding protein 1 OS=Homo sapiens OX=9606 GN=DDB1 PE=1 SV=1	28	1140	126.9	960	23
M0QZM1	Heterogeneous nuclear ribonucleoprotein M (Fragment) OS=Homo sapiens OX=9606 GN=HNRNPM	51	383	40	950	19
Q9NVP1	ATP-dependent RNA helicase DDX18 OS=Homo sapiens OX=9606 GN=DDX18 PE=1 SV=2	36	670	75.4	949	17
Q15717	ELAV-like protein 1 OS=Homo sapiens OX=9606 GN=ELAVL1 PE=1 SV=2	52	326	36.1	931	14
P68104	Elongation factor 1-alpha 1 OS=Homo sapiens OX=9606 GN=EEF1A1 PE=1 SV=1	35	462	50.1	921	16
P52597	Heterogeneous nuclear ribonucleoprotein F OS=Homo sapiens OX=9606 GN=HNRNPF PE=1 SV=3	42	415	45.6	891	10
Q14103	Heterogeneous nuclear ribonucleoprotein D0 OS=Homo sapiens OX=9606 GN=HNRNPD PE=1 SV=1	39	355	38.4	886	15
P49411	Elongation factor Tu, mitochondrial OS=Homo sapiens OX=9606 GN=TUFM PE=1 SV=2	46	452	49.5	883	17
Q9Y5B9	FACT complex subunit SPT16 OS=Homo sapiens OX=9606 GN=SUPT16H PE=1 SV=1	27	1047	119.8	881	21
Q13435	Splicing factor 3B subunit 2 OS=Homo sapiens OX=9606 GN=SF3B2 PE=1 SV=1	24	895	100.2	867	16
O76021	Ribosomal L1 domain-containing protein 1 OS=Homo sapiens OX=9606 GN=RSL1D1 PE=1 SV=3	38	490	54.9	867	17
Q13151	Heterogeneous nuclear ribonucleoprotein A0 OS=Homo sapiens OX=9606 GN=HNRNPA0 PE=1 SV=1	49	305	30.8	866	14
P23246	Splicing factor, proline- and glutamine-rich OS=Homo sapiens OX=9606 GN=SFPQ PE=1 SV=2	36	707	76.1	853	21
P11142	Heat shock cognate 71 kDa protein OS=Homo sapiens OX=9606 GN=HSPA8 PE=1 SV=1	35	646	70.9	852	20
P25705	ATP synthase subunit alpha, mitochondrial OS=Homo sapiens OX=9606 GN=ATP5F1A PE=1 SV=1	44	553	59.7	839	18
Q92621	Nuclear pore complex protein Nup205 OS=Homo sapiens OX=9606 GN=NUP205 PE=1 SV=3	12	2012	227.8	802	21
Q09666	Neuroblast differentiation-associated protein AHNAK OS=Homo sapiens OX=9606 GN=AHNAK PE=1	12	5890	628.7	796	20
P04406	Glyceraldehyde-3-phosphate dehydrogenase OS=Homo sapiens OX=9606 GN=GAPDH PE=1 SV=3	50	335	36	775	15
Q12874	Splicing factor 3A subunit 3 OS=Homo sapiens OX=9606 GN=SF3A3 PE=1 SV=1	31	501	58.8	773	12
P06748	Nucleophosmin OS=Homo sapiens OX=9606 GN=NPM1 PE=1 SV=2	55	294	32.6	772	13
Q9UNX4	WD repeat-containing protein 3 OS=Homo sapiens OX=9606 GN=WDR3 PE=1 SV=1	28	943	106	767	19
Q8WUM0	Nuclear pore complex protein Nup133 OS=Homo sapiens OX=9606 GN=NUP133 PE=1 SV=2	19	1156	128.9	764	15
P31942	Heterogeneous nuclear ribonucleoprotein H3 OS=Homo sapiens OX=9606 GN=HNRNPH3 PE=1 SV=2	54	346	36.9	763	12
Q96KR1	Zinc finger RNA-binding protein OS=Homo sapiens OX=9606 GN=ZFR PE=1 SV=2	26	1074	116.9	762	18
O14979	Heterogeneous nuclear ribonucleoprotein D-like OS=Homo sapiens OX=9606 GN=HNRNPDL PE=1 SV	37	420	46.4	757	12
Q8NI36	WD repeat-containing protein 36 OS=Homo sapiens OX=9606 GN=WDR36 PE=1 SV=1	25	951	105.3	755	17
Q9H583	HEAT repeat-containing protein 1 OS=Homo sapiens OX=9606 GN=HEATR1 PE=1 SV=3	11	2144	242.2	753	18
Q03252	Lamin-B2 OS=Homo sapiens OX=9606 GN=LMNB2 PE=1 SV=4	33	620	69.9	747	15
Q9Y265	RuvB-like 1 OS=Homo sapiens OX=9606 GN=RUVBL1 PE=1 SV=1	42	456	50.2	745	15
Q9UMS4	Pre-mRNA-processing factor 19 OS=Homo sapiens OX=9606 GN=PRPF19 PE=1 SV=1	52	504	55.1	743	15
P62805	Histone H4 OS=Homo sapiens OX=9606 GN=H4C1 PE=1 SV=2	44	103	11.4	736	8
P62873	Guanine nucleotide-binding protein G(I)/G(S)/G(T) subunit beta-1 OS=Homo sapiens OX=9606 GN=G	52	340	37.4	734	12
P06576	ATP synthase subunit beta, mitochondrial OS=Homo sapiens OX=9606 GN=ATP5F1B PE=1 SV=3	39	529	56.5	734	13
P49327	Fatty acid synthase OS=Homo sapiens OX=9606 GN=FASN PE=1 SV=3	10	2511	273.3	731	18
Q9Y2X3	Nucleolar protein 58 OS=Homo sapiens OX=9606 GN=NOP58 PE=1 SV=1	35	529	59.5	731	14
Q9Y230	RuvB-like 2 OS=Homo sapiens OX=9606 GN=RUVBL2 PE=1 SV=3	41	463	51.1	730	15
Q9HCC0	Methylcrotonoyl-CoA carboxylase beta chain, mitochondrial OS=Homo sapiens OX=9606 GN=MCCC	34	563	61.3	709	12
Q96I24	Far upstream element-binding protein 3 OS=Homo sapiens OX=9606 GN=FUBP3 PE=1 SV=2	44	572	61.6	706	19

Accession	Description	Col1	Col2	Col3	Col4	Col5
Q8N1F7	Nuclear pore complex protein Nup93 OS=Homo sapiens OX=9606 GN=NUP93 PE=1 SV=2	28	819	93.4	705	17
P13010	X-ray repair cross-complementing protein 5 OS=Homo sapiens OX=9606 GN=XRCC5 PE=1 SV=3	31	732	82.7	702	17
Q15365	Poly(rC)-binding protein 1 OS=Homo sapiens OX=9606 GN=PCBP1 PE=1 SV=2	52	356	37.5	701	12
Q96E39	RNA binding motif protein, X-linked-like-1 OS=Homo sapiens OX=9606 GN=RBMXL1 PE=1 SV=1	42	390	42.1	698	17
Q8N163	Cell cycle and apoptosis regulator protein 2 OS=Homo sapiens OX=9606 GN=CCAR2 PE=1 SV=2	22	923	102.8	697	14
P36578	60S ribosomal protein L4 OS=Homo sapiens OX=9606 GN=RPL4 PE=1 SV=5	40	427	47.7	693	18
P29692	Elongation factor 1-delta OS=Homo sapiens OX=9606 GN=EEF1D PE=1 SV=5	46	281	31.1	691	9
Q13263	Transcription intermediary factor 1-beta OS=Homo sapiens OX=9606 GN=TRIM28 PE=1 SV=5	27	835	88.5	691	14
Q8IZL8	Proline-, glutamic acid- and leucine-rich protein 1 OS=Homo sapiens OX=9606 GN=PELP1 PE=1 SV=2	18	1130	119.6	679	12
P12956	X-ray repair cross-complementing protein 6 OS=Homo sapiens OX=9606 GN=XRCC6 PE=1 SV=2	31	609	69.8	679	13
P06899	Histone H2B type 1-J OS=Homo sapiens OX=9606 GN=H2BC11 PE=1 SV=3	36	126	13.9	666	5
Q14151	Scaffold attachment factor B2 OS=Homo sapiens OX=9606 GN=SAFB2 PE=1 SV=1	16	953	107.4	660	12
Q2TAY7	WD40 repeat-containing protein SMU1 OS=Homo sapiens OX=9606 GN=SMU1 PE=1 SV=2	34	513	57.5	653	13
U3KQK0	Histone H2B OS=Homo sapiens OX=9606 GN=H2BC15 PE=1 SV=1	27	166	18.8	652	5
Q9H0U4	Ras-related protein Rab-1B OS=Homo sapiens OX=9606 GN=RAB1B PE=1 SV=1	67	201	22.2	650	11
P46087	Probable 28S rRNA (cytosine(4447)-C(5))-methyltransferase OS=Homo sapiens OX=9606 GN=NOP2	22	812	89.2	647	15
Q96DI7	U5 small nuclear ribonucleoprotein 40 kDa protein OS=Homo sapiens OX=9606 GN=SNRNP40 PE=1 S	61	357	39.3	642	12
Q15459	Splicing factor 3A subunit 1 OS=Homo sapiens OX=9606 GN=SF3A1 PE=1 SV=1	19	793	88.8	634	13
Q14980	Nuclear mitotic apparatus protein 1 OS=Homo sapiens OX=9606 GN=NUMA1 PE=1 SV=2	10	2115	238.1	623	14
Q10570	Cleavage and polyadenylation specificity factor subunit 1 OS=Homo sapiens OX=9606 GN=CPSF1 PE=	15	1443	160.8	615	16
Q9BW27	Nuclear pore complex protein Nup85 OS=Homo sapiens OX=9606 GN=NUP85 PE=1 SV=1	26	656	75	613	13
P04792	Heat shock protein beta-1 OS=Homo sapiens OX=9606 GN=HSPB1 PE=1 SV=2	65	205	22.8	612	11
P49748	Very long-chain specific acyl-CoA dehydrogenase, mitochondrial OS=Homo sapiens OX=9606 GN=AC	32	655	70.3	606	14
A0A087WVQ6	Clathrin heavy chain OS=Homo sapiens OX=9606 GN=CLTC PE=1 SV=1	11	1679	191.9	603	13
P42285	Exosome RNA helicase MTR4 OS=Homo sapiens OX=9606 GN=MTREX PE=1 SV=3	26	1042	117.7	601	20
Q9P2I0	Cleavage and polyadenylation specificity factor subunit 2 OS=Homo sapiens OX=9606 GN=CPSF2 PE=1	29	782	88.4	600	13
P62701	40S ribosomal protein S4, X isoform OS=Homo sapiens OX=9606 GN=RPS4X PE=1 SV=2	47	263	29.6	597	14
P55795	Heterogeneous nuclear ribonucleoprotein H2 OS=Homo sapiens OX=9606 GN=HNRNPH2 PE=1 SV=1	33	449	49.2	595	9
Q08945	FACT complex subunit SSRP1 OS=Homo sapiens OX=9606 GN=SSRP1 PE=1 SV=1	20	709	81	592	12
P19338	Nucleolin OS=Homo sapiens OX=9606 GN=NCL PE=1 SV=3	22	710	76.6	591	13
O60832	H/ACA ribonucleoprotein complex subunit DKC1 OS=Homo sapiens OX=9606 GN=DKC1 PE=1 SV=3	36	514	57.6	590	14
P07355	Annexin A2 OS=Homo sapiens OX=9606 GN=ANXA2 PE=1 SV=2	48	339	38.6	585	12
A0A2U3TZH3	Elongation factor 1-alpha OS=Homo sapiens OX=9606 GN=EEF1A2 PE=1 SV=1	27	496	54.3	581	12
A0A2R8Y6G6	Alpha-enolase OS=Homo sapiens OX=9606 GN=ENO1 PE=1 SV=1	34	434	47.3	564	9
Q86XP3	ATP-dependent RNA helicase DDX42 OS=Homo sapiens OX=9606 GN=DDX42 PE=1 SV=1	23	938	102.9	559	11
A0A0D9SF53	ATP-dependent RNA helicase DDX3X OS=Homo sapiens OX=9606 GN=DDX3X PE=1 SV=1	27	733	81.4	559	15
Q15149	Plectin OS=Homo sapiens OX=9606 GN=PLEC PE=1 SV=3	4	4684	531.5	557	14
Q92499	ATP-dependent RNA helicase DDX1 OS=Homo sapiens OX=9606 GN=DDX1 PE=1 SV=2	27	740	82.4	557	16
P62879	Guanine nucleotide-binding protein G(I)/G(S)/G(T) subunit beta-2 OS=Homo sapiens OX=9606 GN=0	44	340	37.3	556	9
D6RBZ0	Heterogeneous nuclear ribonucleoprotein A/B OS=Homo sapiens OX=9606 GN=HNRNPAB PE=1 SV=	32	327	35.7	553	11
P38919	Eukaryotic initiation factor 4A-III OS=Homo sapiens OX=9606 GN=EIF4A3 PE=1 SV=4	35	411	46.8	552	12
P62820	Ras-related protein Rab-1A OS=Homo sapiens OX=9606 GN=RAB1A PE=1 SV=3	63	205	22.7	548	11
J3KTA4	Probable ATP-dependent RNA helicase DDX5 OS=Homo sapiens OX=9606 GN=DDX5 PE=1 SV=1	23	614	69	547	12
P14923	Junction plakoglobin OS=Homo sapiens OX=9606 GN=JUP PE=1 SV=3	25	745	81.7	546	13
P11021	Endoplasmic reticulum chaperone BiP OS=Homo sapiens OX=9606 GN=HSPA5 PE=1 SV=2	27	654	72.3	545	13
Q9UKV3	Apoptotic chromatin condensation inducer in the nucleus OS=Homo sapiens OX=9606 GN=ACIN1 PE	13	1341	151.8	544	13
P50990	T-complex protein 1 subunit theta OS=Homo sapiens OX=9606 GN=CCT8 PE=1 SV=4	34	548	59.6	542	15
Q15269	Periodic tryptophan protein 2 homolog OS=Homo sapiens OX=9606 GN=PWP2 PE=2 SV=2	19	919	102.4	536	11
P22087	rRNA 2'-O-methyltransferase fibrillarin OS=Homo sapiens OX=9606 GN=FBL PE=1 SV=2	43	321	33.8	526	12
A0A1C7CYX9	Dihydropyrimidinase-related protein 2 OS=Homo sapiens OX=9606 GN=DPYSL2 PE=1 SV=1	22	677	73.5	519	9
P12268	Inosine-5'-monophosphate dehydrogenase 2 OS=Homo sapiens OX=9606 GN=IMPDH2 PE=1 SV=2	31	514	55.8	517	11
A0A0R4J2E6	ELAV-like protein OS=Homo sapiens OX=9606 GN=ELAVL4 PE=1 SV=1	33	402	44.5	515	11
Q12769	Nuclear pore complex protein Nup160 OS=Homo sapiens OX=9606 GN=NUP160 PE=1 SV=3	13	1436	162	514	13
Q92797	Symplekin OS=Homo sapiens OX=9606 GN=SYMPK PE=1 SV=2	15	1274	141.1	511	15
Q12788	Transducin beta-like protein 3 OS=Homo sapiens OX=9606 GN=TBL3 PE=1 SV=2	18	808	89	510	10
O94906	Pre-mRNA-processing factor 6 OS=Homo sapiens OX=9606 GN=PRPF6 PE=1 SV=1	14	941	106.9	508	13
P38646	Stress-70 protein, mitochondrial OS=Homo sapiens OX=9606 GN=HSPA9 PE=1 SV=2	23	679	73.6	503	11
P09661	U2 small nuclear ribonucleoprotein A' OS=Homo sapiens OX=9606 GN=SNRPA1 PE=1 SV=2	35	255	28.4	499	10
Q9BXY0	Protein MAK16 homolog OS=Homo sapiens OX=9606 GN=MAK16 PE=1 SV=2	39	300	35.3	499	10
P11940	Polyadenylate-binding protein 1 OS=Homo sapiens OX=9606 GN=PABPC1 PE=1 SV=2	30	636	70.6	499	15
Q8WWY3	U4/U6 small nuclear ribonucleoprotein Prp31 OS=Homo sapiens OX=9606 GN=PRPF31 PE=1 SV=2	31	499	55.4	497	11
P05023	Sodium/potassium-transporting ATPase subunit alpha-1 OS=Homo sapiens OX=9606 GN=ATP1A1 PE	13	1023	112.8	490	10
P27824	Calnexin OS=Homo sapiens OX=9606 GN=CANX PE=1 SV=2	24	592	67.5	485	9
A0A087WTP3	Far upstream element-binding protein 2 OS=Homo sapiens OX=9606 GN=KHSRP PE=1 SV=1	27	711	73	484	12
G5EA30	CUG triplet repeat, RNA binding protein 1, isoform CRA_c OS=Homo sapiens OX=9606 GN=CELF1 PE=	24	514	55.1	483	11
Q15019	Septin-2 OS=Homo sapiens OX=9606 GN=SEPTIN2 PE=1 SV=1	44	361	41.5	478	9
Q96PK6	RNA-binding protein 14 OS=Homo sapiens OX=9606 GN=RBM14 PE=1 SV=2	23	669	69.4	477	11
Q03701	CCAAT/enhancer-binding protein zeta OS=Homo sapiens OX=9606 GN=CEBPZ PE=1 SV=3	15	1054	120.9	476	11
O43172	U4/U6 small nuclear ribonucleoprotein Prp4 OS=Homo sapiens OX=9606 GN=PRPF4 PE=1 SV=2	32	522	58.4	476	10
Q8N8S7	Protein enabled homolog OS=Homo sapiens OX=9606 GN=ENAH PE=1 SV=2	27	591	66.5	470	9
Q9Y490	Talin-1 OS=Homo sapiens OX=9606 GN=TLN1 PE=1 SV=3	8	2541	269.6	470	13
P51149	Ras-related protein Rab-7a OS=Homo sapiens OX=9606 GN=RAB7A PE=1 SV=1	59	207	23.5	467	10
A0A1W2PQ51	Probable ATP-dependent RNA helicase DDX17 OS=Homo sapiens OX=9606 GN=DDX17 PE=1 SV=1	17	731	80.4	467	10
P51148	Ras-related protein Rab-5C OS=Homo sapiens OX=9606 GN=RAB5C PE=1 SV=2	57	216	23.5	460	9
P15924	Desmoplakin OS=Homo sapiens OX=9606 GN=DSP PE=1 SV=3	6	2871	331.6	457	13
P52948	Nuclear pore complex protein Nup98-Nup96 OS=Homo sapiens OX=9606 GN=NUP98 PE=1 SV=4	8	1817	197.5	457	11
H0YFD6	Trifunctional enzyme subunit alpha, mitochondrial OS=Homo sapiens OX=9606 GN=HADHA PE=1 SV	20	792	86.3	457	10
P23528	Cofilin-1 OS=Homo sapiens OX=9606 GN=CFL1 PE=1 SV=3	67	166	18.5	456	8
P31689	DnaJ homolog subfamily A member 1 OS=Homo sapiens OX=9606 GN=DNAJA1 PE=1 SV=2	39	397	44.8	454	10
Q9H0A0	RNA cytidine acetyltransferase OS=Homo sapiens OX=9606 GN=NAT10 PE=1 SV=2	14	1025	115.7	448	12
P62136	Serine/threonine-protein phosphatase PP1-alpha catalytic subunit OS=Homo sapiens OX=9606 GN=	38	330	37.5	444	11
P57740	Nuclear pore complex protein Nup107 OS=Homo sapiens OX=9606 GN=NUP107 PE=1 SV=1	12	925	106.3	443	9
P84103	Serine/arginine-rich splicing factor 3 OS=Homo sapiens OX=9606 GN=SRSF3 PE=1 SV=1	30	164	19.3	436	4
O75691	Small subunit processome component 20 homolog OS=Homo sapiens OX=9606 GN=UTP20 PE=1 SV=	5	2785	318.2	435	12
P51659	Peroxisomal multifunctional enzyme type 2 OS=Homo sapiens OX=9606 GN=HSD17B4 PE=1 SV=3	20	736	79.6	434	9
A0A0A0MQW0	Myelin expression factor 2 OS=Homo sapiens OX=9606 GN=MYEF2 PE=1 SV=1	25	576	61.9	433	10
P52292	Importin subunit alpha-1 OS=Homo sapiens OX=9606 GN=KPNA2 PE=1 SV=1	21	529	57.8	431	8
Q15397	Pumilio homolog 3 OS=Homo sapiens OX=9606 GN=PUM3 PE=1 SV=3	18	648	73.5	428	9
P35579	Myosin-9 OS=Homo sapiens OX=9606 GN=MYH9 PE=1 SV=4	6	1960	226.4	428	7
A0A590UK80	Uncharacterized protein (Fragment) OS=Homo sapiens OX=9606 GN=KPNA2 PE=4 SV=1	9	1090	121	424	9
P62995	Transformer-2 protein homolog beta OS=Homo sapiens OX=9606 GN=TRA2B PE=1 SV=1	29	288	33.6	424	7
Q15061	WD repeat-containing protein 43 OS=Homo sapiens OX=9606 GN=WDR43 PE=1 SV=3	33	677	74.8	420	11
P04899	Guanine nucleotide-binding protein G(i) subunit alpha-2 OS=Homo sapiens OX=9606 GN=GNAI2 PE=	36	355	40.4	418	8
Q9H0D6	5'-3' exoribonuclease 2 OS=Homo sapiens OX=9606 GN=XRN2 PE=1 SV=1	16	950	108.5	418	9
Q9BQ39	ATP-dependent RNA helicase DDX50 OS=Homo sapiens OX=9606 GN=DDX50 PE=1 SV=1	16	737	82.5	415	10
Q5BKZ1	DBIRD complex subunit ZNF326 OS=Homo sapiens OX=9606 GN=ZNF326 PE=1 SV=2	20	582	65.6	414	9
Q15366	Poly(rC)-binding protein 2 OS=Homo sapiens OX=9606 GN=PCBP2 PE=1 SV=1	31	365	38.6	411	8
P61247	40S ribosomal protein S3a OS=Homo sapiens OX=9606 GN=RPS3A PE=1 SV=2	31	264	29.9	411	8
Q99459	Cell division cycle 5-like protein OS=Homo sapiens OX=9606 GN=CDC5L PE=1 SV=2	25	802	92.2	410	12
Q8IY81	pre-rRNA 2'-O-ribose RNA methyltransferase FTSJ3 OS=Homo sapiens OX=9606 GN=FTSJ3 PE=1 SV=	14	847	96.5	410	8

220

Q02809	Procollagen-lysine,2-oxoglutarate 5-dioxygenase 1 OS=Homo sapiens OX=9606 GN=PLOD1 PE=1 SV=	17	727	83.5	409	9
P26641	Elongation factor 1-gamma OS=Homo sapiens OX=9606 GN=EEF1G PE=1 SV=3	26	437	50.1	406	10
P16403	Histone H1.2 OS=Homo sapiens OX=9606 GN=H1-2 PE=1 SV=2	27	213	21.4	406	9
Q13740	CD166 antigen OS=Homo sapiens OX=9606 GN=ALCAM PE=1 SV=2	26	583	65.1	405	9
O60568	Multifunctional procollagen lysine hydroxylase and glycosyltransferase LH3 OS=Homo sapiens OX=9	14	738	84.7	402	7
Q96SI9	Spermatid perinuclear RNA-binding protein OS=Homo sapiens OX=9606 GN=STRBP PE=1 SV=1	11	672	73.6	400	7
P62424	60S ribosomal protein L7a OS=Homo sapiens OX=9606 GN=RPL7A PE=1 SV=2	26	266	30	400	8
P22314	Ubiquitin-like modifier-activating enzyme 1 OS=Homo sapiens OX=9606 GN=UBA1 PE=1 SV=3	11	1058	117.8	398	8
P78371	T-complex protein 1 subunit beta OS=Homo sapiens OX=9606 GN=CCT2 PE=1 SV=4	26	535	57.5	391	9
O15498	Synaptobrevin homolog YKT6 OS=Homo sapiens OX=9606 GN=YKT6 PE=1 SV=1	33	198	22.4	390	5
Q9BVJ6	U3 small nucleolar RNA-associated protein 14 homolog A OS=Homo sapiens OX=9606 GN=UTP14A P	18	771	87.9	385	9
Q14684	Ribosomal RNA processing protein 1 homolog B OS=Homo sapiens OX=9606 GN=RRP1B PE=1 SV=3	16	758	84.4	384	8
P62314	Small nuclear ribonucleoprotein Sm D1 OS=Homo sapiens OX=9606 GN=SNRPD1 PE=1 SV=1	38	119	13.3	384	3
P46782	40S ribosomal protein S5 OS=Homo sapiens OX=9606 GN=RPS5 PE=1 SV=4	39	204	22.9	382	6
P61019	Ras-related protein Rab-2A OS=Homo sapiens OX=9606 GN=RAB2A PE=1 SV=1	38	212	23.5	381	6
P23396	40S ribosomal protein S3 OS=Homo sapiens OX=9606 GN=RPS3 PE=1 SV=2	49	243	26.7	381	9
Q14677	Clathrin interactor 1 OS=Homo sapiens OX=9606 GN=CLINT1 PE=1 SV=1	16	625	68.2	379	7
Q9NW13	RNA-binding protein 28 OS=Homo sapiens OX=9606 GN=RBM28 PE=1 SV=3	15	759	85.7	377	10
P12004	Proliferating cell nuclear antigen OS=Homo sapiens OX=9606 GN=PCNA PE=1 SV=1	49	261	28.8	377	7
P05388	60S acidic ribosomal protein P0 OS=Homo sapiens OX=9606 GN=RPLP0 PE=1 SV=1	41	317	34.3	371	7
P36873	Serine/threonine-protein phosphatase PP1-gamma catalytic subunit OS=Homo sapiens OX=9606 GN	35	323	37	370	9
P60842	Eukaryotic initiation factor 4A-I OS=Homo sapiens OX=9606 GN=EIF4A1 PE=1 SV=1	30	406	46.1	369	8
P30153	Serine/threonine-protein phosphatase 2A 65 kDa regulatory subunit A alpha isoform OS=Homo sap	17	589	65.3	368	8
P30050	60S ribosomal protein L12 OS=Homo sapiens OX=9606 GN=RPL12 PE=1 SV=1	47	165	17.8	366	6
P25685	DnaJ homolog subfamily B member 1 OS=Homo sapiens OX=9606 GN=DNAJB1 PE=1 SV=4	35	340	38	365	10
P46777	60S ribosomal protein L5 OS=Homo sapiens OX=9606 GN=RPL5 PE=1 SV=3	32	297	34.3	365	8
P22234	Multifunctional protein ADE2 OS=Homo sapiens OX=9606 GN=PAICS PE=1 SV=3	23	425	47	365	8
Q8TDN6	Ribosome biogenesis protein BRX1 homolog OS=Homo sapiens OX=9606 GN=BRIX1 PE=1 SV=2	29	353	41.4	364	8
Q9H8Y8	Golgi reassembly-stacking protein 2 OS=Homo sapiens OX=9606 GN=GORASP2 PE=1 SV=3	29	452	47.1	363	7
A0A0U1RRH7	Histone H2A OS=Homo sapiens OX=9606 PE=3 SV=1	27	170	18.5	361	6
P62316	Small nuclear ribonucleoprotein Sm D2 OS=Homo sapiens OX=9606 GN=SNRPD2 PE=1 SV=1	61	118	13.5	357	9
A0A0D9SGF6	Spectrin alpha chain, non-erythrocytic 1 OS=Homo sapiens OX=9606 GN=SPTAN1 PE=1 SV=1	5	2498	287.4	357	10
Q13148	TAR DNA-binding protein 43 OS=Homo sapiens OX=9606 GN=TARDBP PE=1 SV=1	16	414	44.7	355	4
P48681	Nestin OS=Homo sapiens OX=9606 GN=NES PE=1 SV=2	8	1621	177.3	352	8
Q8WTT2	Nucleolar complex protein 3 homolog OS=Homo sapiens OX=9606 GN=NOC3L PE=1 SV=1	16	800	92.5	352	11
Q13217	DnaJ homolog subfamily C member 3 OS=Homo sapiens OX=9606 GN=DNAJC3 PE=1 SV=1	24	504	57.5	351	8
Q7Z3B4	Nucleoporin p54 OS=Homo sapiens OX=9606 GN=NUP54 PE=1 SV=2	24	507	55.4	351	9
Q9H6R4	Nucleolar protein 6 OS=Homo sapiens OX=9606 GN=NOL6 PE=1 SV=2	12	1146	127.5	348	10
P00558	Phosphoglycerate kinase 1 OS=Homo sapiens OX=9606 GN=PGK1 PE=1 SV=3	20	417	44.6	347	6
P62736	Actin, aortic smooth muscle OS=Homo sapiens OX=9606 GN=ACTA2 PE=1 SV=1	26	377	42	347	11
P39023	60S ribosomal protein L3 OS=Homo sapiens OX=9606 GN=RPL3 PE=1 SV=2	27	403	46.1	343	8
Q9UHX1	Poly(U)-binding-splicing factor PUF60 OS=Homo sapiens OX=9606 GN=PUF60 PE=1 SV=1	18	559	59.8	342	7
Q9BXP5	Serrate RNA effector molecule homolog OS=Homo sapiens OX=9606 GN=SRRT PE=1 SV=1	16	876	100.6	341	11
Q9Y3T9	Nucleolar complex protein 2 homolog OS=Homo sapiens OX=9606 GN=NOC2L PE=1 SV=4	13	749	84.9	341	8
Q14498	RNA-binding protein 39 OS=Homo sapiens OX=9606 GN=RBM39 PE=1 SV=2	24	530	59.3	340	9
Q99615	DnaJ homolog subfamily C member 7 OS=Homo sapiens OX=9606 GN=DNAJC7 PE=1 SV=2	27	494	56.4	340	9
E9PL71	Elongation factor 1-delta (Fragment) OS=Homo sapiens OX=9606 GN=EEF1D PE=1 SV=1	37	187	20.8	339	5
H3BPE7	RNA-binding protein FUS OS=Homo sapiens OX=9606 GN=FUS PE=1 SV=1	17	527	53.5	338	7
Q99714	3-hydroxyacyl-CoA dehydrogenase type-2 OS=Homo sapiens OX=9606 GN=HSD17B10 PE=1 SV=3	37	261	26.9	335	5
Q8NFH4	Nucleoporin Nup37 OS=Homo sapiens OX=9606 GN=NUP37 PE=1 SV=1	29	326	36.7	335	7
Q9Y5J1	U3 small nucleolar RNA-associated protein 18 homolog OS=Homo sapiens OX=9606 GN=UTP18 PE=1	17	556	62	335	7
K7EPT8	Glial fibrillary acidic protein (Fragment) OS=Homo sapiens OX=9606 GN=GFAP PE=1 SV=2	16	75	8.4	335	4
Q9BZE4	Nucleolar GTP-binding protein 1 OS=Homo sapiens OX=9606 GN=GTPBP4 PE=1 SV=3	13	634	73.9	334	10
O95758	Polypyrimidine tract-binding protein 3 OS=Homo sapiens OX=9606 GN=PTBP3 PE=1 SV=2	21	552	59.7	334	8
O43809	Cleavage and polyadenylation specificity factor subunit 5 OS=Homo sapiens OX=9606 GN=NUDT21 P	35	227	26.2	333	7
P09172	Dopamine beta-hydroxylase OS=Homo sapiens OX=9606 GN=DBH PE=1 SV=3	16	617	69	332	8
P55084	Trifunctional enzyme subunit beta, mitochondrial OS=Homo sapiens OX=9606 GN=HADHB PE=1 SV=	29	474	51.3	330	9
O43395	U4/U6 small nuclear ribonucleoprotein Prp3 OS=Homo sapiens OX=9606 GN=PRPF3 PE=1 SV=2	24	683	77.5	330	9
E9PEB5	Far upstream element-binding protein 1 OS=Homo sapiens OX=9606 GN=FUBP1 PE=1 SV=1	16	655	68.9	328	8
Q96EE3	Nucleoporin SEH1 OS=Homo sapiens OX=9606 GN=SEH1L PE=1 SV=3	33	360	39.6	328	9
O60341	Lysine-specific histone demethylase 1A OS=Homo sapiens OX=9606 GN=KDM1A PE=1 SV=2	13	852	92.8	327	7
E7ESP4	Integrin alpha-2 OS=Homo sapiens OX=9606 GN=ITGA2 PE=1 SV=1	14	942	102.8	326	7
Q9BVP2	Guanine nucleotide-binding protein-like 3 OS=Homo sapiens OX=9606 GN=GNL3 PE=1 SV=2	19	549	62	325	8
Q8TED0	U3 small nucleolar RNA-associated protein 15 homolog OS=Homo sapiens OX=9606 GN=UTP15 PE=1	19	518	58.4	323	6
P21333	Filamin-A OS=Homo sapiens OX=9606 GN=FLNA PE=1 SV=4	4	2647	280.6	322	7
A0A5F9ZHM4	L-lactate dehydrogenase OS=Homo sapiens OX=9606 GN=LDHB PE=1 SV=1	24	341	37.4	321	6
P62318	Small nuclear ribonucleoprotein Sm D3 OS=Homo sapiens OX=9606 GN=SNRPD3 PE=1 SV=1	55	126	13.9	321	6
Q07021	Complement component 1 Q subcomponent-binding protein, mitochondrial OS=Homo sapiens OX=	27	282	31.3	319	4
Q9BWF3	RNA-binding protein 4 OS=Homo sapiens OX=9606 GN=RBM4 PE=1 SV=1	26	364	40.3	318	7
J3KTL2	Serine/arginine-rich-splicing factor 1 OS=Homo sapiens OX=9606 GN=SRSF1 PE=1 SV=1	39	253	28.3	318	9
P28070	Proteasome subunit beta type-4 OS=Homo sapiens OX=9606 GN=PSMB4 PE=1 SV=4	29	264	29.2	318	5
P55072	Transitional endoplasmic reticulum ATPase OS=Homo sapiens OX=9606 GN=VCP PE=1 SV=4	12	806	89.3	317	7
Q05048	Cleavage stimulation factor subunit 1 OS=Homo sapiens OX=9606 GN=CSTF1 PE=1 SV=1	22	431	48.3	317	6
Q86U42	Polyadenylate-binding protein 2 OS=Homo sapiens OX=9606 GN=PABPN1 PE=1 SV=3	40	306	32.7	316	6
O15240	Neurosecretory protein VGF OS=Homo sapiens OX=9606 GN=VGF PE=1 SV=2	16	615	67.2	315	7
Q5JTH9	RRP12-like protein OS=Homo sapiens OX=9606 GN=RRP12 PE=1 SV=2	8	1297	143.6	315	8
Q9HCS7	Pre-mRNA-splicing factor SYF1 OS=Homo sapiens OX=9606 GN=XAB2 PE=1 SV=2	11	855	99.9	314	7
P57721	Poly(rC)-binding protein 3 OS=Homo sapiens OX=9606 GN=PCBP3 PE=1 SV=2	18	371	39.4	312	5
O43707	Alpha-actinin-4 OS=Homo sapiens OX=9606 GN=ACTN4 PE=1 SV=2	7	911	104.8	307	5
P17301	Integrin alpha-2 OS=Homo sapiens OX=9606 GN=ITGA2 PE=1 SV=1	11	1181	129.2	307	7
P18754	Regulator of chromosome condensation OS=Homo sapiens OX=9606 GN=RCC1 PE=1 SV=1	19	421	44.9	307	5
Q15050	Ribosome biogenesis regulatory protein homolog OS=Homo sapiens OX=9606 GN=RRS1 PE=1 SV=2	21	365	41.2	307	9
Q14576	ELAV-like protein 3 OS=Homo sapiens OX=9606 GN=ELAVL3 PE=2 SV=3	29	367	39.5	306	8
Q8NI27	THO complex subunit 2 OS=Homo sapiens OX=9606 GN=THOC2 PE=1 SV=2	6	1593	182.7	305	7
H3BSH7	U3 small nucleolar RNA-associated protein 4 homolog (Fragment) OS=Homo sapiens OX=9606 GN=U	15	700	77.9	305	7
Q96GQ7	Probable ATP-dependent RNA helicase DDX27 OS=Homo sapiens OX=9606 GN=DDX27 PE=1 SV=2	13	796	89.8	305	9
P98175	RNA-binding protein 10 OS=Homo sapiens OX=9606 GN=RBM10 PE=1 SV=3	12	930	103.5	304	6
P31948	Stress-induced-phosphoprotein 1 OS=Homo sapiens OX=9606 GN=STIP1 PE=1 SV=1	18	543	62.6	303	8
Q8NFH3	Nucleoporin Nup43 OS=Homo sapiens OX=9606 GN=NUP43 PE=1 SV=1	15	380	42.1	302	4
P05556	Integrin beta-1 OS=Homo sapiens OX=9606 GN=ITGB1 PE=1 SV=2	11	798	88.4	301	6
Q9H0S4	Probable ATP-dependent RNA helicase DDX47 OS=Homo sapiens OX=9606 GN=DDX47 PE=1 SV=1	21	455	50.6	299	6
Q9BYG3	MKI67 FHA domain-interacting nucleolar phosphoprotein OS=Homo sapiens OX=9606 GN=NIFK PE=	29	293	34.2	299	6
Q14141	Septin-6 OS=Homo sapiens OX=9606 GN=SEPTIN6 PE=1 SV=4	24	434	49.7	295	7
P08754	Guanine nucleotide-binding protein G(i) subunit alpha OS=Homo sapiens OX=9606 GN=GNAI3 PE=1	20	354	40.5	294	6
P62241	40S ribosomal protein S8 OS=Homo sapiens OX=9606 GN=RPS8 PE=1 SV=2	38	208	24.2	292	6
O43251	RNA binding protein fox-1 homolog 2 OS=Homo sapiens OX=9606 GN=RBFOX2 PE=1 SV=3	25	390	41.3	292	6
Q13838	Spliceosome RNA helicase DDX39B OS=Homo sapiens OX=9606 GN=DDX39B PE=1 SV=1	21	428	49	292	7
E7EPK1	Septin-7 OS=Homo sapiens OX=9606 GN=SEPTIN7 PE=1 SV=2	28	437	50.7	291	8
P05141	ADP/ATP translocase 2 OS=Homo sapiens OX=9606 GN=SLC25A5 PE=1 SV=7	30	298	32.8	290	10
Q8IWA0	WD repeat-containing protein 75 OS=Homo sapiens OX=9606 GN=WDR75 PE=1 SV=1	16	830	94.4	289	7

221

P09874	Poly [ADP-ribose] polymerase 1 OS=Homo sapiens OX=9606 GN=PARP1 PE=1 SV=4	9	1014	113	289	7
P14625	Endoplasmin OS=Homo sapiens OX=9606 GN=HSP90B1 PE=1 SV=1	9	803	92.4	288	8
Q9Y2P8	RNA 3'-terminal phosphate cyclase-like protein OS=Homo sapiens OX=9606 GN=RCL1 PE=1 SV=3	30	373	40.8	284	7
O95219	Sorting nexin-4 OS=Homo sapiens OX=9606 GN=SNX4 PE=1 SV=1	11	450	51.9	284	4
P02786	Transferrin receptor protein 1 OS=Homo sapiens OX=9606 GN=TFRC PE=1 SV=2	11	760	84.8	284	6
P61026	Ras-related protein Rab-10 OS=Homo sapiens OX=9606 GN=RAB10 PE=1 SV=1	35	200	22.5	282	5
Q9Y3I0	RNA-splicing ligase RtcB homolog OS=Homo sapiens OX=9606 GN=RTCB PE=1 SV=1	16	505	55.2	279	6
Q12907	Vesicular integral-membrane protein VIP36 OS=Homo sapiens OX=9606 GN=LMAN2 PE=1 SV=1	29	356	40.2	279	5
P41219	Peripherin OS=Homo sapiens OX=9606 GN=PRPH PE=1 SV=2	11	470	53.6	279	6
P32969	60S ribosomal protein L9 OS=Homo sapiens OX=9606 GN=RPL9 PE=1 SV=1	48	192	21.9	278	5
O00541	Pescadillo homolog OS=Homo sapiens OX=9606 GN=PES1 PE=1 SV=1	14	588	68	278	8
Q9NYF8	Bcl-2-associated transcription factor 1 OS=Homo sapiens OX=9606 GN=BCLAF1 PE=1 SV=2	9	920	106.1	277	7
P62888	60S ribosomal protein L30 OS=Homo sapiens OX=9606 GN=RPL30 PE=1 SV=2	59	115	12.8	273	6
Q9BUJ2	Heterogeneous nuclear ribonucleoprotein U-like protein 1 OS=Homo sapiens OX=9606 GN=HNRNPU	13	856	95.7	272	7
Q02413	Desmoglein-1 OS=Homo sapiens OX=9606 GN=DSG1 PE=1 SV=2	9	1049	113.7	271	6
A0A669KBH5	Alpha-synuclein OS=Homo sapiens OX=9606 GN=SNCA PE=4 SV=1	24	159	16.4	271	3
Q9Y6K1	DNA (cytosine-5)-methyltransferase 3A OS=Homo sapiens OX=9606 GN=DNMT3A PE=1 SV=4	5	912	101.8	270	4
P62269	40S ribosomal protein S18 OS=Homo sapiens OX=9606 GN=RPS18 PE=1 SV=3	42	152	17.7	270	8
P07196	Neurofilament light polypeptide OS=Homo sapiens OX=9606 GN=NEFL PE=1 SV=3	12	543	61.5	269	5
Q12996	Cleavage stimulation factor subunit 3 OS=Homo sapiens OX=9606 GN=CSTF3 PE=1 SV=1	10	717	82.9	269	5
P15880	40S ribosomal protein S2 OS=Homo sapiens OX=9606 GN=RPS2 PE=1 SV=2	25	293	31.3	268	7
Q15907	Ras-related protein Rab-11B OS=Homo sapiens OX=9606 GN=RAB11B PE=1 SV=4	37	218	24.5	268	7
P12277	Creatine kinase B-type OS=Homo sapiens OX=9606 GN=CKB PE=1 SV=1	23	381	42.6	268	5
Q9BSC4	Nucleolar protein 10 OS=Homo sapiens OX=9606 GN=NOL10 PE=1 SV=1	15	688	80.3	267	6
Q6DKI1	60S ribosomal protein L7-like 1 OS=Homo sapiens OX=9606 GN=RPL7L1 PE=1 SV=2	24	255	29.7	266	4
P00338	L-lactate dehydrogenase A chain OS=Homo sapiens OX=9606 GN=LDHA PE=1 SV=2	23	332	36.7	266	6
P14678	Small nuclear ribonucleoprotein-associated proteins B and B' OS=Homo sapiens OX=9606 GN=SNRP	19	240	24.6	266	6
Q9Y2R4	Probable ATP-dependent RNA helicase DDX52 OS=Homo sapiens OX=9606 GN=DDX52 PE=1 SV=3	22	599	67.5	266	9
Q13595	Transformer-2 protein homolog alpha OS=Homo sapiens OX=9606 GN=TRA2A PE=1 SV=1	23	282	32.7	265	5
O00425	Insulin-like growth factor 2 mRNA-binding protein 3 OS=Homo sapiens OX=9606 GN=IGF2BP3 PE=1 S	10	579	63.7	264	4
Q9Y2W1	Thyroid hormone receptor-associated protein 3 OS=Homo sapiens OX=9606 GN=THRAP3 PE=1 SV=2	5	955	108.6	264	6
J3QK89	Calcium homeostasis endoplasmic reticulum protein OS=Homo sapiens OX=9606 GN=CHERP PE=1 SV	7	927	104.9	263	4
P04908	Histone H2A type 1-B/E OS=Homo sapiens OX=9606 GN=H2AC4 PE=1 SV=2	35	130	14.1	261	5
F5H2F4	C-1-tetrahydrofolate synthase, cytoplasmic OS=Homo sapiens OX=9606 GN=MTHFD1 PE=1 SV=2	11	964	104.6	260	8
H3BNC9	Uncharacterized protein OS=Homo sapiens OX=9606 PE=3 SV=2	10	584	64.5	260	3
Q13310	Polyadenylate-binding protein 4 OS=Homo sapiens OX=9606 GN=PABPC4 PE=1 SV=1	17	644	70.7	259	7
O43159	Ribosomal RNA-processing protein 8 OS=Homo sapiens OX=9606 GN=RRP8 PE=1 SV=2	17	456	50.7	259	5
Q9Y224	RNA transcription, translation and transport factor protein OS=Homo sapiens OX=9606 GN=RTRAF P	23	244	28.1	257	4
P55769	NHP2-like protein 1 OS=Homo sapiens OX=9606 GN=SNU13 PE=1 SV=3	38	128	14.2	256	5
Q01780	Exosome component 10 OS=Homo sapiens OX=9606 GN=EXOSC10 PE=1 SV=2	11	885	100.8	255	7
P07237	Protein disulfide-isomerase OS=Homo sapiens OX=9606 GN=P4HB PE=1 SV=3	17	508	57.1	253	8
Q14204	Cytoplasmic dynein 1 heavy chain 1 OS=Homo sapiens OX=9606 GN=DYNC1H1 PE=1 SV=5	3	4646	532.1	253	11
H7C2Q8	EBNA1 binding protein 2, isoform CRA_d OS=Homo sapiens OX=9606 GN=EBNA1BP2 PE=1 SV=1	17	361	40.7	252	5
S4R359	Heterogeneous nuclear ribonucleoprotein K (Fragment) OS=Homo sapiens OX=9606 GN=HNRNPK PE	61	100	10.7	249	4
A0A286YEZ8	Heterogeneous nuclear ribonucleoprotein R (Fragment) OS=Homo sapiens OX=9606 GN=HNRNPR PF	18	141	16.2	248	3
Q92979	Ribosomal RNA small subunit methyltransferase NEP1 OS=Homo sapiens OX=9606 GN=EMG1 PE=1	25	244	26.7	247	5
Q96A72	Protein mago nashi homolog 2 OS=Homo sapiens OX=9606 GN=MAGOHB PE=1 SV=1	45	148	17.3	247	4
P62277	40S ribosomal protein S13 OS=Homo sapiens OX=9606 GN=RPS13 PE=1 SV=2	27	151	17.2	246	4
P17987	T-complex protein 1 subunit alpha OS=Homo sapiens OX=9606 GN=TCP1 PE=1 SV=1	13	556	60.3	246	5
Q9NW64	Pre-mRNA-splicing factor RBM22 OS=Homo sapiens OX=9606 GN=RBM22 PE=1 SV=1	19	420	46.9	246	6
P13674	Prolyl 4-hydroxylase subunit alpha-1 OS=Homo sapiens OX=9606 GN=P4HA1 PE=1 SV=2	16	534	61	244	6
P67809	Y-box-binding protein 1 OS=Homo sapiens OX=9606 GN=YBX1 PE=1 SV=3	23	324	35.9	244	4
Q13283	Ras GTPase-activating protein-binding protein 1 OS=Homo sapiens OX=9606 GN=G3BP1 PE=1 SV=1	18	466	52.1	243	5
Q8WX93	Palladin OS=Homo sapiens OX=9606 GN=PALLD PE=1 SV=3	7	1383	150.5	243	5
Q09161	Nuclear cap-binding protein subunit 1 OS=Homo sapiens OX=9606 GN=NCBP1 PE=1 SV=1	8	790	91.8	242	5
Q14137	Ribosome biogenesis protein BOP1 OS=Homo sapiens OX=9606 GN=BOP1 PE=1 SV=2	13	746	83.6	241	8
Q9Y6D9	Mitotic spindle assembly checkpoint protein MAD1 OS=Homo sapiens OX=9606 GN=MAD1L1 PE=1 S	13	718	83	241	6
Q08170	Serine/arginine-rich splicing factor 4 OS=Homo sapiens OX=9606 GN=SRSF4 PE=1 SV=2	9	494	56.6	240	5
Q9NWT1	p21-activated protein kinase-interacting protein 1 OS=Homo sapiens OX=9606 GN=PAK1IP1 PE=1 SV	19	392	43.9	240	5
E7EX44	Caldesmon OS=Homo sapiens OX=9606 GN=CALD1 PE=1 SV=1	14	557	64.1	239	5
P31350	Ribonucleoside-diphosphate reductase subunit M2 OS=Homo sapiens OX=9606 GN=RRM2 PE=1 SV=	18	389	44.8	239	5
P16435	NADPH--cytochrome P450 reductase OS=Homo sapiens OX=9606 GN=POR PE=1 SV=2	8	677	76.6	239	4
A0A499FHX9	DNA replication licensing factor MCM3 OS=Homo sapiens OX=9606 GN=MCM3 PE=1 SV=1	8	818	91.9	238	5
Q9BQ04	RNA-binding protein 4B OS=Homo sapiens OX=9606 GN=RBM4B PE=1 SV=1	19	359	40.1	236	6
P42166	Lamina-associated polypeptide 2, isoform alpha OS=Homo sapiens OX=9606 GN=TMPO PE=1 SV=2	11	694	75.4	235	5
Q9NXF1	Testis-expressed protein 10 OS=Homo sapiens OX=9606 GN=TEX10 PE=1 SV=2	10	929	105.6	235	7
P83916	Chromobox protein homolog 1 OS=Homo sapiens OX=9606 GN=CBX1 PE=1 SV=1	22	185	21.4	235	3
Q13895	Bystin OS=Homo sapiens OX=9606 GN=BYSL PE=1 SV=3	15	437	49.6	235	5
Q07666	KH domain-containing, RNA-binding, signal transduction-associated protein 1 OS=Homo sapiens OX=	9	443	48.2	235	4
Q9HCD5	Nuclear receptor coactivator 5 OS=Homo sapiens OX=9606 GN=NCOA5 PE=1 SV=1	15	579	65.5	234	5
P62249	40S ribosomal protein S16 OS=Homo sapiens OX=9606 GN=RPS16 PE=1 SV=2	35	146	16.4	233	6
P09382	Galectin-1 OS=Homo sapiens OX=9606 GN=LGALS1 PE=1 SV=2	56	135	14.7	233	5
P21796	Voltage-dependent anion-selective channel protein 1 OS=Homo sapiens OX=9606 GN=VDAC1 PE=1 S	21	283	30.8	233	4
M0R2Z9	SURP and G-patch domain-containing protein 2 OS=Homo sapiens OX=9606 GN=SUGP2 PE=1 SV=1	5	1096	121.5	232	5
P62244	40S ribosomal protein S15a OS=Homo sapiens OX=9606 GN=RPS15A PE=1 SV=2	44	130	14.8	232	6
O14813	Paired mesoderm homeobox protein 2A OS=Homo sapiens OX=9606 GN=PHOX2A PE=1 SV=2	27	284	29.6	230	4
P37108	Signal recognition particle 14 kDa protein OS=Homo sapiens OX=9606 GN=SRP14 PE=1 SV=2	38	136	14.6	230	4
E9PB61	THO complex subunit 4 OS=Homo sapiens OX=9606 GN=ALYREF PE=1 SV=1	21	264	27.5	228	3
Q5JWF2	Guanine nucleotide-binding protein G(s) subunit alpha isoforms XLas OS=Homo sapiens OX=9606 G	8	1037	111	228	6
P52594	Arf-GAP domain and FG repeat-containing protein 1 OS=Homo sapiens OX=9606 GN=AGFG1 PE=1 SV	13	562	58.2	228	3
O60306	RNA helicase aquarius OS=Homo sapiens OX=9606 GN=AQR PE=1 SV=4	5	1485	171.2	227	6
Q9UMX0	Ubiquilin-1 OS=Homo sapiens OX=9606 GN=UBQLN1 PE=1 SV=2	17	589	62.5	227	5
P62906	60S ribosomal protein L10a OS=Homo sapiens OX=9606 GN=RPL10A PE=1 SV=2	29	217	24.8	227	5
P84090	Enhancer of rudimentary homolog OS=Homo sapiens OX=9606 GN=ERH PE=1 SV=1	46	104	12.3	226	5
O43290	U4/U6.U5 tri-snRNP-associated protein 1 OS=Homo sapiens OX=9606 GN=SART1 PE=1 SV=1	9	800	90.2	226	5
Q9NY61	Protein AATF OS=Homo sapiens OX=9606 GN=AATF PE=1 SV=1	8	560	63.1	225	3
P56537	Eukaryotic translation initiation factor 6 OS=Homo sapiens OX=9606 GN=EIF6 PE=1 SV=1	33	245	26.6	225	5
Q16352	Alpha-internexin OS=Homo sapiens OX=9606 GN=INA PE=1 SV=2	16	499	55.4	224	7
P11413	Glucose-6-phosphate 1-dehydrogenase OS=Homo sapiens OX=9606 GN=G6PD PE=1 SV=4	13	515	59.2	223	6
P63096	Guanine nucleotide-binding protein G(i) subunit alpha-1 OS=Homo sapiens OX=9606 GN=GNAI1 PE=	17	354	40.3	223	5
P28289	Tropomodulin-1 OS=Homo sapiens OX=9606 GN=TMOD1 PE=1 SV=1	23	359	40.5	223	5
Q9BZJ0	Crooked neck-like protein 1 OS=Homo sapiens OX=9606 GN=CRNKL1 PE=1 SV=4	7	848	100.4	222	5
Q9UHD8	Septin-9 OS=Homo sapiens OX=9606 GN=SEPTIN9 PE=1 SV=2	16	586	65.4	222	5
Q52LJ0	Protein FAM98B OS=Homo sapiens OX=9606 GN=FAM98B PE=1 SV=2	14	433	45.5	221	6
Q9UHG3	Prenylcysteine oxidase 1 OS=Homo sapiens OX=9606 GN=PCYOX1 PE=1 SV=3	11	505	56.6	221	4
Q9UKD2	mRNA turnover protein 4 homolog OS=Homo sapiens OX=9606 GN=MRTO4 PE=1 SV=2	23	239	27.5	220	5
A0A087WWS1	THO complex subunit 1 OS=Homo sapiens OX=9606 GN=THOC1 PE=1 SV=1	12	657	75.6	220	5
A0A1W2PRS1	Lysosome membrane protein 2 (Fragment) OS=Homo sapiens OX=9606 GN=SCARB2 PE=1 SV=1	13	519	58.1	220	5
Q99567	Nuclear pore complex protein Nup88 OS=Homo sapiens OX=9606 GN=NUP88 PE=1 SV=2	13	741	83.5	219	5
A0A2R8Y5A3	Catenin beta-1 OS=Homo sapiens OX=9606 GN=CTNNB1 PE=1 SV=1	7	783	85.6	217	5

ID	Description					
P61313	60S ribosomal protein L15 OS=Homo sapiens OX=9606 GN=RPL15 PE=1 SV=2	27	204	24.1	216	5
O00560	Syntenin-1 OS=Homo sapiens OX=9606 GN=SDCBP PE=1 SV=1	23	298	32.4	216	4
Q9C0J8	pre-mRNA 3' end processing protein WDR33 OS=Homo sapiens OX=9606 GN=WDR33 PE=1 SV=2	7	1336	145.8	215	5
P29401	Transketolase OS=Homo sapiens OX=9606 GN=TKT PE=1 SV=3	9	623	67.8	215	3
Q9BUQ8	Probable ATP-dependent RNA helicase DDX23 OS=Homo sapiens OX=9606 GN=DDX23 PE=1 SV=3	12	820	95.5	214	7
P25398	40S ribosomal protein S12 OS=Homo sapiens OX=9606 GN=RPS12 PE=1 SV=3	39	132	14.5	213	4
Q9NV31	U3 small nucleolar ribonucleoprotein protein IMP3 OS=Homo sapiens OX=9606 GN=IMP3 PE=1 SV=1	40	184	21.8	213	5
P78316	Nucleolar protein 14 OS=Homo sapiens OX=9606 GN=NOP14 PE=1 SV=3	8	857	97.6	211	6
K7EJV9	60S ribosomal protein L23a (Fragment) OS=Homo sapiens OX=9606 GN=RPL23A PE=1 SV=1	35	170	19.4	210	7
P61020	Ras-related protein Rab-5B OS=Homo sapiens OX=9606 GN=RAB5B PE=1 SV=1	32	215	23.7	210	5
P61106	Ras-related protein Rab-14 OS=Homo sapiens OX=9606 GN=RAB14 PE=1 SV=4	19	215	23.9	210	4
P40926	Malate dehydrogenase, mitochondrial OS=Homo sapiens OX=9606 GN=MDH2 PE=1 SV=3	15	338	35.5	209	3
P55735	Protein SEC13 homolog OS=Homo sapiens OX=9606 GN=SEC13 PE=1 SV=3	16	322	35.5	209	3
O43175	D-3-phosphoglycerate dehydrogenase OS=Homo sapiens OX=9606 GN=PHGDH PE=1 SV=4	12	533	56.6	209	5
Q9Y3B4	Splicing factor 3B subunit 6 OS=Homo sapiens OX=9606 GN=SF3B6 PE=1 SV=1	37	125	14.6	208	4
B7ZLQ5	Probable global transcription activator SNF2L1 OS=Homo sapiens OX=9606 GN=SMARCA1 PE=1 SV=1	7	1070	124.2	208	6
Q13409	Cytoplasmic dynein 1 intermediate chain 2 OS=Homo sapiens OX=9606 GN=DYNC1I2 PE=1 SV=3	13	638	71.4	208	4
Q01813	ATP-dependent 6-phosphofructokinase, platelet type OS=Homo sapiens OX=9606 GN=PFKP PE=1 SV	8	784	85.5	206	3
P55081	Microfibrillar-associated protein 1 OS=Homo sapiens OX=9606 GN=MFAP1 PE=1 SV=2	16	439	51.9	206	5
Q9HDC9	Adipocyte plasma membrane-associated protein OS=Homo sapiens OX=9606 GN=APMAP PE=1 SV=2	16	416	46.5	205	7
P20340	Ras-related protein Rab-6A OS=Homo sapiens OX=9606 GN=RAB6A PE=1 SV=3	29	208	23.6	203	5
Q12931	Heat shock protein 75 kDa, mitochondrial OS=Homo sapiens OX=9606 GN=TRAP1 PE=1 SV=3	9	704	80.1	203	6
O75694	Nuclear pore complex protein Nup155 OS=Homo sapiens OX=9606 GN=NUP155 PE=1 SV=1	6	1391	155.1	202	5
P35221	Catenin alpha-1 OS=Homo sapiens OX=9606 GN=CTNNA1 PE=1 SV=1	8	906	100	202	5
P62829	60S ribosomal protein L23 OS=Homo sapiens OX=9606 GN=RPL23 PE=1 SV=1	40	140	14.9	202	5
D6RER5	Septin-11 OS=Homo sapiens OX=9606 GN=SEPTIN11 PE=1 SV=1	15	432	49.8	201	5
Q15417	Calponin-3 OS=Homo sapiens OX=9606 GN=CNN3 PE=1 SV=1	27	329	36.4	201	6
P27694	Replication protein A 70 kDa DNA-binding subunit OS=Homo sapiens OX=9606 GN=RPA1 PE=1 SV=2	15	616	68.1	201	4
O00566	U3 small nucleolar ribonucleoprotein protein MPP10 OS=Homo sapiens OX=9606 GN=MPHOSPH10	14	681	78.8	201	5
Q8TDD1	ATP-dependent RNA helicase DDX54 OS=Homo sapiens OX=9606 GN=DDX54 PE=1 SV=2	7	881	98.5	200	4
Q02543	60S ribosomal protein L18a OS=Homo sapiens OX=9606 GN=RPL18A PE=1 SV=2	26	176	20.7	198	4
Q15428	Splicing factor 3A subunit 2 OS=Homo sapiens OX=9606 GN=SF3A2 PE=1 SV=2	15	464	49.2	197	5
J3KN66	Torsin-1A-interacting protein 1 OS=Homo sapiens OX=9606 GN=TOR1AIP1 PE=1 SV=1	9	599	67.8	197	4
Q9Y2Z0	Protein SGT1 homolog OS=Homo sapiens OX=9606 GN=SUGT1 PE=1 SV=3	17	365	41	197	5
G3V3A4	SNW domain-containing protein 1 OS=Homo sapiens OX=9606 GN=SNW1 PE=1 SV=1	10	571	65.4	196	5
Q16629	Serine/arginine-rich splicing factor 7 OS=Homo sapiens OX=9606 GN=SRSF7 PE=1 SV=1	13	238	27.4	196	3
O60264	SWI/SNF-related matrix-associated actin-dependent regulator of chromatin subfamily A member 5	6	1052	121.8	196	6
P0C0S5	Histone H2A.Z OS=Homo sapiens OX=9606 GN=H2AZ1 PE=1 SV=2	31	128	13.5	196	4
P45973	Chromobox protein homolog 5 OS=Homo sapiens OX=9606 GN=CBX5 PE=1 SV=1	27	191	22.2	196	4
P62917	60S ribosomal protein L8 OS=Homo sapiens OX=9606 GN=RPL8 PE=1 SV=2	25	257	28	195	7
Q9H501	ESF1 homolog OS=Homo sapiens OX=9606 GN=ESF1 PE=1 SV=1	7	851	98.7	195	4
P09012	U1 small nuclear ribonucleoprotein A OS=Homo sapiens OX=9606 GN=SNRPA PE=1 SV=3	33	282	31.3	194	7
P00387	NADH-cytochrome b5 reductase 3 OS=Homo sapiens OX=9606 GN=CYB5R3 PE=1 SV=3	18	301	34.2	194	3
P16104	Histone H2AX OS=Homo sapiens OX=9606 GN=H2AX PE=1 SV=2	22	143	15.1	194	4
P62280	40S ribosomal protein S11 OS=Homo sapiens OX=9606 GN=RPS11 PE=1 SV=3	40	158	18.4	194	6
O00267	Transcription elongation factor SPT5 OS=Homo sapiens OX=9606 GN=SUPT5H PE=1 SV=1	7	1087	120.9	193	5
Q9UHD9	Ubiquilin-2 OS=Homo sapiens OX=9606 GN=UBQLN2 PE=1 SV=2	11	624	65.7	193	4
Q9H307	Pinin OS=Homo sapiens OX=9606 GN=PNN PE=1 SV=5	10	717	81.6	193	6
O00148	ATP-dependent RNA helicase DDX39A OS=Homo sapiens OX=9606 GN=DDX39A PE=1 SV=2	13	427	49.1	192	5
P35606	Coatomer subunit beta' OS=Homo sapiens OX=9606 GN=COPB2 PE=1 SV=2	9	906	102.4	192	6
Q8NCA5	Protein FAM98A OS=Homo sapiens OX=9606 GN=FAM98A PE=1 SV=2	5	518	55.2	190	3
Q02978	Mitochondrial 2-oxoglutarate/malate carrier protein OS=Homo sapiens OX=9606 GN=SLC25A11 PE=	16	314	34	190	3
P62913	60S ribosomal protein L11 OS=Homo sapiens OX=9606 GN=RPL11 PE=1 SV=2	38	178	20.2	189	6
A0A0A0MRM9	Nucleolar and coiled-body phosphoprotein 1 (Fragment) OS=Homo sapiens OX=9606 GN=NOLC1 PE	9	708	74.6	189	6
O95716	Ras-related protein Rab-3D OS=Homo sapiens OX=9606 GN=RAB3D PE=1 SV=1	17	219	24.3	189	3
Q9NWH9	SAFB-like transcription modulator OS=Homo sapiens OX=9606 GN=SLTM PE=1 SV=2	6	1034	117.1	189	5
Q9Y333	U6 snRNA-associated Sm-like protein LSm2 OS=Homo sapiens OX=9606 GN=LSM2 PE=1 SV=1	40	95	10.8	189	2
Q9Y4W2	Ribosomal biogenesis protein LAS1L OS=Homo sapiens OX=9606 GN=LAS1L PE=1 SV=2	8	734	83	188	5
Q9Y3Y2	Chromatin target of PRMT1 protein OS=Homo sapiens OX=9606 GN=CHTOP PE=1 SV=2	21	248	26.4	188	4
O00203	AP-3 complex subunit beta-1 OS=Homo sapiens OX=9606 GN=AP3B1 PE=1 SV=3	7	1094	121.2	187	6
O15042	U2 snRNP-associated SURP motif-containing protein OS=Homo sapiens OX=9606 GN=U2SURP PE=1 S	5	1029	118.2	187	5
Q9GZR7	ATP-dependent RNA helicase DDX24 OS=Homo sapiens OX=9606 GN=DDX24 PE=1 SV=1	12	859	96.3	186	6
Q9NYU2	UDP-glucose:glycoprotein glucosyltransferase 1 OS=Homo sapiens OX=9606 GN=UGGT1 PE=1 SV=3	3	1555	177.1	185	3
Q9NYH9	U3 small nucleolar RNA-associated protein 6 homolog OS=Homo sapiens OX=9606 GN=UTP6 PE=2 S	11	597	70.1	185	5
Q9UIG0	Tyrosine-protein kinase BAZ1B OS=Homo sapiens OX=9606 GN=BAZ1B PE=1 SV=2	4	1483	170.8	185	4
Q96AG4	Leucine-rich repeat-containing protein 59 OS=Homo sapiens OX=9606 GN=LRRC59 PE=1 SV=1	17	307	34.9	184	2
O96019	Actin-like protein 6A OS=Homo sapiens OX=9606 GN=ACTL6A PE=1 SV=1	19	429	47.4	184	5
F8VXC8	SWI/SNF complex subunit SMARCC2 OS=Homo sapiens OX=9606 GN=SMARCC2 PE=1 SV=1	4	1245	136.1	184	4
Q15286	Ras-related protein Rab-35 OS=Homo sapiens OX=9606 GN=RAB35 PE=1 SV=1	18	201	23	182	3
Q9NY93	Probable ATP-dependent RNA helicase DDX56 OS=Homo sapiens OX=9606 GN=DDX56 PE=1 SV=1	15	547	61.6	182	6
O95721	Synaptosomal-associated protein 29 OS=Homo sapiens OX=9606 GN=SNAP29 PE=1 SV=1	29	258	29	181	5
P35658	Nuclear pore complex protein Nup214 OS=Homo sapiens OX=9606 GN=NUP214 PE=1 SV=2	4	2090	213.5	181	5
A0A0A0MT49	Transcription activator BRG1 OS=Homo sapiens OX=9606 GN=SMARCA4 PE=1 SV=1	3	1681	188.7	180	4
O00505	Importin subunit alpha-4 OS=Homo sapiens OX=9606 GN=KPNA3 PE=1 SV=2	15	521	57.8	180	6
P56182	Ribosomal RNA processing protein 1 homolog A OS=Homo sapiens OX=9606 GN=RRP1 PE=1 SV=1	17	461	52.8	179	5
P46781	40S ribosomal protein S9 OS=Homo sapiens OX=9606 GN=RPS9 PE=1 SV=3	30	194	22.6	179	8
P38117	Electron transfer flavoprotein subunit beta OS=Homo sapiens OX=9606 GN=ETFB PE=1 SV=3	24	255	27.8	178	5
Q09028	Histone-binding protein RBBP4 OS=Homo sapiens OX=9606 GN=RBBP4 PE=1 SV=3	12	425	47.6	178	5
Q96B26	Exosome complex component RRP43 OS=Homo sapiens OX=9606 GN=EXOSC8 PE=1 SV=1	18	276	30	178	3
Q53F19	Nuclear cap-binding protein subunit 3 OS=Homo sapiens OX=9606 GN=NCBP3 PE=1 SV=2	6	620	70.5	178	3
P20339	Ras-related protein Rab-5A OS=Homo sapiens OX=9606 GN=RAB5A PE=1 SV=2	26	215	23.6	178	4
P61006	Ras-related protein Rab-8A OS=Homo sapiens OX=9606 GN=RAB8A PE=1 SV=1	18	207	23.7	176	4
O15226	NF-kappa-B-repressing factor OS=Homo sapiens OX=9606 GN=NKRF PE=1 SV=2	9	690	77.6	176	4
A0A087WUZ3	Spectrin beta chain OS=Homo sapiens OX=9606 GN=SPTBN1 PE=1 SV=1	2	2366	274.7	175	4
A0A087WV75	Neural cell adhesion molecule 1 OS=Homo sapiens OX=9606 GN=NCAM1 PE=1 SV=1	7	884	97.3	175	4
P07737	Profilin-1 OS=Homo sapiens OX=9606 GN=PFN1 PE=1 SV=2	51	140	15	175	5
A0A087WY31	YTH domain-containing family protein 3 OS=Homo sapiens OX=9606 GN=YTHDF3 PE=1 SV=1	7	588	64.5	175	3
P48047	ATP synthase subunit O, mitochondrial OS=Homo sapiens OX=9606 GN=ATP5PO PE=1 SV=1	20	213	23.3	174	3
Q8IUH3	RNA-binding protein 45 OS=Homo sapiens OX=9606 GN=RBM45 PE=1 SV=1	13	476	53.5	174	4
Q9H8H0	Nucleolar protein 11 OS=Homo sapiens OX=9606 GN=NOL11 PE=1 SV=1	9	719	81.1	173	4
Q14157	Ubiquitin-associated protein 2-like OS=Homo sapiens OX=9606 GN=UBAP2L PE=1 SV=2	5	1087	114.5	173	3
Q9H0L4	Cleavage stimulation factor subunit 2 tau variant OS=Homo sapiens OX=9606 GN=CSTF2T PE=1 SV=1	8	616	64.4	173	4
Q6PD62	RNA polymerase-associated protein CTR9 homolog OS=Homo sapiens OX=9606 GN=CTR9 PE=1 SV=1	4	1173	133.4	173	4
G5EA09	Syndecan binding protein (Syntenin), isoform CRA_a OS=Homo sapiens OX=9606 GN=SDCBP PE=1 SV	18	318	34.8	172	3
Q8IX12	Cell division cycle and apoptosis regulator protein 1 OS=Homo sapiens OX=9606 GN=CCAR1 PE=1 SV	5	1150	132.7	172	4
P26373	60S ribosomal protein L13 OS=Homo sapiens OX=9606 GN=RPL13 PE=1 SV=4	20	211	24.2	172	5
E7EWR4	Cleavage stimulation factor subunit 2 OS=Homo sapiens OX=9606 GN=CSTF2 PE=1 SV=1	10	597	62.9	172	5
Q14692	Ribosome biogenesis protein BMS1 homolog OS=Homo sapiens OX=9606 GN=BMS1 PE=1 SV=1	5	1282	145.7	171	4
P54289	Voltage-dependent calcium channel subunit alpha-2/delta-1 OS=Homo sapiens OX=9606 GN=CACNA	7	1103	124.5	171	5
Q9Y221	60S ribosome subunit biogenesis protein NIP7 homolog OS=Homo sapiens OX=9606 GN=NIP7 PE=1 S	35	180	20.4	170	4

223

Accession	Description					
P62753	40S ribosomal protein S6 OS=Homo sapiens OX=9606 GN=RPS6 PE=1 SV=1	20	249	28.7	170	5
Q15637	Splicing factor 1 OS=Homo sapiens OX=9606 GN=SF1 PE=1 SV=4	12	639	68.3	169	5
O43681	ATPase GET3 OS=Homo sapiens OX=9606 GN=GET3 PE=1 SV=2	18	348	38.8	169	5
Q16643	Drebrin OS=Homo sapiens OX=9606 GN=DBN1 PE=1 SV=4	7	649	71.4	169	3
P31040	Succinate dehydrogenase [ubiquinone] flavoprotein subunit, mitochondrial OS=Homo sapiens OX=9	6	664	72.6	168	2
O75340	Programmed cell death protein 6 OS=Homo sapiens OX=9606 GN=PDCD6 PE=1 SV=1	16	191	21.9	167	3
B0QY89	Eukaryotic translation initiation factor 3 subunit L OS=Homo sapiens OX=9606 GN=EIF3L PE=1 SV=1	6	607	70.9	167	3
O43347	RNA-binding protein Musashi homolog 1 OS=Homo sapiens OX=9606 GN=MSI1 PE=1 SV=1	18	362	39.1	166	4
M0QYS1	60S ribosomal protein L13a (Fragment) OS=Homo sapiens OX=9606 GN=RPL13A PE=1 SV=2	21	210	24.2	164	4
O75367	Core histone macro-H2A.1 OS=Homo sapiens OX=9606 GN=MACROH2A1 PE=1 SV=4	14	372	39.6	163	4
P42704	Leucine-rich PPR motif-containing protein, mitochondrial OS=Homo sapiens OX=9606 GN=LRPPRC PI	4	1394	157.8	162	4
Q9BV38	WD repeat-containing protein 18 OS=Homo sapiens OX=9606 GN=WDR18 PE=1 SV=2	13	432	47.4	162	5
Q86W42	THO complex subunit 6 homolog OS=Homo sapiens OX=9606 GN=THOC6 PE=1 SV=1	15	341	37.5	162	4
Q9BSJ8	Extended synaptotagmin-1 OS=Homo sapiens OX=9606 GN=ESYT1 PE=1 SV=1	5	1104	122.8	161	4
E9PQ57	mRNA export factor OS=Homo sapiens OX=9606 GN=RAE1 PE=1 SV=1	12	437	47.8	161	3
Q96QD9	UAP56-interacting factor OS=Homo sapiens OX=9606 GN=FYTTD1 PE=1 SV=3	13	318	35.8	161	3
Q92769	Histone deacetylase 2 OS=Homo sapiens OX=9606 GN=HDAC2 PE=1 SV=2	12	488	55.3	160	5
Q14697	Neutral alpha-glucosidase AB OS=Homo sapiens OX=9606 GN=GANAB PE=1 SV=3	6	944	106.8	160	4
Q9UJZ1	Stomatin-like protein 2, mitochondrial OS=Homo sapiens OX=9606 GN=STOML2 PE=1 SV=1	14	356	38.5	160	3
A0A3F2YNY6	Pre-mRNA-processing factor 40 homolog A OS=Homo sapiens OX=9606 GN=PRPF40A PE=1 SV=1	5	994	112.3	159	3
I3L1P4	Proline-, glutamic acid- and leucine-rich protein 1 (Fragment) OS=Homo sapiens OX=9606 GN=PELP1	37	148	15.1	159	3
P46940	Ras GTPase-activating-like protein IQGAP1 OS=Homo sapiens OX=9606 GN=IQGAP1 PE=1 SV=1	3	1657	189.1	158	4
P63104	14-3-3 protein zeta/delta OS=Homo sapiens OX=9606 GN=YWHAZ PE=1 SV=1	13	245	27.7	158	2
P20338	Ras-related protein Rab-4A OS=Homo sapiens OX=9606 GN=RAB4A PE=1 SV=3	20	218	24.4	157	4
P50395	Rab GDP dissociation inhibitor beta OS=Homo sapiens OX=9606 GN=GDI2 PE=1 SV=2	12	445	50.6	157	3
P37198	Nuclear pore glycoprotein p62 OS=Homo sapiens OX=9606 GN=NUP62 PE=1 SV=3	8	522	53.2	156	4
A6NMH8	Tetraspanin OS=Homo sapiens OX=9606 GN=CD81 PE=1 SV=1	16	274	29.8	156	2
P50454	Serpin H1 OS=Homo sapiens OX=9606 GN=SERPINH1 PE=1 SV=2	14	418	46.4	155	4
Q01518	Adenylyl cyclase-associated protein 1 OS=Homo sapiens OX=9606 GN=CAP1 PE=1 SV=5	9	475	51.9	155	3
Q13242	Serine/arginine-rich splicing factor 9 OS=Homo sapiens OX=9606 GN=SRSF9 PE=1 SV=1	19	221	25.5	155	4
O95639	Cleavage and polyadenylation specificity factor subunit 4 OS=Homo sapiens OX=9606 GN=CPSF4 PE=	13	269	30.2	154	2
Q13492	Phosphatidylinositol-binding clathrin assembly protein OS=Homo sapiens OX=9606 GN=PICALM PE=	7	652	70.7	154	3
Q15084	Protein disulfide-isomerase A6 OS=Homo sapiens OX=9606 GN=PDIA6 PE=1 SV=1	5	440	48.1	153	2
Q99623	Prohibitin-2 OS=Homo sapiens OX=9606 GN=PHB2 PE=1 SV=2	16	299	33.3	153	4
O43818	U3 small nucleolar RNA-interacting protein 2 OS=Homo sapiens OX=9606 GN=RRP9 PE=1 SV=1	22	475	51.8	152	5
P31150	Rab GDP dissociation inhibitor alpha OS=Homo sapiens OX=9606 GN=GDI1 PE=1 SV=2	12	447	50.6	152	3
K7ER00	Phenylalanine--tRNA ligase alpha subunit OS=Homo sapiens OX=9606 GN=FARSA PE=1 SV=1	5	548	62.4	152	3
Q9BVI4	Nucleolar complex protein 4 homolog OS=Homo sapiens OX=9606 GN=NOC4L PE=1 SV=1	10	516	58.4	152	5
Q9UKX7	Nuclear pore complex protein Nup50 OS=Homo sapiens OX=9606 GN=NUP50 PE=1 SV=2	12	468	50.1	152	4
Q15007	Pre-mRNA-splicing regulator WTAP OS=Homo sapiens OX=9606 GN=WTAP PE=1 SV=2	10	396	44.2	151	3
Q9Y3F4	Serine-threonine kinase receptor-associated protein OS=Homo sapiens OX=9606 GN=STRAP PE=1 SV	10	350	38.4	151	2
A0A0A6YYL6	Protein RPL17-C18orf32 OS=Homo sapiens OX=9606 GN=RPL17-C18orf32 PE=3 SV=1	11	228	26.4	151	2
P35232	Prohibitin OS=Homo sapiens OX=9606 GN=PHB PE=1 SV=1	16	272	29.8	150	3
P39656	Dolichyl-diphosphooligosaccharide--protein glycosyltransferase 48 kDa subunit OS=Homo sapiens C	10	456	50.8	148	4
Q12800	Alpha-globin transcription factor CP2 OS=Homo sapiens OX=9606 GN=TFCP2 PE=1 SV=2	8	502	57.2	148	3
P34897	Serine hydroxymethyltransferase, mitochondrial OS=Homo sapiens OX=9606 GN=SHMT2 PE=1 SV=3	13	504	56	148	5
A0A286YFF7	Palmitoyl-protein thioesterase 1 OS=Homo sapiens OX=9606 GN=PPT1 PE=1 SV=1	14	335	37.1	148	3
P35611	Alpha-adducin OS=Homo sapiens OX=9606 GN=ADD1 PE=1 SV=2	6	737	80.9	147	3
P62304	Small nuclear ribonucleoprotein E OS=Homo sapiens OX=9606 GN=SNRPE PE=1 SV=1	70	92	10.8	147	4
Q9BZK7	F-box-like/WD repeat-containing protein TBL1XR1 OS=Homo sapiens OX=9606 GN=TBL1XR1 PE=1 SV	7	514	55.6	147	3
P62266	40S ribosomal protein S23 OS=Homo sapiens OX=9606 GN=RPS23 PE=1 SV=3	29	143	15.8	145	4
P49792	E3 SUMO-protein ligase RanBP2 OS=Homo sapiens OX=9606 GN=RANBP2 PE=1 SV=2	2	3224	358	145	4
P61204	ADP-ribosylation factor 3 OS=Homo sapiens OX=9606 GN=ARF3 PE=1 SV=2	28	181	20.6	145	4
Q16630	Cleavage and polyadenylation specificity factor subunit 6 OS=Homo sapiens OX=9606 GN=CPSF6 PE=	8	551	59.2	144	3
E9PI41	Exosome complex component RRP41 (Fragment) OS=Homo sapiens OX=9606 GN=EXOSC4 PE=1 SV=	12	261	28.3	144	2
Q14152	Eukaryotic translation initiation factor 3 subunit A OS=Homo sapiens OX=9606 GN=EIF3A PE=1 SV=1	3	1382	166.5	144	3
Q15738	Sterol-4-alpha-carboxylate 3-dehydrogenase, decarboxylating OS=Homo sapiens OX=9606 GN=NSDI	13	373	41.9	143	4
P42696	RNA-binding protein 34 OS=Homo sapiens OX=9606 GN=RBM34 PE=1 SV=2	7	430	48.5	143	3
P49368	T-complex protein 1 subunit gamma OS=Homo sapiens OX=9606 GN=CCT3 PE=1 SV=4	10	545	60.5	143	5
O75525	KH domain-containing, RNA-binding, signal transduction-associated protein 3 OS=Homo sapiens OX	14	346	38.8	143	4
O60664	Perilipin-3 OS=Homo sapiens OX=9606 GN=PLIN3 PE=1 SV=3	7	434	47	142	2
Q15836	Vesicle-associated membrane protein 3 OS=Homo sapiens OX=9606 GN=VAMP3 PE=1 SV=3	40	100	11.3	142	2
Q9BTD8	RNA-binding protein 42 OS=Homo sapiens OX=9606 GN=RBM42 PE=1 SV=1	6	480	50.4	140	2
Q8WVC0	RNA polymerase-associated protein LEO1 OS=Homo sapiens OX=9606 GN=LEO1 PE=1 SV=1	6	666	75.4	139	3
Q92922	SWI/SNF complex subunit SMARCC1 OS=Homo sapiens OX=9606 GN=SMARCC1 PE=1 SV=3	5	1105	122.8	139	4
Q8N1N4	Keratin, type II cytoskeletal 78 OS=Homo sapiens OX=9606 GN=KRT78 PE=1 SV=2	7	520	56.8	139	4
P40227	T-complex protein 1 subunit zeta OS=Homo sapiens OX=9606 GN=CCT6A PE=1 SV=3	8	531	58	139	4
A0A0J9YXF2	Paraoxonase 2, isoform CRA_a OS=Homo sapiens OX=9606 GN=PON2 PE=1 SV=1	12	375	41.5	139	3
P84098	60S ribosomal protein L19 OS=Homo sapiens OX=9606 GN=RPL19 PE=1 SV=1	13	196	23.5	138	2
P50914	60S ribosomal protein L14 OS=Homo sapiens OX=9606 GN=RPL14 PE=1 SV=4	14	215	23.4	138	3
P35268	60S ribosomal protein L22 OS=Homo sapiens OX=9606 GN=RPL22 PE=1 SV=2	20	128	14.8	138	3
P46821	Microtubule-associated protein 1B OS=Homo sapiens OX=9606 GN=MAP1B PE=1 SV=2	2	2468	270.5	138	3
Q13330	Metastasis-associated protein MTA1 OS=Homo sapiens OX=9606 GN=MTA1 PE=1 SV=2	5	715	80.7	137	3
P68400	Casein kinase II subunit alpha OS=Homo sapiens OX=9606 GN=CSNK2A1 PE=1 SV=1	8	391	45.1	137	2
O43169	Cytochrome b5 type B OS=Homo sapiens OX=9606 GN=CYB5B PE=1 SV=3	39	150	16.7	137	3
Q9H7B2	Ribosome production factor 2 homolog OS=Homo sapiens OX=9606 GN=RPF2 PE=1 SV=2	15	306	35.6	137	4
Q92733	Proline-rich protein PRCC OS=Homo sapiens OX=9606 GN=PRCC PE=1 SV=1	8	491	52.4	136	2
D6REX3	Protein transport protein Sec31A OS=Homo sapiens OX=9606 GN=SEC31A PE=1 SV=1	4	1251	136.1	136	4
Q68CQ4	Digestive organ expansion factor homolog OS=Homo sapiens OX=9606 GN=DIEXF PE=1 SV=2	6	756	87	136	5
Q01081	Splicing factor U2AF 35 kDa subunit OS=Homo sapiens OX=9606 GN=U2AF1 PE=1 SV=3	13	240	27.9	136	2
P28331	NADH-ubiquinone oxidoreductase 75 kDa subunit, mitochondrial OS=Homo sapiens OX=9606 GN=N	6	727	79.4	135	3
O43684	Mitotic checkpoint protein BUB3 OS=Homo sapiens OX=9606 GN=BUB3 PE=1 SV=1	20	328	37.1	135	5
Q9NQ29	Putative RNA-binding protein Luc7-like 1 OS=Homo sapiens OX=9606 GN=LUC7L PE=1 SV=1	12	371	43.7	135	4
E9PNQ8	Thy-1 membrane glycoprotein (Fragment) OS=Homo sapiens OX=9606 GN=THY1 PE=1 SV=1	18	165	18.2	133	2
Q8N6H7	ADP-ribosylation factor GTPase-activating protein 2 OS=Homo sapiens OX=9606 GN=ARFGAP2 PE=1	8	521	56.7	133	4
D6W5Y5	Cold inducible RNA binding protein, isoform CRA_c OS=Homo sapiens OX=9606 GN=CIRBP PE=1 SV=	4	297	31.9	133	2
P55060	Exportin-2 OS=Homo sapiens OX=9606 GN=CSE1L PE=1 SV=3	3	971	110.3	132	4
O75494	Serine/arginine-rich splicing factor 10 OS=Homo sapiens OX=9606 GN=SRSF10 PE=1 SV=1	9	262	31.3	131	3
Q6RFH5	WD repeat-containing protein 74 OS=Homo sapiens OX=9606 GN=WDR74 PE=1 SV=1	11	385	42.4	131	3
O43795	Unconventional myosin-Ib OS=Homo sapiens OX=9606 GN=MYO1B PE=1 SV=3	4	1136	131.9	131	4
Q13123	Protein Red OS=Homo sapiens OX=9606 GN=IK PE=1 SV=3	8	557	65.6	131	4
Q9NQT4	Exosome complex component RRP46 OS=Homo sapiens OX=9606 GN=EXOSC5 PE=1 SV=1	16	235	25.2	131	2
P46783	40S ribosomal protein S10 OS=Homo sapiens OX=9606 GN=RPS10 PE=1 SV=1	15	165	18.9	131	3
P08133	Annexin A6 OS=Homo sapiens OX=9606 GN=ANXA6 PE=1 SV=3	7	673	75.8	131	4
Q14146	Unhealthy ribosome biogenesis protein 2 homolog OS=Homo sapiens OX=9606 GN=URB2 PE=1 SV=2	2	1524	170.4	130	3
Q13206	Probable ATP-dependent RNA helicase DDX10 OS=Homo sapiens OX=9606 GN=DDX10 PE=1 SV=2	5	875	100.8	130	3
Q99733	Nucleosome assembly protein 1-like 4 OS=Homo sapiens OX=9606 GN=NAP1L4 PE=1 SV=1	10	375	42.8	130	3
O95208	Epsin-2 OS=Homo sapiens OX=9606 GN=EPN2 PE=1 SV=3	4	641	68.4	130	2
P49750	YLP motif-containing protein 1 OS=Homo sapiens OX=9606 GN=YLPM1 PE=1 SV=4	3	2146	241.5	130	4
Q5T749	Keratinocyte proline-rich protein OS=Homo sapiens OX=9606 GN=KPRP PE=1 SV=1	6	579	64.1	130	2

Accession	Description	1	2	3	4	5
O75915	PRA1 family protein 3 OS=Homo sapiens OX=9606 GN=ARL6IP5 PE=1 SV=1	16	188	21.6	129	2
A0A0B4J203	Protein kinase domain-containing protein OS=Homo sapiens OX=9606 PE=3 SV=1	4	849	94.6	128	2
Q99470	Stromal cell-derived factor 2 OS=Homo sapiens OX=9606 GN=SDF2 PE=1 SV=2	22	211	23	128	2
O00629	Importin subunit alpha-3 OS=Homo sapiens OX=9606 GN=KPNA4 PE=1 SV=1	13	521	57.9	128	4
Q16576	Histone-binding protein RBBP7 OS=Homo sapiens OX=9606 GN=RBBP7 PE=1 SV=1	8	425	47.8	128	4
D6RHJ3	Calnexin (Fragment) OS=Homo sapiens OX=9606 GN=CANX PE=1 SV=8	22	78	8.5	128	2
F2Z2X0	Nucleoside diphosphate kinase OS=Homo sapiens OX=9606 GN=NME4 PE=1 SV=1	18	233	25.4	127	3
Q7RTV0	PHD finger-like domain-containing protein 5A OS=Homo sapiens OX=9606 GN=PHF5A PE=1 SV=1	35	110	12.4	127	4
P18124	60S ribosomal protein L7 OS=Homo sapiens OX=9606 GN=RPL7 PE=1 SV=1	23	248	29.2	127	5
Q9Y5S9	RNA-binding protein 8A OS=Homo sapiens OX=9606 GN=RBM8A PE=1 SV=1	26	174	19.9	126	2
D3DQV9	Eukaryotic translation initiation factor 4 gamma 2 (Fragment) OS=Homo sapiens OX=9606 GN=EIF4G	5	907	102.3	126	3
P25789	Proteasome subunit alpha type-4 OS=Homo sapiens OX=9606 GN=PSMA4 PE=1 SV=1	13	261	29.5	125	3
O60287	Nucleolar pre-ribosomal-associated protein 1 OS=Homo sapiens OX=9606 GN=URB1 PE=1 SV=4	2	2271	254.2	125	3
Q92900	Regulator of nonsense transcripts 1 OS=Homo sapiens OX=9606 GN=UPF1 PE=1 SV=2	5	1129	124.3	124	4
Q99536	Synaptic vesicle membrane protein VAT-1 homolog OS=Homo sapiens OX=9606 GN=VAT1 PE=1 SV=2	10	393	41.9	124	2
P49736	DNA replication licensing factor MCM2 OS=Homo sapiens OX=9606 GN=MCM2 PE=1 SV=4	5	904	101.8	124	3
Q9H3N1	Thioredoxin-related transmembrane protein 1 OS=Homo sapiens OX=9606 GN=TMX1 PE=1 SV=1	13	280	31.8	123	3
P62714	Serine/threonine-protein phosphatase 2A catalytic subunit beta isoform OS=Homo sapiens OX=960	16	309	35.6	123	3
A0A494C0W0	Poly(A)-specific ribonuclease PARN OS=Homo sapiens OX=9606 GN=PARN PE=1 SV=1	6	664	76.3	123	3
B7Z4C8	60S ribosomal protein L31 OS=Homo sapiens OX=9606 GN=RPL31 PE=1 SV=1	25	130	15.1	123	3
V9GZ56	U6 snRNA-associated Sm-like protein LSm4 (Fragment) OS=Homo sapiens OX=9606 GN=LSM4 PE=1 S	21	238	25.7	122	4
O43447	Peptidyl-prolyl cis-trans isomerase H OS=Homo sapiens OX=9606 GN=PPIH PE=1 SV=1	30	177	19.2	122	3
P48449	Lanosterol synthase OS=Homo sapiens OX=9606 GN=LSS PE=1 SV=1	4	732	83.3	122	2
H0YKD8	60S ribosomal protein L28 OS=Homo sapiens OX=9606 GN=RPL28 PE=1 SV=1	16	170	19.1	121	4
Q9UHB6	LIM domain and actin-binding protein 1 OS=Homo sapiens OX=9606 GN=LIMA1 PE=1 SV=1	4	759	85.2	121	2
O00264	Membrane-associated progesterone receptor component 1 OS=Homo sapiens OX=9606 GN=PGRMC	19	195	21.7	121	2
Q9UHB9	Signal recognition particle subunit SRP68 OS=Homo sapiens OX=9606 GN=SRP68 PE=1 SV=2	6	627	70.7	121	2
Q14344	Guanine nucleotide-binding protein subunit alpha-13 OS=Homo sapiens OX=9606 GN=GNA13 PE=1 S	9	377	44	120	3
Q8NAV1	Pre-mRNA-splicing factor 38A OS=Homo sapiens OX=9606 GN=PRPF38A PE=1 SV=1	12	312	37.5	120	3
A0A0C4DG17	40S ribosomal protein SA OS=Homo sapiens OX=9606 GN=RPSA PE=1 SV=1	14	300	33.3	119	2
Q9UBS4	DnaJ homolog subfamily B member 11 OS=Homo sapiens OX=9606 GN=DNAJB11 PE=1 SV=1	10	358	40.5	119	2
Q9UKF6	Cleavage and polyadenylation specificity factor subunit 3 OS=Homo sapiens OX=9606 GN=CPSF3 PE=	8	684	77.4	119	4
P50991	T-complex protein 1 subunit delta OS=Homo sapiens OX=9606 GN=CCT4 PE=1 SV=4	8	539	57.9	119	3
P45880	Voltage-dependent anion-selective channel protein 2 OS=Homo sapiens OX=9606 GN=VDAC2 PE=1 S	11	294	31.5	118	2
Q15287	RNA-binding protein with serine-rich domain 1 OS=Homo sapiens OX=9606 GN=RNPS1 PE=1 SV=1	10	305	34.2	118	3
P61254	60S ribosomal protein L26 OS=Homo sapiens OX=9606 GN=RPL26 PE=1 SV=1	21	145	17.2	117	4
P12814	Alpha-actinin-1 OS=Homo sapiens OX=9606 GN=ACTN1 PE=1 SV=2	3	892	103	116	3
O43242	26S proteasome non-ATPase regulatory subunit 3 OS=Homo sapiens OX=9606 GN=PSMD3 PE=1 SV=	9	534	60.9	116	4
Q96I25	Splicing factor 45 OS=Homo sapiens OX=9606 GN=RBM17 PE=1 SV=1	10	401	44.9	116	3
P49458	Signal recognition particle 9 kDa protein OS=Homo sapiens OX=9606 GN=SRP9 PE=1 SV=2	26	86	10.1	116	2
Q13510	Acid ceramidase OS=Homo sapiens OX=9606 GN=ASAH1 PE=1 SV=5	6	395	44.6	115	2
Q9UKA9	Polypyrimidine tract-binding protein 2 OS=Homo sapiens OX=9606 GN=PTBP2 PE=1 SV=1	10	531	57.5	115	3
A0A2R8Y7H4	Ribose-phosphate pyrophosphokinase OS=Homo sapiens OX=9606 GN=PRPS1 PE=1 SV=1	9	321	35.3	115	2
P50502	Hsc70-interacting protein OS=Homo sapiens OX=9606 GN=ST13 PE=1 SV=2	9	369	41.3	114	3
Q71DI3	Histone H3.2 OS=Homo sapiens OX=9606 GN=H3C15 PE=1 SV=3	34	136	15.4	113	3
Q01130	Serine/arginine-rich splicing factor 2 OS=Homo sapiens OX=9606 GN=SRSF2 PE=1 SV=4	14	221	25.5	113	3
O14828	Secretory carrier-associated membrane protein 3 OS=Homo sapiens OX=9606 GN=SCAMP3 PE=1 SV	8	347	38.3	113	2
P62854	40S ribosomal protein S26 OS=Homo sapiens OX=9606 GN=RPS26 PE=1 SV=3	23	115	13	113	2
P08621	U1 small nuclear ribonucleoprotein 70 kDa OS=Homo sapiens OX=9606 GN=SNRNP70 PE=1 SV=2	14	437	51.5	112	4
P54886	Delta-1-pyrroline-5-carboxylate synthase OS=Homo sapiens OX=9606 GN=ALDH18A1 PE=1 SV=2	4	795	87.2	112	2
P62081	40S ribosomal protein S7 OS=Homo sapiens OX=9606 GN=RPS7 PE=1 SV=1	22	194	22.1	111	4
Q9H8H2	Probable ATP-dependent RNA helicase DDX31 OS=Homo sapiens OX=9606 GN=DDX31 PE=1 SV=2	4	851	94	111	3
P49755	Transmembrane emp24 domain-containing protein 10 OS=Homo sapiens OX=9606 GN=TMED10 PE=	23	219	25	111	3
P62851	40S ribosomal protein S25 OS=Homo sapiens OX=9606 GN=RPS25 PE=1 SV=1	24	125	13.7	111	3
P50402	Emerin OS=Homo sapiens OX=9606 GN=EMD PE=1 SV=1	10	254	29	110	2
Q6UXN9	WD repeat-containing protein 82 OS=Homo sapiens OX=9606 GN=WDR82 PE=1 SV=1	10	313	35.1	110	3
P60228	Eukaryotic translation initiation factor 3 subunit E OS=Homo sapiens OX=9606 GN=EIF3E PE=1 SV=1	11	445	52.2	110	4
P27348	14-3-3 protein theta OS=Homo sapiens OX=9606 GN=YWHAQ PE=1 SV=1	9	245	27.7	110	2
A0A0A6YYJ8	Putative RNA-binding protein Luc7-like 2 OS=Homo sapiens OX=9606 GN=LUC7L2 PE=4 SV=1	7	458	54.2	110	3
P49959	Double-strand break repair protein MRE11 OS=Homo sapiens OX=9606 GN=MRE11 PE=1 SV=3	3	708	80.5	110	2
Q96AC1	Fermitin family homolog 2 OS=Homo sapiens OX=9606 GN=FERMT2 PE=1 SV=1	4	680	77.8	109	2
Q9H4L4	Sentrin-specific protease 3 OS=Homo sapiens OX=9606 GN=SENP3 PE=1 SV=2	8	574	65	109	3
H0YJ66	Dehydrogenase/reductase SDR family member 7 (Fragment) OS=Homo sapiens OX=9606 GN=DHRS	7	399	44.8	108	2
Q7Z4W1	L-xylulose reductase OS=Homo sapiens OX=9606 GN=DCXR PE=1 SV=2	16	244	25.9	108	3
A0A0U1RQQ9	SCY1-like protein 2 OS=Homo sapiens OX=9606 GN=SCYL2 PE=1 SV=1	5	933	104	108	3
P56545	C-terminal-binding protein 2 OS=Homo sapiens OX=9606 GN=CTBP2 PE=1 SV=1	8	445	48.9	108	3
P09429	High mobility group protein B1 OS=Homo sapiens OX=9606 GN=HMGB1 PE=1 SV=3	13	215	24.9	108	2
P00505	Aspartate aminotransferase, mitochondrial OS=Homo sapiens OX=9606 GN=GOT2 PE=1 SV=3	6	430	47.5	108	2
Q5SSJ5	Heterochromatin protein 1-binding protein 3 OS=Homo sapiens OX=9606 GN=HP1BP3 PE=1 SV=1	7	553	61.2	107	3
Q9BPW8	Protein NipSnap homolog 1 OS=Homo sapiens OX=9606 GN=NIPSNAP1 PE=1 SV=1	13	284	33.3	107	2
Q13642	Four and a half LIM domains protein 1 OS=Homo sapiens OX=9606 GN=FHL1 PE=1 SV=4	8	323	36.2	107	2
Q01469	Fatty acid-binding protein 5 OS=Homo sapiens OX=9606 GN=FABP5 PE=1 SV=3	24	135	15.2	107	3
Q13601	KRR1 small subunit processome component homolog OS=Homo sapiens OX=9606 GN=KRR1 PE=1 SV	8	381	43.6	107	3
Q9UI30	Multifunctional methyltransferase subunit TRM112-like protein OS=Homo sapiens OX=9606 GN=TRI	17	125	14.2	107	2
P33992	DNA replication licensing factor MCM5 OS=Homo sapiens OX=9606 GN=MCM5 PE=1 SV=5	6	734	82.2	107	3
Q13363	C-terminal-binding protein 1 OS=Homo sapiens OX=9606 GN=CTBP1 PE=1 SV=2	8	440	47.5	107	4
Q99832	T-complex protein 1 subunit eta OS=Homo sapiens OX=9606 GN=CCT7 PE=1 SV=2	7	543	59.3	106	4
P51572	B-cell receptor-associated protein 31 OS=Homo sapiens OX=9606 GN=BCAP31 PE=1 SV=3	12	246	28	106	2
Q9UQ80	Proliferation-associated protein 2G4 OS=Homo sapiens OX=9606 GN=PA2G4 PE=1 SV=3	10	394	43.8	106	2
D6RJF2	Polyadenylate-binding protein-interacting protein 1 (Fragment) OS=Homo sapiens OX=9606 GN=PAI	12	200	22.6	106	2
Q7L2E3	ATP-dependent RNA helicase DHX30 OS=Homo sapiens OX=9606 GN=DHX30 PE=1 SV=1	2	1194	133.9	106	2
Q5SY16	Polynucleotide 5'-hydroxyl-kinase NOL9 OS=Homo sapiens OX=9606 GN=NOL9 PE=1 SV=1	7	702	79.3	105	3
P53621	Coatomer subunit alpha OS=Homo sapiens OX=9606 GN=COPA PE=1 SV=2	4	1224	138.3	104	3
Q15363	Transmembrane emp24 domain-containing protein 2 OS=Homo sapiens OX=9606 GN=TMED2 PE=1	12	201	22.7	104	2
Q9Y3B9	RRP15-like protein OS=Homo sapiens OX=9606 GN=RRP15 PE=1 SV=2	9	282	31.5	104	2
P55209	Nucleosome assembly protein 1-like 1 OS=Homo sapiens OX=9606 GN=NAP1L1 PE=1 SV=1	6	391	45.3	104	3
Q8TDI0	Chromodomain-helicase-DNA-binding protein 5 OS=Homo sapiens OX=9606 GN=CHD5 PE=1 SV=1	2	1954	222.9	103	3
O60684	Importin subunit alpha-7 OS=Homo sapiens OX=9606 GN=KPNA6 PE=1 SV=1	5	536	60	103	2
Q13610	Periodic tryptophan protein 1 homolog OS=Homo sapiens OX=9606 GN=PWP1 PE=1 SV=1	6	501	55.8	103	2
O60701	UDP-glucose 6-dehydrogenase OS=Homo sapiens OX=9606 GN=UGDH PE=1 SV=1	7	494	55	103	2
J3QQ67	60S ribosomal protein L18 (Fragment) OS=Homo sapiens OX=9606 GN=RPL18 PE=1 SV=1	21	190	21.8	102	4
O00422	Histone deacetylase complex subunit SAP18 OS=Homo sapiens OX=9606 GN=SAP18 PE=1 SV=1	17	153	17.6	102	2
Q13162	Peroxiredoxin-4 OS=Homo sapiens OX=9606 GN=PRDX4 PE=1 SV=1	19	271	30.5	101	2
P23284	Peptidyl-prolyl cis-trans isomerase B OS=Homo sapiens OX=9606 GN=PPIB PE=1 SV=2	13	216	23.7	101	2
P48643	T-complex protein 1 subunit epsilon OS=Homo sapiens OX=9606 GN=CCT5 PE=1 SV=1	9	541	59.6	101	3
Q8N684	Cleavage and polyadenylation specificity factor subunit 7 OS=Homo sapiens OX=9606 GN=CPSF7 PE=	7	471	52	101	2
O60231	Pre-mRNA-splicing factor ATP-dependent RNA helicase DHX16 OS=Homo sapiens OX=9606 GN=DHX	2	1041	119.2	100	2
Q96DH6	RNA-binding protein Musashi homolog 2 OS=Homo sapiens OX=9606 GN=MSI2 PE=1 SV=1	9	328	35.2	100	2
Q5SRE5	Nucleoporin NUP188 homolog OS=Homo sapiens OX=9606 GN=NUP188 PE=1 SV=1	1	1749	195.9	100	2
Q8N7H5	RNA polymerase II-associated factor 1 homolog OS=Homo sapiens OX=9606 GN=PAF1 PE=1 SV=2	6	531	59.9	100	2

A0A0B4J1V8	HCG2039996 OS=Homo sapiens OX=9606 GN=PPAN-P2RY11 PE=3 SV=1	7	794	87.9	100	3
Q14247	Src substrate cortactin OS=Homo sapiens OX=9606 GN=CTTN PE=1 SV=2	4	550	61.5	99	2
Q15942	Zyxin OS=Homo sapiens OX=9606 GN=ZYX PE=1 SV=1	7	572	61.2	98	2
P04844	Dolichyl-diphosphooligosaccharide--protein glycosyltransferase subunit 2 OS=Homo sapiens OX=96	9	631	69.2	98	3
P63244	Receptor of activated protein C kinase 1 OS=Homo sapiens OX=9606 GN=RACK1 PE=1 SV=3	9	317	35.1	98	2
Q9UDY4	DnaJ homolog subfamily B member 4 OS=Homo sapiens OX=9606 GN=DNAJB4 PE=1 SV=1	8	337	37.8	98	2
P41250	Glycine--tRNA ligase OS=Homo sapiens OX=9606 GN=GARS1 PE=1 SV=3	4	739	83.1	98	2
P30041	Peroxiredoxin-6 OS=Homo sapiens OX=9606 GN=PRDX6 PE=1 SV=3	18	224	25	98	3
Q12972	Nuclear inhibitor of protein phosphatase 1 OS=Homo sapiens OX=9606 GN=PPP1R8 PE=1 SV=2	10	351	38.5	97	2
A0A1W2PQ47	Squalene synthase OS=Homo sapiens OX=9606 GN=FDFT1 PE=1 SV=1	7	476	53.6	97	2
Q8IXT5	RNA-binding protein 12B OS=Homo sapiens OX=9606 GN=RBM12B PE=1 SV=2	4	1001	118	97	3
J3KMZ8	Zinc finger protein ubi-d4 OS=Homo sapiens OX=9606 GN=DPF2 PE=1 SV=1	8	405	45.8	96	2
P29558	RNA-binding motif, single-stranded-interacting protein 1 OS=Homo sapiens OX=9606 GN=RBMS1 PE	7	406	44.5	96	2
P63173	60S ribosomal protein L38 OS=Homo sapiens OX=9606 GN=RPL38 PE=1 SV=2	36	70	8.2	96	2
Q9H7Z7	Prostaglandin E synthase 2 OS=Homo sapiens OX=9606 GN=PTGES2 PE=1 SV=1	10	377	41.9	96	2
Q9UBQ5	Eukaryotic translation initiation factor 3 subunit K OS=Homo sapiens OX=9606 GN=EIF3K PE=1 SV=1	11	218	25	96	2
P11387	DNA topoisomerase 1 OS=Homo sapiens OX=9606 GN=TOP1 PE=1 SV=2	4	765	90.7	95	2
Q6PJT7	Zinc finger CCCH domain-containing protein 14 OS=Homo sapiens OX=9606 GN=ZC3H14 PE=1 SV=1	3	736	82.8	95	2
P20290	Transcription factor BTF3 OS=Homo sapiens OX=9606 GN=BTF3 PE=1 SV=1	23	206	22.2	95	2
Q15291	Retinoblastoma-binding protein 5 OS=Homo sapiens OX=9606 GN=RBBP5 PE=1 SV=2	7	538	59.1	95	2
M0QXB4	Coatomer protein complex, subunit epsilon, isoform CRA_g OS=Homo sapiens OX=9606 GN=COPE P	12	331	36.9	95	2
P18077	60S ribosomal protein L35a OS=Homo sapiens OX=9606 GN=RPL35A PE=1 SV=2	28	110	12.5	94	4
Q9NPE3	H/ACA ribonucleoprotein complex subunit 3 OS=Homo sapiens OX=9606 GN=NOP10 PE=1 SV=1	38	64	7.7	94	2
A0A0A0MSW4	Phosphatidylinositol transfer protein beta isoform OS=Homo sapiens OX=9606 GN=PITPNB PE=1 SV=	16	271	31.6	94	2
Q9Y5Q9	General transcription factor 3C polypeptide 3 OS=Homo sapiens OX=9606 GN=GTF3C3 PE=1 SV=1	3	886	101.2	93	2
P26368	Splicing factor U2AF 65 kDa subunit OS=Homo sapiens OX=9606 GN=U2AF2 PE=1 SV=4	11	475	53.5	93	3
Q00325	Phosphate carrier protein, mitochondrial OS=Homo sapiens OX=9606 GN=SLC25A3 PE=1 SV=2	9	362	40.1	93	3
O75208	Ubiquinone biosynthesis protein COQ9, mitochondrial OS=Homo sapiens OX=9606 GN=COQ9 PE=1 S	12	318	35.5	93	2
Q13200	26S proteasome non-ATPase regulatory subunit 2 OS=Homo sapiens OX=9606 GN=PSMD2 PE=1 SV=	3	908	100.1	93	2
Q96T37	RNA-binding protein 15 OS=Homo sapiens OX=9606 GN=RBM15 PE=1 SV=2	4	977	107.1	92	2
Q9P035	Very-long-chain (3R)-3-hydroxyacyl-CoA dehydratase 3 OS=Homo sapiens OX=9606 GN=HACD3 PE=	10	362	43.1	92	2
Q96G21	U3 small nucleolar ribonucleoprotein protein IMP4 OS=Homo sapiens OX=9606 GN=IMP4 PE=1 SV=1	10	291	33.7	91	2
O60716	Catenin delta-1 OS=Homo sapiens OX=9606 GN=CTNND1 PE=1 SV=1	4	968	108.1	91	3
Q8WXF1	Paraspeckle component 1 OS=Homo sapiens OX=9606 GN=PSPC1 PE=1 SV=1	7	523	58.7	91	3
Q92598	Heat shock protein 105 kDa OS=Homo sapiens OX=9606 GN=HSPH1 PE=1 SV=1	3	858	96.8	91	2
E9PH57	Transcription factor 4 OS=Homo sapiens OX=9606 GN=TCF4 PE=1 SV=2	3	773	83.4	90	2
Q53GQ0	Very-long-chain 3-oxoacyl-CoA reductase OS=Homo sapiens OX=9606 GN=HSD17B12 PE=1 SV=2	7	312	34.3	90	2
Q13185	Chromobox protein homolog 3 OS=Homo sapiens OX=9606 GN=CBX3 PE=1 SV=4	14	183	20.8	90	2
P35613	Basigin OS=Homo sapiens OX=9606 GN=BSG PE=1 SV=2	8	385	42.2	90	2
P39019	40S ribosomal protein S19 OS=Homo sapiens OX=9606 GN=RPS19 PE=1 SV=2	19	145	16.1	89	3
Q9UK61	Protein TASOR OS=Homo sapiens OX=9606 GN=TASOR PE=1 SV=3	1	1670	188.9	89	2
P56199	Integrin alpha-1 OS=Homo sapiens OX=9606 GN=ITGA1 PE=1 SV=2	2	1179	130.8	89	3
Q9BXS5	AP-1 complex subunit mu-1 OS=Homo sapiens OX=9606 GN=AP1M1 PE=1 SV=3	6	423	48.6	89	2
A0A0G2JLB3	Glucosylceramidase OS=Homo sapiens OX=9606 GN=GBA PE=1 SV=1	5	536	59.6	88	2
P49720	Proteasome subunit beta type-3 OS=Homo sapiens OX=9606 GN=PSMB3 PE=1 SV=2	16	205	22.9	88	2
Q8NDT2	Putative RNA-binding protein 15B OS=Homo sapiens OX=9606 GN=RBM15B PE=1 SV=3	3	890	97.1	88	2
P36776	Lon protease homolog, mitochondrial OS=Homo sapiens OX=9606 GN=LONP1 PE=1 SV=2	3	959	106.4	87	2
O14980	Exportin-1 OS=Homo sapiens OX=9606 GN=XPO1 PE=1 SV=1	4	1071	123.3	87	3
O96008	Mitochondrial import receptor subunit TOM40 homolog OS=Homo sapiens OX=9606 GN=TOMM40	9	361	37.9	87	2
Q8IWZ8	SURP and G-patch domain-containing protein 1 OS=Homo sapiens OX=9606 GN=SUGP1 PE=1 SV=2	5	645	72.4	87	2
P00491	Purine nucleoside phosphorylase OS=Homo sapiens OX=9606 GN=PNP PE=1 SV=2	9	289	32.1	87	2
Q13427	Peptidyl-prolyl cis-trans isomerase G OS=Homo sapiens OX=9606 GN=PPIG PE=1 SV=2	4	754	88.6	87	2
Q9NZZ3	Charged multivesicular body protein 5 OS=Homo sapiens OX=9606 GN=CHMP5 PE=1 SV=1	19	219	24.6	86	2
P42766	60S ribosomal protein L35 OS=Homo sapiens OX=9606 GN=RPL35 PE=1 SV=2	19	123	14.5	85	2
P17480	Nucleolar transcription factor 1 OS=Homo sapiens OX=9606 GN=UBTF PE=1 SV=1	4	764	89.4	85	2
Q9P2J5	Leucine--tRNA ligase, cytoplasmic OS=Homo sapiens OX=9606 GN=LARS1 PE=1 SV=2	2	1176	134.4	84	2
Q02878	60S ribosomal protein L6 OS=Homo sapiens OX=9606 GN=RPL6 PE=1 SV=3	11	288	32.7	84	3
Q9BRJ7	Tudor-interacting repair regulator protein OS=Homo sapiens OX=9606 GN=NUDT16L1 PE=1 SV=1	17	211	23.3	84	3
Q13177	Serine/threonine-protein kinase PAK 2 OS=Homo sapiens OX=9606 GN=PAK2 PE=1 SV=3	6	524	58	84	2
P04843	Dolichyl-diphosphooligosaccharide--protein glycosyltransferase subunit 1 OS=Homo sapiens OX=96	6	607	68.5	83	3
G3V5Z7	Proteasome subunit alpha type OS=Homo sapiens OX=9606 GN=PSMA6 PE=1 SV=1	8	252	28.1	83	2
P62306	Small nuclear ribonucleoprotein F OS=Homo sapiens OX=9606 GN=SNRPF PE=1 SV=1	40	86	9.7	83	2
A6NKG5	Retrotransposon-like protein 1 OS=Homo sapiens OX=9606 GN=RTL1 PE=3 SV=3	1	1358	155	83	2
P05455	Lupus La protein OS=Homo sapiens OX=9606 GN=SSB PE=1 SV=2	6	408	46.8	82	2
P05386	60S acidic ribosomal protein P1 OS=Homo sapiens OX=9606 GN=RPLP1 PE=1 SV=1	52	114	11.5	82	2
P41091	Eukaryotic translation initiation factor 2 subunit 3 OS=Homo sapiens OX=9606 GN=EIF2S3 PE=1 SV=3	8	472	51.1	82	2
Q5VW26	Nuclear factor 1 OS=Homo sapiens OX=9606 GN=NFIB PE=1 SV=1	4	570	63.4	82	2
P27708	CAD protein OS=Homo sapiens OX=9606 GN=CAD PE=1 SV=3	1	2225	242.8	81	2
Q13523	Serine/threonine-protein kinase PRP4 homolog OS=Homo sapiens OX=9606 GN=PRPF4B PE=1 SV=3	2	1007	116.9	81	2
Q9BRX8	Peroxiredoxin-like 2A OS=Homo sapiens OX=9606 GN=PRXL2A PE=1 SV=1	12	229	25.7	81	2
Q15024	Exosome complex component RRP42 OS=Homo sapiens OX=9606 GN=EXOSC7 PE=1 SV=3	9	291	31.8	81	2
P12273	Prolactin-inducible protein OS=Homo sapiens OX=9606 GN=PIP PE=1 SV=1	18	146	16.6	81	2
P16401	Histone H1.5 OS=Homo sapiens OX=9606 GN=H1-5 PE=1 SV=3	13	226	22.6	80	2
P54136	Arginine--tRNA ligase, cytoplasmic OS=Homo sapiens OX=9606 GN=RARS1 PE=1 SV=2	4	660	75.3	80	2
P62312	U6 snRNA-associated Sm-like protein LSm6 OS=Homo sapiens OX=9606 GN=LSM6 PE=1 SV=1	38	80	9.1	80	3
P63010	AP-2 complex subunit beta OS=Homo sapiens OX=9606 GN=AP2B1 PE=1 SV=1	3	937	104.5	80	2
P62195	26S proteasome regulatory subunit 8 OS=Homo sapiens OX=9606 GN=PSMC5 PE=1 SV=1	8	406	45.6	79	2
O00232	26S proteasome non-ATPase regulatory subunit 12 OS=Homo sapiens OX=9606 GN=PSMD12 PE=1 S	7	456	52.9	79	3
Q9Y678	Coatomer subunit gamma-1 OS=Homo sapiens OX=9606 GN=COPG1 PE=1 SV=1	3	874	97.7	79	2
Q9H2U1	ATP-dependent DNA/RNA helicase DHX36 OS=Homo sapiens OX=9606 GN=DHX36 PE=1 SV=2	4	1008	114.7	79	2
Q9BWJ5	Splicing factor 3B subunit 5 OS=Homo sapiens OX=9606 GN=SF3B5 PE=1 SV=1	33	86	10.1	79	2
P33993	DNA replication licensing factor MCM7 OS=Homo sapiens OX=9606 GN=MCM7 PE=1 SV=4	3	719	81.3	79	2
O15371	Eukaryotic translation initiation factor 3 subunit D OS=Homo sapiens OX=9606 GN=EIF3D PE=1 SV=1	4	548	63.9	79	2
P08579	U2 small nuclear ribonucleoprotein B'' OS=Homo sapiens OX=9606 GN=SNRPB2 PE=1 SV=1	7	225	25.5	78	2
J3KR12	Uncharacterized protein OS=Homo sapiens OX=9606 PE=4 SV=1	9	359	36.7	78	2
Q9ULX3	RNA-binding protein NOB1 OS=Homo sapiens OX=9606 GN=NOB1 PE=1 SV=1	6	412	46.6	78	2
A1L020	RNA-binding protein MEX3A OS=Homo sapiens OX=9606 GN=MEX3A PE=1 SV=1	6	520	54.1	78	2
P62258	14-3-3 protein epsilon OS=Homo sapiens OX=9606 GN=YWHAE PE=1 SV=1	9	255	29.2	77	2
Q14444	Caprin-1 OS=Homo sapiens OX=9606 GN=CAPRIN1 PE=1 SV=2	3	709	78.3	77	2
P16949	Stathmin OS=Homo sapiens OX=9606 GN=STMN1 PE=1 SV=3	16	149	17.3	77	2
Q5SRQ6	Casein kinase II subunit beta OS=Homo sapiens OX=9606 GN=CSNK2B PE=1 SV=2	12	234	26.9	77	2
P62263	40S ribosomal protein S14 OS=Homo sapiens OX=9606 GN=RPS14 PE=1 SV=3	9	151	16.3	77	2
Q9Y3B2	Exosome complex component CSL4 OS=Homo sapiens OX=9606 GN=EXOSC1 PE=1 SV=1	13	195	21.4	76	2
Q92522	Histone H1.10 OS=Homo sapiens OX=9606 GN=H1-10 PE=1 SV=1	13	213	22.5	76	2
A0A3B3IT92	DNA helicase OS=Homo sapiens OX=9606 GN=MCM4 PE=1 SV=1	3	904	100.7	76	2
Q7Z3K3	Pogo transposable element with ZNF domain OS=Homo sapiens OX=9606 GN=POGZ PE=1 SV=2	2	1410	155.2	75	2
P07197	Neurofilament medium polypeptide OS=Homo sapiens OX=9606 GN=NEFM PE=1 SV=3	3	916	102.4	75	2
Q04837	Single-stranded DNA-binding protein, mitochondrial OS=Homo sapiens OX=9606 GN=SSBP1 PE=1 SV	16	148	17.2	75	2
P60953	Cell division control protein 42 homolog OS=Homo sapiens OX=9606 GN=CDC42 PE=1 SV=2	12	191	21.2	75	2
Q96ST2	Protein IWS1 homolog OS=Homo sapiens OX=9606 GN=IWS1 PE=1 SV=2	4	819	91.9	75	2

J3KPS3	Fructose-bisphosphate aldolase OS=Homo sapiens OX=9606 GN=ALDOA PE=1 SV=1	8	368	39.8	75	2
Q9ULR0	Pre-mRNA-splicing factor ISY1 homolog OS=Homo sapiens OX=9606 GN=ISY1 PE=1 SV=3	11	285	33	72	2
H7C561	Splicing factor 1 (Fragment) OS=Homo sapiens OX=9606 GN=SF1 PE=1 SV=8	9	291	30.1	72	2
O43148	mRNA cap guanine-N7 methyltransferase OS=Homo sapiens OX=9606 GN=RNMT PE=1 SV=1	6	476	54.8	71	2
Q9UHA3	Probable ribosome biogenesis protein RLP24 OS=Homo sapiens OX=9606 GN=RSL24D1 PE=1 SV=1	12	163	19.6	71	2
P34932	Heat shock 70 kDa protein 4 OS=Homo sapiens OX=9606 GN=HSPA4 PE=1 SV=4	3	840	94.3	71	2
P06756	Integrin alpha-V OS=Homo sapiens OX=9606 GN=ITGAV PE=1 SV=2	5	1048	116	70	2
Q8WVV9	Heterogeneous nuclear ribonucleoprotein L-like OS=Homo sapiens OX=9606 GN=HNRNPLL PE=1 SV=	4	542	60	69	2
O95831	Apoptosis-inducing factor 1, mitochondrial OS=Homo sapiens OX=9606 GN=AIFM1 PE=1 SV=1	4	613	66.9	69	2
O95696	Bromodomain-containing protein 1 OS=Homo sapiens OX=9606 GN=BRD1 PE=1 SV=1	2	1058	119.4	67	2
Q9Y5A9	YTH domain-containing family protein 2 OS=Homo sapiens OX=9606 GN=YTHDF2 PE=1 SV=2	4	579	62.3	67	2
P51513	RNA-binding protein Nova-1 OS=Homo sapiens OX=9606 GN=NOVA1 PE=1 SV=2	5	507	51.7	67	2
P23919	Thymidylate kinase OS=Homo sapiens OX=9606 GN=DTYMK PE=1 SV=4	10	212	23.8	67	2
Q15046	Lysine--tRNA ligase OS=Homo sapiens OX=9606 GN=KARS1 PE=1 SV=3	4	597	68	67	2
Q99575	Ribonucleases P/MRP protein subunit POP1 OS=Homo sapiens OX=9606 GN=POP1 PE=1 SV=2	3	1024	114.6	66	2
Q9BQ67	Glutamate-rich WD repeat-containing protein 1 OS=Homo sapiens OX=9606 GN=GRWD1 PE=1 SV=1	7	446	49.4	66	2
Q9Y3A2	Probable U3 small nucleolar RNA-associated protein 11 OS=Homo sapiens OX=9606 GN=UTP11 PE=1	11	253	30.4	64	2
P18669	Phosphoglycerate mutase 1 OS=Homo sapiens OX=9606 GN=PGAM1 PE=1 SV=2	10	254	28.8	64	2
Q53GS9	U4/U6.U5 tri-snRNP-associated protein 2 OS=Homo sapiens OX=9606 GN=USP39 PE=1 SV=2	4	565	65.3	63	2
Q99497	Parkinson disease protein 7 OS=Homo sapiens OX=9606 GN=PARK7 PE=1 SV=2	7	189	19.9	63	2
F8VRH0	Poly(rC)-binding protein 2 (Fragment) OS=Homo sapiens OX=9606 GN=PCBP2 PE=1 SV=2	17	310	32	63	2
Q92917	G-patch domain and KOW motifs-containing protein OS=Homo sapiens OX=9606 GN=GPKOW PE=1 !	4	476	52.2	63	2
Q99453	Paired mesoderm homeobox protein 2B OS=Homo sapiens OX=9606 GN=PHOX2B PE=1 SV=2	7	314	31.6	63	2
J3KQE5	GTP-binding nuclear protein Ran (Fragment) OS=Homo sapiens OX=9606 GN=RAN PE=1 SV=1	10	234	26.8	60	2
A0A590UJL8	H3.2 histone (putative) (Fragment) OS=Homo sapiens OX=9606 GN=H3-2 PE=1 SV=1	9	79	9.1	57	3
P50570	Dynamin-2 OS=Homo sapiens OX=9606 GN=DNM2 PE=1 SV=2	3	870	98	56	2
P57723	Poly(rC)-binding protein 4 OS=Homo sapiens OX=9606 GN=PCBP4 PE=2 SV=1	5	403	41.5	56	2
Q8NE71	ATP-binding cassette sub-family F member 1 OS=Homo sapiens OX=9606 GN=ABCF1 PE=1 SV=2	2	845	95.9	55	2
O43823	A-kinase anchor protein 8 OS=Homo sapiens OX=9606 GN=AKAP8 PE=1 SV=1	2	692	76.1	55	2
Q8WVM7	Cohesin subunit SA-1 OS=Homo sapiens OX=9606 GN=STAG1 PE=1 SV=3	1	1258	144.3	55	2
P08559	Pyruvate dehydrogenase E1 component subunit alpha, somatic form, mitochondrial OS=Homo sapi	5	390	43.3	54	2
F8W727	60S ribosomal protein L32 OS=Homo sapiens OX=9606 GN=RPL32 PE=1 SV=1	11	153	18	52	2